AD-A125 687 ADVANCES IN GUIDANCE AND CONTROL SYSTEMS(U) ADVISORY GROUP FOR AEROSPACE RESEARCH AND DEVELOPMENT NEUILLY-SUR-SEINE (FRANCE) JAN 83 AGARD-CP-321 1/3

UNCLASSIFIED F/G 17/7 NL

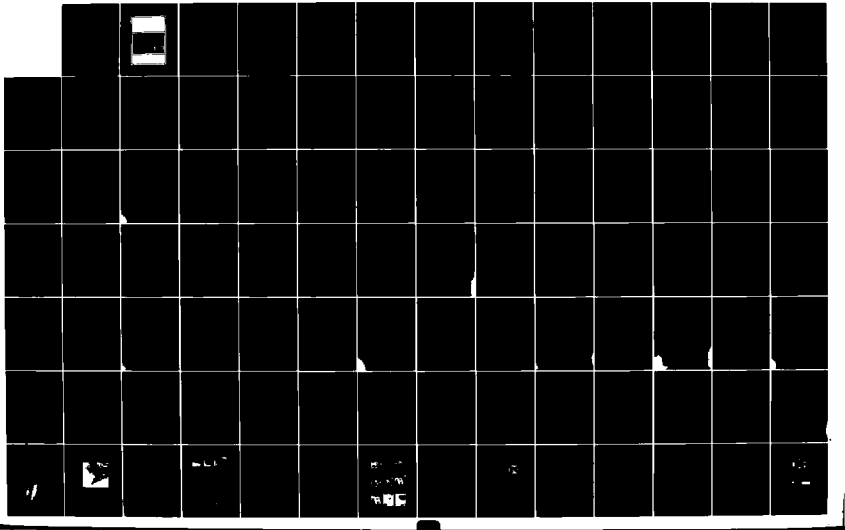

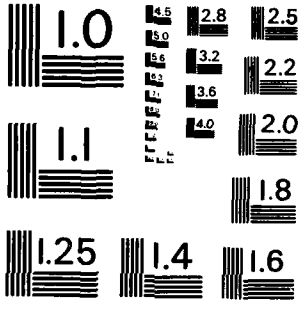

MICROCOPY RESOLUTION TEST CHART
NATIONAL BUREAU OF STANDARDS - 1963 - A

(1)

AGARD-CP-321

AGARD

ADVISORY GROUP FOR AEROSPACE RESEARCH & DEVELOPMENT

7 RUE ANCELLE 92200 NEUILLY SUR SEINE FRANCE

AGARD CONFERENCE PROCEEDINGS No. 321

Advances in Guidance and Control Systems

NORTH ATLANTIC TREATY ORGANIZATION

DISTRIBUTION AND AVAILABILITY
ON BACK COVER

AGARD-CP-321

NORTH ATLANTIC TREATY ORGANIZATION

ADVISORY GROUP FOR AEROSPACE RESEARCH AND DEVELOPMENT

(ORGANISATION DU TRAITE DE L'ATLANTIQUE NORD)

AGARD Conference Proceedings No.321

ADVANCES IN GUIDANCE AND CONTROL SYSTEMS

Papers presented at the Guidance and Control Panel 35th Symposium held in
Lisbon, Portugal, 12–14 October 1982.

THE MISSION OF AGARD

The mission of AGARD is to bring together the leading personalities of the NATO nations in the fields of science and technology relating to aerospace for the following purposes:

- Exchanging of scientific and technical information;
- Continuously stimulating advances in the aerospace sciences relevant to strengthening the common defence posture;
- Improving the co-operation among member nations in aerospace research and development;
- Providing scientific and technical advice and assistance to the North Atlantic Military Committee in the field of aerospace research and development;
- Rendering scientific and technical assistance, as requested, to other NATO bodies and to member nations in connection with research and development problems in the aerospace field;
- Providing assistance to member nations for the purpose of increasing their scientific and technical potential;
- Recommending effective ways for the member nations to use their research and development capabilities for the common benefit of the NATO community.

The highest authority within AGARD is the National Delegates Board consisting of officially appointed senior representatives from each member nation. The mission of AGARD is carried out through the Panels which are composed of experts appointed by the National Delegates, the Consultant and Exchange Programme and the Aerospace Applications Studies Programme. The results of AGARD work are reported to the member nations and the NATO Authorities through the AGARD series of publications of which this is one.

Participation in AGARD activities is by invitation only and is normally limited to citizens of the NATO nations.

Published January 1983

ISBN 92-835-0324-4

Printed by Specialised Printing Services Ltd
40 Chigwell Lane, Loughton, Essex, IG10 3TZ

PREFACE

Many significant advances in optimal control theory, synthesis techniques and design methodology have taken place since the last symposium held in this area in 1973.

The rapidly developing technologies in computation, data distribution systems, computer aided design methods and data bases now permit application of theories and synthesis methods heretofore impractical.

The increased emphasis on functional and performance capability at reduced cost suggests application of technologies and methods for more common use of information and higher levels of integration.

The purpose of this meeting is to review and discuss all aspects of these emerging technologies ranging from theory through applications including aircraft, missiles, space vehicles and unmanned vehicles.

* * * * *

Des progrès nombreux et importants en matière de théorie de contrôle optimal, de techniques de synthèse et de méthodes conceptuelles ont été réalisés depuis le dernier symposium consacré à ce domaine en 1973.

L'évolution rapide des technologies dans le domaine du calcul, des systèmes de diffusion de données, des études automatisées et des bases de données permet désormais l'application de théories et de méthodes de synthèses jusqu'ici irréalisables.

L'importance croissante donnée aux capacités fonctionnelles et opérationnelles à coût réduit conduit à l'application de technologies et de méthodes permettant un partage plus poussé dans l'utilisation de l'information et des niveaux d'intégration plus élevés.

Cette réunion se propose de passer en revue et d'examiner tous les aspects des technologies qui se font jour actuellement et qui vont du domaine de la théorie à celui de l'application en ce qui concerne les avions, les missiles, les véhicules spatiaux et les véhicules non pilotés.

AGARD GUIDANCE AND CONTROL PANEL OFFICERS

Panel Chairman:	Mr R.S.Vaughn, US
Panel Deputy Chairman:	Dr R.C.Onken, GE
Panel Executive:	Mr B.M.Heliot

PROGRAMME COMMITTEE FOR THE 35th GCP SYMPOSIUM

Programme Chairman:	Mr M.A.Ostgaard, US
Members:	IPA O.Rossignol, FR Dr Ing. R.C.Onken, GE Ir. P.Kant, NE Eng A.Alves Vieira, PO Mr G.C.Howell, UK

HOST COORDINATOR

Eng A.Alves Vieira

CONTENTS

* Issued in classified publication CP-321 (Supplement)

† To appear as a separate AGARD publication

* Issued in classified publication CP-321 (Supplement)

PROGRESS AND PITFALLS IN ADVANCED FLIGHT CONTROL SYSTEMS

Duane McRuer
President and Technical Director

Systems Technology, Inc.
13766 S. Hawthorne Blvd.
Hawthorne, CA 90250

SUMMARY

The conjunction of multiple-fail-operational fly-by-wire flight control and high-performance new aircraft technology has been, in the main, a favorable one. Major weight and volume reductions and performance enhancements have been achieved by automatic and manual flight control system (FCS) integration, and the basic airframe can now truly be optimized for performance properties such as low drag, maximum maneuverability, low observables, etc., without considering some of the traditional penalties imposed by stability and control requirements. Instead, the new flight control technology can redress stability and control imbalances and even provide flying quality characteristics that border on the absolute optimum.

This new technology is not an unmixed blessing. Greater FCS complexity and cost are obvious disadvantages, but other unfavorable effects are more subtle, being of the nature of side effects which accompany the favorable major effects. Three of these are discussed and illustrated with examples in this paper.

The first is associated with the flight control and flying qualities of unstable relaxed static stability aircraft. In solving the control problem an "equivalent vehicle" is created in which the key dynamic properties comprise a mix of FCS and airframe parameters. Unfortunately, the equivalent vehicle dynamics may no longer correspond to those of conventional aircraft. Instead, they are different in kind as well as degree. There are very few flying quality data that are appropriate for such systems and, not surprisingly, existing criteria are difficult or impossible to apply directly. Such data as do exist are summarized and implications for possible criteria developed.

The second issue is the accumulation of lags and delays resulting when stick and flexible mode suppression filters, high-frequency actuation dynamics, computational delays, etc., are combined. These give rise to a net effective time lag or delay in the vehicle dynamics as seen by the pilot which, if excessive, can cause serious piloting problems.

The third example focuses on some of the peculiarities associated with sampled, as contrasted with continuous, control.

INTRODUCTION

A great deal of attention has recently been given to the technological ways and means of improving aircraft energy efficiency and various aspects of aircraft performance. A leading approach has been the development of new control concepts which can be used in conjunction with aircraft configuration tailoring to achieve the features desired. The key to success has been the reduction to operational practice of multiple-redundant, fly-by-wire (or light), fail-operational flight control systems.

The practical acceptance of fail-operational FCS was an enormous step forward. This has become commonplace for relatively short-time tasks, such as autoland (e.g., Ref. 1 notes that by 1980 the Trident had made more than 50,000 in-service automatic landings). Then, the further progress of technology for multiple-redundant fail-operational systems and experience in many operational aircraft have been accompanied by major expansions in the activities which can be accomplished by flight control. These include a cornucopia of functions intended to permit extensions in performance envelopes — longitudinal and lateral stability enhancement, span load modification, elastic mode suppression, ride smoothing, flutter prevention, envelope limiting/stretching, etc. These have been studied, and to some extent applied, over the last decade and are grouped under the general heading of active control technology (Refs. 1-8). Military and space applications have led the way, although the National Aeronautics and Space Administration and the transport aircraft manufacturers have devoted considerable effort to commercial transport applications, primarily in an attempt to reduce direct operating costs via fuel savings (e.g., Refs. 9-11).

In its most modern manifestations, as exemplified by the Space Shuttle and new fighters entering the inventory, multiple fail-operational fly-by-wire flight control technology provides both for major weight and volume reductions and performance enhancements in the primary flight control system elements and for optimization of the basic airframe. The airframe performance optimization can include a wide variety of properties such as drag reduction, L/D improvement, maximum usable maneuverability, low observabilities, longer fatigue life, etc. The new control technology permits this to be accomplished without some of the constraints and traditional penalties imposed by stability and control or flying quality requirements. Indeed, the new flight control technology can redress stability and control imbalances which earlier would have been considered to be excessive, while at the same time provide flying quality characteristics which border on an absolute optimum — if only someone could define what that is! Because the systems are of very high integrity and are typically arranged to be multiple fail-operative, essentially any imaginable aircraft-alone stability deficiency can be corrected as long as sufficient control power is available.

In some respects, however, this wonderful new technological marriage is not an unmixed blessing. The obvious handmaidens associated with greater complexity and cost are well known in kind if not fully appreciated in degree. Other unfavorable aspects are more subtle, being of the nature of side effects

which accompany the favorable major effects. Three of these are discussed and illustrated in this paper. They are:

Flight Control/Aircraft System Dynamics and Flying Qualities

Accumulation of Lags and Delays

Digital System Peculiarities

FLIGHT CONTROL/AIRCRAFT SYSTEM DYNAMICS AND FLYING QUALITIES

Many of the aircraft performance and energy efficiency benefits available in advanced aircraft are gained at the expense of reduced aircraft-alone stability. While each configuration has its own special considerations, typically the optimized aircraft-alone longitudinal dynamics will be statically unstable in some parts of the flight regime. To correct the stability deficiencies a number of feedback system architectures are possible, although all share certain properties. In the discussion below a particularly simple system is selected as a representative example. The characteristics of the aircraft/augmentation system are developed, idealized as a "superaugmented" aircraft, and then contrasted with the characteristics of a conventional statically stable aircraft. This comparison will show that a properly designed augmentor can result in attitude response characteristics which are identical in form to those of the conventional aircraft short period mode. But, the parameters which govern the conventional and superaugmented responses are entirely different in their origin and may be significantly different in their quantitative values. Fundamentally this is due to the displacement of aircraft stability and control parameters by some equally fundamental control system parameters as the dominant entities in the responses.

For normally augmented statically stable airplanes the effective aircraft characteristics may still be close enough to conventional for one to stretch existing flying quality criteria using such concepts as "equivalent systems." For superaugmented aircraft, on the other hand, such extensions may not be possible or pertinent. This brings new flying qualities considerations, and hence new FCS specification possibilities, to the fore.

To provide a context for comparing some of the conventional/superaugmentation differences, attention is focused on high workload pilot/aircraft control operations as the central flying qualities issue. With this orientation precision path control is put forth as the key control task to explore.

The exploration starts with a summary of the fundamental flying quality differences between superaugmented and conventional aircraft, within the path control context. These differences are then examined for their consequences viewed in the light of existing data. Exemplary sets of response boundaries for relaxed static stability (RSS) aircraft are used as "strawmen" backdrops for comparing pertinent conventional and superaugmented system data. The comparisons made show that superaugmented aircraft are fundamentally different, and that new FCS criteria and flying quality data are needed. Finally, some partial and tentative suggestions for FCS specification are advanced as interim measures.

An Exemplary FCS to Correct RSS Aircraft Stability Deficiencies

Relaxed static stability (near neutral or unstable static margins) is perhaps the most ubiquitous feature of advanced aircraft which are optimized as composite flight control/airframe systems. To correct the consequent reduced short-period damping and low undamped natural frequency or short-period divergence, and, at the same time, significantly improve the aircraft flying qualities and reduce pilot workload, a variety of full-authority FCS systems can be constructed. The system finally selected for a particular application will depend on many considerations and tradeoffs. Problems of instrumentation and sensing, including biases and sensor excitation by disturbances, control system compensation needed for flight condition changes, etc., must enter into comparative consideration of practical systems. The transition from one flight phase to another, the effective dynamics presented to the pilot, and the response of the augmented aircraft to external disturbances are also affected by the particular feedbacks chosen and must be considered in fundamental comparisons of candidate systems. These features and the consequences on effective aircraft dynamics of many candidate feedback control possibilities are treated in detail in, for example, Ref. 12.

To permit the development of some flying quality issues a typical example of an FCS suitable for RSS aircraft is posed here. The issues drawn will, of course, pertain explicitly only to the example system, although some can be generalized for other system possibilities. The flight control system selected is shown in Fig. 1. This system performs six functions, as follows:

- Creates a high degree of effective static stability for the augmented aircraft.
- Improves the damping of the effective short-period mode.
- Eliminates the phugoid as a long period, lowly damped oscillation.
- Provides a pitch rate command/attitude hold platform for piloted control.
- Regulates against external disturbances, with emphasis on pitch attitude maintenance rather than weathercocking.
- Provides automatic up-elevator compensation for turning flight.

As a flight-critical system, all the system elements except possibly those involved in turn compensation would be multiply redundant. This is one reason for basing the system on pitch rate sensors which are simple, hardy, relatively insensitive to bias errors, and easily made part of a minimum complexity multiple-redundant system. With skewed sensors, for instance, six rate gyros oriented so that their

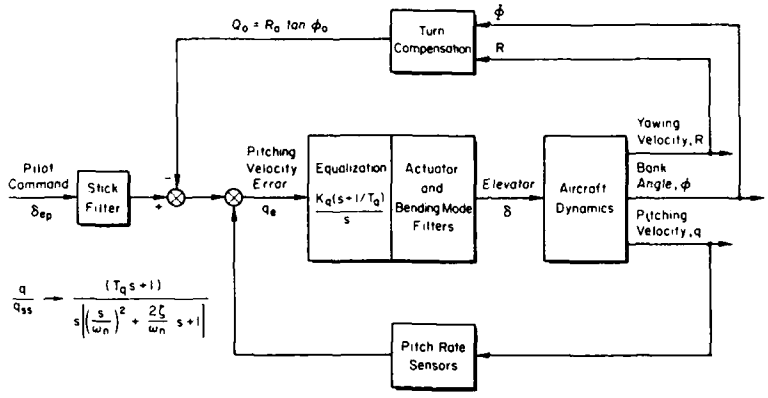

Figure 1. Typical Pitch SAS for Highly Augmented Aircraft

input axes are perpendicular to the faces of a dodecahedron can provide dual fail-operate capability for rates in all three axes.

The basic low-frequency control law for the Fig. 1 FCS, which drives the elevator servo with a signal proportional to pitch rate error, q_e, and the integral of pitch rate error, q_e/s, is simply:

$$\delta = K_q q_e + \frac{K_q/T_q}{s} q_e \tag{1}$$

Consequently, the augmentor as a stabilizer creates a pitching moment proportional to $\int q\,dt$ and one proportional to q. The first term creates an effective derivative $M_{\int q}$ (akin to M_θ) which corrects for the static instability, damps the phugoid, etc., while the second term augments the pitch damping derivative, M_q. When the aircraft-alone dynamics include a divergence, the aircraft/FCS combination will be a conditionally stable system. That is, a minimum gain, K_q, is needed to rid the system of any divergence due to the aircraft-alone static instability. At the other extreme, the maximum gain possible is set by the closed-loop system stability limits. If the aircraft is considered only as a rigid body, these limits will depend primarily on the high-frequency lags due to the actuator, rate sensor, and other computational or filter dynamics within the closed-loop system. When aircraft flexible mode properties are also included, they too will also affect the closed-loop system stability and maximum gain. For the moment all the higher frequency lags will be neglected.

When the saturation characteristics of the aircraft control surface (and surface rates) are taken into account, the maximum gain may be further restricted. The higher the open-loop gain, K_q, of the augmentor, the smaller the pitching velocity error needed to saturate the control. The pilot command input can be deliberately limited to avoid saturating the controls, but external disturbances cannot. Indeed, the possibility of control saturation due to shears and other atmospheric disturbances is one reason for the selection of the Fig. 1 system. Some competing stabilization possibilities result in systems which are not as tolerant to external disturbances and which, therefore, cause significantly higher probabilities of limiting elevator positions.

Although this particular exemplary system has many advantages and has been used on a number of aircraft (e.g., the Space Shuttle Orbiter and some modern fighters), it has its own peculiarities. For instance, the presence of the forward loop integrator, while needed for either a pitch rate or normal acceleration system to accomplish the static stability function, can be troublesome in some flight phases involving transient changes in trim conditions (e.g., takeoff) if not properly accounted for by using appropriate synchronizers or flight-phase-tailored functional modes. On the other hand, this system is the simplest one available which accomplishes the functions listed above. It was actually selected for an example, however, because it serves as an excellent paradigm and point of departure for developing the types of flying qualities issues involved in heavily augmented RSS aircraft.

The changes in the linear dynamics of an unstable aircraft due to the control system will be illustrated below using a system survey of the closed-loop system. This survey, given in Fig. 2, consists of a number of complementary root locus and frequency response plots. The aircraft dynamics considered are those of a generic RSS transport, with numerical values which represent a cruise condition with a 5 percent negative static margin (Ref. 13).

Figure 2a is a conventional s-plane root locus which shows the closed-loop roots of the system as control system gain, K_q, is increased. The starting points are the poles of the airplane located at $-1/T_{sp_2}$ (located in the right half of the s-plane, indicating its character as a divergence), $-1/T_{sp_1}$ (on the real axis in the left half plane), and the phugoid $[\zeta_p, \omega_p]$ (a lightly damped complex pair near the origin). The control system also has a pole at s = 0 due to the integrator. This is not shown on the plots because it exactly cancels a free s in the numerator of the airplane pitch rate due to elevator deflection, q/δ, transfer function. As the controller gain, K_q, is increased, the corrective moments applied to the airplane by the elevator modify the poles of the closed-loop system. Some of these at very high gain approach the zeros of the open-loop system. There are three open-loop zeros in the Fig. 1

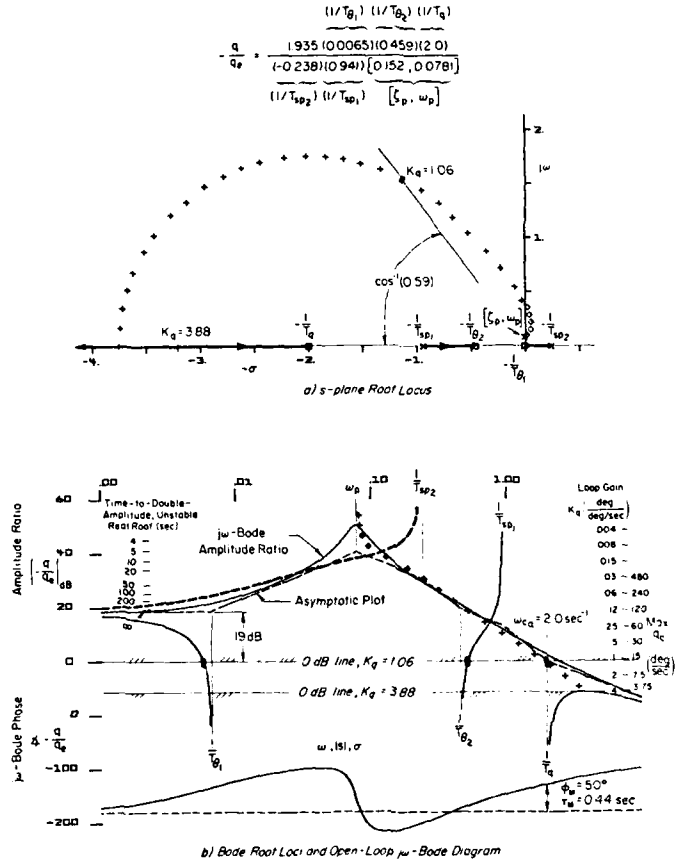

Figure 2. System Survey for Example RSS Aircraft/Augmentation System Dynamics (Cruise, Static Margin = -5% c̄; q, ∫q dt + δ Closure, $1/T_q$ = 2.0, Ref. 13)

augmentor. Two are airplane characteristics, located at $-1/T_{\theta_1}$, in the left half plane but very near the origin, and at $-1/T_{\theta_2}$, well out the real axis in the left half plane. The control system lead time constant, T_q, is shown in Fig. 2a as the zero at $-1/T_q$.

The perambulations of the closed-loop roots as controller gain varies, while nicely depicted on the s-plane root locus, can also be shown with controller gain and associated quantities as an ordinate, rather than as a parameter along the plot. This is accomplished with the so-called Bode root locus. It uses semi-log presentations for conventional open-loop system frequency response (jω-Bode plot of amplitude ratio and phase) and Bode root locus constructions (root loci with Bode format), wherein gain is an independent variable on the plot. Figure 2 presents these diagrams. The ordinate is an amplitude ratio plot of the open-loop transfer function expressed in decibels, while the abscissa is a logarithmic scale of several general "frequencies." When the plot is a conventional Bode frequency response plot, the "frequency" is a real one, ω in rad/sec. Complex components of the root locus use undamped natural frequencies, $|s|$ or ω_n, in rad/sec. Finally, real roots are also shown here as σ, with units of 1/sec. Thus, interpretation of the abscissa depends on the particular curve, and is either ω, $|s|$, or σ.

The conventional jω Bode diagram consists of separate amplitude ratio and phase plots for the total open-loop transfer function with $s = j\omega$. The jω amplitude ratio, and its asymptotes, and phase angles are shown in Fig. 2. The breakpoints on the asymptotic plot apply to all the Bode plot forms and occur at values of "frequency" equal to magnitudes of the open-loop poles and zeros.

Following the loci of Fig. 2a, b as gain is increased the various airplane modes are modified as follows:

1) The airplane short-period divergence, $1/T_{sp_2}$, is decreased as gain, K_q, is increased; becomes stabilized as it passes through the jω-axis; and finally terminates on the airplane zero at $-1/T_{\theta_1}$ as gain approaches infinity.

2) The short-period subsidence, with time constant T_{sp_1}, proceeds along the real axis to the right toward $-1/T_{\theta_2}$. Part of the damping given up by this subsidence is transferred as an increase in damping to the divergence.

3) The phugoid, which for the airplane-alone is stable but lightly damped ($\zeta_p = 0.152$), is initially driven toward instability as the augmentor gain is increased. For controller gains $0.004 < K_q < 0.06$ deg/deg/sec the closed-loop phugoid is unstable. This is the portion of the locus depicted with ◇◇◇. For gains greater than this the phugoid is stable and the nearly circular arc of Fig. 2a corresponds to the nearly constant slope of 40 dB/decade on the Bode root locus in Fig. 2b. This arc is nearly centered on the control system at $-1/T_q$. Also, the radius of the nearly circular segment is approximately $|1/T_q|$. As gain is increased further, the undamped natural frequency, damping, and damping ratio of this quadratic mode increases until ultimately $\zeta_p' = 1^*$ when the arc hits the real axis. The undamped natural frequency of this critically damped mode is just slightly less than $2/T_q$. The real axis is encountered for a gain of approximately $K_q = 3.88$, after which the complex roots divide into two real roots. One, as is shown on both the Fig. 2 plots, goes into the $1/T_q$ control system lead, while the other progresses indefinitely out the high-frequency asymptote.

The system with $K_q = 1.06$ reflects several different good control system design, response, and stability considerations. These include:

- Responses which are similar to those of low-order, well-damped, rapidly responding systems. This implies that the low-frequency open-loop poles are, in their closed-loop manifestations, driven nearly into open-loop zeros, such that they nearly cancel. Examples on Fig. 2 for the $K_q = 1.06$ reference 0 dB line are the close proximity of the lead at $1/T_{\theta_1}$ with the closed-loop pole, shown as ■, stemming from the divergence, and a similar proximity of the lead at $1/T_{\theta_2}$ to the pole arising from the short-period subsidence. It also implies a well-damped dominant mode, as given by the quadratic $[\zeta_p', \omega_p'] = [0.59, 1.92]$.

- Insensitivity of the response to gain changes. This is illustrated by the nearly vertical slopes of the loci in Fig. 2b as they drive into $1/T_{\theta_1}$ and $1/T_{\theta_2}$ around the reference crossover region. Because the slopes are so steep small changes in gain, or for that matter small changes in the open-loop aerodynamics which change $1/T_{\theta_1}$ and $1/T_{\theta_2}$, will not materially affect the near cancellation of these closed-loop leads and lags. Thus, such shifts will hardly effect any changes in the response.

- System stability with large stability margins. In the present example of the conditionally stable system, a margin of 19 dB exists on the low-gain end relative to the reference $K_q = 1.06$. Thus, nearly a factor of 10 in gain reduction would be needed to get back to the divergence. At the high-frequency end, the crossover of $\omega_c = 2$ rad/sec (which incidentally sets the desired controller gain at $K_q = 1.06$) is consistent with a phase margin, ϕ_M, of 50 deg and a delay margin, τ_M, of 0.44 sec. Thus, high frequency lags or parameter uncertainties currently ignored in the design would have to contribute 50 deg of phase lag, or the equivalent of a pure time delay of 0.44 sec, before the closed-loop system would be neutrally stable at the gain selected.

- Well damped and rapidly responding closed-loop system dominant mode(s) to resist and thereby reduce the effects of disturbances. In the present example the dominant mode is the oscillation stemming from the phugoid which, for the nominal controller gain, has a damping ratio of 0.59 and an undamped natural frequency of 1.92 rad/sec. This mode is therefore both stiff and well damped.

- Closed-loop system bandwidth which is sufficiently large that the augmented airplane is responsive to pilot command without requiring pilot anticipation or compensation for precision control. In the present case the system as seen by the pilot is rate-command with a bandwidth near the crossover frequency of 2 rad/sec.

- The control system gain should be low enough so that the augmentor is very seldom saturated. Saturation may be viewed as reducing the gain and thus progressing from the nominal 0 dB line closed-loop roots back toward those of the open-loop aircraft. When completely saturated, the effective controller gain approaches zero and the effective aircraft dynamics are those of the airplane alone. Unfortunately, in this event the pilot also has no control available in one direction, since the surfaces are saturated. These kinds of considerations are easy to show on the plot of Fig. 2 as commanded pitching velocities which would just saturate the system when gains are set at particular levels. Scales showing the maximum pitching velocity commandable without saturation, $q_{c\,max}$, is given on the right side of the Bode root locus plot next to that for the controller gain, K_q, in linear units. Another useful scale for partial saturation and other low-gain operations is given on the far left side. This shows the time to double amplitude of the divergent root at the several gain levels (in essence this is a cross-plot of the locus from $1/T_{sp_2}$ toward the $1/T_{\theta_1}$ lead). For instance, a divergence with 6 sec time to double amplitude corresponds to a gain K_q of 0.010 deg/deg/sec. This is an enormous reduction in effective loop gain (factor of 388) in terms of saturation or other gain reduction phenomena, showing that the system is quite robust at the nominal value of $K_q = 1.06$.

The description above, even though of a summary overview character, may appear tedious. The net effect, however, of a well-tempered design is straightforward. It is that the closed-loop pitching velocity response to a step input will have the approximate form:

---

*The prime on ζ_p' indicates it is a closed-loop damping ratio of a quadratic mode which started, at zero gain, from the phugoid ζ_p, ω_p.

$$\frac{q}{q_{ss}} \doteq \frac{(T_q s + 1)}{s\left[(s/\omega_n)^2 + (2\zeta/\omega_n)s + 1\right]} \qquad (2)$$

The ζ and ω_n in the denominator are those of the closed-loop oscillatory mode which progressed from the phugoid, while the lead time constant, T_q, is the controller lead. The approximation takes advantage of the fact that the short-period subsidence and divergence are both modified by the effects of feedback control and, for favored gains, do not even appear in the pitching velocity response since they are nearly cancelled by the airplane leads at $1/T_{\theta_1}$ and $1/T_{\theta_2}$. Feedback control has thus provided us with a low-order effective system as far as pitch attitude response to pilot inputs is concerned. It is in fact identical in form to that of the short period of a statically stable conventional airplane. This is especially apparent in the time response for the total system shown in Fig. 3a. There the characteristic initial ramp-like, nearly constant pitch acceleration rise with the overshoot and subsequent return looks very similar to the exemplary time response of Fig. 3b for a conventional aircraft with a large static margin.

There is an important difference between the time responses of Figs. 3a and 3b in that the closed-loop system response for Fig. 3a is that for all time rather than just the first few seconds. For the conventional aircraft the Fig. 3b response will be succeeded by the phugoid long period oscillation.

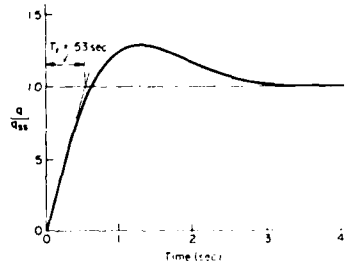

a) Augmented Aircraft Attitude Dynamics in Cruise Flight

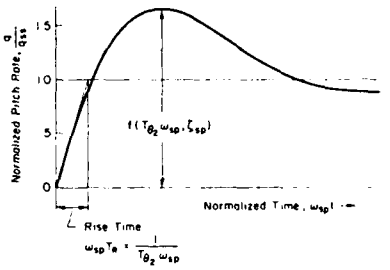

General Form

$$\frac{q}{q_{ss}} = \frac{(T_{\theta_2}s + 1)}{s\left[\left(\frac{s}{\omega_{sp}}\right)^2 + \frac{2\zeta_{sp}}{\omega_{sp}}s + 1\right]}$$

b) Short-Period Attitude Dynamics for a Conventional Aircraft With Large Static Stability

Figure 3. Pitch Rate Response for Step Control Surface Input

In Fig. 3 the pitching velocity, q, for a step elevator is given in normalized form, scaled by the steady-state pitching velocity, q_{ss}. The time scale in Fig. 3b is non-dimensionalized using $\omega_{sp}t$ as the time variable. Notice that the non-dimensionalized rise time, $\omega_{sp}T_R$, depends only on the product of the lead time constant, T_{θ_2}, and the short-period undamped natural frequency, ω_{sp}. Interestingly enough, the peak overshoot also depends only on this product and the damping ratio, ζ_{sp}. Figure 4a (Ref. 14) shows this overshoot as a function of the $T_{\theta_2}\omega_{sp}$ product, with ζ_{sp} as a parameter. Because of the $(T_{\theta_2}s + 1)$ lead in q/q_{ss}, there is an overshoot even when the damping ratio is critical ($\zeta_{sp} = 1$). For nominal well-damped cases, the overshoot depends as much on the separation between $1/T_{\theta_2}$ and ω_{sp} as it does on ζ_{sp}. $1/T_{\theta_2}$, being dependent on the lift curve slope, C_{L_α}, as scaled by speed and density, is an aircraft parameter set mainly by wing configuration, whereas ω_{sp} can be adjusted by shifting the aircraft's balance, i.e., the c.g. location. The more forward the c.g., the greater the weathercock stability, and the stiffer the short period mode; hence, from Fig. 4a, the greater the overshoot (for a given $1/T_{\theta_2}$ and ζ_{sp}). Similarly, the rise time decreases as the short-period undamped natural frequency is increased. Rise time is given approximately by:

$$T_R \doteq \frac{1}{T_{\theta_2}\omega_{sp}^2} \doteq \frac{Z_w}{M_\alpha} \qquad (3)$$

Lift curve slope and rise time thus vary together, as does the peak overshoot for a fixed ω_{sp}.

In the exemplary case study for the highly augmented RSS aircraft, pitch attitude response lead, T_q, came from the augmentor lead rather than from the airplane T_{θ_2}. In fact, the airplane pitch attitude lead, T_{θ_2}, is not even present in the pitch rate response, since it was essentially canceled by the closed-loop subsidence originating at $1/T_{sp_1}$. Also, the undamped natural frequency and damping, while superficially similar to the short period, depend instead primarily upon the control system lead time constant, T_q (which set the circular arc along which the ζ_p', ω_p' closed-loop roots proceeded), and the total open loop gain, K_qM_δ, which located ζ_p', ω_p' at a given spot along this arc. These parameters are associated predominantly with the highest frequency and next highest frequency asymptotes of the Fig. 2b Bode diagram. Using just these two high frequency asymptotes as an approximation for the total system, it is easy to show that the approximate values of ω_n and ζ are given by:

$$\omega_n^2 = \frac{K_qM_\delta}{T_q} = \frac{\omega_{ca}}{T_q} \qquad (4)$$

and

$$\zeta = \frac{1}{2}\sqrt{K_qT_qM_\delta} = \frac{1}{2}\sqrt{T_q\omega_{ca}} \qquad (5)$$

Also, the approximate normalized rise time is

$$\omega_nT_R = \frac{1}{T_q\omega_n} = \frac{1}{\sqrt{T_q\omega_{ca}}} \qquad (6)$$

Here the quantity $\omega_{c_a} = K_q M_\delta$ is the crossover frequency of the 0 dB line with the high-frequency asymptote. The subscript "a" distinguishes it from the crossover frequency ω_c, which is based on the value where the open-loop $j\omega$-Bode amplitude ratio crosses the 0 dB line.

The limiting case heavily augmented RSS aircraft in which the airplane pitch attitude lead T_{θ_2} no longer appears in the effective augmented aircraft pitch dynamics is referred to here as "superaugmented". The superaugmented distinction is made to highlight that superaugmented aircraft have attitude characteristics which depend primarily on the crossover frequency, $\omega_{c_a} = K_q M_\delta$, and the controller lead T_q, and that these characteristics may differ in kind from those of even fairly heavily augmented conventional craft. In this sense, superaugmented aircraft are an idealization which may not always be approached by heavily augmented aircraft. On the other hand, the Space Shuttle is an ideal example of a superaugmented aircraft, for $1/T_{\theta_2}$ is completely suppressed in its pitch attitude response and is replaced by a control system lead. Supersugmentation is a useful concept because it is sufficiently idealized to simplify the drawing of issues and understanding, while not so far removed from reality as to make the considerations academic.

By way of comparison of the key pitch attitude response parameters, Table 1 summarizes the attitude lead and quadratic mode characteristics of q/q_{ss} for a conventional aircraft short period and for an idealized superaugmented aircraft.

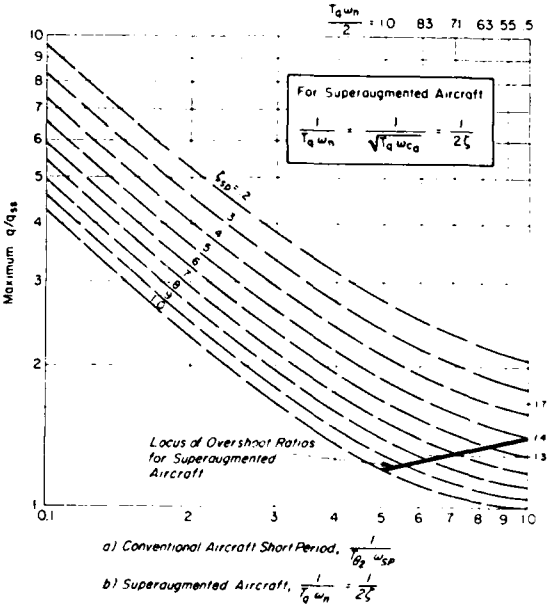

Figure 4. Maximum Pitch Rate Overshoot Variation

TABLE 1. COMPARISON OF PITCH ATTITUDE RESPONSE GOVERNING PARAMETERS FOR CONVENTIONAL AND SUPERAUGMENTED AIRCRAFT

DYNAMIC PROPERTY	CONVENTIONAL		SUPERAUGMENTED	
	PARAMETERS	PRIMARY DESIGN FACTORS	PARAMETERS	PRIMARY DESIGN FACTORS
Lead Time Constant T	$\frac{1}{T_{\theta_2}} \approx -Z_w + \frac{Z_\delta}{M_\delta} M_w$	Set Predominantly by Airframe: C_{L_α}; wing; Maneuver Margin; $C_{M_{CL}}$; Tail	T_q	Governed predominantly by closed-loop control system Stability, Response, and Margins **Control System Parameters** T_q - Lead time constant K_q - Gain **Airframe Parameter** M_δ - Surface effectiveness (C_{m_δ})
Undamped Natural Frequency ω_n	$\omega_{sp}^2 = Z_w M_q - M_\alpha$		$\omega_n^2 = \frac{\omega_{c_a}}{T_q} = \frac{K_q}{T_q}[M_\delta]$	
Normalized Rise Time $\omega_n T_r$ Rise Time T_r	$\frac{1}{T_{\theta_2} \omega_{sp}}$		$\frac{1}{T_q \omega_n} = \sqrt{\frac{T_q}{\omega_{c_a}}} = \sqrt{\frac{T_q}{K_q[M_\delta]}}$	
Damping Ratio ζ	$(\zeta\omega)_{sp} = -(Z_w + M_q + M_{\dot{\alpha}})$	C_{L_α}; Wing C_{m_q}; Tail Pitch Damper	$\zeta = \frac{\sqrt{T_q \omega_{c_a}}}{2} = \frac{1}{2}\sqrt{K_q T_q [M_\delta]}$	
Delay Time τ_d		Actuator and Manual Control lags		Actuator lag + Stick filters + Bending Mode filters + Computational delays

For the conventional airplane, covered at the left, the table reiterates that the attitude lead and short-period undamped natural frequency, and hence the rise time, depend primarily on aircraft configuration characteristics and the way the aircraft is balanced. The damping ratio also is predominantly a function of configuration, although a pitch damper can provide a good deal of design latitude.

For the superaugmented aircraft, the discussion of the example emphasized the relative lack of sensitivity to aircraft configuration characteristics and the relative importance of the controller properties as they affect the closed-loop aircraft/augmenter system. The primary design factors described there were considerations of a closed-loop character, including the system stability, response, bandwidth, stability margins, etc. The most important composite factor underlying the dynamics of the superaugmented vehicle is the crossover frequency (of the asymptote), ω_{ca}. This quantity is an indication of:

- The total system gain comprising both controller (K_q) and aircraft control effectiveness (M_δ) parameters.
- The system bandwidth, which indicates the frequency range of good command following and disturbance suppression.
- The rapidity of system response, i.e., rise time $T_R = 1/\omega_{ca}$.
- The system damping ratio, in that ω_{ca} is a key factor (together with the controller lead time constant, T_q) in setting the damping ratio, ζ.

The first three properties of the crossover frequency listed above are qualitatively applicable to all feedback control systems which have a low-pass closed-loop character. The fourth property is a special one for superaugmented systems which share the specific characteristics of the example case. It is one reflection of the idealized superaugmented situation wherein only two parameters, the attitude lead (T_q) and crossover frequency (ω_{ca}), define all the system input/output characteristics except the overall response scaling between output and input.

Another manifestation of the two-parameter character of the idealized superaugmented aircraft can be seen in connection with the maximum pitch rate overshoot. The superaugmented version of Fig. 4 is shown in Fig. 4b. The possible variation in damping ratio, overshoot, and normalized rise time is encompassed by the straight line superimposed on the background plot. Notice that for a normalized rise time of 1, the damping ratio is 0.5 and the undamped natural frequency is $1/T_q$. At the other end is a normalized rise time of 0.5, accompanied by a $\zeta = 1$ and an $\omega_n = 2/T_q$. Any system between these two extremes has excellent closed-loop control, system stability, and margins. Again the parameters which set the actual location on the attainable line are the crossover frequency, ω_{c_a}, and the control system lead time constant, T_q.

A major distinction can also be made between the superaugmented and conventional aircraft with reference to the aerodynamic characteristics which underlie their responses. For the conventional aircraft, even in the short period, the stability derivatives Z_w, M_q, and $M_{\dot{\alpha}}$ together with their variations with flight condition, are major governing parameters. When the complete three-degree-of-freedom airplane characteristics are also taken into account, several more derivatives become important (e.g., Z_u, M_u, X_w, etc.). In contrast, to the extent that the system can be made to approach the superaugmented characteristics, the aerodynamic parameters of importance reduce to the surface effectiveness, M_δ.

Precision Path Control

Those aircraft control functions which demand the greatest pilot attention and skill require primary consideration in flying qualities assessments. Probably the most demanding high workload pilot/aircraft closed-loop control operations involve precision path control in unfavorable environmental conditions. All flight phases require some form of path control, which incorporates both flight path changes and flight path maintenance or regulation. In most ordinary flight circumstances path control, while an essential pilot skill, is nonetheless a relatively benign and low-stress function. On the other hand, when the path task is itself very demanding and the environment unfavorable (e.g., low visibility approach and landing in turbulence and shear), the precision path control task becomes exceedingly exacting. Thus <u>precision path control</u> is used here as the control task to explore the effects of heavy augmentation on closed-loop pilot/aircraft system flying qualities.

A block diagram that indicates the pilot's activities in precision path control is shown in Fig. 5. On the right the augmented aircraft has path deviation and pitch attitude as the output variables stemming from aircraft dynamics which are forced by external atmospheric disturbances and the pilot control output, δ. The augmented aircraft itself is a closed-loop system comprising the airplane-alone and augmentation system. Thus, the sensors, computation, and actuation elements involved in the feedback control augmentation system, as well as the aircraft alone, are encompassed by the "Augmented Aircraft Pitch Dynamics" block in Fig. 5. (An underlying assumption in this diagram is that other aircraft control effectors such as throttle or flap are not being continuously modulated by pilot control action; trim management using these aircraft effectors, however, is not excluded.)

Even though trimmed precisely, the augmented aircraft will not by itself maintain exactly the prescribed path and attitude in the presence of disturbances. Consequently, the pilot must exert control not only to establish the desired path but also to correct any deviations from the desired attitude and path. This is accomplished by the pilot acting as a closed-loop controller, which means simply that the pilot's control output is dependent on (i.e., a function of) path deviation and attitude. Thus, a component of the pilot's control output is correlated with an attitude error, and another component is correlated with the difference between the desired and actual path. This relationship is depicted in the Fig. 5 block diagram as a "series" pilot closure, i.e., the pilot's action on path deviation acts in series with, and provides an internal "attitude command" for, the pilot's action on attitude error. These pilot activities are represented in Fig. 5 by the symbolic transfer characteristics Y_{p_h} and Y_{p_θ}. Several research studies using elaborate and detailed measurements of just this situation (e.g., Refs. 15 and 16) indicate that this series structure and general pilot behavior control model is appropriate for

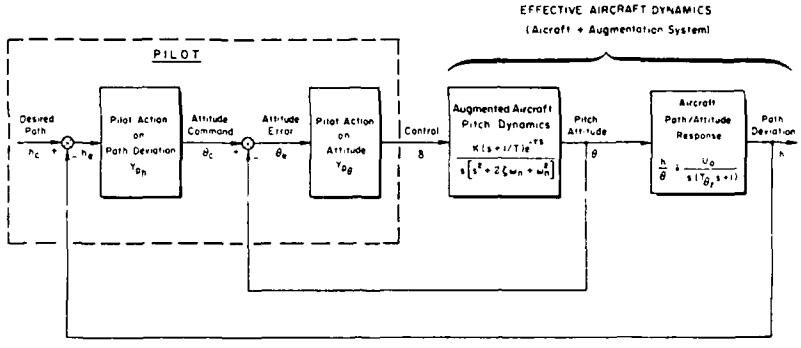

Figure 5. Closed-Loop Precision Path Control with Attitude Control Inner Loop

path control situations. In essence, the pilot's higher-frequency control actions are devoted primarily to attitude so that the "inner" attitude loop is tightly closed, and the attitude is well regulated. This tight inner loop makes possible the effective closure of the "outer" path deviation loop without excessive pilot equalization or compensation. Without good control of attitude the pilot would have to be way ahead of any path changing trends, requiring very difficult anticipation and high workload. (Examples include altitude control using only airspeed and altimeter or control during approach using only airspeed and the raw ILS glidepath data.) If the attitude loop is difficult for the pilot to interact with and close (i.e., if the augmented aircraft pitch attitude dynamics are deficient in that they require excessive pilot compensation and attentional workload), attitude control will suffer directly and path control indirectly.

It will evolve below that a key issue in the differences between the flying qualities of conventionally augmented aircraft and superaugmented aircraft resides in the differences in the transfer characteristics for the augmented pitch attitude and the similarities for the path/attitude response. By focusing on these facets we can expose the major differences between heavy and conventional augmentation without an elaborate argument involving the pilot's detailed control actions. It is extremely important to recognize, however, that the closed-loop piloting aspects are a central issue in that the pilot's assessment of the suitability of the aircraft inherently depends upon his actions required to accomplish control. (As an adaptive controller the pilot adjusts his control actions as needed to compensate for the aircraft dynamics; so different aircraft dynamics mean different pilot actions and different pilot assessments.) Thus, the feedback loop structure and what the pilot actions are on path deviation and attitude are of central concern to set the context of the control task. Yet, within this context, one can focus primarily on the augmented aircraft pitch dynamics and the aircraft path/attitude response to explore differences between conventional and highly-augmented aircraft.

The aircraft blocks in Fig. 5 show the transfer characteristics in fairly general form for the pitch attitude dynamics and for the path/attitude response dynamics. The time constant T_{θ_2} is often referred to as the path/attitude "lag" time constant. This stems from its appearance in the denominator of h/θ. For a step pitch attitude change, the flight path angle, γ, or the rate of change of path deviation, $\dot{h}$, will respond exponentially, with the time lag T_{θ_2}. Because $1/T_{\theta_2} \doteq -Z_w$, which in turn is proportional to the lift curve slope of the airplane, C_{L_α}, this path-to-attitude time lag is a direct function of the fundamental performance characteristics of the airplane. Once the wing is designed (and C_{L_α} set by a given wing configuration), T_{θ_2} for a given flight condition cannot be changed without direct-lift control. As a flight path lag T_{θ_2} is an extremely important factor in the attainable path precision as it limits the pilot's outer loop control bandwidth even if the pitch attitude dynamics are perfect. This lag and, accordingly, the aircraft path/attitude response block in Fig. 5 is the same for both conventional and superaugmented aircraft.

Marked differences occur in the Augmented Aircraft Pitch Dynamics block. For conventional airplanes, the lead time constant, T, in Fig. 5 is T_{θ_2}. Thus the attitude lead and the path lag are the same quantity, fixed by the same aircraft configuration feature (the lift curve slope). The undamped natural frequency and damping ratio of the augmented aircraft pitch dynamics are, in this case, $\zeta = \zeta_{sp}$ and $\omega_n = \omega_{sp}$. Consequently, for a conventional aircraft the pitch and path dynamics are predominantly dependent on the three variables, T_{θ_2}, ζ_{sp}, and ω_{sp}, which in turn depend on the lift curve slope, the weathercock stability, and the pitch damping. For the superaugmented aircraft the attitude lead is no longer T_{θ_2}, but the control system lead T_q, while the undamped natural frequency and damping ratio are unrelated to those of the conventional short period. Thus, the augmented aircraft pitch attitude dynamics are potentially fundamentally different than those of a conventionally augmented aircraft.

Not the least important of these differences is the replacement of the T_{θ_2} lead by T_q, for now the attitude lead is not the same as the path/altitude response lag. On existing superaugmented vehicles, there is often a substantial difference between these two properties. For instance, on the Shuttle Orbiter, in a typical approach flight condition the value of $1/T_{\theta_2}$ is about 0.54 sec^{-1} whereas $1/T_q$ is 1.5 sec^{-1} (Ref. 17). Similarly, for the example RSS transport in cruise $1/T_{\theta_2}$ is 0.46 sec^{-1} while $1/T_q$ is 2 sec^{-1}.

Fundamental Flying Quality Consequences for Superaugmented Aircraft

As demonstrated above the distinction between conventional and superaugmented closed loop aircraft/augmentation system dynamics is present in the pitch attitude characteristics block. Although the forms are the same, the parameters are different in both the numerator lead and the denominator quadratic which describes the aircraft's high frequency (short-time) attitude response characteristics. In review, the key distinctions made are:

- The aircraft path/attitude response, h/θ, is the same for both conventional and superaugmented aircraft;
- The augmented aircraft pitch attitude short-term characteristics differ in that:
  1) The lead T_{θ_2} for the conventional aircraft is the same as the path/attitude lag, whereas the lead for the superaugmented aircraft T_q may be quite different from T_{θ_2}.
  2) The undamped natural frequency and damping of the effective short-period mode for the conventional aircraft depends primarily on aircraft flight condition, weathercock stability, and pitch damping (sometimes augmented).
  3) The undamped natural frequency and damping for the superaugmented aircraft depends predominantly on the augmentation system (lead and ζ_{sp}) and aircraft control effectiveness (M_δ) parameters.
- The low frequency and trim characteristics for the conventional aircraft are not reflected by the short-period attitude dynamics approximation, whereas the superaugmented aircraft pitch attitude dynamics are appropriate for low frequency and trim.

With these differences now established as at least idealizations, the key question is what effect, if any, do they have on flying qualities and hence on desirable FCS characteristics? Unfortunately, the answer to this question is not yet in. A resume of current status on these issues will be given below.

At the outset it should be recognized that almost all of the criteria and the very great preponderance of flying quality research data which underlie the various flying quality criteria were obtained on aircraft in the conventional category. The flying quality data base for heavily augmented and superaugmented aircraft is exceedingly sparse. In fact, much of the available data base and even some of the relevant criteria in the existing or proposed Military Specification (Refs. 18 and 19) cannot be used directly for superaugmented aircraft. A recently completed study in which all available criteria were considered for a particular superaugmented aircraft — the Space Shuttle Orbiter — showed that they were sometimes inapplicable or gave very ambiguous and confusing results (Ref. 17).

One of the pioneering attempts to specify the flying qualities of a relaxed static stability vehicle derives from the Space Shuttle Orbiter. Because this vehicle under piloted control is always an "effective vehicle" which inherently intermingles airframe-alone with some augmentation, this specification from the outset considered only the aircraft/FCS closed-loop system characteristics. The Shuttle flight control system is flight crucial, so no attention was paid to the aircraft-alone dynamics in the requirements. The specifications also relate directly to the pitch attitude control, with no specific mention to path control features. The statements are given in two parts. The first part is qualitative and states that the system shall provide a pitch rate output proportional to pilot inputs. This is accomplished using an augmentation system which is equivalent to the example used here (Fig. 1). The second part is more quantitative in character and provides limits on the maximum and minimum steady-state pitch rates that can be commanded and a time domain boundary specification for transient responses. Only the latter is of interest here. The original subsonic pitch rate response boundaries, from Ref. 20, are shown in Fig. 6. These boundaries have shifted somewhat dur g the Shuttle's development, with the present (Ref. 21) set also shown in Fig. 6. The third set of boundaries in Fig. 6 are rise time and settling time criteria proposed by NLR for transport aircraft with rate command/attitude hold flight control systems (Ref. 22). Their definition for rise time differs from that used here. It is

T_{rise} = the time in which the pitch rate response to a step type control input reaches 90 percent of the final steady state value.

The NLR Settling time is the time after which the pitch rate response remains within a band from 90 percent to 110 percent of the final steady state value. All the criteria of Fig. 6 were originally based on simulation data.

The transient responses for the exemplary RSS transport, given in Fig. 3a, falls within the time response boundaries shown in Fig. 6, although it nudges the upper boundary.

While we hold no thesis for any of the pitch rate time response boundaries of Fig. 6, they do encompass the responses for the example RSS aircraft and (except for an initial delay time) are generally compatible with the Shuttle itself, which is also an RSS aircraft. By adding the NLR proposed rise and settling time limits the composite Fig. 6 becomes a summary of time-domain envelope criteria specifically proposed for aircraft with rate command/attitude hold FCS. The boundaries can thus at least be considered exemplary, and can be used as a

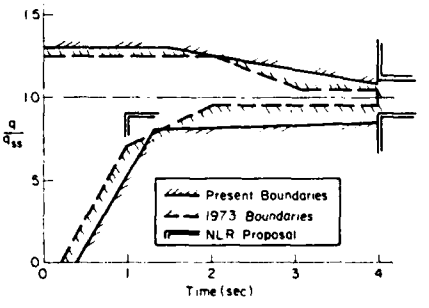

Figure 6. Exemplary Time Domain Response Boundaries for Pitch Rate Response of RSS Aircraft

convenient framework from which to consider possible distinctions between conventional and superaugmented aircraft. They shall be used as strawmen below to serve as a backdrop for data comparisons.

The best and most current set of flight data for conventional aircraft precision path control is probably the landing and approach higher order system (LAHOS) study of Ref. 23. These experiments used the Calspan variable stability NT-33 aircraft in an approach and landing task. The evaluation flights were continued through touchdown. A large number of configurations were evaluated, usually by two pilots, with repeat evaluations being made randomly for many of the configurations. Six of these configurations have been selected as being particularly relevant to the points at issue here. While all six meet the NLR rise time criterion, three of the six selected LAHOS configurations exceeded the exemplary time domain RSS aircraft boundaries, and three had responses within those boundaries. Both sets are shown in Fig. 7. With a pilot rating of 3-1/2 as a boundary between desirable and undesirable workload, corresponding approximately to the MIL-Spec Level 1 flying quality category, Fig. 7a indicates that conventional configurations with good flying qualities may not meet the exemplary RSS boundaries. On the other hand, the three configurations which have responses which fall within the exemplary boundaries have overall pilot ratings between 6 and 7. It will be recalled that pilot ratings of 6.5 correspond to conditions where adequate performance cannot be attained with a tolerable pilot workload. These configurations, therefore, demand excessive workload and pilot compensation for control purposes. They are all poor from the flying qualities standpoint, and border on the unsafe by virtue of the poor control and high workload. Incidently, the flight path/attitude lag for both good and bad configurations is $1/T_{\theta_2} = 0.714\ sec^{-1}$. Since this feature is the same for all, the rating differences are probably associated with the attitude component of precision path control.

Thus, the LAHOS data indicate that conventional aircraft which do meet the exemplary boundaries can have poor flying qualities whereas those which do not can have good flying qualities. Indeed, the marked similarity between some of those responses shown in Fig. 7b and the response of the example RSS superaugmented aircraft in Fig. 3a could be used to support a contention that the flying qualities of the example RSS aircraft would be poor. [Logically, however, all that can be said to this point is that the exemplary boundaries are not suitable to define good flying qualities for conventional aircraft.]

There is, of course, another interpretation. This is quite simply that, as has been emphasized all along, superaugmented aircraft are different in their characteristics and are not necessarily appropriately judged by data from conventional configurations. With this interpretation, the exemplary boundaries or something similar could conceivably still encompass the responses of heavily or superaugmented aircraft which have good flying qualities. Unfortunately, there are very few data available which apply to heavily augmented aircraft as considered herein and even less data which are pertinent to the idealized superaugmented condition. A very recent study, however, does contain one data point which does indeed approach the superaugmented situation. This appears in Ref. 24, which examined the handling qualities of large airplanes in the approach and landing phase using the USAF-AFWAL/Calspan Total In-Flight Simulator. The study simulated a 453,600 kg statically unstable airplane as the RSS baseline vehicle. Several control systems to stabilize the aircraft were examined. Among these was one which corresponded to the augmentor of Fig. 1. One of the cases studied had sufficiently high control system gain to approach the superaugmentation idealization. This response is shown in Fig. 8. The overshoot, while less than the maximum in the exemplary boundary is extended somewhat further and the rise time is also fairly large. In fact the response is just outside the NLR proposed rise and settling time limits. Nonetheless, this pitch rate response is not too far removed from the exemplary boundaries. This configuration was evaluated by both evaluation pilots used in the study and received generally good ratings. In its second evaluation by one pilot it was given a Cooper-Harper rating of 1 which is extremely unusual (the same pilot initially evaluated it as 4). The pilot commentary indicates initial problems in trim, basically in attempting to "Keep the airspeed and attitude organized." After familiarization, however, the same pilot noted that "Airspeed control is excellent. Once I get it trimmed up it virtually holds

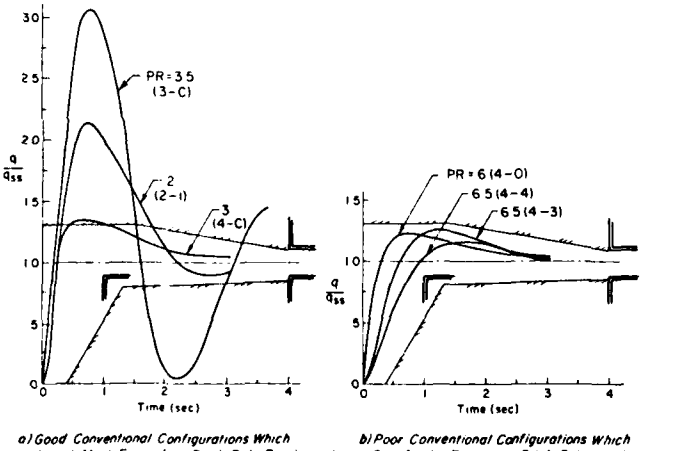

a) Good Conventional Configurations Which do not Meet Exemplary Pitch Rate Requirements

b) Poor Conventional Configurations Which Satisfy the Exemplary Pitch Rate Requirements

Figure 7. Comparison of Conventional Configurations with Exemplary Time Domain Boundaries for RSS Aircraft [Configurations are identified as, e.g. (3-C) from Ref. 23].

the airspeed, holds attitude, and stays trimmed in turns." The other pilot indicated that "airspeed control was good, predictable." His summary comment was "No major problems, an excellent airplane." From these comments it would appear that in precision path control, a superaugmented configuration may indeed exhibit good flying qualities. There does appear to be a potential familiarization problem, although this is rapidly overcome. This one flight data point, considered in company with the LAHOS data of Fig. 7, goes a long way toward justifying a position that heavily augmented RSS aircraft, especially as they approach the superaugmented condition, cannot satisfactorily be judged by criteria or compared with data from conventional aircraft.

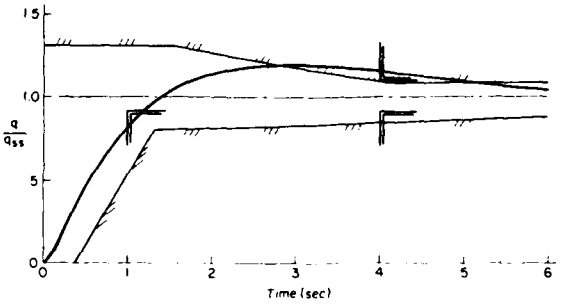

Figure 8. Flight Simulated Superaugmented Airplane Response for Approach and Landing (Ref. 24); $1/T_{\theta_2} = 0.53$ sec^{-1}, $1/T_q = 1$ sec^{-1}

Can one currently go much further in laying out tentative FCS specifications for idealized superaugmented aircraft? There is another solid data set available which can be culled for further insight. Reference 22 includes moving-base ground simulations of a large number of rate-command, attitude hold systems for an RSS version of the Fokker F-28 transport. A small subset (four flight conditions) approached superaugmented status in that their attitude dynamics: were rate command/attitude hold; had a dominant attitude lead time constant T_q which was significantly different from T_{θ_2}; were nearly insensitive to T_{θ_2}, which was nearly cancelled by a neighboring pole; approximated the superaugmented q/q_{ss} response form of Eq. 2. Figure 9 shows the four "F" configurations for Ref. 22 which are close to superaugmented. Interestingly, the three-pilot average Cooper-Harper ratings for these highly-augmented RSS configurations put the exemplary boundaries in a much more favorable light then the LAHOS data of Fig. 7. Pilot comments for configurations F-3 and F-4 ranged from "Favorable pitch control properties leading to reduced pilot workload" (F-3), to "Very good pitch control and stabilization properties" (F-4). The F-4 configuration has since been flight simulated in the USAF/Calspan TIFS (Ref. 25). The flight result had a three-pilot average Cooper-Harper rating of 3.7 [1 pilot "3", 2 pilots "4"], in contrast with the CHPR of 2.3 [2 pilots "2", 1 pilot "3"] for the moving base results. Unfortunately, the F-4 configuration is very close to "conventional" in that the effective attitude lead is not far removed from T_{θ_2}.

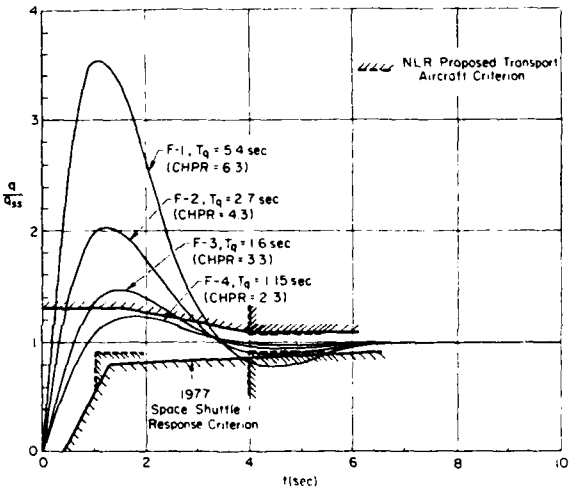

Figure 9. Normalized Indicial q Response of Ref. 22 "F" Configurations Compared to Exemplary Criteria ($T_{\theta_2} = 1.4$ sec)

When all is said and done, it now appears that parts of the exemplary boundaries of Fig. 6 are probably adequate for highly augmented aircraft which approach the superaugmented ideal. The NLR rise time and the present shuttle upper bound would appear to offer excellent guidelines for precision path and attitude control in approach and landing. The NLR settling time requirement is also pertinent although it is a bit less stringent than the upper boundary. For a lower boundary the 1973 shuttle envelope might be faired into the NLR rise time criterion to provide an interim envelope. However, it should be plain that more data are needed to solidify such interim time domain guidelines into a more solid and reliable FCS specification.

ACCUMULATION OF LAGS AND DELAYS INTRODUCED BY THE CONTROL SYSTEM

A common feature of all heavily augmented aircraft is the introduction by the control system of additional lags which may tend to delay the actual aircraft response buildup. The idealized responses shown in Fig. 3 start with an instantaneous pitching acceleration for a step control surface input. In actuality, this response will appear more as shown in Fig. 10. Because of the lags, after a step input is instantaneously applied there will be a very gradual buildup before the pitching acceleration begins to ramp off. This initial buildup delay is easily measured by a delay time τ_d. Although the discussion of this delay has been deferred to this point, it is the last item listed in the Table I comparison of pitch attitude response parameters for conventional and superaugmented aircraft.

In all the responses and example analyses described previously, the explicit assumption was that actuation, sensing, filtering, and other real system lags were ignored. The delay time accounts for these. In the conventional aircraft, τ_d will be due primarily to the surface actuator and any additional lags that may be present in the manual control system. It, characteristically, is relatively small. Typical actuators, for example, appear like first order systems with time constants on the order of 0.05 sec or so for small amplitudes of movement. Thus, for a conventional airplane with a state of the

art, fully powered, surface actuating system and manual control system, the effective time delay may typically be less than 1/10 sec.

With heavily augmented or supersugmented aircraft, additional considerations enter. As it turns out, all tend to increase the delay time. The baseline is, of course, the surface actuator shared with a conventional counterpart. The relaxed static stability aircraft which relies on the augmentation to restore favorable stability properties demands a controller-aircraft system minimum bandwidth which is characteristically greater than that present with a damping only augmentor. Because of this, the augmentation system bandwidth for rigid body control comes closer to intruding on the higher frequency flexible modes of the aircraft. So that these flexible modes do not become important in the aircraft/augmentor system stability, filters are often used in the control system to attenuate system signals which may arise due to the lower frequency lightly-damped flexible modes. This can be done using either low pass or notch filtering. Over the low frequency range associated with pilot control, either type of filter will appear as an effective lag.

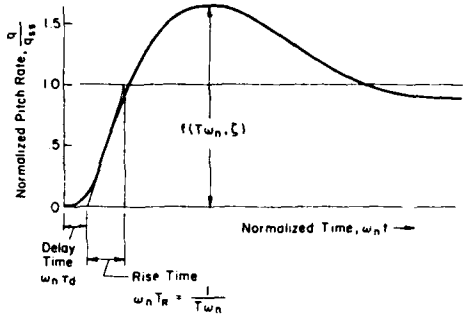

General Form:

$$\frac{q}{q_{ss}} = \frac{(Ts+1)}{s\left[\left(\frac{s}{\omega_n}\right)^2 + \frac{2\zeta}{\omega_n}s + 1\right]}$$

Figure 10. General Pitch Rate Response to Step Pilot Input

In the augmentation system filters are sometimes required for certain sensors, such as normal accelerometers, to reduce unwanted inputs from the local vibratory environment. These filters also add to the net lag. Further, in the controller itself, a number of quite small time constant or pure time delay elements may be present. For instance, if the controller is digital, pure time delays are introduced due to computing operations, and filtering may be inserted for anti-aliasing at the input and smoothing digital to analog conversions at the output.

Finally, if the pilot command input is accomplished via a sidestick or low-force-input control column in a fly-by-wire controller installation, the manipulator will transmit both the desirable coherent pilot command signals and undesirable pilot-induced noise. The latter may be the small random fluctuations in pilot control precision commonly referred to as remnant, or may be more excessive in vibratory environments. In either event, the pilot-induced noise is ordinarily quite wide band, whereas the appropriate control signals are much narrower in frequency content. The manipulator signal accordingly may require filtering before it is presented to the flight controller.

All of these types of filtering and time delays are called out in the exemplary Fig. 1 augmentation system. Their associated lags are individually quite small. However, unless great care is taken in the detailed design of the manipulator and other controller characteristics, they can add up to a sizable quantity. In fact, for the ALT version of the Space Shuttle Orbiter, such time delays approached 0.25 sec. This excessive delay pushed the ALT version of the Shuttle pitch rate response to or past the lower boundary of its own specification (Fig. 6). As demonstrated in Ref. 26 this effective delay in the ALT orbiter played an important role in the pilot induced oscillation encountered in Free Flight 5 during the approach and landing sequence. This, and similar instances in advanced fighters which are also RSS aircraft, has caused a great deal of emphasis to be placed on the effects of such delays.

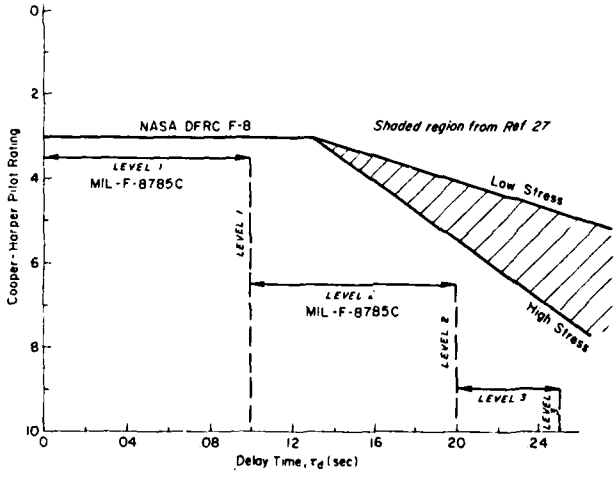

Figure 11. Comparison of MIL-F-8785C Time Delay Requirements with Data from Ref. 27

While the flying qualities problems which may arise from excessive effective delay time are quite well understood, the quantitative picture is still clouded. The existing military specification, MIL-F-8785C (Ref. 18) puts forth requirements for allowable time delays as a function of flying qualities levels. These are shown in Fig. 11. The origins of the time delay requirements of Ref. 30 are not well documented and these bounds were set up shortly after the basic problems were perceived to be a critical issue.

On the other hand, Ref. 27 shows the boundaries from data developed for approaches and landing using the NASA DFRF F8 DFBW airplane. The high stress and low stress bounds depend on task precision. For Level 1 the MIL SPEC may be a bit too stringent ($\tau_d < 0.1$ sec), since the NASA data do not show a major

shift until $\tau_d \triangleq 0.12 - 0.14$ sec. If Cooper-Harper ratings of 6-1/2 are taken as an upper limit, then the high stress boundary would indicate that delay times somewhat less than 0.22 sec (contrasted with the MIL SPEC 0.20 sec) might be permissible.

It must be recognized that delay time cannot be viewed as an uncoupled entity. Instead, it is intrinsically connected with other flying quality metrics, such as rise time. A system with a short rise time can surely accommodate more delay than a system with a longer rise time. Both time delay and rise time affect the attainable bandwidth of piloted control. This is recognized as one of the alternate specification factors in Ref. 19.

It is especially important in connection with delay time, as in most of the other flying quality issues brought up in this paper, that precision control with high stress or high urgency conditions be emphasized in design and testing. Otherwise the importance of some of these issues in operational flight precision and safety will be missed. A very large time delay could be accommodated, for example, if the aircraft is lined up well out on final approach and no urgent correction is required or extreme disturbance is present.

DIGITAL SYSTEM PECULIARITIES

While existing full-time multiple-redundant fly-by-wire flight control systems have both analog and digital representatives (e.g., the F-16 is analog, F-18 and Shuttle are digital), the majority in the future will almost certainly be digital. When contrasted with the behavior of continuous analog systems digital FCS exhibit some interesting peculiarities. These include sampling, serial processing of data, and finite word length. For future manned systems any word length problems are likely to be insignificant. Serial processing results in order of call effects which can create a small incremental time delay that sometimes requires careful consideration in an FCS. The sampling features are the most important and need a bit more discussion.

Periodic sampling is a linear operation, yet it is peculiar in that a sinusoidal input will beget an infinity of frequencies in the output, and the output waveform will, on the average, be delayed. As an approximation, the transmission of a sinusoid through a sampling and hold operation described by an impulse sampler with sampling rate 1/T samples/second and a hold circuit with transfer function $(1 - e^{-Ts})/s$, will be given by the describing function

$$N(T, j\omega) = \left.\frac{1 - e^{-Ts}}{Ts}\right|_{s = j\omega}$$

$$= \frac{e^{j\omega(T/2)} - e^{-j\omega(T/2)}}{2j} \frac{1}{\omega(T/2)} e^{-j\omega(T/2)} \qquad (7)$$

$$= \frac{\sin(\omega T/2)}{\omega T/2} e^{-j\omega(T/2)}$$

This describing function implies a time delay of 1/2 the sampling interval, and an amplitude ratio reduction when input frequencies approach twice the sampling rate. In most cases the delay is the main problem since it is a component of the total delay time τ_d.

A more precise and satisfying way to show the loop transmission and stability effects of sampling is direct digital system analysis in the w-domain (Refs. 28 and 29). This uses a complex variable w which is derived as a bilateral transformation in terms of the z transform used in conventional sampled data analysis. w is defined as

$$w = \frac{2}{T}\left(\frac{z - 1}{z + 1}\right); \qquad (8)$$

$$z = -\frac{(w - 2/T)}{(w + 2/T)} \qquad (9)$$

Recalling that $z = e^{Ts}$, w becomes

$$w = \frac{2}{T}\left(\frac{e^{Ts} - 1}{e^{Ts} + 1}\right) \qquad (10)$$

$$= \frac{2}{T} \tanh \frac{Ts}{2}$$

One feature of the w domain is that stability boundaries are not associated with the unit circle as it is in the z-domain, but with the entire left half w plane similar to the s-domain. Another characteristic of surpassing importance is that w approaches s as the sampling interval T approaches zero. These two features permit the carryover into the digital world of many continuous system design procedures, techniques, and insights.

One such technique is the use of w transforms to provide a digital system equivalent of the Laplace transform for continuous systems. Bode diagrams, root locus plots, multiloop analyses, and many rules of thumb will then all work well using w as the complex variable instead of s. An abbreviated transform

TABLE 2. AN ABBREVIATED TRANSFORM TABLE

s-PLANE	z-PLANE	z-PLANE (ZOH)	w-PLANE
$\frac{1}{s}$	$\frac{z}{z-1}$	$\frac{T}{z-1}$	$\frac{-\frac{T}{2}w+1}{w}$
$\frac{1}{s^2}$	$\frac{Tz}{(z-1)^2}$	$\frac{\frac{T^2}{2}(z+1)}{(z-1)^2}$	$\frac{-\frac{T}{2}w+1}{w^2}$
$\frac{1}{s^3}$	$\frac{T^2z(z+1)}{2(z-1)^3}$	$\frac{\frac{T^3}{6}(z^2+4z+1)}{(z-1)^3}$	$\frac{(-\frac{T}{2}w+1)(-\frac{T}{\sqrt{12}}w+1)(\frac{T}{\sqrt{12}}w+1)}{w^3}$
$\frac{a}{s+a}$	$\frac{az}{z-e^{-aT}}$	$\frac{1-e^{-aT}}{z-e^{-aT}}$	$\frac{\frac{2}{T}\left\lfloor\frac{(1-e^{-aT})}{(1+e^{-aT})}(-\frac{T}{2}w+1)\right\rfloor}{w+\frac{2}{T}\left\lfloor\frac{(1-e^{-aT})}{(1+e^{-aT})}\right\rfloor}$
$\frac{b}{s^2+b^2}$	$\frac{zS}{z^2-(2C)z+1}$	$\frac{\frac{(1-C)}{b}(z+1)}{z^2-(2C)z+1}$	$\frac{\frac{4}{T^2}\left\lfloor\frac{(1-C)}{b(1+C)}(-\frac{T}{2}w+1)\right\rfloor}{w^2+\frac{4}{T^2}\left\lfloor\frac{(1-C)}{(1+C)}\right\rfloor}$
$\frac{s}{s^2+b^2}$	$\frac{z(z-C)}{z^2-(2C)z+1}$	$\frac{(\frac{S}{b})(z-1)}{z^2-(2C)z+1}$	$\frac{\frac{2}{T}\left\lfloor\frac{S}{b(1+C)}(w)(-\frac{T}{2}w+1)\right\rfloor}{w^2+\frac{4}{T^2}\left\lfloor\frac{(1-C)}{(1+C)}\right\rfloor}$
$\frac{b}{(s+a)^2+b^2}$	$\frac{ze^{-aT}S}{z^2-(2e^{-aT}C)z+e^{-2aT}}$	$\frac{\frac{b-e^{-aT}(aS+bC)}{a^2+b^2}z+\frac{be^{-2aT}-e^{-aT}(bC-aS)}{a^2+b^2}}{z^2-(2e^{-aT}C)z+e^{-2aT}}$	$\frac{\frac{2}{T}\left\lfloor\frac{b(1-e^{-2aT})-2aSe^{-aT}}{(a^2+b^2)(1+2e^{-aT}C+e^{-2aT})}\right\rfloor\left\{w+\frac{2}{T}\left\lfloor\frac{b(1+e^{-2aT})-2bCe^{-aT}}{b(1-e^{-2aT})-2aSe^{-aT}}\right\rfloor\right\}(-\frac{T}{2}w+1)}{w^2+\frac{4}{T}\left\lfloor\frac{(1-e^{-2aT})}{1+2e^{-aT}C+e^{-2aT}}\right\rfloor w+\frac{4}{T^2}\left\lfloor\frac{1-2e^{-aT}C+e^{-2aT}}{1+2e^{-aT}C+e^{-2aT}}\right\rfloor}$
$\frac{s+a}{(s+a)^2+b^2}$	$\frac{z(z-e^{-aT}C)}{z^2-(2e^{-aT}C)z+e^{-2aT}}$	$\frac{\frac{a+e^{-aT}(bS-aC)}{a^2+b^2}z+\frac{ae^{-2aT}-e^{-aT}(bS+aC)}{a^2+b^2}}{z^2-(2e^{-aT}C)z+e^{-2aT}}$	$\frac{\frac{2}{T}\left\lfloor\frac{a(1-e^{-2aT})+2bSe^{-aT}}{(a^2+b^2)(1+2e^{-aT}C+e^{-2aT})}\right\rfloor\left\{w+\frac{2}{T}\left\lfloor\frac{a(1+e^{-2aT})-2aCe^{-aT}}{a(1-e^{-2aT})+2bSe^{-aT}}\right\rfloor\right\}(-\frac{T}{2}w+1)}{w^2+\frac{4}{T}\left\lfloor\frac{(1-e^{-2aT})}{1+2e^{-aT}C+e^{-2aT}}\right\rfloor w+\frac{4}{T^2}\left\lfloor\frac{1-2e^{-aT}C+e^{-2aT}}{1+2e^{-aT}C+e^{-2aT}}\right\rfloor}$

C = cos bT S = sin bT

K-15

table is given in Table 2. A key point to notice there is that the w transforms, when viewed as transfer function-like entities, all exhibit a right-half plane zero at w = 2/T. This, of course, stems from the sample and hold. When loops are closed around w transfer functions this zero has the expected but unfortunate property of drawing the loci from some system pole(s) toward or into the unstable region. The effect is very similar to that caused by the pure time delay approximation of T/2 in Eq. 7 (which itself could have been approximated by a non-minimum phase lead (1 - sT/2).

Another interesting feature of the w domain is a shift in poles and zeros as one goes from s to w. Consider, for instance the first-order lag a/(s + a).

$$\frac{a}{s+a} \rightarrow \frac{\frac{2}{T}\left(\frac{1-e^{-aT}}{1+e^{-aT}}\right)\left(1-\frac{Tw}{2}\right)}{w+\frac{2}{T}\left(\frac{1-e^{-aT}}{1+e^{-aT}}\right)} \tag{11}$$

$$= \frac{a'\left(1-\frac{Tw}{2}\right)}{w+a'}$$

where $a' = (2/T)\left(1-e^{-aT}\right)/\left(1+e^{-aT}\right) = (2/T)\tanh(aT/2)$. Using the hyperbolic tangent series expansion the value of a' for sampling rates which are high relative to the s-plane pole magnitude a, i.e., for aT/2 << 1, becomes

$$a' = a\left[1-\frac{1}{3}\left(\frac{aT}{2}\right)^2+\frac{2}{15}\left(\frac{aT}{2}\right)^4-\cdots\right] \tag{12}$$

Thus, when "a" is small compared with the sampling rate the s-plane pole at s = -a is an excellent approximation to the w-plane pole at w = -a'. At lower rates (or larger values of "a") the effect of sampling is to reduce the magnitude a' of the w-plane pole relative to the s-plane pole magnitude, a.

If these concepts are now applied to FCS analysis considerations the first-order effect of sampling is to introduce the rhp numerator zero at -2/T, while the second-order effects are to change the magnitude of the poles and zeros in the w transfer functions from those of the s-domain transfer function. Ordinarily the FCS sampling rate will be large relative to the FCS frequencies of interest (except, perhaps, for flexible modes) so the addition of a zero at s = +2/T in the regular continuous transfer functions will often provide an adequate approximation for FCS stability and dominant mode response purposes. When higher frequency modes impinge on the sampling region these approximations no longer apply and the more exact w-domain poles and zeros should be used.

With the high sample rates of next generation digital FCS for manned aircraft the sampling effects noted above are not as likely to cause trouble on the actual aircraft as they are earlier in the simulation phase of development. There are particular concerns with closed-loop man-in-the-loop simulation with actual hardware. Remarkably, analog computers have almost disappeared from many research and development facilities which are now run on a totally digital basis. In a typical simulation the aircraft characteristics may be programmed onto a digital computer which may also run a moving-base apparatus and parts of a visual display attachment. The mathematical models of the vehicle may be very complex and include many nonlinear characteristics, lots of lookup tables, and so forth. The result often is a full computer which represents a continuous airframe by a fundamentally digital characterization with relatively low update rates. Now, when an actual digital flight controller with a frame rate of 80-100/s is used in conjunction with a 20/s digital simulation of a continuous airplane, the simulated stability and control properties of the aircraft will suffer the shifts described above. Unrealistic delays which affect the pilot's ratings and workload assessment will appear. Further, if these "digital airplane" effects are not properly accounted for even the basic aircraft/augmenter system may exhibit difficulties which are really only imaginary. There have been times when the actual airplane was needed to fully appreciate the FCS capabilities!

REFERENCES

1. Howard, R. W., "Progress in the Use of Automatic Flight Controls in Safety Critical Applications," Aeron. J., Vol. 84, Oct. 1980, pp. 316-326.

2. McRuer, D., and D. Graham, "Eighty Years of Flight Control: Triumphs and Pitfalls of the Systems Approach," J. Guidance and Control, Vol. 4, No. 4, July-Aug. 1981, pp. 353-362.

3. Burns, B. R. A., "Fly-by-Wire and Control-Configured Vehicles — Rewards and Risks," Aeron. J., Vol. 79, Feb. 1975, pp. 51-58.

4. Impact of Active Control Technology on Airplane Design, AGARD CP-157, June 1975.

5. Advanced Control Technology and Its Potential for Future Transport Aircrft, NASA TM X-3409, Aug. 1976.

6. McRuer, D., "New Trends and Problem Areas in Automatic Flight Control," Israel J. of Technology, Vol. 15, Jan. 1977, pp. 1-10.

7. Integrity in Electronic Flight Control Systems, AGARD AG-224, Apr. 1977.

8. Simpson, A., and H. P. Y. Hitch, "Active Control Technology," Aeron. J., Vol. 81, June 1977.

9. Shomber, H. A., "Application of Integrated Active Controls to Future Transports," AIAA Paper 79-1654, 1979.

10. Urie, D. M., et al., Accelerated Development and Flight Evaluation of Active Controls Concepts for Subsonic Transport Aircraft, 2 vols., NASA CR-159097 and CR-159098, Sept. 1979.

11. Hitch, H. P. Y., "Active Controls for Civil Aircraft," Aeron. J., Vol. 83, No. 826, Oct. 1979, pp. 389-398.

12. McRuer, D. T., I. L. Ashkenas, and D. Graham, Aircraft Dynamics and Automatic Control, Princeton University Press, 1973.

13. McRuer, Duane and Thomas T. Myers, Handling Qualities of Aircraft with Relaxed Static Stability and Advanced Flight Control System. Vol. II: Ramifications of Flight-Critical Heavily-Augmented Relaxed Static Stability Airplane Characteristics on Flying Qualities, Systems Technology, Inc. TR-1178-1-II, Aug. 1982.

14. Stapleford, Robert L., and Irving L. Ashkenas, "Longitudinal Short-Period Handling Quality Requirements," Section IV," and Appendix, in R. L. Stapleford, Irving L. Ashkenas, et al., Analysis of Several Handling Quality Topics Pertinent to Advanced Manned Aircraft, AFFDL-TR-67-2, June 1967.

15. Stapleford, R. L., S. J. Craig, and J. A. Tennant, Measurement of Pilot Describing Functions in Single-Controller Multiloop Tasks, NASA CR-1238, Jan. 1969.

16. Weir, D. H., and D. T. McRuer, Pilot Dynamics for Instrument Approach Tasks: Full Panel Multiloop and Flight Director Operations, NASA CR-2019, May 1972.

17. Myers, T. T., D. E. Johnston, and D. McRuer, Space Shuttle Flying Qualities and Flight Control System Assessment Study, NASA CR 170391, June 1982.

18. "Flying Qualities of Piloted Airplanes," MIL-F-8785C, Nov. 1980.

19. Hoh, R. H., D. G. Mitchell, I. L. Ashkenas, et al., Proposed MIL Standard and Handbook — Handling Qualities of Piloted Airplanes, Vol. 2, AFWAL-TR-82-3081, July 1982.

20. Klinar, W. J., D. W. Gilbert, et al., Flying Qualities Requirements for the Orbiter Utilizing Closed-Loop, Fly-by-Wire Control of Vehicle Response Parameters, NASA MCS-C7151, Rev. 1, Dec. 1973.

21. Requirements/Definition Document, Flight Control, Part 1 Configuration, Performance and Functional Requirements, Rockwell International Space Division, Report SD72-SH-0105, Vol. 1, Book 2, Part 1A, July 1977.

22. Mooij, H. A., W. P. deBoer, and M. F. C. von Gool, Determination of Low-Speed Longitudinal Maneuvering Criteria for Transport Aircraft with Advanced Flight Control Systems, National Aerospace Laboratory (NLR) TR 79127U, 20 Dec. 1979.

23. Smith, Rogers E., Effect of Control System Dynamics on Fighter Approach and Landing Longitudinal Flying Qualities, Vol. I, AFFDL-TR-78-122, Mar. 1978.

24. Weingarten, N. C., and C. R. Chalk, In-Flight Investigation of Large Airplane Flying Qualities for Approach and Landing, to be issued as AFWAL 81-3118, July 1981.

25. Mooij, H. A. and M. F. C. von Gool, "Handling Qualities of Transports with Advanced Flight Control Systems," Criteria for Handling Qualities of Military Aircraft, AGARD CP-333, June 1982.

26. Teper, Gary L., Richard J. DiMarco, and Irving L. Ashkenas, Analyses of Shuttle Orbiter Approach and Landing Conditions, NASA CR-163108, July 1981.

27. Berry, D. T., B. G. Powers, K. J. Szalai, and R. J. Wilson, "A Summary of an In-Flight Evaluation of Control System Pure Time Delays During Landing Using the F-8 DFBW Airplane," A Collection of Technical Papers: Proceedings of AIAA Atmospheric Flight Mechanics Conference, August 11-13, 1980, Danvers, MA, pp. 561-571.

28. Whitbeck, R. F. and L. G. Hofmann, "Digital Control Law Synthesis with w'-Domain," J. Guidance and Control, Vol. 1, No. 5, Sept.-Oct. 1978, pp. 319-326.

29. Franklin, G. F., and J. D. Powell, Digital Control of Dynamic Systems, Addison-Wesley, 1980.

30. Whitbeck, Richard F. and L. G. Hofmann, Analysis of Digital Flight Control Systems with Flying Qualities Applications. Vol. II: Technical Report, AFFDL-TR-78-115, Sept. 1978.

REALISATION DE REGULATEURS DE POURSUITE AMELIORES POUR LE PILOTAGE DES AVIONS A GRANDE MANOEUVRABILITE

par Omer L. MERCIER
Office National d'Etudes et de Recherches Aérospatiales (ONERA)
92320 Châtillon (France)

RESUME

La commande multivariable des avions à manœuvrabilité élevée, dans un domaine de vol étendu, est un sujet qui a reçu une attention croissante depuis quelques années. Du point de vue de l'automaticien, ce sujet est tout à fait voisin du problème de l'asservissement de poursuite dans la mesure où un vecteur de variables de sorties est asservi à suivre des variables de consigne évoluant arbitrairement. Ce problème est encore compliqué par le fait que, dans le domaine de manœuvre envisagé, le modèle dynamique est fortement nonlinéaire, variable le long du domaine de vol, et sujet à de sévères erreurs ou variations. Cependant, les objectifs de pilotage doivent être atteints tout en respectant les spécifications de qualités de vol. En outre, la poursuite doit être assurée malgré l'action continue de perturbations extérieures et la turbulence basse-fréquence doit être compensée. Des défauts importants des régulateurs issus des méthodes classiques sont cités et une théorie améliorée du régulateur linéaire-quadratique à deux niveaux est présentée. Apliquée au pilotage d'un avion d'arme, ce schéma de régulation permet de commander de manière précise des manœuvres de grande amplitude en dépit d'erreurs ou variations de modèle, tout en isolant les spécifications concernant les qualités de vol de celles qui caractérisent le rejet des perturbations extérieures. La manière dont des non-conformités de modèle ou des nonlinéarités sont tolérées est mise en évidence par des simulations numériques.

ABSTRACT

The multivariable control of an highly maneuvering aircraft in an extended flight envelope has been receiving a growing attention in recent years. From the control designer point of view, it bears close relationship to the servomechanism problem in the sense that a vector of output variables is regulated to track continuously set command variables. This tracking problem is further complicated by the fact that, in the range of considered maveuvers, the dynamic model is highly nonlinear, variable about the flight domain and prone to severe modeling errors and variations. Yet, piloting objectives must be met while satisfying handling qualities specifications. In addition, tracking must be maintained under continuously acting external disturbances and low-frequency turbulence must be rejected. Important defects of classical methods are shown and an improved theory is presented and applied to the fighter control problem. Tolerance of model mismatch and nonlinearities is especially demonstrated in numerical simulations.

INTRODUCTION

En référence au système nonlinéaire

$$\begin{aligned} \dot{x} &= f(x,u), && x \in \mathbb{R}^n,\ u \in \mathbb{R}^m, \\ z &= g(x), && z \in \mathbb{R}^p, \end{aligned} \tag{1}$$

Le problème de poursuite optimale est la réalisation d'une loi de commande en boucle fermée u(.) telle que la sortie z suive asymptotiquement un vecteur de consigne donné z_d, soit

$$\lim_{t \to \infty} \left[z(t) - z_d(t) \right] = 0,$$

en dépit de perturbations persistantes et de variations de modèle.

Un défaut commun aux lois de commande actuellement considérées est qu'elles requièrent la connaissance précise des variables d'équilibre x^e et u^e, solutions de $\dot{x}^e = f(x^e,u^e) = 0$ et $g(x^e) = z_d$, correspondant à la solution de régime permanent de (1), pour fonctionner correctement. Or, la solution de ces équations nonlinéaires est difficile à calculer. Bien plus, ce calcul des valeurs d'équilibre x^e et u^e est compliqué par les inévitables erreurs et variations de modèle et par l'addition de perturbations extérieures.

Même en utilisant des lois de commande de Type-1, c'est-à-dire avec action intégrale, l'utilisation de valeurs d'équilibre inexactes a pour résultat des conflits d'objectifs pour le régulateur de poursuite et de graves défauts de convergence malgré une stabilité apparemment satisfaisante. Il est donc approprié de rechercher des lois de commande qui éliminent le besoin de connaître ces valeurs d'équilibre.

En outre, lorsque l'équation du système nonlinéaire (1) est sujette à des erreurs de modèle ou à des perturbations inconnues, les écarts entre les variables d'état et de commande et leurs valeurs d'équilibre respectives ne s'annulent plus individuellement : les fonctions de coût traditionnellement utilisées ne convergent donc plus. Ce problème mathématique amplifie les autres difficultés, surtout si l'on souhaite exploiter les avantages de cette fonction de coût quadratique, par exemple pour accroitre la robustesse ou la marge multivariable du système contrôlé (voir [1,2]).

Dans cette communication, une théorie améliorée du régulateur de poursuite est présentée, résolvant tous les problèmes des approches classiques. L'exposé est tout particulièrement orienté sur la manière de réaliser des lois de commande de pilotage pour un avion d'arme moderne. Une structure de contrôleur à deux niveaux, inspirée des idées exprimées dans [3-5], est utilisée pour faciliter le respect des contraintes opérationnelles sur les variables d'état et de commande ainsi que des spécifications concernant les qualités de vol.

II. DESCRIPTION DU REGULATEUR A DEUX NIVEAUX

Le premier niveau du régulateur, représenté en Fig. 1, sous forme de schéma-bloc, est un filtre de conditionnement des consignes, comprenant un modèle de l'avion linéarisé au voisinage du vol horizontal, caractérisé par $(x_0, u_0, z_0 = Cx_0)$, soit

$$\begin{aligned} \delta\dot{x}_m &= A\,\delta x_m + B\,\delta u_m, & \delta x_m &\in \mathbb{R}^n,\ \delta u_m \in \mathbb{R}^m, \\ \delta z_m &= C\,\delta x_m, & \delta z_m &\in \mathbb{R}^p, \end{aligned} \tag{2}$$

où $\delta x_m = x_m - x_0$, $\delta u_m = u_m - u_0$, $\delta z = z_m - z_0$.

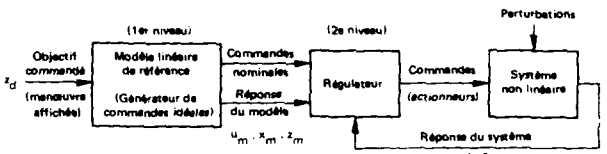

Fig. 1 – Configuration générale du régulateur à deux niveaux.

Une loi de commande de Type-1 est appliquée à δu_m pour stabiliser le système augmenté $(\delta\dot{x}_m^T, e_m^T)$,

où $e_m \triangleq z_m - z_d$, c'est-à-dire pour assurer la convergence de z_m vers z_d avec une dynamique imposée. Le régulateur de ralliement de modèle (2e niveau), qui utilise la commande δu_m à la manière d'un "feedforward", est réalisé de manière à assurer la convergence des variables de sorties z de l'avion nonlinéaire perturbé vers celles du modèle, z_m.

Aux écarts entre le mouvement non linéaire perturbé (1) de l'avion et le mouvement linéaire du premier niveau est associé un modèle linéarisé

$$\begin{aligned} \delta\dot{x} &= f(x,u) - A\,\delta x_m - B\,\delta u_m = A\,\delta x + B\,\delta u + \delta_1, \\ e &= g(x) - g(x_m) = C\,\delta x + \delta_2, \end{aligned} \tag{3}$$

$\delta x \in \mathbb{R}^n$, $\delta u \in \mathbb{R}^m$, $e \in \mathbb{R}^p$, où $\delta x = x - x_m = x - \delta x_m - x_0$, $\delta u = u - u_m = u - \delta u_m - u_0$, également au voisinage du vol horizontal et à une valeur particulière de l'incidence et de la pression dynamique (ρV^2). La quantité δ_1 est un vecteur rassemblant les perturbations extérieures ainsi que les erreurs de modèle et de linéarisation. δ_2 contient les résidus de linéarisation de g(x).

Ce modèle est utilisé pour élaborer la loi de commande, également de Type-1, qui sera appliquée à l'avion nonlinéaire (1). Cette loi linéaire est choisie de manière à stabiliser le système augmenté $[\delta\dot{x}^T, e^T]^T$, où $e \triangleq z - \delta z_m - z_0$ c'est-à-dire de manière à assurer la convergence de z vers $\delta z_m + z_0$, et donc de z vers z_d, avec une dynamique imposée et en dépit de perturbations constantes δ_1. En même temps, cette loi tranquilise le système contrôlé (puisque $\delta\dot{x} \to 0$) à une valeur de régime permanent qui n'est pas connue puisque dépendant des caractéristiques réelles de l'avion ainsi que des perturbations extérieures. Enfin, pour toute la classe des perturbations δ_1 pour lesquelles le mouvement contrôlé de (3) sera stable, la loi considérée sera également stabilisante pour le système nonlinéaire (1). L'architecture générale du régulateur de pilotage est représentée sur la Fig. 2.

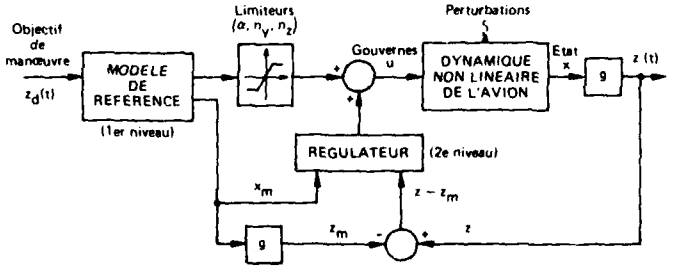

Fig. 2 – Architecture du régulateur de pilotage.

La philosophie de la régulation à 2 niveaux apparait donc maintenant :

1/ Le premier niveau permet de définir la réponse (δx_m , δu_m , δz_m) d'un modèle idéalisé de l'avion, linéaire et sans saturations de gouvernes. La dynamique en boucle fermée de ce système satisfait les spécifications de manœuvrabilité et de qualités de vol. Sa rapidité est dictée par les amplitudes de gouvernes souhaitées pour réaliser des manœuvres d'intensité moyenne ainsi que par les limitations concernant les facteurs de charge.

2/ Le deuxième niveau réalise un asservissement rapide du mouvement nonlinéaire de l'avion vers la réponse du modèle (1er niveau), en dépit d'erreurs de modèle (méconnaissance des coefficients aérodynamiques, variations de paramètres, couplages gyroscopiques, effets de la pesanteur, etc.) et des perturbations atmosphériques. On verra plus loin que cet asservissement est précis en ce qui concerne les variables de manœuvre (z, z_d) mais "souple" en ce qui concerne les autres variables d'état.

En l'absence de perturbations ou d'erreurs de modèle ou de linéarisation, donc au premier ordre, $\delta u = \delta u_m$: l'avion recopie donc l'évolution du modèle. En raison de sa dynamique rapide, le second niveau joue également un rôle d'anti-turbulence. Cependant, puisque ces gains rapides ne s'appliquent qu'aux écarts entre le mouvement de l'avion réel et les réponses modèle, ils n'ont pas pour effet d'entrainer la mise en saturation de toutes les gouvernes à la moindre sollicitation du manche par le pilote. Les actions respectives des deux niveaux sont illustrées sur la fig. 3.

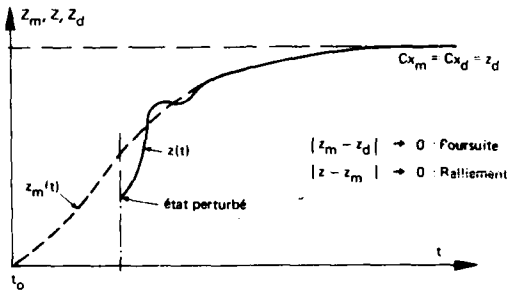

Fig. 3 – Distinction entre régulation de "poursuite" (1er niveau) et de "ralliement" (2ème niveau).

Ce partage des "responsabilités" entre les deux niveaux du régulateur de pilotage est apparemment la seule manière de résoudre le compromis impossible entre la satisfaction des spécifications de qualités de vol et l'usage de gains rapides, nécessaires au vol à haute incidence. On remarquera que l'architecture décrite est compatible non seulement avec l'usage de limiteurs d'incidence ou de facteurs de charge mais aussi avec le choix, pour le premier niveau, de lois de commande à double mode, c'est-à-dire munies de gains dépendant de l'intensité de la manœuvre affichée par le pilote.

Choix du point de linéarisation : Si le vol horizontal stabilisé a été retenu comme point de linéarisation pour les modèles (2) et (3) , ce choix est peu critique et n'est dicté que par des raisons de commodité. On n'exige en effet de ces modèles qu'un réalisme minimum rendant compte au premier ordre mais avec cohérence des relations de cause à effet existant entre les différentes variables du mouvement de l'avion non contrôlé ainsi que des évolutions relatives des différentes variables à l'occasion d'une manœuvre donnée de faible amplitude. On verra plus loin que les lois de commande proposées s'accommodent en réalité très bien d'écarts notables avec la dynamique réelle par suite d'erreurs sur certains coefficients ou à l'occasion de manœuvres de grande amplitude.

III. FORMULATION MATHEMATIQUE ET CALCUL DES LOIS DE COMMANDE

Considérant le modèle linéarisé (2) du premier niveau, la commande stabilisatrice δu_m, assurant la convergence de z_m vers z_d, est choisie de manière à minimiser la fonction de coût

$$J_m = \int_0^\infty \left[\delta x_m^T Q_1^m \delta x_m + (z_m - z_d)^T Q_2^m (z_m - z_d) + \delta u_m^T R^m \delta u_m \right] dt. \qquad (4)$$

La loi de commande est obtenue directement de la forme

$$\delta u_m = K_1^m \delta x_m + K_2^m \int_0^t (\delta z_m + z_0 - z_d) dt + \delta u_{m_0}. \qquad (5)$$

Les gains K_1^m et K_2^m sont tels que

$$\begin{bmatrix} K_1^m & K_2^m \end{bmatrix} \triangleq - (R^m)^{-1} \begin{bmatrix} B \\ 0 \end{bmatrix} P = - (R^m)^{-1} B \begin{bmatrix} P_{11} & P_{12} \end{bmatrix},$$

où

$$P \triangleq \begin{bmatrix} P_{11} & P_{12} \\ P_{12}^T & P_{22} \end{bmatrix}$$

est solution de l'équation matricielle de dimension (n+p)

$$PF + F^TP - PG(R^m)^{-1}G^TP + Q = 0, \tag{6}$$

avec $F = \begin{bmatrix} A & 0 \\ C & 0 \end{bmatrix}$, $G = \begin{bmatrix} B \\ 0 \end{bmatrix}$ et $Q = \begin{bmatrix} Q_1^m & 0 \\ 0 & Q_2^m \end{bmatrix}$.

δu_{m_0} est une quantité permettant optionnellement(+) d'initialiser optimalement les braquages des gouvernes en fonction de l'état initial $\delta x_m(0)$ et de la manœuvre commandée z_d, suivant

$$\delta u_{m_0} = -(B^TP_{11}B)^{-1}B^T\left\{\left[P_{11}(A+BK_1^m) + P_{12}C\right]\delta x_m(0) - P_{12}z_d\right\}$$

de manière à hâter les mouvements transitoires (cf. [6]).

Dans le cas considéré ici en ce qui concerne le choix du vecteur z, la paire matricielle (F,G) étant stabilisable et la paire (H,F) étant observable, où $H=\begin{bmatrix} 0_p & I_p \end{bmatrix}$, il suffit que Ker L $\subset$ Ker H, avec $L \triangleq Q^{\frac{1}{2}}$ pour qu'il existe une solution unique à l'équation (6), minimisant J_m et faisant tendre asymptotiquement $e'_m \triangleq H\left[\delta\dot{x}_m^T \; e_m^T\right]^T$ vers zéro et donc e_m vers z_d. Lorsque ces conditions ne sont pas verifiées, en particulier si la paire (F,G) n'est pas stabilisable, des tests spécifiques portant sur L, développés dans [6], permettent de s'assurer que e_m tend vers zéro.

Considérant maintenant le second niveau, c'est-à-dire la régulation proprement dite de l'avion, la commande δu qui stabilize le modèle linéarisé (3) est choisie de manière à minimiser la fonction de coût suivante

$$J_a = \int_0^\infty \left[\delta\dot{x}^TQ_1\delta\dot{x} + e^TQ_2e + \xi^TQ_3\xi + \delta u^TR\delta u\right]dt, \tag{7}$$

où $\xi = \dot{y} - A_ry$, $y = Dx$, $\delta x = x - x_m = x - \delta x_m - x_0$, $\delta u = u - u_m$, $e = z - z_m = z - \delta z_m - z_0$, et où A_r est une matrice stable arbitrairement choisie permettant de spécifier avec une facilité accrue un modèle (implicite) de convergence des réponses du système perturbé (1) vers les trajectoires à grande amplitude du modèle de poursuite (2) [7]. La loi de commande est de la forme

$$\delta u = \delta u_0 + K_1\delta x + K_2\int_0^t\left[g(x) - \delta z_m - z_0\right]d\tau, \tag{8}$$

où les matrices de gains K_1 et K_2 sont programmées et où la quantité δu_0 peut être prise égale à zéro si les intégrateurs de (8) sont initialisés de manière synchrone avec ceux de (5). La commande réellement appliquée à l'avion est bien sûr donnée par

$$u = \delta u + \delta u_m - u_0, \tag{9}$$

où u_0 est la commande nécessaire à l'équilibrage de l'avion au point de linéarisation choisi.

Les gains K_1 et K_2 de (8) sont tels que

$$\begin{bmatrix} K_1 & K_2 \end{bmatrix} = -R'^{-1}\left[S + G^TP\right],$$

où P est solution de l'équation matricielle de dimension (n+p)

$$PF' + F'^TP - PGR'^{-1}G^TP + Q - S^TR'^{-1}S = 0, \tag{10}$$

dans laquelle $F' = F - GR'^{-1}S$, $R' = R + B^TD^TQ_3DB$, $S = \begin{bmatrix} B^TD^TQ_3(DA-A_rD) & 0 \end{bmatrix}$,

$$Q = \begin{bmatrix} Q_1 + (DA-A_rD)^TQ_3(DA-A_rD) & 0 \\ 0 & Q_2 \end{bmatrix},$$

et où F et G sont telles que définies plus haut.

Un choix arbitraire des variables de consigne est possible, incluant des variables d'angle, de vitesse, d'accélération, un choix mixte sur les différents axes, voire des fonctions non-linéaires de ces variables. La formulation proposée pour le calcul de la loi de commande est donc compatible avec toutes les combinaisons de variables actuellement étudiées pour le pilotage par objectifs ("maneuver control") des avions modernes. Dans le cas considéré ici en ce qui concerne le choix de z, le système (3) étant stabilisable et observable du point de vue du triplet matriciel (H,F,G), il suffit que Ker L $\subset$ Ker H, avec $L = Q^{\frac{1}{2}}$, pour que (10) admette une solution P unique, minimisant J_a et faisant tendre asymptotiquement δx et e vers zéro (cf. [6]).

Du point de vue théorique, l'introduction de pénalités à la fois sur les dérivées des variables d'état et sur les dérivées des commandes est récente [8,9]. Les fonctions de coût quadratiques (4) et (7) convergent, même en cas d'erreurs ou de défaut de conformité du modèle. Les lois de commande qui en résultent sont telles que :

(+)Une logique d'initialisation des commandes et de remise à zéro des intégrateurs lorsque z_d a été modifié de manière significative étant encore en cours de mise au point, la valeur $u_{m_0}=0$ est prise dans les simulations présentées en Section IV.

1) la stabilité "en vitesse" du mouvement de l'avion perturbé, c'est-à-dire $\dot{x} \to 0$ quand $t \to \infty$ est assurée, et que

2) la convergence asymptotique (ralliement sans erreur) de $z=g(x)$ vers $z_m=g(\delta x_m+x_0)$ et donc de $z = g(x)$ vers $z_d(t)$ est réalisée,

ceci dans un large domaine de vol, qui n'est pas actuellement entièrement quantifié mais qui inclut des manœuvres mettant les gouvernes fréquemment en saturation.

On pourra bien sûr discuter de la nécessité de disposer de lois de commande précises pour le pilotage d'un avion. S'il est certain qu'une telle précision n'est pas requise dans la plupart des manœuvres rapides de l'avion (ex. interception ou combat tournoyant), elle est cependant désirable pour certaines tâches (ex. pointage d'armes, vol en formation, ravitaillement en vol, atterrissage ou apontage) qui exigent du pilote une attention et une charge de travail telles qu'il importe de lui faciliter la conduite du vol de l'avion.

La mise en œuvre des lois de commande (5 et (8-9) ne requiert pas la connaissance ds valeurs d'équilibre (l'équilibrage statique de l'avion est automatique). Cet aspect est secondaire pour le choix de la loi (5) puisque, par définition, le système dynamique du premier niveau est invariant et non perturbé ; le calcul des valeurs d'équilibre serait donc aisé (cf. [10]). Il est cependant d'une importance majeure pour la loi de commande du deuxième niveau. L'équilibrage automatique est particulièrement utile pour le passage en transsonique dans des positions variées et pour compenser les perturbations habituelles du vol. Enfin, en raison de la tolérance aux erreurs et variations de modèle, la loi (8) permet de réaliser des manœuvres de grande amplitude.

Parce que les lois de commande (5) et (8) sont obtenues directement et sans approximations algébriques comme dans certaines autres méthodes, les pénalités de J_m et J_a sont faciles à choisir et à adapter. Une démarche particulièrement facile consiste en effet à exploiter les relations de sensibilité entre les pôles du système contrôlé et les éléments des matrices de pénalité de la fonction de coût. On améliore ainsi un placement de poles initial en agissant, par une méthode de gradient, de manière coordonnée sur tous les éléments des matrices Q et R de J_m et de J_a (cf. [11-12]), ce que l'intuition seule ne peut parvenir à réaliser.

Relations de transfert : Avec les notations utilisées plus haut, la relation d'entrée-sortie du premier niveau s'exprime, dénotant les transformées de Laplace par des majuscules, définissant $Z_d = \mathcal{L}[\delta z_d = z_d - z_0]$, et avec $\delta u_{m_0} = \delta u_0 = 0$,

$$\delta X_m(s) = -T_1(s)\left[BK_2^m \delta Z_d(s) - s\delta x_m(0)\right],$$

avec

$$T_1(s) = \left[s^2 I - s(A+BK_1^m) - BK_2^m C\right]^{-1}.$$

De même, omettant δ_2, le deuxième niveau satisfait la relation de transfert

$$\delta X(s) = sT_2(s)\left\{\delta x(0) + \mathcal{L}[\delta_1]\right\},$$

$$T_2(s) = \left[s^2 I - s(A+BK_1) - BK_2 C\right]^{-1}.$$

Utilisant le fait que $\delta x = x - x_m = x - \delta x_m - x_0$, les écarts $\Delta x = x - x_0$ de l'état de l'avion par rapport au point de linéarisation satisfont l'équation

$$\Delta X(s) = -T_1(s)BK_2\,\delta Z_d(s) + sT_2(s)\left\{\mathcal{L}(\delta_1) + \Delta x(0) - \delta x_m(0)\right\} + sT_1(s)\,\delta x_m(0).$$

Il apparait donc clairement que le second niveau est totalement **TRANSPARENT** vis à vis des consignes δx_m (qui agissent bien à la manière d'un "feedforward") et que la convergence de z(t) vers $z_d(t)$ n'est conditionnée que par $T_1(s)$, c'est-à-dire par la dynamique du premier niveau. La dynamique du deuxième niveau n'intervient que dans la compensation des perturbations extérieures et des erreurs d'initialisation de la manœuvre. Elle peut donc être arbitrairement rapide, étant sans incidence sur les qualités de manœuvrabilité de l'avion.

Il apparait en outre que, du fait de la nature proportionnelle et intégrale des lois de commande qui crée des zéros de transmission bloqueurs, z(t) converge sans erreur vers $z_d(t)$ dans la mesure où les perturbations tendent vers $Z_d(s) - sC(BK_2C)^{-1}\mathcal{L}[\delta_1(t)]$. On réduira donc l'effet des erreurs de modèle ou des perturbations en accroissant le produit BK_2, ou du moins sa restriction au sous-espace observable par z.

IV - SIMULATION NUMERIQUE DE L'AVION CONTROLE

La méthodologie présentée dans les sections précédentes a été appliquée à un avion de combat relativement typique ($C_{m\alpha}$ =-0.3) muni de quatre (m=4) gouvernes dont une gouverne de force latérale directe, avec pour choix des variables d'objectifs (p=4)

$$z = \left[v,\ p_a,\ q,\ r\right]$$

où v, p_a, q et r dénotent respectivement la vitesse de dérapage, le taux de roulis autour du vecteur vitesse, la vitesse de tangage et la vitesse de lacet. En fonction des variables d'état, p_a s'exprime par la relation nonlinéaire $p_a = (pu + qv + rw) / V$,
où p, w et u dénotent respectivement la vitesse de roulis en axes avion, la composante normale de la vitesse (incidence) et la composante longitudinale de cette vitesse, avec $V=(u^2+v^2+w^2)^{\frac{1}{2}}$. Pour les besoins de la commande, le modèle dynamique retenu est d'ordre n=5 et comprend les variables $x = [v,w,p,q,r]$. Les variables u, ϕ (angle de roulis) et θ (assiette longitudinale) sont intégrées séparément.

Les simulations qui sont présentées ici se rapportent à un choix de matrices de pénalités des fonctions de coût J_m et J_a qui est donné dans le Tableau 1. Ces valeurs n'ont ici qu'une valeur indicative et ne sauraient être interprétées comme des conclusions ou des recommandations. Il en résulte pour le modèle de référence (premier niveau) des valeurs propres caractérisant le processus de poursuite qui sont données sur le Tableau 2. Outre les valeurs propres, le Tableau 2 contient aussi la matrice de projection M transformant la matrice $A_C^M = A - R^{m-1}GP$ sous la forme bloc-diagonale de Schur ; cette matrice indique donc comment se projettent les variables "canoniques" du mouvement contrôlé dans l'espace physique (variables canoniques $=x^e=Mx$). On observe par exemple que $\lambda_1 = \overline{\lambda_2}$ et λ_7 se rapportent au mouvement longitudinal seul et que le mouvement associé à λ_3 se projette principalement sur $(r_m - r_d)$ tout en ayant des composantes non nulles sur les autres variables du mouvement latéral.

Tableau 1 – Matrices de pénalité utilisées.

a) Premier niveau

$$Q_1^m = \begin{bmatrix} 1.0000E-04 & 0. & 0. & 0. & 0. \\ 0. & 1.0000E-04 & 0. & 0. & 0. \\ 0. & 0. & 1.0000E-03 & 0. & 0. \\ 0. & 0. & 0. & 1.0000E-03 & 0. \\ 0. & 0. & 0. & 0. & 1.0000E-03 \end{bmatrix}$$

$$Q_2^m = \begin{bmatrix} 1.0000E-03 & 0. & 0. & 0. \\ 0. & 1.0000E+01 & 0. & 0. \\ 0. & 0. & 1.0000E+02 & 0. \\ 0. & 0. & 0. & 1.0000E+04 \end{bmatrix}$$

$$R^m = \begin{bmatrix} 1.0000E+00 & 0. & 0. & 0. \\ 0. & 1.0000E+00 & 0. & 0. \\ 0. & 0. & 1.0000E+00 & 0. \\ 0. & 0. & 0. & 1.0000E+00 \end{bmatrix}$$

$$Q_1 = \begin{bmatrix} 1.0000E-04 & 0. & 0. & 0. & 0. \\ 0. & 1.0000E-04 & 0. & 0. & 0. \\ 0. & 0. & 1.0000E-03 & 0. & 0. \\ 0. & 0. & 0. & 1.0000E-03 & 0. \\ 0. & 0. & 0. & 0. & 1.0000E-03 \end{bmatrix}$$

$$Q_2 = \begin{bmatrix} 1.0000E-03 & 0. & 0. & 0. \\ 0. & 1.0000E+01 & 0. & 0. \\ 0. & 0. & 1.0000E+02 & 0. \\ 0. & 0. & 0. & 1.0000E+04 \end{bmatrix}$$

$$R = \begin{bmatrix} 1.0000E-01 & 0. & 0. & 0. \\ 0. & 1.0000E-01 & 0. & 0. \\ 0. & 0. & 1.0000E-01 & 0. \\ 0. & 0. & 0. & 1.0000E-01 \end{bmatrix}$$

$$D = \begin{bmatrix} 1.0000E+00 & 0. & 0. & 0. & 0. \\ 0. & 0. & 9.9870E-01 & 0. & 2.5840E-02 \\ 0. & 0. & 0. & 1.0000E+00 & 0. \\ 0. & 0. & 0. & 0. & 1.0000E+00 \end{bmatrix}$$

$$A_r = \begin{bmatrix} -5.0000E+00 & 0. & 0. & 0. \\ 0. & -3.0000E+00 & 0. & 0. \\ 0. & 0. & -1.2000E+00 & 0. \\ 0. & 0. & 0. & -1.5000E+00 \end{bmatrix}$$

b) Deuxième niveau

$$Q_3 = \begin{bmatrix} 1.0000E-04 & 0. & 0. & 0. \\ 0. & 1.0000E-04 & 0. & 0. \\ 0. & 0. & 1.0000E-04 & 0. \\ 0. & 0. & 0. & 1.0000E-04 \end{bmatrix}$$

Tableau 2 – Pôles du processus de poursuite (1er niveau).

i	$Re(\lambda_i)$	$Im(\lambda_i)$	EXPRESSION EN F DES VARIABLES D ETAT $\dot{v}_m$	$\dot{w}_m$	$\dot{p}_m$	$\dot{q}_m$	$\dot{r}_m$	e_v	e_p	e_q	e_r
1	-1.22E+01	1.23E+01	0.	2.95E-02	0.	1.86E+00	0.	0.	0.	2.47E+02	0.
2	-1.22E+01	-1.23E+01	0.	2.16E-02	0.	1.87E+01	0.	0.	0.	1.99E+02	0.
3	-1.05E+01	1.08E+01	1.31E-02	0.	-9.83E-02	0.	-5.90E+00	1.18E-02	-5.28E-02	0.	-2.55E+02
4	-1.05E+01	-1.08E+01	6.99E-03	0.	-6.52E-03	0.	-1.84E+01	5.98E-03	1.19E-01	0.	-1.30E+02
5	-3.38E+00	3.17E+00	1.49E-02	0.	4.90E-01	0.	1.43E+00	1.13E-02	8.74E+00	0.	2.62E+01
6	-3.38E+00	-3.17E+00	1.03E-02	0.	2.26E+00	0.	5.75E+00	7.04E-03	6.03E+00	0.	1.13E+01
7	-1.08E+00	0.	0.	9.71E-01	0.	-1.86E+00	0.	0.	0.	-2.46E+02	0.
8	-4.28E-01	3.63E-01	4.37E-03	0.	3.46E-01	0.	-3.65E-01	1.15E+00	1.94E+00	0.	-1.52E+01
9	-4.28E-01	-3.63E-01	3.09E+00	0.	-4.45E-01	0.	1.44E+01	1.29E+00	-1.82E+01	0.	7.06E+02

Les valeurs propres caractérisant le deuxième niveau, c'est-à-dire le régime perturbé de l'avion par rapport à la trajectoire commandée, sont indiquées dans le Tableau 3 côte-à-côte avec la matrice de projection de l'espace modal dans l'espace physique. On remarque que les pôles du deuxième niveau sont plus rapides que ceux du premier ; ils pourraient d'ailleurs l'être encore davantage en fonction des résultats de la simulation de l'avion en vol perturbé, actuellement en cours. Tous ces pôles sont facilement et séparément ajustables, la difficulté du problème résidant uniquement dans le choix d'une bonne configuration, ce qui constitue un problème non encore résolu.

Tableau 3 – Pôles du processus de ralliement (2e niveau).

i	$Re(\lambda_i)$	$Im(\lambda_i)$	EXPRESSION EN F DES VARIABLES D ETAT $\dot{v}$	$\dot{w}$	$\dot{p}$	$\dot{q}$	$\dot{r}$	e_v	e_p	e_q	e_r
1	-1.98E+01	1.66E+01	1.73E-02	0.	1.35E-02	0.	-5.23E+00	1.05E-02	4.10E-01	0.	2.43E+02
2	-1.98E+01	-1.66E+01	4.92E-03	0.	1.63E-02	0.	-8.48E+00	2.95E-03	1.24E-01	0.	-7.95E+01
3	-1.87E+01	1.87E+01	0.	2.78E-02	0.	1.34E+00	0.	0.	0.	2.41E+02	0.
4	-1.87E+01	-1.87E+01	0.	2.08E-02	0.	1.19E+01	0.	0.	0.	1.92E+02	0.
5	-5.87E+00	5.66E+00	-2.46E-03	0.	1.14E+00	0.	2.48E+00	-1.60E-03	3.87E-02	0.	-1.01E+01
6	-5.87E+00	-5.66E+00	-2.22E-02	0.	-1.18E+00	0.	-2.84E+00	-1.32E-02	-1.33E+01	0.	-3.02E+01
7	-1.39E+00	0.	2.34E+00	0.	-4.32E-01	0.	9.77E+00	1.59E+00	-1.28E+01	0.	4.65E+02
8	-1.08E+00	0.	0.	9.72E-01	0.	-1.33E+00	0.	0.	0.	-2.40E+02	0.
9	-6.78E-01	0.	1.65E+00	0.	-2.03E-01	0.	6.72E+00	2.33E+00	-8.11E+00	0.	3.34E+02

La Fig. 4 montre l'évolution de l'avion contrôlé à l'occasion d'une mise en roulis rapide (p_{a_d}= 90°/s autour du vecteur vitesse), à 230 m/s. Les différentes courbes montrent les évolutions respectives du premier niveau (trait discontinu) et du deuxième niveau (trait continu). Les mouvements périodiques des

gouvernes ont pour objet la compensation cyclique des effets de la pesanteur. Sur ces courbes comme sur les suivantes, les gains sont constants (non-programmés selon α).

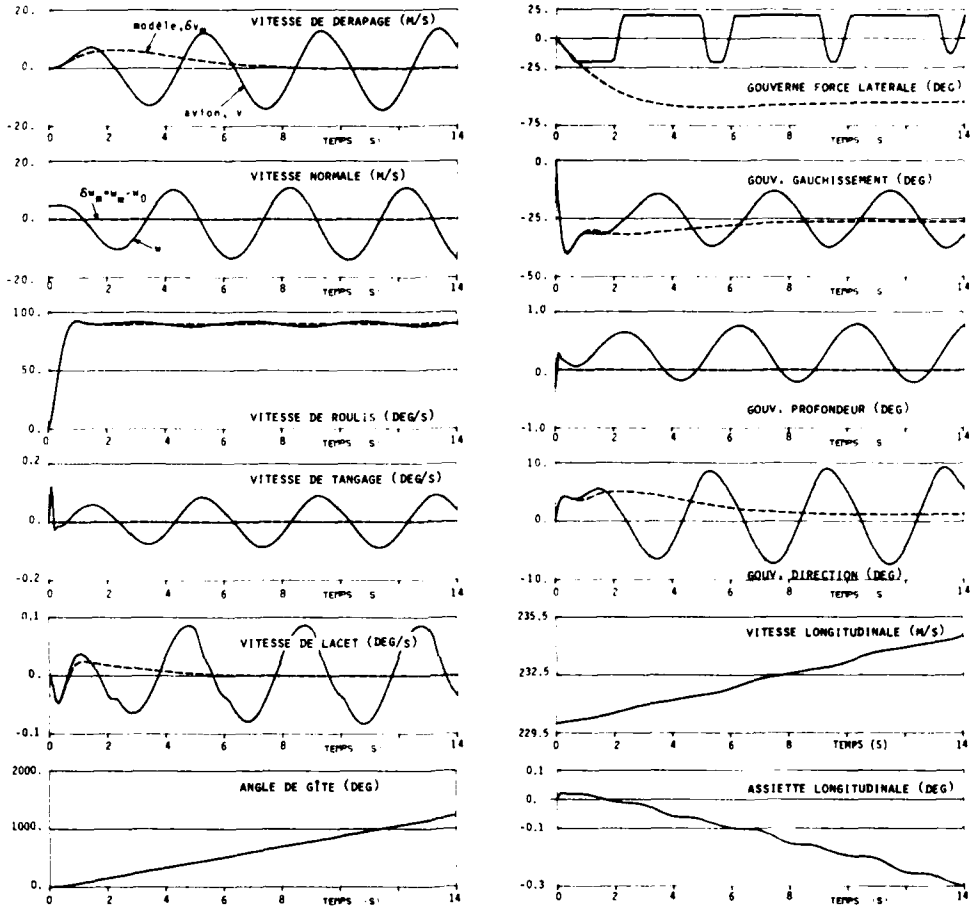

Fig. 4 – Simulation de l'avion contrôlé (commande de roulis constant).

La Fig. 5 montre l'évolution de l'avion contrôlé dans une manœuvre conjuguant un piqué constant (q_d=-10°/S, $t \in [0,7s]$) et une perturbation importante de roulis réalisée par le créneau p_{a_d}=-180°/s, $t \in [4.5,5s]$ et p_{a_d}=+180°/s, $t \in [5,5.5s]$. Dans cette situation, les vitesses angulaires de l'avion sont suffisantes pour le placer dans une situation instable d'auto-tonneau. Les évolutions des différentes courbes révèlent en effet de légères perturbations transitoires du mouvement de l'avion réel. Le fait que cette manœuvre était réellement instable pour l'avion non-contrôlé (en réalité, un point de bifurcation est dépassé [13]) est démontré sur la Fig. 6, où les commandes du mouvement latéral sont annulés après 6.5 secondes, les mouvements de grande amplitude de v,p et r ne disparaissant que lorsque q est ramené à zéro.

La Fig. 7 montre une mise en virage de l'avion. Les dernières simulations présentées concernent enfin le fonctionnement en mode dégradé, où une perturbation de roulis ($\Delta C_{l} = 1.5\times10^{-3}$) et de tangage ($\Delta C_m=4\times10^{-3}$) est appliquée à l'avion en même temps que le C_m est annulé (les gains étant calculés par rapport à la situation nominale de $C_{m\alpha}$ non nul). Il s'agit d'abord d'une manœuvre de roulis constant, représentée sur la Fig. 8, et que l'on comparera avec la Fig. 4. Il s'agit enfin de la manœuvre de piqué largement perturbée en roulis telle que déjà considérée ; elle est représentée sur la Fig. 9 que l'on comparera avec la Fig. 5 (cas non perturbé). Il résulte de ces comparaisons que l'avion contrôlé s'accommode de perturbations extérieures et d'erreurs importantes de modèle, de manière relativement transparente pour le pilote et en tous cas sans erreur pour les variables de réponse.

Des travaux actuels visent à montrer la tolérance de ces lois vis-à-vis de servo-gouvernes ou de capteurs à bande passante limitée ainsi qu'à accroitre cette tolérance. Avec les mêmes gains, la loi de commande considérée dans les simulations déjà décrites tolère ainsi la présence sur chaque canal d'une servo-gouverne modélisée comme un premier ordre ayant une fréquence de coupure de 4 Hz (pôle à -25.13). En deçà, sans être instable, l'avion sollicité pour les mêmes manoeuvres que celles qui ont été décrites est excessivement perturbé et difficilement pilotable. Des résultats complémentaires, incluant des simulations en présence de pertubations atmosphériques, seront présentés dans une prochaine publication.

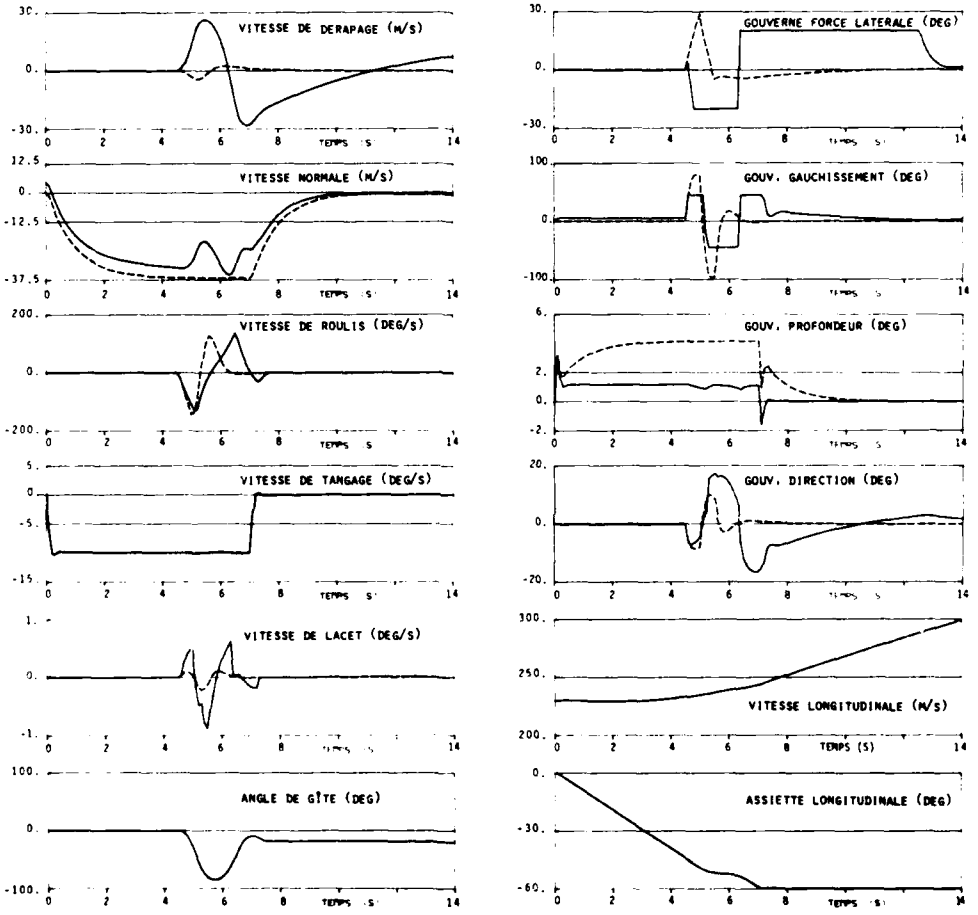

Fig. 5 – Simulation de l'avion contrôlé (mise en situation d'auto-tonneau en piqué).

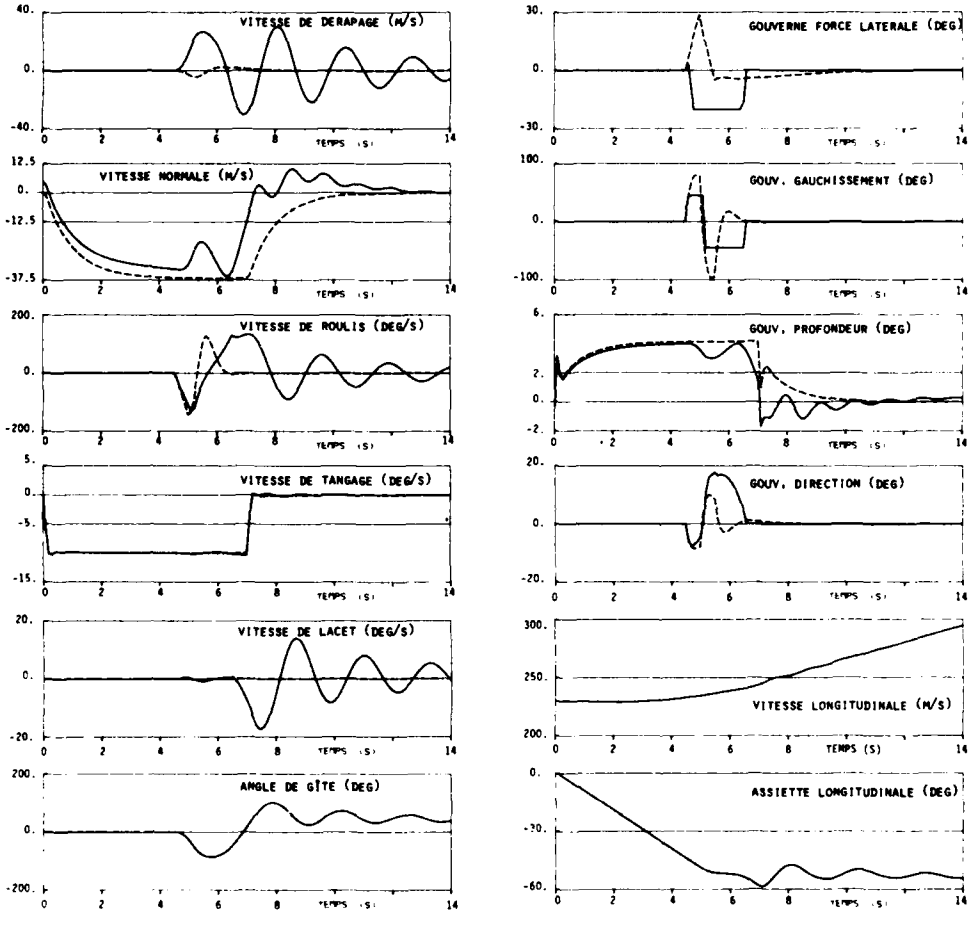

Fig. 6 – Simulation du mouvement de l'avion (mise en situation d'auto-tonneau, commandes latérales annulées après 6.5 s.

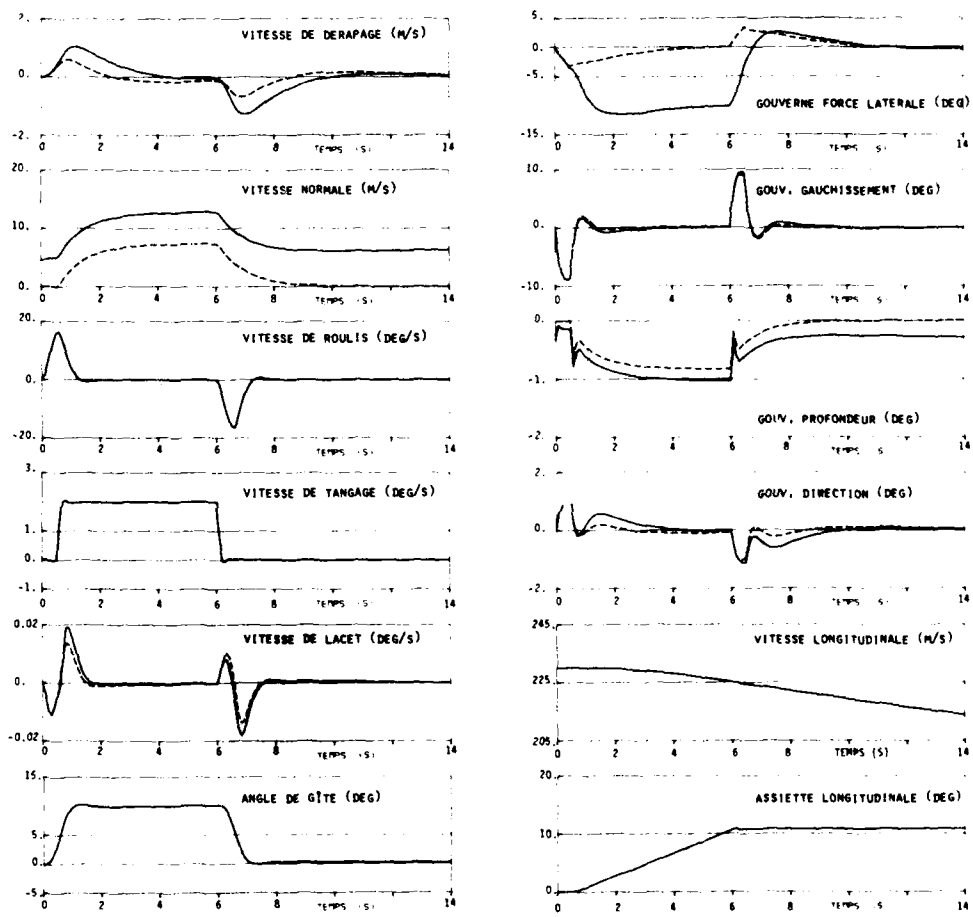

Fig. 7 – Simulation de l'avion contrôlé (virage commandé).

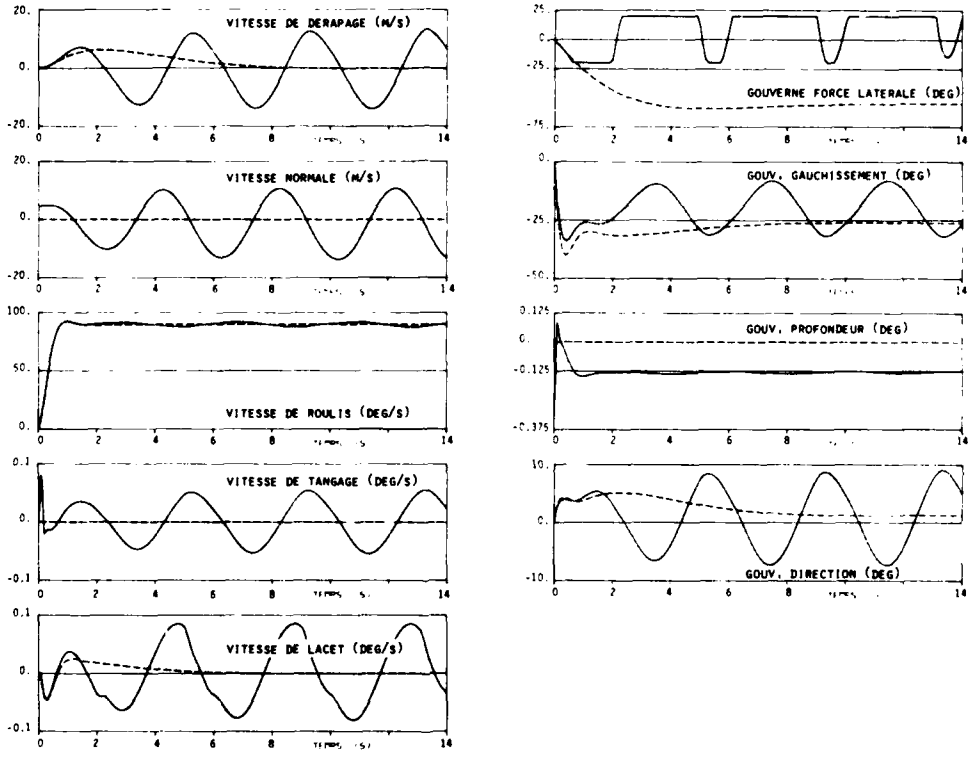

Fig. 8 – Simulation de l'avion contrôlé (commande de roulis constant avec erreur de modèle).

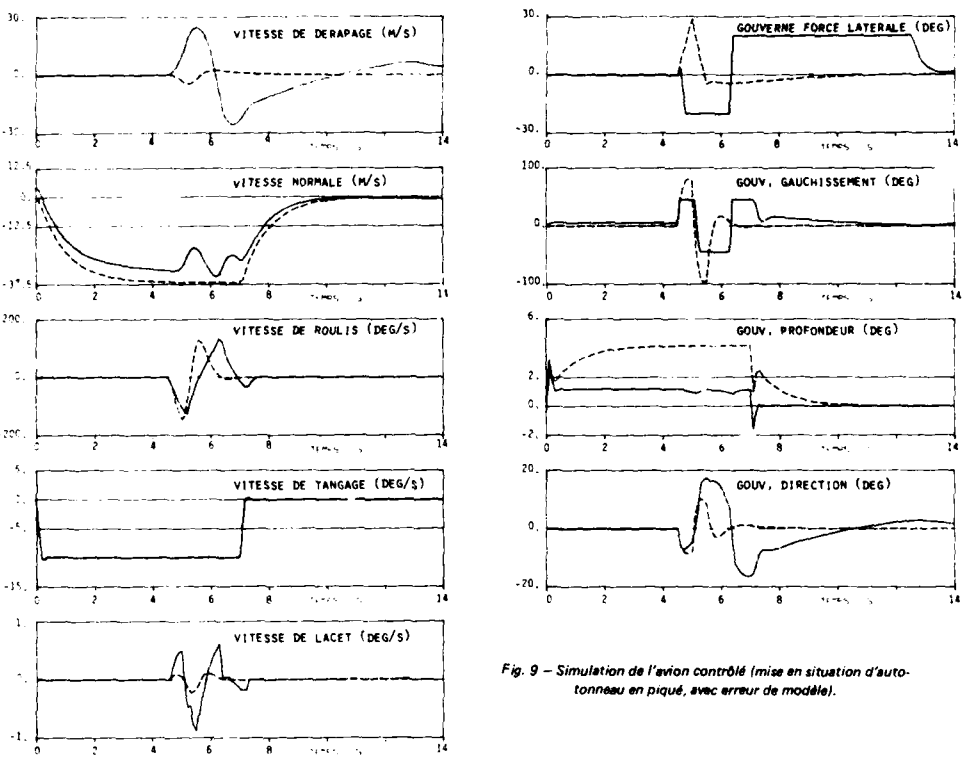

Fig. 9 – Simulation de l'avion contrôlé (mise en situation d'auto-tonneau en piqué, avec erreur de modèle).

V - CONCLUSION

Une philosophie de commande a été proposée pour les régulateurs de pilotage des avions de la prochaine génération. Elle permet de satisfaire à la fois les spécifications concernant les qualités de vol et celles qui concernent le rejet de perturbations extérieures. Un même régulateur, éventuellement au moyen de gouvernes additionnelles non-classiques, peut donc prendre en charge le pilotage multivariable et l'anti-turbulence sans que ces fonctions s'opposent (leur action non coordonnée réduit en effet le domaine de vol). Une méthodologie a été présentée pour faire la synthèse complète de ces lois de commande. Elles ont été illustrées par des simulations dans des manœuvres d'amplitude raisonnablement élevées faisant saturer plusieurs gouvernes et ceci en présence d'erreurs de modèle. Les simulations présentées ici se rapportent à un avion relativement classique, statiquement stable ; appliquées à un avion très manœuvrable, les performances observées sont évidemment bien supérieures. La mise en œuvre de ces lois requiert pour le premier niveau la programmation d'un système dynamique d'ordre 5 muni de gains programmés ; le second niveau se ramenant -quant à lui- à une simple "boite à gains", éventuellement programmés.

On remarquera enfin que la structure de ce régulateur de pilotage à deux niveaux s'insère parfaitement dans une chaîne plus complexe, par exemple pour réaliser une boucle de navigation. Ainsi, sur la Fig. 10, les sorties du régulateur de navigation peuvent consister en un vecteur de manœuvres désirées z_d, agissant comme affichage pour le régulateur de pilotage. Le sélecteur de mode représenté peut avoir pour entrées :

1) l'affichage par le manche ou le palonnier, pour le pilotage "toutes manœuvres",
2) les sorties d'un auto-pilote de navigation,
3) les sorties d'autres régulateurs spécialisés tels que les régulateurs de tir, cette dernière stratégie ayant été déjà décrite dans [14-15].

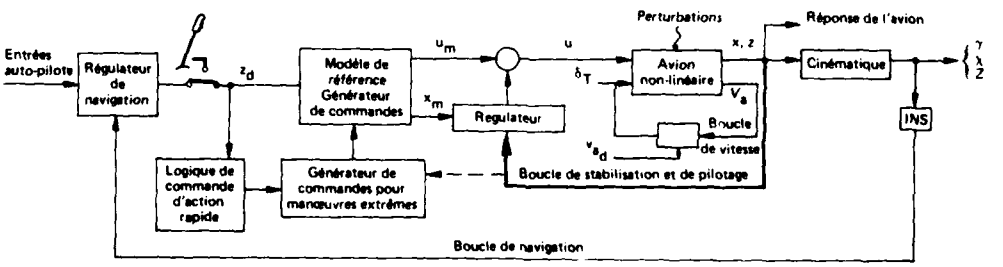

Fig. 10 – Coordination des boucles de pilotage et de navigation.

REFERENCES

1. Mercier, O.L. et Bourlès, H., Développement de lois de pilotage multivariables robustes pour les avions futurs. Rapport Technique ONERA n° 4/7224 SY, Décembre 1981.

2. Bourlès, H., et Mercier, O.L., Marges de stabilité et robustesse structurelle généralisées des régulateurs linéaires-quadratiques multivariables, Revue RAIRO Automatique, Vol. 16, 1, Janvier 1982, 49-70.

3. Tiroshi, I., et Elliott, J.R., Explicit Model Following Control Scheme Incorporating Integral Feedback. J. Aircraft, Vol. 11, 6, Juin 1974, 364-366.

4. Tyler, J.S., Jr. The Characteristics of Model-following Systems as Synthesized by Optimal Control. IEEE Trans., Vol. AC-9, 5, Octobre 1964, 485-498.

5. Trankle, T.L. et Bryson, A.E., Jr. Control Logic to Track Outputs of a Command Generator, J. Guidance and Control, Vol. 1, 2 Mars-Avril 1978, 130-135.

6. Bourlès, H., et Mercier, O.L., La régulation de poursuite optimale quadratique multivariable des systèmes linéaires perturbés, Revue RAIRO Automatique, Vol. 16, 4, Octobre 1982.

7. Kreindler, E., et Rothschild, D., Model-Following in Linear-Quadratic Optimization. AIAA Journal, Vol. 14, Juillet 1976, 835-842.

8. Sandell, N.R., et Athans, M., On type-L multivariable linear systems. Automatica, Vol. 9, 1, Janvier 1973, 131-136.

9. Gustafsson, S.E., A theory for optimal P.I. control of multivariable linear systems. Acta Polytechnica Scandinavica, Math. and Comp. Sci. Series, Helsinki, 17, 1975.

10. Kirszenblat, A., Calcul d'un système de commande à deux niveaux du mouvement nonlinéaire d'un avion. Note Technique ONERA n° 1979-7, Septembre 1979 ; ESA Tech. Transl. TT-614.

11. Mercier, O.L., Gradients et sensibilités asociés aux problèmes de commande linéaires-quadratiques-gaussiens. Rapport Technique n° 1/3534 SN, 1982.

12. Mercier, O.L., Joannic, Y., et Moreigne, O., Mise au point interactive des régulateurs linéaires-quadratiques par action directe et sélective sur les pôles du système contrôlé. Accepté pour publication, Symp. d'Informatique Appliquée de l'IASTED, 15-17 Mars 1983, Lille (France).

13. Guicheteau, P., Application de la théorie des bifurcations à l'étude des pertes de contrôle sur avion de combat. Proc. AGARD-FMP Symp. "Combat Aircraft Manoeuvrability", Florence, 5-8 Octobre 1981, La Recherche Aérospatiale, n° 2, Mars-Avril 1982, 61-73.

14. Dang Vu, B., Multivariable aircraft control by manoeuvre commands. An application to air-to-ground gunnery. Proc. 12e Congrès ICAS, Munich, RFA, 12-17 Octobre 1980.

15. Dang Vu , B., Pilotage d'un avion par objectifs. Application au tir canon air-sol. La Recherche Aérospatiale, n° 3, Mai-Juin 1981, 149-159.

MICROPROCESSOR IMPLEMENTATION OF FAST-SAMPLING DIRECT DIGITAL FLIGHT-MODE CONTROLLERS

Prof B Porter, Dr A Bradshaw, Dr A Garis, and Dr M A Woodhead
Department of Aeronautical and Mechanical Engineering
University of Salford
Salford M5 4WT
England

SUMMARY

The general results of Bradshaw and Porter [1],[2] are extended to allow for a computational time-delay of up to one sampling period by a simple modification of the control algorithms. The resulting control algorithms are simple to implement and provide tight non-interacting control. Their efficiency and effectiveness are demonstrated by the presentation of the results of a laboratory microprocessor implementation in which the controllers are required to effect fuselage pitch pointing and vertical translation manoeuvres in the case of an analogue computer representation of the YF-16 aircraft.

1. INTRODUCTION

The general results of Bradshaw and Porter [1],[2] for discrete-time tracking systems indicate that tight non-interacting control is, in general, achievable by the implementation of fast-sampling error-actuated controllers. Indeed, the efficiency and effectiveness of such controllers has been demonstrated by their application to the YF-16 aircraft where they are required to effect fuselage pitch pointing and vertical translation manoeuvres [3]. Implicit in these controllers, however, was the assumption that the computational time delay is small compared with the sampling period. In some cases, this assumption may not be valid and it is necessary to compensate for the time delay. Indeed, if no such compensation is provided the resulting tracking system will have either very poor performance or will be unstable.

The general results of Bradshaw and Porter [1],[2] can be extended to allow for a computational time delay of one sampling period if the control algorithm is appropriately modified. The resulting control algorithms are simple to implement and provide tight non-interacting control. Their efficiency and effectiveness are demonstrated by the presentation of the results of a laboratory microprocessor implementation in which the controllers are required to effect fuselage pitch pointing and vertical translation manoeuvres in the case of an analogue computer representation of the YF-16 aircraft.

2. DISCRETE-TIME TRACKING SYSTEMS WITH FINITE TIME-DELAY COMPENSATION

2.1 System Configuration

In general, high-performance discrete-time tracking systems with finite time-delay compensation consist of linear multivariable plants governed on the continuous-time set $T = [0,+\infty)$ by state, output, and measurement equations of the respective forms

$$\begin{bmatrix}\dot{x}_1(t)\\ \dot{x}_2(t)\end{bmatrix} = \begin{bmatrix}A_{11} & A_{12}\\ A_{21} & A_{22}\end{bmatrix}\begin{bmatrix}x_1(t)\\ x_2(t)\end{bmatrix} + \begin{bmatrix}0\\ B_2\end{bmatrix}u(t) \quad , \tag{1}$$

$$y(t) = [C_1 \ , \ C_2]\begin{bmatrix}x_1(t)\\ x_2(t)\end{bmatrix} \quad , \tag{2}$$

and

$$w(t) = [F_1 \ , \ F_2]\begin{bmatrix}x_1(t)\\ x_2(t)\end{bmatrix} \quad , \tag{3}$$

together with fast-sampling error-actuated digital controllers governed on the discrete-time set $T_T = \{0,T,2T,\ldots\}$ by control-law equations of the form

$$s(kT) = f\{K_0 e(kT)+K_1 z(kT)\} \tag{4}$$

and computational time-delay compensation equations of the form

$$r(kT) = s(kT) - \gamma r\{(k-1)T\} \tag{5}$$

where

$$e(kT) = v(kT) - w(kT) \quad , \tag{6}$$

and

$$z(kT) = z(o) + T\sum_{j=0}^{j=k-1} e(jT) \quad . \tag{7}$$

In equations (1) to (7), $x_1(t) \in R^{n-\ell}$, $x_2(t) \in R^{\ell}$, $u(t) \in R^{\ell}$, $y(t) \in R^{\ell}$, $w(t) \in R^{\ell}$, $A_{11} \in R^{(n-\ell)x(n-\ell)}$, $A_{12} \in R^{(n-\ell)x\ell}$, $A_{21} \in R^{\ell x(n-\ell)}$, $A_{22} \in R^{\ell x\ell}$, $B_2 \in R^{\ell x\ell}$, $C_1 \in R^{\ell x(n-\ell)}$, $C_2 \in R^{\ell x\ell}$, $F_1 \in R^{\ell x(n-\ell)}$, $F_2 \in R^{\ell x\ell}$, rank $C_2B_2 < \ell$, rank $F_2B_2 = \ell$, $r(kT) \in R^{\ell}$, $s(kT) \in R^{\ell}$, $v(kT) \in R^{\ell}$, $e(kT) \in R^{\ell}$, $z(kT) \in R^{\ell}$, $K_o \in R^{\ell x\ell}$, $K_1 \in R^{\ell x\ell}$, $f = 1/T$ is the sampling frequency, and $\gamma \in R$ is the delay compensation parameter. Since the computational time delay is one sampling period, the digital controller is required to generate the control input vector

$$u(t) = r\{(k-1)T\} \ , \ t \in [kT,(k+1)T) \ , \ kT \in T_T \quad , \tag{8}$$

so as to cause the output vector $y(t)$ to track any constant command input vector $v(t)$ on T_T in the sense that

$$\lim_{k\to\infty}\{v(kT)-y(kT)\} = 0 \tag{9}$$

as a consequence of the fact that the error vector $e(t) = v(t) - w(t)$ assumes the steady-state value

$$\lim_{k\to\infty} e(kT) = \lim_{k\to\infty}\{v(kT)-w(kT)\} = 0 \tag{10}$$

for arbitrary initial conditions. In case

$$[F_1 \ , \ F_2] = [C_1+MA_{11} \ , \ C_2+MA_{12}] \quad , \tag{11}$$

it is evident from equations (2), (3), and (11) that the vector

$$w(t) - y(t) = [MA_{11} \ , \ MA_{12}]\begin{bmatrix} x_1(t) \\ x_2(t) \end{bmatrix} \tag{12}$$

of extra measurements is such that $v(kT)$ and $y(kT)$ satisfy the tracking condition (9) for any $M \in R^{\ell x(n-\ell)}$ if $e(kT)$ satisfies the steady-state condition (10), since equation (1) clearly implies that

$$\lim_{t\to\infty}[A_{11} \ , \ A_{12}]\begin{bmatrix} x_1(t) \\ x_2(t) \end{bmatrix} = 0 \tag{13}$$

in any steady state. However, the condition that rank $F_2B_2 = \ell$ requires that C_2 and A_{12} are such that M can be chosen so that

$$\text{rank } F_2 = \text{rank}(C_2+MA_{12}) = \ell \quad . \tag{14}$$

If the control input vectors are stored in the manner of Koepcke [4] by introducing the extra state variables

$$q\{(k+1)T\} = Tu(kT) \quad , \tag{15}$$

then it is evident from equations (1) to (7) and (15) that such discrete-time tracking systems are governed on T_T by state and output equations of the respective forms

$$\begin{bmatrix} z\{(k+1)T\} \\ x_1\{(k+1)T\} \\ x_2\{(k+1)T\} \\ q\{(k+1)T\} \end{bmatrix} = \begin{bmatrix} I_\ell \ , & -TF_1 \ , & TF_2 \ , & 0 \\ 0 \ , & \Phi_{11} \ , & \Phi_{12} \ , & f\Psi_1 \\ 0 \ , & \Phi_{21} \ , & \Phi_{22} \ , & f\Psi_2 \\ K_1 \ , & -K_oF_1 \ , & -K_oF_2 \ , & -\gamma I_\ell \end{bmatrix}\begin{bmatrix} z(kT) \\ x_1(kT) \\ x_2(kT) \\ q(kT) \end{bmatrix} + \begin{bmatrix} TI_\ell \\ 0 \\ 0 \\ K_o \end{bmatrix} v(kT) \tag{16}$$

and

$$y(kT) = [0 \ , \ C_1 \ , \ C_2 \ , \ 0]\begin{bmatrix} z(kT) \\ x_1(kT) \\ x_2(kT) \\ q(kT) \end{bmatrix} \quad , \tag{17}$$

where

$$\begin{bmatrix} \Phi_{11} \ , & \Phi_{12} \\ \Phi_{21} \ , & \Phi_{22} \end{bmatrix} = \exp\left\{\begin{bmatrix} A_{11} \ , & A_{12} \\ A_{21} \ , & A_{22} \end{bmatrix}T\right\} \tag{18}$$

and

$$\begin{bmatrix}\Psi_1\\ \Psi_2\end{bmatrix} = \int_0^T \exp\left\{\begin{bmatrix}A_{11} & A_{12}\\ A_{21} & A_{22}\end{bmatrix}t\right\}\begin{bmatrix}0\\ B_2\end{bmatrix}dt \quad . \tag{19}$$

2.2 System Analysis

The transfer function matrix relating the plant output vector to the command input vector of the closed-loop discrete-time tracking system governed by equations (16) and (17) is clearly

$$G(\lambda) = [0 \ , \ C_1 \ , \ C_2 \ , \ 0]\begin{bmatrix}\lambda I_\ell - I_\ell & , & TF_1 & , & TF_2 & , & 0\\ 0 & , & \lambda I_{n-\ell} - \Phi_{11} & , & -\Phi_{12} & , & -f\Psi_1\\ 0 & , & -\Phi_{21} & , & \lambda I_\ell - \Phi_{22} & , & -f\Psi_2\\ -K_1 & , & K_0F_1 & , & K_0F_2 & , & \lambda I_\ell + \gamma I_\ell\end{bmatrix}^{-1}\begin{bmatrix}TI_\ell\\ 0\\ 0\\ K_0\end{bmatrix} \tag{20}$$

and the fast-sampling tracking characteristics of this system can accordingly be elucidated by invoking the results of Porter and Shenton [5] from the singular perturbation analysis of transfer function matrices. Indeed, since it follows from equations (18) and (19) that

$$\lim_{f\to\infty} f\begin{bmatrix}\Phi_{11} - I_{n-\ell} & , & \Phi_{12}\\ \Phi_{21} & , & \Phi_{22} - I_\ell\end{bmatrix} = \begin{bmatrix}A_{11} & , & A_{12}\\ A_{21} & , & A_{22}\end{bmatrix} \tag{21}$$

and

$$\lim_{f\to\infty} f\begin{bmatrix}\Psi_1\\ \Psi_2\end{bmatrix} = \begin{bmatrix}0\\ B_2\end{bmatrix} \quad , \tag{22}$$

these results indicate that as $f \to \infty$ the transfer function matrix $G(\lambda)$ assumes the asymptotic form

$$\Gamma(\lambda) = \tilde{\Gamma}(\lambda) + \hat{\Gamma}(\lambda) \tag{23}$$

where

$$\tilde{\Gamma}(\lambda) = C_o(\lambda I_n - I_n - TA_o)^{-1}TB_o \quad , \tag{24}$$

$$\hat{\Gamma}(\lambda) = C_2(\lambda(\lambda+\gamma-1)I_\ell - \gamma I_\ell - A_4)^{-1}B_2K_o \quad , \tag{25}$$

$$A_o = \begin{bmatrix}-K_o^{-1}K_1 & , & 0\\ A_{22}F_2^{-1}K_o^{-1}K_1 & , & A_{11} - A_{12}F_2^{-1}F_1\end{bmatrix}, \tag{26}$$

$$B_o = \begin{bmatrix}0\\ A_{12}F_2^{-1}\end{bmatrix} \quad , \tag{27}$$

$$C_o = [C_2F_2^{-1}K_o^{-1}K_1 \ , \ C_1 - C_2F_2^{-1}F_1] \quad , \tag{28}$$

and

$$A_4 = -B_2K_oF_2 \quad . \tag{29}$$

It follows from equations (23), (24), and (26) that the 'slow' modes $\mathcal{I}_s$ of the tracking system correspond as $f \to \infty$ to the poles $\mathcal{I}_1 \cup \mathcal{I}_2$ of $\Gamma(\lambda)$ where

$$\mathcal{I}_1 = \{\lambda \in C : |\lambda I_\ell - I_\ell + TK_o^{-1}K_1| = 0\} \tag{30}$$

and

$$\mathcal{I}_2 = \{\lambda \in C : |\lambda I_{n-\ell} - I_{n-\ell} - TA_{11} + TA_{12}F_2^{-1}F_1| = 0\} \quad , \tag{31}$$

and from equations (23), (25), and (29) that the 'fast' modes $\mathcal{I}_f$ of the tracking system correspond as $f \to \infty$ to the poles $\mathcal{I}_3$ of $\hat{\Gamma}(\lambda)$ where

$$\mathcal{I}_3(\lambda) = \{\lambda \in C : |\lambda(\lambda+\gamma-1)I_\ell - \gamma I_\ell + F_2B_2K_o| = 0\} \quad . \tag{32}$$

Furthermore, it follows from equations (24), (26), (27), and (28) that the 'slow' transfer function matrix

$$\tilde{\Gamma}(\lambda) = (C_1 - C_2F_2^{-1}F_1)(\lambda I_{n-\ell} - I_{n-\ell} - TA_{11} + TA_{12}F_2^{-1}F_1)^{-1}TA_{12}F_2^{-1} \tag{33}$$

and from equations (25) and (29) that the 'fast' transfer function matrix

$$\hat{\Gamma}(\lambda) = C_2F_2^{-1}(\lambda(\lambda+\gamma-1)I_\ell - I_\ell + F_2B_2K_o)^{-1}F_2B_2K_o \quad . \tag{34}$$

It is evident from these results that the computational time-delay has no affect on the 'slow' modes as $f \to \infty$ but that the 'fast' modes are crucially affected as $f \to \infty$. Indeed, in case no time-delay compensation is used so that $\gamma = 0$, it is evident from equation (32) that at least some of the 'fast' modes will be unstable.

2.3 System Synthesis

It is evident from equations (11), (13), (16), and (17) that tracking will occur in the sense of equation (9) provided only that

$$Z_s \cup Z_f \subset \mathcal{D}^- \tag{35}$$

where $\mathcal{D}^-$ is the open unit disc. In view of equations (30), (31), and (32), the 'slow' and 'fast' modes will satisfy the tracking requirement (35) for sufficiently small sampling periods T, the time-delay compensation parameter γ and the controller matrices K_0, K_1, and M are chosen such that $Z_1 \subset \mathcal{D}^-$, $Z_2 \subset \mathcal{D}^-$, and $Z_3 \subset \mathcal{D}^-$. Indeed, if full time-delay compensation is employed, $\gamma = 1$ and stability of the 'fast' modes is assured by requiring that

$$F_2 B_2 K_0 = \mathrm{diag}(\sigma_1, \sigma_2, \ldots, \sigma_\ell) \tag{36}$$

where $1-\sigma_j \in R \cap \mathcal{D}^-$ $(j=1,2,\ldots,\ell)$. Moreover, if in addition M is chosen such that both $\tilde{\Gamma}(\lambda)$ and $\hat{\Gamma}(\lambda)$ are diagonal transfer function matrices, then it is evident that increasingly non-interacting tracking will occur as $f \to \infty$.

3. DIRECT DIGITAL FLIGHT-MODE CONTROL SYSTEMS WITH FINITE TIME-DELAY COMPENSATION

3.1 Vertical Translation Manoeuvre

In the vertical translation manoeuvre, the linearised longitudinal dynamics of the YF-16 aircraft flying at a Mach number of 0.8 at sea level are governed on T by state and output equations of the respective forms [3]

$$\begin{bmatrix} \dot{x}_1(t) \\ \dot{x}_2(t) \\ \dot{x}_3(t) \end{bmatrix} = \begin{bmatrix} 0 & 1 & 0 \\ 0 & -2.068 & 10.029 \\ 0 & 0.985 & -2.155 \end{bmatrix} \begin{bmatrix} x_1(t) \\ x_2(t) \\ x_3(t) \end{bmatrix} + \begin{bmatrix} 0 & 0 \\ -35.44 & -5.124 \\ -0.238 & -0.308 \end{bmatrix} \begin{bmatrix} u_1(t) \\ u_2(t) \end{bmatrix} \tag{37}$$

and

$$\begin{bmatrix} y_1(t) \\ y_2(t) \end{bmatrix} = \begin{bmatrix} 1 & 0 & 0 \\ 0 & 0 & 1 \end{bmatrix} \begin{bmatrix} x_1(t) \\ x_2(t) \\ x_3(t) \end{bmatrix} \tag{38}$$

where $x_1(t)$ is the change in pitch angle, $x_2(t)$ is the rate of change of pitch angle, $x_3(t)$ is the change in angle of attack, $u_1(t)$ is the elevator deflection, and $u_2(t)$ is the flaperon deflection. Hence, in case $\{\sigma_1,\sigma_2\} = \{1,1\}$, $\gamma = 1$, $K_1 = K_0$, and

$$M = \begin{bmatrix} 0.25 \\ 0 \end{bmatrix} , \tag{39}$$

it follows from equations (3), (8), and (36) that the corresponding transducers and fast-sampling error-actuated digital controllers with finite time-delay compensation are governed on T and T_T by the respective measurement and control-law equations

$$\begin{bmatrix} w_1(t) \\ w_2(t) \end{bmatrix} = \begin{bmatrix} 1 & 0.25 & 0 \\ 0 & 0 & 1 \end{bmatrix} \begin{bmatrix} x_1(t) \\ x_2(t) \\ x_3(t) \end{bmatrix} \tag{40}$$

and

$$\begin{bmatrix} u_1(kT) \\ u_2(kT) \end{bmatrix} = f\left\{ \begin{bmatrix} -0.127 & 0.528 \\ 0.098 & -3.655 \end{bmatrix} \begin{bmatrix} e_1(kT) \\ e_2(kT) \end{bmatrix} + \begin{bmatrix} -0.127 & 0.528 \\ 0.098 & -3.655 \end{bmatrix} \begin{bmatrix} z_1(kT) \\ z_2(kT) \end{bmatrix} \right\} - \begin{bmatrix} u_1\{(k-1)T\} \\ u_2\{(k-1)T\} \end{bmatrix} . \tag{41}$$

It is evident from equations (30), (31), and (32) that $Z_1 = \{1-T, 1-T\}$, $Z_2 = \{1-4T\}$, and $Z_3 = \{0,0\}$. It is also evident from equations (23), (33), and (34) that the asymptotic transfer function matrix assumes the diagonal form

$$\Gamma(\lambda) = \begin{bmatrix} \frac{4T}{\lambda-1+4T} & , & 0 \\ 0 & , & \frac{1}{\lambda^2} \end{bmatrix} \tag{42}$$

and therefore that the direct digital flight-mode control system for the vertical translation manoeuvre of the aircraft, with a time delay of one sampling period in the implementation of the control action, will exhibit increasingly non-interacting tracking behaviour as $f \to \infty$ when the piecewise-constant control input vector $[u_1(t) \ , \ u_2(t)]^T = [u_1(kT) \ , \ u_2(kT)]^T$, $t \in [kT,(k+1)T)$, $kT \in \mathcal{T}_T$, is generated by the fast-sampling digital controller governed on $\mathcal{T}_T$ by equation (41).

3.2 Fuselage Pitch Pointing Manoeuvre

In the fuselage pitch pointing manoeuvre, the linearised longitudinal dynamics of the YF-16 aircraft flying at a Mach number of 0.8 at sea level are governed on $\mathcal{T}$ by state and output equations of the respective forms [3]

$$\begin{bmatrix} \dot{x}_1(t) \\ \dot{x}_2(t) \\ \dot{x}_3(t) \end{bmatrix} = \begin{bmatrix} 0 & , & 1 & , & 0 \\ 0 & , & -2.068 & , & 10.029 \\ 0 & , & 0.985 & , & -2.155 \end{bmatrix} \begin{bmatrix} x_1(t) \\ x_2(t) \\ x_3(t) \end{bmatrix} + \begin{bmatrix} 0 & , & 0 \\ -35.44 & , & -5.124 \\ -0.238 & , & -0.308 \end{bmatrix} \begin{bmatrix} u_1(t) \\ u_2(t) \end{bmatrix} \tag{43}$$

and

$$\begin{bmatrix} y_1(t) \\ y_2(t) \end{bmatrix} = \begin{bmatrix} 1 & , & 0 & , & 0 \\ 1 & , & 0 & , & -1 \end{bmatrix} \begin{bmatrix} x_1(t) \\ x_2(t) \\ x_3(t) \end{bmatrix} \tag{44}$$

where $x_1(t)$ is the change in pitch angle, $x_2(t)$ is the rate of change of pitch angle, $x_3(t)$ is the change in angle of attack, $u_1(t)$ is the elevator deflection, and $u_2(t)$ is the flaperon deflection. Hence, in case $\{\sigma_1,\sigma_2\} = \{1,1\}$, $K_1 = K_0$, and

$$M = \begin{bmatrix} 0.25 \\ 0 \end{bmatrix}, \tag{45}$$

it follows from equations (3), (8), and (36) that the corresponding transducers and fast-sampling error-actuated digital controllers with finite time-delay compensation are governed on $\mathcal{T}$ and $\mathcal{T}_T$ by the respective measurement and control-law equations

$$\begin{bmatrix} w_1(t) \\ w_2(t) \end{bmatrix} = \begin{bmatrix} 1 & , & 0.25 & , & 0 \\ 1 & , & 0 & , & -1 \end{bmatrix} \begin{bmatrix} x_1(t) \\ x_2(t) \\ x_3(t) \end{bmatrix} \tag{46}$$

and

$$\begin{bmatrix} u_1(kT) \\ u_2(kT) \end{bmatrix} = f\left\{ \begin{bmatrix} -0.127 & , & 0.528 \\ 0.098 & , & -3.655 \end{bmatrix} \begin{bmatrix} e_1(kT) \\ e_2(kT) \end{bmatrix} + \begin{bmatrix} -0.127 & , & 0.528 \\ 0.098 & , & -3.655 \end{bmatrix} \begin{bmatrix} z_1(kT) \\ z_2(kT) \end{bmatrix} \right\} - \begin{bmatrix} u_1\{(k-1)T\} \\ u_2\{(k-1)T\} \end{bmatrix} . \tag{47}$$

It is evident from equations (30), (31), and (32) that $\mathcal{Z}_1 = \{1-T,1-T\}$, $\mathcal{Z}_2 = \{1-4T\}$, and $\mathcal{Z}_3 = \{0,0\}$. It is also evident from equations (23), (33), and (34) that the asymptotic transfer function matrix assumes the diagonal form

$$\Gamma(\lambda) = \begin{bmatrix} \frac{4T}{\lambda-1+4T} & , & 0 \\ 0 & , & \frac{1}{\lambda^2} \end{bmatrix} \tag{48}$$

and therefore that the direct digital flight-mode control system for the fuselage pitch pointing manoeuvre of the aircraft, with a time delay of one sampling period in the implementation of the control action, will exhibit increasingly non-interacting tracking behaviour as $f \to \infty$ when the piecewise-constant control input vector $[u_1(t) \ , \ u_2(t)]^T = [u_1(kT) \ , \ u_2(kT)]^T$, $t \in [kT,(k+1)T)$, $kT \in \mathcal{T}_T$, is generated by the fast-sampling digital controller governed on $\mathcal{T}_T$ by equation (47).

4. LABORATORY MICROPROCESSOR IMPLEMENTATION STUDIES

4.1 Apparatus

The laboratory apparatus [6] for the study of the microprocessor implementation of such controllers consists of an EAI180 analogue computer for the simulation of a linearised model of the plant (equations (37) and (38) or (43) and (44)), a microprocessor system based on the M6800 MPU for the computation of the controller equations, and a data-acquisition system for data handling and processing between the controller and the plant.

The microprocessor system is focussed upon the M68SAC1 Stand Alone Computer module. This module provides the user with a means of efficiently interfacing the MPU to peripheral devices through an Mc6850 ACIA or an Mc6820 PIA depending upon the data-format required. In addition, this module is interfaced with an external memory module, MM568103, of 2K RAM and an arithmetic processor unit module, M68MM14, to improve the efficiency of the arithmetic manipulations.

The data-acquisition system consists of a high-level A/D module, M68MM15A, and an analogue output D/A module, MP7104. Both these modules include multiplexers, amplifiers, filters, and sample and hold circuits.

4.2 Vertical Translation Manoeuvre

The simulated behaviour of the YF-16 aircraft in the vertical translation mode when controlled in accordanced with equation (41) is shown in Fig 1 when the command input vector is 'ramped up' in 2 sec to the steady value $[v_1(t) \ , \ v_2(t)]^T = [0 \ , \ 2]^T$ deg. In these tests, a sampling period of 0.05 sec is used and it is evident that high-accuracy non-interacting tracking behaviour is achieved despite the time delay of one sampling period in the control action. Furthermore, it is apparent from Fig 1 that the vertical translation manoeuvre is effected without the use of excessive transient control surface deflections.

4.3 Fuselage Pitch Pointing Manoeuvre

The simulated behaviour of the YF-16 aircraft in the fuselage pitch pointing mode when controlled in accordance with equation (47) is shown in Fig 2 when the command input vector is 'ramped up' in 1 sec to the steady value $[v_1(t) \ , \ v_2(t)]^T = [2 \ , \ 0]^T$ deg. In these tests, a sampling period of 0.05 sec is used and it is evident that high-accuracy non-interacting tracking behaviour is achieved despite the time delay of one sampling period in the control action. Furthermore, it is apparent from Fig 2 that the fuselage pitch pointing manoeuvre is effected without the use of excessive transient control surface deflections.

5. CONCLUSION

The general results of Bradshaw and Porter [1],[2] have been extended to allow for a computational time delay of up to one sampling period by a simple modification of the control algorithms. The resulting control algorithms are simple to implement and provide tight non-interacting control. Their efficiency and effectiveness have been demonstrated by the presentation of the results of a laboratory microprocessor implementation in which the controllers were required to effect fuselage pitch pointing and vertical translation manoeuvres in the case of an analogue computer representation of the YF-16 aircraft.

6. REFERENCES

[1] A Bradshaw and B Porter, "Singular perturbation methods in the design of tracking systems incorporating fast-sampling error-actuated controllers", Int J Systems Sci, Vol 12, 1981, pp 1181-1191.

[2] A Bradshaw and B Porter, "Singular perturbation methods in the design of tracking systems incorporating inner-loop compensators and fast-sampling error-actuated controllers", Int J Systems Sci, Vol 12, 1981, pp 2107-1220.

[3] B Porter and A Bradshaw, "Design of direct digital flight-mode control systems for high-performance aircraft", Proc IEEE National Aerospace and Electronics Conference, Dayton, USA, May 1981.

[4] R W Koepcke, "On the control of linear systems with pure time-delay", Trans ASME J of Basic Engineering, Vol 87, 1965, pp 74-80.

[5] B Porter and A T Shenton, "Singular perturbation analysis of the transfer function matrices of a class of multivariable linear systems", Int J Control, Vol 21, 1975, pp 655-660.

[6] A Garis, "Fast-sampling direct digital flight-mode control systems", PhD Thesis, University of Salford, 1981.

7. ACKNOWLEDGEMENT

This research was sponsored by the Air Force Flight Dynamics Laboratory, AFWAL/FIGL, Wright-Patterson AFB, United States Air Force, under Contract F49620-81-C-0026.

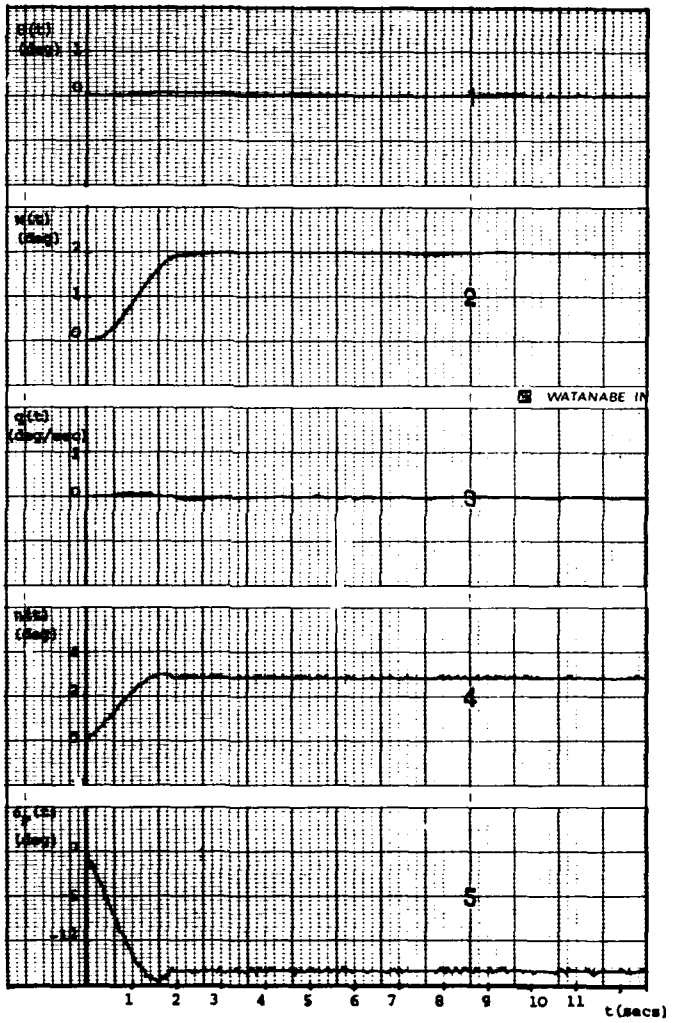

FIGURE 1

Vertical Translation Mode , T = 1/20 secs
Time-delay of 1/20 secs in the control action
Flight condition: M = 0.8 at sea level

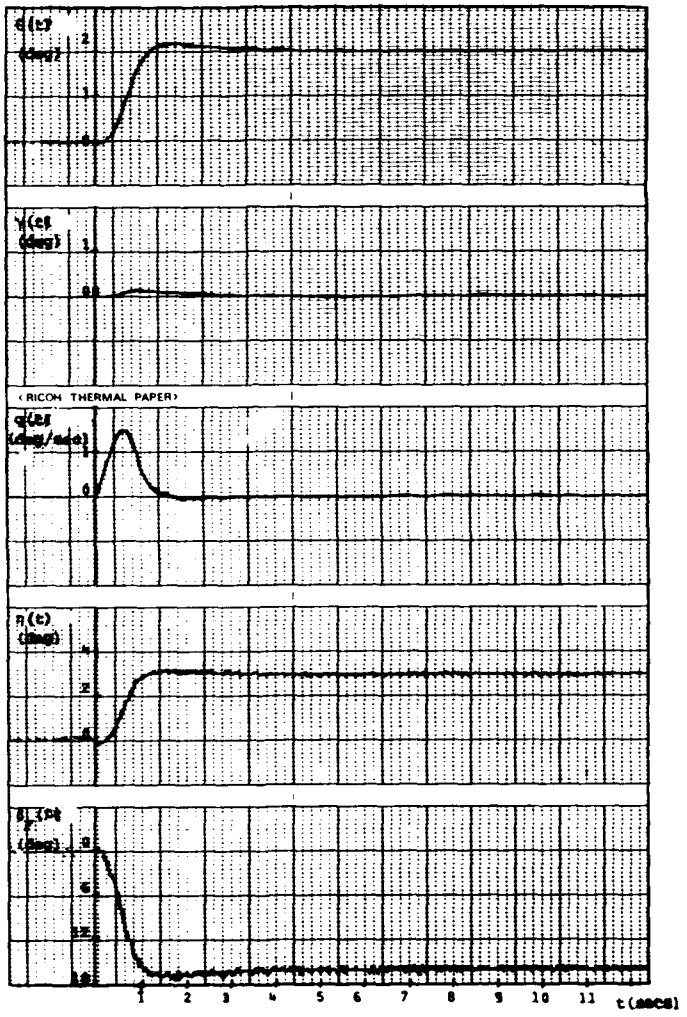

FIGURE 2
Pitch Pointing Mode , T = 1/20 secs
Time-delay of 1/20 secs in the control action
Flight condition: M = 0.8 at sea level

DESIGN OF A HELICOPTER AUTOPILOT BY MEANS OF LINEARIZING TRANSFORMATIONS

G. Meyer, R. L. Hunt, and R. Su
NASA Ames Research Center, Moffett Field, California, U.S.A., 94035

SUMMARY

A method for designing automatic flight control systems for aircraft that have complex characteristics and operational requirements, such as the powered-lift STOL and V/STOL configurations, is presented. The method is effective for a large class of dynamic systems that require multiaxis control and that have highly coupled nonlinearities, redundant controls, and complex multidimensional operational envelopes. The method exploits the possibility of linearizing the system over its operational envelope by transforming the state and control. The linear canonical forms used in the design are described, and necessary and sufficient conditions for linearizability are stated. The control logic has the structure of an exact model follower with linear decoupled model dynamics and possibly nonlinear plant dynamics. The design method is illustrated with an application to a helicopter autopilot design.

1. INTRODUCTION

Consider in general terms the control-system design problem. Let us take the usual hardware/software model of the problem in which the hardware consists of the plant together with all the sensors and actuators which are connected to a digital computer, and in which the software embodies the complete control strategy. The hardware is fixed; we may change only the software, over which, however, we have full control. So one may say that since the underlying physical process is to remain fixed, only its representation may be changed. If this point of view is taken, then much of the control-system design problem may be interpreted in terms of transformations.

This paper outlines a design approach that is being developed from the transformations point of view, and describes an application to the control of a helicopter. This approach, first outlined in Ref. 1, has been applied to several aircraft of increasing complexity, and the completely automatic flight-control system was first tested on a DHC-6. The reference trajectory used in the flight test exercised a substantial part of the operational envelope of the aircraft. Despite disturbances and variations in plant dynamics, the system performed well (see Ref. 2). Next, the technique was applied to the Augmentor Wing Jet STOL Research aircraft, the successful flight tests of which are reported in Ref. 3. Methods for providing pilot inputs to this design were examined in Ref. 4, and application of the scheme to the control of an A-7 aircraft for carrier landing and testing in manned simulation is reported in Refs. 5 and 6. The design method is currently being applied to the UH-1H helicopter, again with the substantial portion of the operational envelope of this aircraft being used.

The key concept of the approach is to simplify the representation of the plant dynamics by means of a change of coordinates of the state and control. The design proceeds in three steps. First, the given nonlinear system – possibly time-varying, multiaxis, and cross-coupled – is transformed into a constant, decoupled linear representation. Second, standard linear and nonlinear design techniques, such as Bode plots, pole placement, LQG, and phase plane, are used to design a control law for this simple representation. And third, the resulting control law is transformed back out into the original coordinates to obtain the control law in terms of the available controls.

The mathematical foundation for the approach is provided by modern differential geometry, the necessary and sufficient conditions for linearizing have been established, and the theory is given in Refs. 7-15.

2. CANONICAL FORM

Suppose that the given natural representation S_1 of the physical process is given by the state x_1, control u_1, and field f_1,

$$\dot{x}_1 = f_1(x_1,u_1) \tag{1}$$

and that we wish to change S_1 into S_2 with state x_2, control u_2, and field f_2,

$$\dot{x}_2 = f_2(x_2,u_2) \tag{2}$$

This change will be accomplished, and hence a large part of the design problem solved, once we construct the appropriate transformations of the state and control,

$$x_2 = T(x_1) \tag{3a}$$

$$u_1 = W(x_1,u_2) \tag{3b}$$

which relate S_1 to S_2 so that for all admissible (x_1,u_2),

$$\frac{\partial T}{\partial x_1}(x_1) f_1[x_1,W(x_1,u_2)] = f_2[T(x_1),u_2] \tag{4}$$

The function W is the control law.

The construction of the transformation (T,W) is often greatly simplified by the introduction of an intermediate canonical representation S_0 as shown in Fig. 1. To obtain (T_{12},W_{12}), which links S_1 to S_2, both S_1 and S_2 are first transformed into the canonical representation S_0. Then

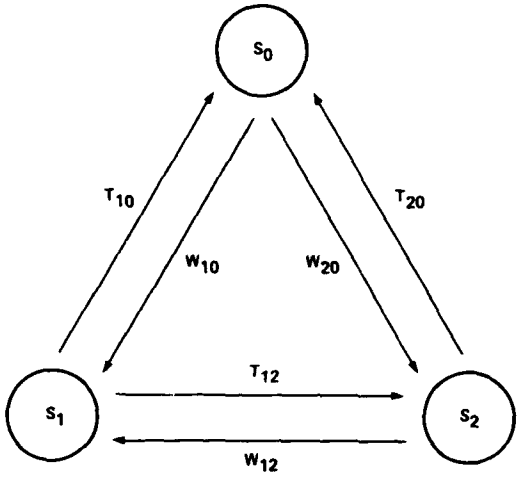

Fig. 1. Manipulation of system representations.

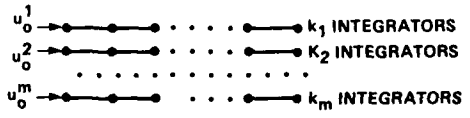

Fig. 2. Diagram of Brunovsky form.

$$T_{12} = T_{20}^{-1}T_{10} \tag{5a}$$

$$W_{12} = W_{10}W_{20}^{-1} \tag{5b}$$

In the design procedure being described, the Brunovsky form (Ref. 14) is taken to be canonical. In linear theory this form is basic. It consists of decoupled strings of integrators which may be diagrammed as shown in Fig. 2 where each dot represents a scalar integrator.

The number of strings, which may be of different lengths, equals the number of controls which itself equals the number of Kronecker indexes $k_1 \geq k_2 \geq \ldots \geq k_m$. The lengths of the ith string is given by k_i and the dimension of the state space

$$n = \sum_{i=1}^{m} k_i \ .$$

Let the canonical state $x_0 \in R^n$ control $u_0 \in R^m$, and denote the canonical field f_0 by

$$\dot{x}_0 = A_0x_0 + B_0u_0 \tag{6}$$

According to linear theory any constant, linear, controllable system may be viewed as a nonsingular transformation of an appropriate Brunovsky form. Thus, if S_1 is given by the state $x_1 \in R^n$, control $u_1 \in R^m$, and field

$$\dot{x}_1 = A_1x_1 + B_1u_1 \tag{7}$$

with controllable (A_1,B_1), then there is a Brunovsky form that can be transformed into S_1 by means of nonsingular transformations (T,W nonsingular)

$$x_1 = T^{-1}x_0 \tag{8a}$$

$$u_1 = Wu_0 + Qx_1 \tag{8b}$$

Of course, S_0 may also be transformed into nonlinear and time-varying systems without any loss of information by allowing the transformations in Eq. (8) to be nonlinear and time-varying but still nonsingular:

$$x_1 = T^{-1}(x_0,t) \tag{9a}$$

$$u_1 = W(x_1,u_0,t) \tag{9b}$$

This fact gives rise to our design procedure. When presented with a nonlinear system S_1, the first step is to try to linearize the system over its whole operational envelope by constructing (T,W) which maps S_1 into S_0. Then a control law is synthesized for the much simpler S_0. Finally, the S_0 control law is transformed into the coordinates of S_1 to obtain the control law for S_1.

3. TRANSFORMABILITY

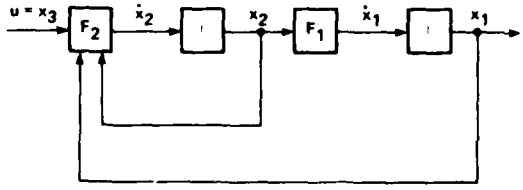

Fig. 3. An example of a block triangular system.

A class of systems particularly amenable to this approach has the following form. The control $u \in R^m$, the state $x \in R^m \times R^m \times \ldots \times R^m$ and the field f is without transmission zeroes and invertible. An example is shown in Fig. 3. In this example, the state $x \in R^m \times R^m$, the control $u \in R^m$, and the field f,

$$\left.\begin{aligned} \dot{x}_1 &= F_1(x_1,x_2,t) \\ \dot{x}_2 &= F_1(x_1,x_2,u,t) \end{aligned}\right\} \tag{10}$$

and F_1 and F_2 are invertible relative to $(x_2,\dot{x}_1)$ and $(u,\dot{x}_2)$. That is, functions h_1 and h_2 can be constructed so that if

$$\left.\begin{aligned} x_2 &= h_1(x_1,\dot{x}_1,t) \\ u &= h_2(x_1,x_2,\dot{x}_2,t) \end{aligned}\right\} \tag{11}$$

then

$$\left.\begin{aligned} F_1[x_1,h_1(x_1,\dot{x}_1,t),t] &= \dot{x}_1 \\ F_2[x_1,x_2,h_2(x_1,x_2,\dot{x}_2,t),t] &= \dot{x}_2 \end{aligned}\right\} \tag{12}$$

on the operational envelope. Because of the form of Eq. (10), such systems will be called block-triangular.

For this example, the canonical form S_0 has m Kronecker indexes, all equal to 2. The state $x^\circ \in R^m \times R^m$, the control $u^\circ \in R^m$, and the field,

$$\left.\begin{aligned} \dot{x}_1^\circ &= x_2^\circ \\ \dot{x}_2^\circ &= u^\circ \end{aligned}\right\} \tag{13}$$

The map linking Eq. (10) with Eq. (13) may be obtained by letting $x_1 = x_1^\circ(t)$ and pushing, as it were, the time-history $x_1^\circ(t)$ upstream through f to obtain $u(t)$. Thus,

$$\left.\begin{aligned} x_1 &= x_1^\circ \\ \dot{x}_1 &= \dot{x}_1^\circ = x_2^\circ \\ x_2 &= h_1(x_1^\circ, x_2^\circ, t) \\ \dot{x}_2 &= \frac{\partial h_1}{\partial x_1} x_2^\circ + \frac{\partial h_1}{\partial x_2} u^\circ + \frac{\partial h_1}{\partial t} \\ u &= h_2(x_1^\circ, x_2^\circ, \dot{x}_2, t) \end{aligned}\right\} \tag{14}$$

In general, the canonical form S_0 of a block triangular S_1 will have m Kronecker indexes, all equal to n/m where n is the dimension of the state space of S_1.

This procedure of constructing the linearizing transformations will fail if S_1 does have transmission zeroes. In that case, one obtains differential equation constraints on u, thereby destroying its status as an independent control variable. Nevertheless, such systems may still be linearizable. For example, the scalar system

$$\begin{pmatrix} \dot{x}_1 \\ \dot{x}_2 \\ \dot{x}_3 \end{pmatrix} = \begin{pmatrix} x_2 \\ x_3 \\ 0 \end{pmatrix} + \begin{pmatrix} -x_3 \\ 0 \\ 1 \end{pmatrix} u \tag{15}$$

is linearized by the transformation

$$\left.\begin{aligned} x_1^\circ &= x_1 + \frac{1}{2}(x_3)^2 \\ x_2^\circ &= x_2 \\ x_3^\circ &= x_3 \\ u &= u^\circ \end{aligned}\right\} \tag{16}$$

On the other hand it will be shown that the system

$$\begin{pmatrix} \dot{x}_1 \\ \dot{x}_2 \\ \dot{x}_3 \end{pmatrix} = \begin{pmatrix} x_2 \\ x_3 \\ 0 \end{pmatrix} + \begin{pmatrix} -x_2 \\ 0 \\ 1 \end{pmatrix} u \tag{17}$$

is not linearizable; the nonlinearity in this case is intrinsic and cannot be removed by a change of coordinates. The conditions under which linearization is possible are summarized next.

Let $x \in R^n$, $u \in R^m$, and the field

$$\dot{x} = F(x,u) \tag{18}$$

There are four conditions for this system to be linearizable. First, it is necessary to be able to construct a new control variable, ϕ,

$$\left.\begin{aligned} \phi &= h^{-1}(x,u) \\ u &= h(x,\phi) \end{aligned}\right\} \tag{19}$$

so that ϕ enters linearly into the field:

$$F[x,h(x,\phi)] = f(x) + \sum_{i=1}^{m} g_i(x)\phi_i \tag{20}$$

The remaining three conditions are technical, and they are best expressed by means of Lie brackets defined as follows. If f and g are C^∞ vector fields on R^n, the Lie bracket of f and g is

$$[f,g] = \frac{\partial g}{\partial x} f - \frac{\partial f}{\partial x} g \tag{21}$$

and we set

$$(ad^{0}f,g) = g$$

$$(ad^{1}f,g) = [f,g]$$

$$(ad^{2}f,g) = [f,[f,g]]$$

$$\vdots$$

$$(ad^{k}f,g) = [f,(ad^{k-1}f,g)]$$

A collection of C^{∞} vector fields $h_1,h_2,\ldots,h_r$ on R^n is involutive if there exist C^{∞} functions γ_{ijk} with

$$[h_i,h_j] = \sum_{k=1}^{r} \gamma_{ijk} h_k \,, \quad 1 \le i \,, \quad j \le r \,, \quad i \ne j$$

Now, suppose that we wish to transform Eq. (20) into S_0 with Kronecker indexes $k_1 \ge k_2 \ge \ldots \ge k_m$. Define the sets

$$C = \{g_1,[f_1g_1],\ldots,(ad^{k_1-1}f_1g_1),$$
$$g_2,[f_1g_2],\ldots,(ad^{k_2-1}f_1g_2),$$
$$\ldots\ldots\ldots\ldots\ldots\ldots$$
$$g_m,[f_1g_m],\ldots,(ad^{k_m-1}f_1g_m)\}$$

$$C_j = \{g_1,[f_1g_1],\ldots,(ad^{k_j-2}f_1g_1),$$
$$g_2,[f_1g_2],\ldots,(ad^{k_j-2}f_1g_2),$$
$$\ldots\ldots\ldots\ldots\ldots\ldots$$
$$g_m,[f_1g_m],\ldots,(ad^{k_j-2}f_1g_m)\}; \quad \text{for} \quad j = 1, 2, \ldots, m$$

Then it can be shown that the transformation is possible if and only if at each admissible x,

1. The set of C spans an n-dimensional space
2. Each C_j is involutive for $j = 1, 2, \ldots, m$
3. The span of C_j equals the span of $C_j \cap C$ for $j = 1, 2, \ldots, m$

For a linear field, $\dot{x} = Ax + Bu$, the spanning condition (1) or C is equivalent to controllability, rank $(B, AB, \ldots, A^{n-1}B) = n$. The other conditions are automatically satisfied. The new coordinate surface $T_i(x) =$ constant in a plane through the origin in the old state space. For nonlinear field, $T_i(x) =$ constant will be a general surface. The involutivity condition (2) guarantees that this surface is constructible from local conditions (integrability theorem of Frobenius).

Suppose we wish to transform system (17) into S_0 with $k = 3$. Here the set $C = \{g,[f,g],(ad^2f,g)\}$ spans R^3. But the $C_1 = \{g,[f,g],[g,[f,g]]\}$ also spans R^3; therefore, system (17) is not transformable into S_0. For further details on the transformation theory see Refs. 7-15. Let us turn our attention next to the control structure in which these ideas of transformability may be implemented in practical cases.

4. EXACT MODEL FOLLOWER

If the plant S_1 is equivalent to a system S_2 in the sense that each can be transformed into the other by nonsingular transformations, then one may construct an exact model follower in which the plant S_1 will, except for disturbances, follow exactly the system S_2, which is interpreted as being the model. Let the system representing the tracking error be denoted by S_3. The three systems, are related to each other and to the Brunovsky form S_0 as shown in Fig. 4.

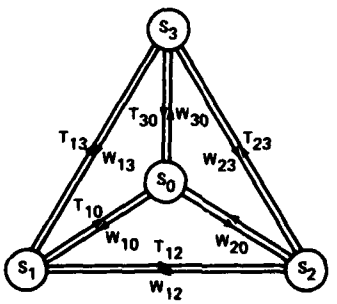

Fig. 4. Plant S_1, model S_2, and regulator S_3.

Now consider the structure of the model follower as shown in Fig. 5. There are five subsystems: model servo, regulator, plant, and two transformations. The desired system behavior is defined in the model servo. The model servo law may be nonlinear, time-varying, and dynamic. The TW-map (T_{23},W_{23}) transforms the S_2 system

$$\dot{x}_2^m = f_2(x_2^m,u_2^m) \tag{22}$$

into S_3,

$$\dot{x}_3^m = f_3(x_3^m,u_3^m) \tag{23}$$

The TW-map (T_{13},W_{13}) transforms the plant S_1

$$\dot{x}_1 = f_1(x_1,u_1) \tag{24}$$

into S_3

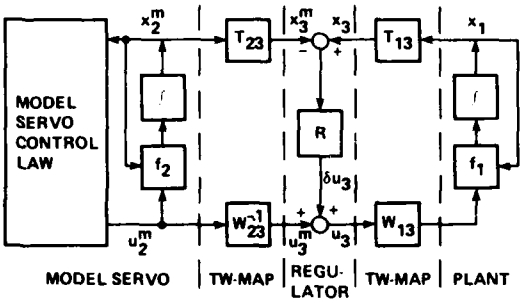

Fig. 5. Structure of the model follower.

$$\dot{x}_3 = f_3(x_3,u_3) \tag{25}$$

That is, when seen through the TW-map (T_{13},W_{13}) in terms of (x_3,u_3), the plant looks like Eq. (25); which is also how the model looks through the TW-map (T_{23},W_{23}).

In the absence of disturbances and with proper initialization of the model (i.e., $x_2^m(0) = T_{12}[x_1(0$ the plant will follow the model exactly in the sense that the error defined by

$$e_3 = x_3 - x_3^m \tag{26}$$

will be zero for $t \geq 0$. In a realistic situation, disturbances, say, d, are present, and they are controlled by means of the regulator which transforms the tracking error e_3 into corrective control δu_3. The error dynamics are given by

$$\dot{e}_3 = f_3(x_3,u_3) - f_3(x_3^m,u_3^m) \tag{27}$$

which for small errors simplifies to

$$\dot{e} = \frac{\partial f_3}{\partial x_3} e_3 + \frac{\partial f_3}{\partial u_3} \delta u_3 + d$$

In particular, if S_3 is chosen to coincide with S_0, so that $f_3 = f_0$, then without approximation,

$$\dot{e}_0 = A_0 e_0 + B_0 \delta u_0 + d \tag{28}$$

It may be noted that the regulator need not be gain-scheduled; that function is accomplished automatically by the TW-map.

This completes the outline of the design approach. Consider next an application to a helicopter.

5. THE PLANT-A HELICOPTER

The helicopter will be represented by a rigid body moving in three-dimensional space in response to gravity, aerodynamics, and propulsion. The state,

$$x = (r,v,C,\omega)^T \in X \subset R^3 \times R^3 \times SO(3) \times R^3 \tag{29}$$

where r and v are the inertial coordinates of body center-of-mass position and velocity, respectively, and C is the direction cosine matrix of the body-fixed axes relative to the runway-fixed axes (taken to be inertial). The attitude C moves on the sphere SO(3). The body coordinates of angular velocity are represented by ω.

The controls,

$$u = (u^M,u^P)^T \in U \subset R^3 \times R \tag{30}$$

where u^M is the three-axis moment control, that is, roll cyclic and pitch cyclic, which tilt the main-rotor thrust, and the tail-rotor collective, which controls the yaw moment; and u^P is the main-rotor collective, which controls the main-rotor thrust.

The effectively 12-dimensional state equation consists of the translational and rotational kinematic and dynamic equations:

$$\left.\begin{aligned} \dot{r} &= v \\ \dot{v} &= f^F(x,u) \\ \dot{C} &= S(\omega)C \\ \dot{\omega} &= f^M(x,u) \end{aligned}\right\} \tag{31}$$

where f^F and f^M are the total force and moment generation processes, and (x,u) are defined by Eqs. (29) and (30). This is the natural representation S_1 of the helicopter.

Consider next the transformation of Eqs. (31) into a Brunovsky form S_0 by means of the transformations $u = W(x,u_0)$ and $x_0 = T(x)$.

6. THE TW-MAP

In general, the moment generation process f^M is invertible with respect to the pair $(\dot{\omega},u^M)$, and for the restricted class of maneuvers being considered in this experiment (i.e., no 360° rolls), f^F is invertible with respect to the pair $(\dot{v}_3,u^P)$. Thus, in the present case for the set of angular and vertical acceleration commands restricted to the set

$$U_{\dot{\omega}} = \{(\dot{\omega}_i,\dot{v}_3) : |\dot{\omega}_i| \le 1.0 \text{ rad/sec}^2, \quad i = 1,2,3, \ |\dot{v}_3| \le 0.5 \text{ g}\} \tag{32}$$

a function $h^M: X \times U_{\dot{\omega}} \to U$ can be constructed so that if

$$u = h^M[x,(\dot{\omega}_0,\dot{v}_{30})] \tag{33}$$

then

$$\left.\begin{aligned} \dot{\omega} &= \dot{\omega}_0 \\ \dot{v}_3 &= \dot{v}_{30} \end{aligned}\right\} \tag{34}$$

If $(\dot{\omega}_0,\dot{v}_{30})$ are chosen to be the new independent control variables to replace the natural controls (u^M,u^P), then the state equation (31) becomes the following:

$$\left.\begin{aligned} \dot{r} &= v \\ \begin{pmatrix}\dot{v}_1\\ \dot{v}_2\end{pmatrix} &= f^{\circ}(r,v,C) + \epsilon\, f^1[r,v,C,\omega,(\dot{\omega}_0,\dot{v}_{30})] \\ \dot{v}_3 &= \dot{v}_{30} \\ \dot{C} &= S(\omega)C \\ \dot{\omega} &= \dot{\omega}_0 \end{aligned}\right\} \tag{35}$$

where $\epsilon = 1$ and f^1 is such that $f^1[r,v,C,0,(0,0)] = 0$.

The function f° is invertible with respect to the pair, $\{[\dot{v}_1,\dot{v}_2,E_3(\psi)],C\}$ in which $E_3(\psi)$ is an elementary rotation about the runway z-axis, representing the heading of the helicopter.

$$E_3(\psi) = \begin{pmatrix} \cos\psi & \sin\psi & 0 \\ -\sin\psi & \cos\psi & 0 \\ 0 & 0 & 1 \end{pmatrix} \tag{36}$$

If the horizontal acceleration commands are restricted to the set

$$U_{\dot{v}} = \{(\dot{v}_1,\dot{v}_2) : |\dot{v}_i| \le 0.5 \text{ g}, \quad i = 1,2\} \tag{37}$$

then a function $h^F : R^3 \times R^3 \times U_{\dot{v}} \times SO(2) \to SO(3)$ can be constructed so that the helicopter attitude given by

$$C_0 = h^F[r,v,\dot{v}_0,E_3(\psi_0)] \tag{38}$$

results in the commanded acceleration,

$$\dot{v} = \dot{v}_0 \tag{39}$$

Equations (33) and (38) are the trim equations of the helicopter (31) without the parasitic effects ($\epsilon = 0$ in Eq. (35)). That is, for a given motion $\{r(t),E_3[\psi(t)]\}, t \ge 0$, the corresponding trim state and control may be computed as follows:

$$\left.\begin{aligned} r_0 &= r(t) \\ v_0 &= \dot{r}(t) \\ C_0 &= h^F(r_0,v_0,\dot{v}_0(t),E_3[\psi_0(t)]) \\ \omega_0 &= q[\dot{C}_0(t)C_0^T] \\ \dot{\omega}_0 &= \dot{\omega}_0(t) \\ u_0 &= h^M[r_0,v_0,C_0,\omega_0,(\dot{\omega}_0,\dot{v}_{30})] \end{aligned}\right\} \tag{40}$$

where the function q extracts ω from $S(\omega) = \dot{C}C^T$. The required time derivatives in Eq. (40) are computable provided that the motion (r,E_3) is generated by the strings of integrators shown in Fig. 6 where a dot represents a scalar integrator, and $y^5 \in R^4$ is an independent control variable. The system shown in Fig. 6 (Kronecker indexes $(4,4,2,2)$) will be taken as the canonical model of the helicopter. The canonical variables will be denoted by y rather than x_0 to reduce the number of subscripts. The transformation and feedback that change the natural representation (Eq. (31)) to the canonical representation are approximately the following.

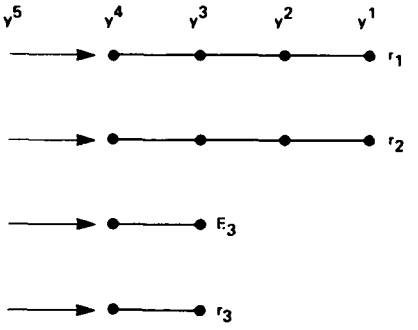

Fig. 6. Canonical model of helicopter.

The coordinate change, $y = T(x)$, is given by

$$\left.\begin{aligned} y^1 &= (y^1_1, y^1_2)^T = (r_1, r_2)^T \\ y^2 &= (y^2_1, y^2_2)^T = (v_1, v_2)^T \\ y^3 &= (y^3_1, y^3_2, y^3_3, y^3_4)^T = (f^\circ_1, f^\circ_2, E_3(\psi), r_3)^T \\ y^4 &= (y^4_1, y^4_2, y^4_3, y^4_4)^T = \left(\frac{\partial f^\circ}{\partial C}\,\omega, \omega_3, r_3\right)^T \end{aligned}\right\} \quad (41)$$

where

$$\cos\psi = c_{11}/c,\ \sin\psi = c_{12}/c,\ c = (c^2_{11} + c^2_{12})^{1/2},\ \text{and}\ (c_{ij}) = C\ .$$

The control variable change, $u = w(x,y^5)$ is defined in two steps:

$$\begin{aligned} \dot{\omega} &= \begin{pmatrix} \frac{\partial f^\circ}{\partial C} \\ 0\ \ 0\ \ 1 \end{pmatrix}^{-1} \begin{pmatrix} y^5_1 \\ y^5_2 \\ y^5_3 \end{pmatrix} \\ \dot{v}_3 &= y^5_4 \end{aligned} \quad (42)$$

and

$$u = h^M[r, v, C, \omega, (\dot{\omega}, \dot{v}_3)] \quad (43)$$

The effects of the various approximations made in the construction of these transformations are relegated to the regulator.

7. MODEL SERVO AND REGULATOR

The field of the model S_2 is chosen to be canonical as defined in Fig. 6. The design of the three trajectory channels of the model servo is shown in Fig. 7. There are four 3-axis integrators. Two axes correspond to the horizontal strings (r_1, r_2) in Fig. 6. The third axis represents the vertical (r_3) string, but with two additional smoothing integrators. The exceedingly simple structure of the field (i.e., linear, decoupled) greatly simplifies the servo design process. The inner loop $(a_0, \dot{a}_0)$ is designed to be an acceleration servo whose input a_I is the sum of coarse acceleration command a^* from the coarse command generator, and δa_0 which is generated by the outer loop to smoothly reduce any discontinuities in the commanded position and velocity vectors, r^* and v^*, respectively. The acceleration servo bandwidth is 0.63 rad/sec. The bandwidth of the outer loop is 0.1 rad/sec. Large position errors are reduced at the rate of 6 m/sec.

The heading model servo is shown in Fig. 8. It is designed to have two scalar integrators corresponding to the E_3 string in Fig. 6. The heading error,

$$e_{\psi_0} = \cos\psi_0 \sin\psi^* - \sin\psi_0 \cos\psi^* \quad (44)$$

is computed in the q-block. Block S represents, together with the integrator, the kinematic equation of E_3.

The model reference state y_0 and control y^5_0 in Fig. 5 are defined (see Figs. 6-8) as follows:

$$\left.\begin{aligned} y^1_0 &= (r_{10}, r_{20})^T \\ y^2_0 &= (v_{10}, v_{20})^T \\ y^3_0 &= [a_{10}, a_{20}, E_3(\psi_0), r_{30}]^T \\ y^4_0 &= (\dot{a}_{10}, \dot{a}_{20}, \omega_{30}, v_{30})^T \\ y^5_0 &= (\ddot{a}_{10}, \ddot{a}_{20}, \dot{\omega}_{30}, a_{30})^T \end{aligned}\right\} \quad (45)$$

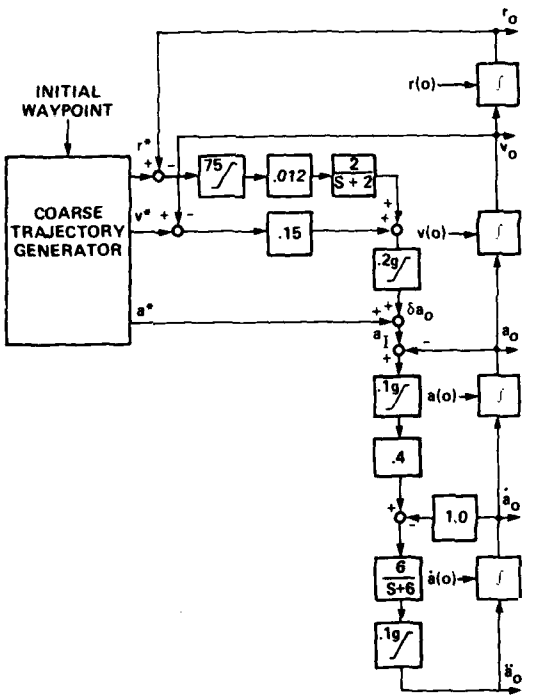

Fig. 7. Model servo-trajectory, $r = (r_1, r_2, r_3)$.

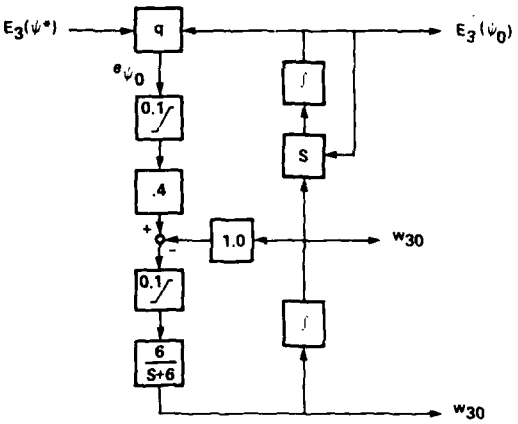

Fig. 8. Model servo-heading $E_3(.)_0$.

The field of the regulator S_3 is also chosen to be canonical S_0. The regulator design is outlined in Figs. 9-11.

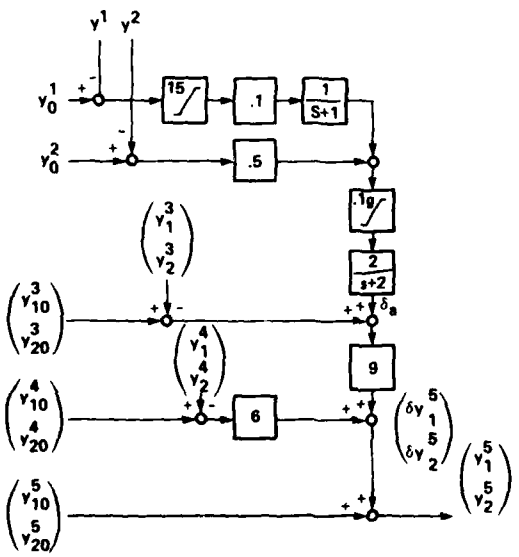

Fig. 9. Regulator-horizontal axes.

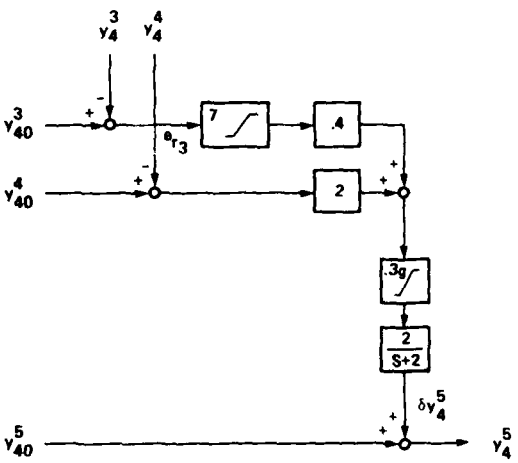

Fig. 10. Regulator – vertical channel.

The estimated canonical state y is computed from the estimated natural state by means of the transformation T defined by Eq. (41). The outer loop of the horizontal channels (Fig. 9) has a bandwidth of 0.3 rad/sec, with a 3 m/sec large-error reduction rate and 0.1-g authority limit. The inner loop bandwidth is 3 rad/sec. The vertical channel, shown in Fig. 10, has a bandwidth of 0.63 rad/sec, a 1.5-m/sec large-error reduction speed, and 0.3-g authority. Finally, the heading channel is regulated as shown in Fig. 11, where the heading error is given by

$$e_\psi = \cos\psi \sin\psi_o - \sin\psi \cos\psi_o \qquad (46)$$

The bandwidth of the heading regulator is 3 rad/sec.

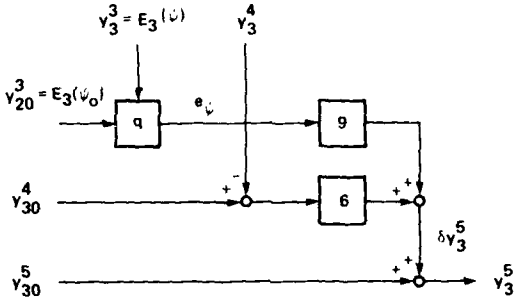

Fig. 11. Regulator – the heading channel.

The total regulator output, δy^5, is added to the open-loop command, y_o^5, resulting in the total canonical control, y^5. It is then transformed by means of the W-map given by Eqs. (42) and (43) into the natural control u which, in turn, drives the actual plant.

8. SYSTEM PERFORMANCE

The results of a manned simulation are summarized in this section. The code was implemented on the flight computer to be used in the flight test, and the mathematical model of the helicopter (UH-1H) was driven through the actual hydraulics.

The experimental flightpath is defined by a set of way points, segments of lines and helixes, and a speed profile, as shown in Figs. 12 and 13. As can be seen from Fig. 12, the flightpath is a closed curve. The time dependence is shown in Fig. 13.

The experiment, which consists of automatically flying this trajectory, exercises the system over a wide range of flight conditions. The helicopter is taken from hover (way-point 1 in Fig. 12) to high-speed (50 m/sec) accelerating, turning, and ascending flight. This input to the system is coarse, with a variety of discontinuities. The required smoothing is provided by the model servo discussed in the preceding section.

For the data presented, the helicopter was flown manually to the point * marked in Fig. 12. There the automatic system was engaged. It takes about 500 sec for the helicopter to go once around the flightpath. Unlike the coarse accelerations in Fig. 13, the model accelerations are smooth, as is the vertical velocity, v_{zo}. The second panel in Fig. 14 (labeled "acceleration error") shows the effects of the neglected parasitic terms on acceleration. The acceleration errors are quite small – less than 0.05 g. The regulator controls these effects by means of position errors. The resulting horizontal error is less than 2 m, and the vertical error is below 0.5 m. The speed error, $e_v = \|v\| - \|v_{oi}\|$, is below 0.5 m/sec.

Thus, the performance of the design in the simulation tests was good, and, at this writing, flight tests are in progress.

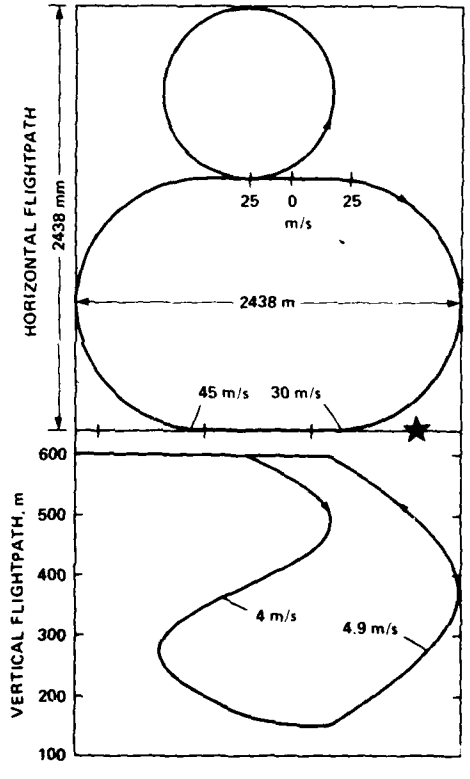

Fig. 12. Experimental flightpath shown in horizontal and vertical planes.

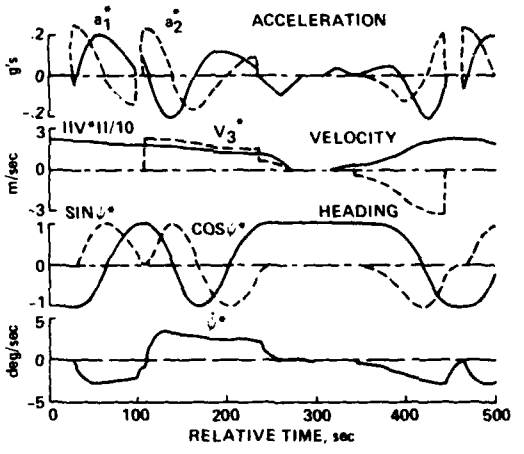

Fig. 13. Time-dependence of the coarse command.

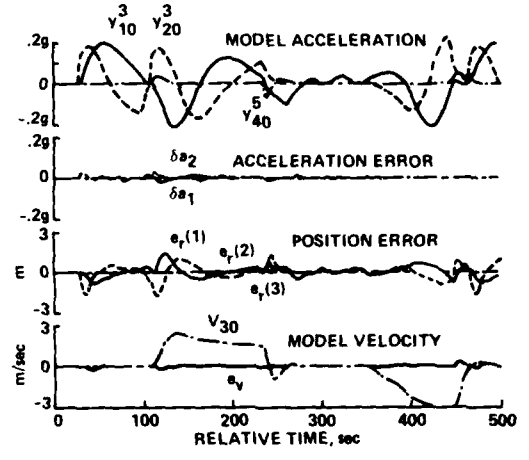

Fig. 14. System response – canonical variables.

REFERENCES

1. Meyer, G., and Cicolani, L., A Formal Structure for Advanced Flight Control Systems. NASA TN D-7940, 1975.

2. Wehrend, W. R., Jr., and Meyer, G., Flight Tests of the Total Automatic Flight Control System (TAFCOS) Concept on a DHC-6 Twin Otter Aircraft. NASA TP-1513, 1980.

3. Meyer, G., and Cicolani, L., Applications of Nonlinear System Inverses to Automatic Flight Control Design – System Concepts and Flight Evaluations. Theory and Applications of Optimal Control in Aerospace Systems, P. Kant., ed., AGARDograph 251, 1980.

4. Wehrend, W. R., Jr., Pilot Control through the TAFCOS Automatic Flight Control System. NASA TM-81152, 1979.

5. Smith, G. A., and Meyer, G., Total Aircraft Flight Control System Balanced Open- and Closed-Loop Control with Dynamic Trimmaps. AIAA 3rd Digital Avionics Conference, Dallas, Texas, 1979. (Published in IEEE proceedings.)

6. Smith, G. A., and Meyer, G., Application of the Concept of Dynamic Trim Control to Automatic Landing of Carrier Aircraft. NASA TP-1512, 1980.

7. Krener, A. J., On the Equivalence of Control Systems and Linearization of Nonlinear Systems. SIAM J. Control, vol. 11, 1973, pp. 670-676.

8. Brockett, R. W., Feedback Invariants for Nonlinear Systems. IFAC Congress, Helsinki, 1978.

9. Jakubcyzk, B., and Respondek, W., On Linearization of Control Systems. Bull. Acad. Polon. Sci., Ser. Sci. Math. Astronom. Phys., vol. 28, 1980, pp. 517-522.

10. Hunt, L. R., and Su, R., Linear Equivalents of Linear Time-Varying Systems. International Symposium on Mathematical Theory of Networks and Systems, 1981, pp. 119-123.

11. Hunt, L. R., and Su, R., Control of Nonlinear Time-Varying Systems. IEEE Conference on Decision and Control, 1981, pp. 558-563.

12. Hunt, L. R., Su, R., and Meyer, G., Global Transformations of Nonlinear Systems. To appear in IEEE Trans. on Autom. Control, vol. 27, 1982.

13. Hunt, L. R., Su, R., and Meyer, G., Multi-Input Nonlinear Systems. To appear in Differential Geometric Control Theory Conference, Birkhäuser, Boston, Cambridge, Mass., 1982.

14. Brunovsky, P., A Classification of Linear Controllable Systems. Kibernetika (Praha), vol. 5, 1970, pp. 173-188.

15. Meyer, G., The Design of Exact Nonlinear Model Followers. Joint Automatic Control Conference, FA-3A, 1981.

SYSTEMATIC COMPUTER AIDED CONTROL DESIGN

Georg Grübel and Gerhard Kreisselmeier

DFVLR-Institut für Dynamik der Flugsysteme

Oberpfaffenhofen

D-8031 Wessling

F.R. Germany

Summary

Computerized synthesis techniques of modern control theory are in widespread use, but a number of fundamental design problems still remain. We call them: the design specifications problem, the free design parameter problem, the plant complexity versus controller simplicity problem and the dirty design environment problem. A design procedure which comes close to solving these design problems is recommended: It is an iterative design technique using a performance index vector which provides a systematic guidance for the designer to take care of multiple design objectives simultaneously and individually. As a design tool unconstrained parameter optimization is used. A practical application is briefly reported: The design of a robust control loop for a fighter aircraft where 42 performance criteria of 9 different sorts have been considered simultaneously.

1. Introduction

The ultimately achievable performance of a control system is limited by hardware constraints such as the dynamics of the plant, the actuators, and the sensors. The actually achieved performance is, in addition, a product of control design: The specification of a controller structure and the tuning of the controller parameters determine how well the design objectives are met within the given limitations. Hence, in order to improve control performance one should improve the control design as well as the underlying design procedures.

Design is a trade-off between various competing objectives. These objectives reflect the properties a good system should satisfy. They are rarely complete and quantitatively specified at the outset. Rather they are an open list and formulated in qualitative terms such as: The control system should be
- "fast and smooth" in response to reference inputs, there should be
- "small static and dynamic errors" due to disturbances. The system should have a
- "good stability margin" in order to
- "tolerate 'large' parameter variations and modelling inaccuracies." But the system should also have a
- "well limited bandwidth" and "low feedback gains" in order to be
- "insensitive with respect to measurement noise". Furthermore control action should be
- "well within actuator saturation limits" and so on ...

The designer has to satisfy all these objectives in the best possible way. How can this be achieved?

2. Problems when Using Synthesis Techniques of Modern Control Theory

Modern control theory using state feedback and observers e.g. for linear optimal control, pole placement, decoupling, and disturbance accomodation, provides much insight into the analysis and synthesis of linear systems. Combining this conceptual insight with the numerical efficiency of a digital computer results in a set of useful tools to assist the design process. But although such computerized control synthesis techniques are in widespread use, a number of fundamental design problems still remain:

The Design Specifications Problem: A synthesis technique of modern control theory usually focuses on one type of design specification only (e.g. pole location; decoupling; disturbance accomodation) and is based on an exact numerical specification (e.g. all pole positions, exact decoupling, exact asymptotic disturbance accomodation for prespecified frequencies). This requests the designer to map all design objectives onto a single type of mathematical criterion (e.g. pole placement) which often narrows too much the designer's overall view of system performance. Furthermore an exact quantitative specification of design objectives is rarely possible in practice. What about a combination of different types of criteria to cover the overall system performance? What about specifying bounds rather than specifying exact numerical values for performance measures?

The Free Design Parameter Problem: The free design parameters in the Riccati formalism are the weighting coefficients in the cost functional. How to choose these weighting coefficients systematically? How to choose pole locations as the free design parameters in a pole placement approach? What about additional free parameters in, say, a full order state observer? To solve these decision problems, an iterative design loop is necessary based on an analysis of the overall system performance and notably the plant limitations. Is there a strategy available for systematically reaching an overall compromise?

The Plant Complexity vs. Controller Simplicity Problem: Modern control theory provides analytical relations between the structure of the plant and the structure of a suitable controller. This means: Simple plant models yield simple controllers, complex plant models yield complex controllers. What about simple controllers for complex plants which, as we know, often do very well in practice? We need an efficient design procedure for simple controllers taking into account realistic and thereby rather complex plant models. Why not use parameter optimization?

The Dirty Design Environment Problem: Modern control theory yields neat solutions for neat problems. Unfortunately, the design environment in practice is rather dirty. What about plant nonlinearities, parameter uncertainties, changing characteristics and control saturation? Can we handle such effects directly without the need to transcribe them into the linear framework of modern control synthesis?

These design problems when using synthesis techniques of modern control theory are conceptual ones: They are consequences of a search for analytical solutions, where the computer serves only the purpose of fast numerical evaluations of (complex) analytical relations. They cannot be removed by using faster computers or by improving the man-computer interface. What we need for control design is a multi-objective design procedure with a systematic decision strategy as a complement to control theory and the use of computers as fast searching devices for finding a "best" solution in a (nonlinearly defined) set of possible candidates.

In order to handle multiple design objectives in a systematic way, they have to be formulated by mathematical criteria. This is a question of control theory, where either the state space or the frequency domain may turn out to be more appropriate for quantifying a particular design objective. Control theory also helps to decide what kind of design criteria have to be included for a special design purpose and it yields some qualitative insight into conflicting demands. But control theory yields no strategy to handle design as a multiple-criteria decision problem as it naturally results out of the multitude of different design objectives which have to be considered. Hence we are looking for a systematic framework which guides the designer to cope with a multiple-criteria control design problem.

3. Systematic Design Via a Performance Index Vector and Parameter Optimization

A design procedure which comes close to solve most of the above mentioned design problems has been suggested in [1]. It has proven to be very useful in various practical designs and can be summarized as follows:

Given a plant, and given a suitably chosen controller structure with free parameters $\underline{k} = [k_1,\ldots,k_n]$ the design problem is to determine suitable values for $\underline{k}$.

In order that the design can proceed in a systematic fashion it is necessary that all design objectives are taken care of explicitly in the design. Therefore, every design objective shall be rated quantitatively by means of a suitable performance index $J_i(\underline{k})$.

A performance index $J_i(\underline{k})$ is called suitable if $J_i(\underline{k}') < J_i(\underline{k}'')$ means that $\underline{k}'$ satisfies the i-th control objective better than $\underline{k}''$ does, and if $J_i(\underline{k})$ is a sufficiently smooth function.

For ease of notation we define the performance vector $\underline{J}(\underline{k}) = [J_1(\underline{k}),\ldots,J_L(\underline{k})]$. Moreover, for any two real vectors $\underline{x}$, $\underline{y}$ we say that $\underline{x} < \underline{y}$ if for all components $x_i \leq y_i$ and $\underline{x} \neq \underline{y}$.

Iterative Technique for a Systematic Design

The design technique is iterative, where each design iteration (the ν-th, say) comprises two steps:

Step 1: Choose a vector of design parameters $\underline{c}^\nu$ ($c_i^\nu > 0$) such that

$$\underline{J}(\underline{k}^{\nu-1}) < \underline{c}^\nu < \underline{c}^{\nu-1}. \tag{1}$$

Step 2: Find $\underline{k}^\nu$ and $\alpha_o < 1$ such that

$$\underline{J}(\underline{k}^\nu) < \alpha_o \underline{c}^\nu. \tag{2}$$

The design iteration is initialized by using an initial guess $\underline{k}^o$ for the controller parameters and by taking $\underline{c}^o$ sufficiently large.

In step 1 of every design iteration, $\underline{c}^\nu$ has to be chosen where (1) provides a well defined margin. This choice determines the design direction. Step 2 then provides the margin for the next design iteration.

It is desirable that this margin be as large as possible, i.e. α_o should be as small as possible.

After the ν-th design iteration we have from (3), (2) that

$$\underline{J}(\underline{k}^{\nu}) < \underline{c}^{\nu-1} < \underline{c}^{\nu-2} < \ldots < \underline{c}^{0}, \tag{3a}$$

i.e. we have a monotonically decreasing sequence of design vectors and the performance vector has become less than all of them. This establishes the systematic behaviour of the design process.

Design Tool

Basically, any method which is able to perform step 2 of the design iterations can serve as a design tool. Here we shall focus on a method which, in addition, tends to make α_0 as small as possible.

The smallest value of α_0 satisfying $\underline{J}(\underline{k}) < \alpha_0 \underline{c}^{\nu}$ is given (as a function of $\underline{k}$) by

$$\alpha_0(\underline{k}) = \max_{1 \le i \le L} \{J_i(\underline{k})/c_i^{\nu}\}. \tag{4}$$

Since $\alpha_0(\underline{k})$ is not continuously differentiable everywhere, we consider a smooth, i.e. at least C^2 twice continuously differentiable approximation $\alpha(\underline{k})$ instead, where

$$\alpha(\underline{k}) = \frac{1}{\sigma} \ln \sum_{i=1}^{L} \exp\{\sigma J_i(\underline{k})/c_i^{\nu}\} \tag{5}$$

and $\sigma > 0$ is arbitrary. It can be verified that

$$\alpha(\underline{k}) = \alpha_0(\underline{k}) + \frac{1}{\sigma} \ln \sum_{i=1}^{L} \exp\{\sigma[\frac{J_i(\underline{k})}{c_i^{\nu}} - \alpha_0(\underline{k})]\} \tag{6}$$

Hence $0 \le \alpha - \alpha_0 \le (\ln L)/\sigma$, i.e. α can be made as close to α_0 as desired by choice of σ.

The minimization of $\alpha(\underline{k})$ (for example, by applying Powell's method for function minimization without calculating derivatives [21]) can now be used as a design tool for performing step 2 in each design iteration.

The sequence of design iterations finally terminates when the minimization of $\alpha(\underline{k})$ results in a $\underline{k}^{\nu}$ with $\alpha_0(\underline{k}^{\nu}) \ge 1$.

As in all parameter optimization problems there is a possibility of local minima. Therefore, instead of using efficient local optimization algorithms such as Powell's [21], one may as well use global optimization algorithms such as random search algorithms. However, the latter are known to be less efficient.

Note also that the use of optimization algorithms which assume that the function to be minimized is twice continuously differentiable (which most efficient local algorithms do), requires that the performance indices themselves must be twice continuously differentiable. This imposes a certain restriction on the mathematical formulation of performance indices.

4. Practical Application Considerations

The above design procedure using a performance index vector and parameter optimization solves most of the design problems stated in section 2:

The design procedure provides a systematic framework to take care of multiple design objectives simultaneously and individually. The design objectives can be formulated by criteria of different kind either in state space or frequency domain. Hence the design specifications problem can be tackled in the most direct way. However, the design procedure does not provide a priori guidelines what design objectives are appropriate for a particular design problem. It remains in the designer's responsibility to decide what design criteria he shall use. This decision must be based on his knowledge of control theory and the operational requirements he has to satisfy.

The design procedure provides a systematic guidance for the designer to cope with the free design parameter problem: For each individual perfomance index J_i there is associated a free design parameter c_i which can be chosen by the designer within a well-defined margin. Typically, one starts with sufficiently large values for the design parameters and then successively reduces them so as to improve certain criteria while keeping possible deteriorations of others in tolerable bounds. Whatever choice c_i^{ν} in the given margin is taken, it is always guaranteed that $J_i \le c_i^{\nu}$ and hence a possible degradation of the performance index J_i is well bounded. If $c_i^{\nu} = J_i(\underline{k}^{\nu-1})$ is chosen, then an improvement of J_i is guaranteed provided only that such an improvement is possible at all at the expense of degrading other performance indices. This allows to explore the design possibilities, and to reach a desirable trade-off between competing objectives, step by step.

In each step it is the responsibility of the designer to decide upon the design direction, i.e. which performance index shall be improved and what is a permissible expense in degr.ding other performance indices. The design procedure then guarantees a step by step monotonic improvement in the direction specified by the designer. The admissible margins of the design parameters which are updated in each design iteration, yield some information how easy or difficult it is to reach the individual design objectives. Hence this design procedure makes it possible to explore the system's limitations in control design.

The design approach is well suited to deal with practical controller realization constraints. This is a consequence of using parameter optimization as a design tool instead of using an analytical control synthesis technique. There is no "controller simplicity vs. plant complexity problem" as we called it earlier. The designer can specify the controller structure at will. He is free to combine control considerations with technical realizability constraints. This freedom, however, calls much at the designer's experience and physical insight into the type of system to be controlled. Furthermore, in view of the numerical convergence properties of parameter optimization, one also has to take some care in mathematically specifying the controller structure, i.e. in parameterizing the control law: There must not be redundant parameters. In addition, the free parameter to be optimized should have the same order of magnitude, i.e. proper scaling may be necessary. On the other hand, the freedom to specify a controller structure makes it possible to develop a proper structure in an iterative process: Start with a simple structure, say a P-I controller, and extend it successively by additional dynamic degrees of freedom, i.e. use a higher order controller, if the design iterations yield no further improvement with the formerly chosen structure. In this way, one can explore the trade-offs between controller simplicity and control system performance.

The design procedure is open to handle complex, nonlinear systems. There is no conceptual necessity for linearized or low order plant models. But there may be computer time limitations: In view of parameter optimization the performance indices have to be evaluated very often and hence sufficiently fast. For nonlinear systems there are usually no analytical relations for such evaluations, rather the performance indices have to be computed on the basis of system simulations. This limits the complexity of system models to be used by the speed of available computers and the efficiency of available simulation software.

For practical applications of the design procedure via performance index vector and parameter optimization, a user-oriented, modular design software package REMVG [3] is available. This design package has been successfully applied in solving various non-standard design p oblems. One such application is briefly described in the next section.

5. Application Example: Robust Control Loop Design for a Fighter Aircraft

This application is well documented in [4]. Here we shall give a brief overview of the problem to be handled, the sort and number of performance indices used and the final result.

Control problem: For a fighter aircraft (type F-4C) a stability augmentation system shall be designed to improve the longitudinal handling qualities. This shall be achieved with a fixed gain controller which covers the whole flight envelope without gain scheduling. Furthermore only pitch rate ($\dot{\theta}$), the variable to be controlled, shall be used for feedback. As structure of the controller, a third-order compensator has been specified, where ten constant controller parameters k_j are to be assigned (figure 1). The longitudinal motion of the aircraft is modeled by a linearized second order short period motion description of the aircraft plus a first order actuator system. In the flight envelope, five (extreme) flight conditions shall be considered (figure 2).

Performance Criteria: The following performance criteria are specified for each of the five selected flight conditions.

Trajectory criteria for step response:

$$1)\quad J_i(k) = \int_0^{T_1} [\dot{\theta}_1(t) - \dot{\theta}_m(\alpha_1 \cdot t)]^2 dt \qquad (i = 1,\ldots 5)$$

Here $\dot{\theta}_m$ is a desired, normalized step response modeled by a second-order sytem, α_i denote different time scales for each individual flight condition.

$$2)\quad J_{5+i}(k) = \int_0^{T_1} [\dot{\theta}_1(t) - \dot{\theta}_1(\alpha_i \cdot t)]^2 dt \qquad (i = 1,\ldots 5)$$

Here $\dot{\theta}_1$ is the associated rate of elevator motion.

Trajectory criteria for disturbance rejection:

$$3)\quad J_{10+i}(\underline{k}) = \int_{t_i}^{T_i} \ldots \quad (i = 1,\ldots 5)$$

Here t_i denote the desired settling times, after which the pitch rate regulation error is to be uniformly less in magnitude than 5 per cent of the initial perturbation.

$$4)\quad J_{15+i}(\underline{k}) = \int_{o}^{T_i'} [\dot{\eta}_i(t)]^2 dt \quad (i = 1,\ldots 5)$$

Here $\dot{\eta}_i$ is the associated rate of elevator motion for disturbance rejection.

Eigenvalue criteria:

To guarantee a desired degree of damping:

$$5)\quad J_{20+i}(\underline{k}) = [\mathrm{Im}(\lambda)\ \mathrm{Re}(\lambda)]_{max}^{(i)} \quad (i = 1,\ldots 5)$$

To guarantee a desired degree of absolute stability:

$$6)\quad J_{25+i}(\underline{k}) = \exp\{[\mathrm{Re}(\lambda)]_{max}^{(i)}\} \quad (i = 1,\ldots 5)$$

To limit the maximum eigenfrequency in order to avoid structural mode excitation:

$$7)\quad J_{30+i}(\_) = |\lambda|_{max}^{(i)} . \quad (i = 1,\ldots 5)$$

Controller coefficients criteria:

To bound the controller eigenvalues:

$$8)\quad J_{35+j}(\underline{k}) = 1/|k_j| \quad (j = 1.2.3)$$

To limit feedback gains:

$$9)\quad J_{35+j}(\underline{k}) = |k_j| . \quad (j = 4,\ldots 7)$$

Hence in this control design, 9 different sorts of performance criteria are used. The total number of performance criteria is 42. The number of controller parameters to be designed is 10.

Result:

The final design result is shown in figures 3 and 4: It was possible to design a fixed gain controller which covers the entire flight envelope without gain scheduling and which uses pitch rate feedback only. This novel result has been achieved in about 20 design steps, where each design step required about 60 s computer time on a AMDAHL 470/V6 computer. More details and results can be found in [4].

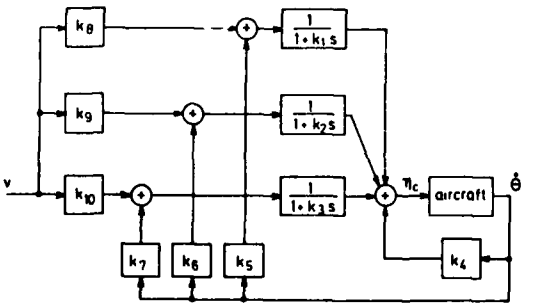

Figure 1:
Compensator structure (3^{rd} order)
Parameters to be designed $k_1 \ldots k_{10}$

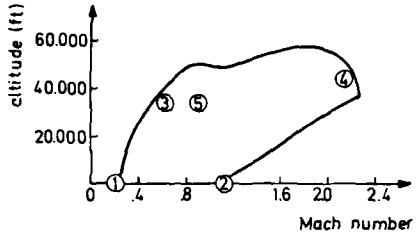

Figure 2: Flight envelope F - 4C
Flight conditions considered 1 ... 5

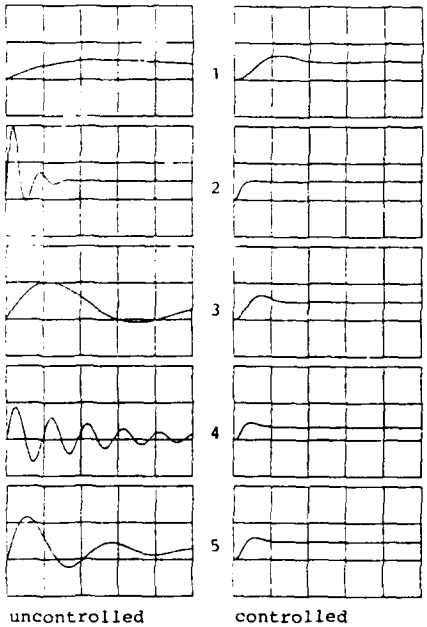

Figure 3: Command step response $\dot{\theta}$
Flight conditions 1 ... 5

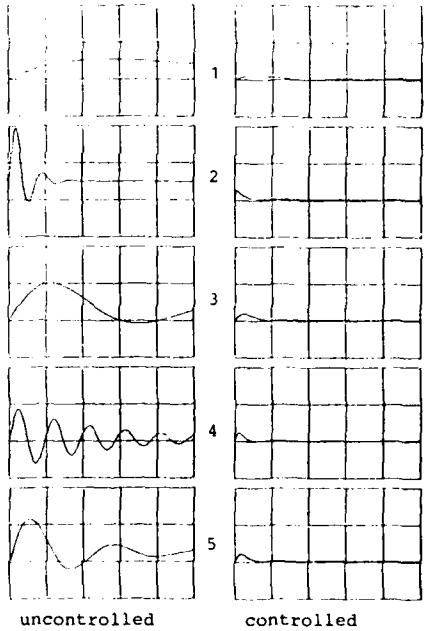

Figure 4: Disturbance step response $\dot{\theta}$
Flight conditions 1 ... 5

Literature

[1] Kreisselmeier, G., Steinhauser, R. — Systematic Control Design by Optimizing a Vector Performance Index.
IFAC Symposium on Computer Aided Design of Control Systems, Zürich (Switzerland), Aug. 1979, pp. 113-117.

[2] Powell, M.J.D. — An Efficient Method for Finding the Minimum of a Function of Several Variables Without Calculating Derivatives.
Computer Journal 7 (1964), pp. 155-162.

[3] Steinhauser, R. — Systematische Auslegung von Reglern durch Optimieren eines vektoriellen Gütekriteriums - Durchführung des Reglerentwurfes mit dem Programm REMVG.
DFVLR-Institut für Dynamik der Flugsysteme, Report No. DFVLR-Mitt. 80-18, 1980.

[4] Kreisselmeier, G., Steinhauser, R. — Application of Vector Performance Optimization to a Robust Control Loop Design for a Fighter Aircraft
DFVLR-Institute for Flight Systems Dynamics, Report No. DFVLR-FB 80-14, 1980.
Also to appear in Int. Journal of Control.

DIGITAL IMPLEMENTATION OF A LASER ACTIVE FLIGHT CONTROL SYSTEM WITH PROCESSED DECOUPLED STATES

by
ACHILLE DANESI

School of Aerospace Engineering, Rome University
Via Eudossiana, 16 - 00184 Rome, Italy

SUMMARY

This study follows a previous author's work (Ref. 1) where a new laser probe was presented as a detector of air mass wind shear perturbation ahead of the vehicle; the probe informations are applied to a lateral digital autopilot input generating the necessary sideslip corrections minimizing trajectory errors due to the wind shear effects. Here the results of the state variable decoupling theory are applied to decouple the roll and yaw lateral motion as required to satisfy independently maneuvering and trajectory following specifications. The rudder channel gains, yielding the decoupling process and forcing the vehicle transient behaviour to reproduce the desidered response, are computed and the resulting multi-input-multi-out-put autopilot feedback structure is described. The software and hardware aspects of the digital autopilot, including the laser package and microprocessors resolving the desidered control laws, are presented and the system simulation results are shown for the evaluation of the system dynamical behaviour in response to a wind shear perturbation.

LIST OF SYMBOLS

β	sideslip angle
p	roll rate
r	yaw rate
φ	bank angle
ψ	heading angle
β_a	drift angle
β_t	crosstrack angle
ψ_{Rif}	heading reference
w_y	lateral wind component
u_a	control variable for the subsystem S_a (u_a, φ)
u_r	control variable for the subsystem S_r (u_r, r)
r_a	reference input for the subsystem S_a (u_a, φ)
r_r	reference input for the subsystem S_r (u_r, r)

1. INTRODUCTION

In Ref.1 has been shown the basic information regarding the design of an airborne laser doppler sensor allowing the simultaneous measurements of the two-dimensional body axes components of the airmass velocity in a unperturbed point ahead of the vehicle to predict the wind shear onset just in advance to correct its effects and reduce consistently the tracking errors due to this cause. The essential kinematic requirement in the design of the wind velocity was to gather the wind velocity information sufficiently in advance to allow the autopilot to carry out the corrective actions, generally involving high yaw rates, provided by the autopilot rudder channel. The laser velocimeter signal, together with heading error information, is employed to generate, at the rudder channel input, a signal with magnitude proportional to the crosstrack angle which is continuously forced to a null value by a feedback process. This means to drift the vehicle, in presence of wind shear gradient, to an angle appropiate to align continuously the ground speed vector with a variable reference direction. Since the roll and yaw motions are coupled in the original control system, where they are adjusted for satisfactory tracking characteristics, the modified control strategy may result inadequate to cope simultaneously the tracking and wind shear requirements. The design objectives have been achieved decoupling the roll and jaw motions in the original control system and adjusting separately the bank angle and yaw rate. In the following sections the theory of the state variable decoupled linear system is applied to the lateral dynamics of the Shuttle Orbiter vehicle.

2. ROLL-YAW DECOUPLING

The theory on state variables decoupled linear system (Ref.2) has been

applied to decouple the roll and yaw modes of the Shuttle Orbiter lateral dynamis. A generalized program has been prepared to design decoupled flight control systems and the basic theoretical equations involved in it and the numerical results for the case treated are summarized in the following.

The basic vehicle lateral dynamic is described by a fourth order state equation involving two inputs:

$$\dot{\underline{x}}\,(t) = A\,\underline{x}\,(t) + B\,\underline{u}\,(t) \tag{1}$$

with state and control vectors defined:

$$\underline{x}\,(t) = [\ \beta(t),\ p(t),\ r(t),\ \varphi(t)\ ] \tag{2}$$
$$\underline{u}\,(t) = [\ u_a(t),\ u_r(t)\ ] \tag{3}$$

The numerical state and control matrices for the case treated are shown in Table 1; the (2x4) selection matrix is introduced to define the output vector:

$$\underline{y}\,(t) = C\,\underline{x}\,(t) = [\ r(t),\quad \varphi(t)\ ]^T \tag{4}$$

consisting of the basic state variables, the yaw rate and the bank angle which, when associated respectively to the control variables u_r and u_a, will provide the two desidered decoupled subsystems:

$$S_a = [\ u_a,\ \varphi\ ] \qquad S_r = [\ u_r,\ r\ ] \tag{5}$$

The first step in decoupling the two subsystems (5) is to define the subsystems order:

$$p_i = d_i + 1$$

where d_i is the decoupling index:

$$d_i = \min_j\ (j : C_i\,A^j\,B); \quad i = 1,2; \quad j = 0,1,2,3$$

As result of the application of these relations, the two subsystems (5) appear respectively as a first and second order systems. The decoupling process applied to the system (1) will be based on the control law:

$$\underline{u}\,(t) = K\,\underline{x}\,(t) + G\,\underline{r}\,(t) \tag{6}$$

where $\underline{r}\,(t)$ is an input vector applied externally to the decoupled system. The (2x2) input matrix G and the (2x4) feedback matrix K are defined in the following form:

$$G = \bar{B}^{-1} \qquad K = -\,\bar{B}^{-1}\,\bar{A} \tag{7}$$

$$\bar{B} = \begin{bmatrix} C_1 A^{d_1} B & C_2 A^{d_1} B \end{bmatrix}^T$$

$$\bar{A} = \begin{bmatrix} C_1 A^{d_1+1} & C_2 A^{d_2+1} \end{bmatrix}^T$$

The control law (6) solves the decoupling problem if and only if the matrix $\bar{B}$ is not singular, as has been proved for the case at hand. The numerical values of the G and K matrices are indicated in Table 1. In Fig.1 is depicted the feedback structure of the control system allowing the two lateral state variables r and φ to be regulated independently by the the autopilot rudder and aileron channel in response to the respective set point values. The closed loop representation of the decoupled system will be:

$$\begin{aligned} \dot{\underline{x}}(t) &= A_d\,\underline{x}\,(t) + B_d\,\underline{v}\,(t) \\ \underline{y}(t) &= C\,\underline{x}\,(t) \\ A_d &= A + B\,K \\ B_d &= B\,G \end{aligned} \tag{8}$$

The integrator poles of the system (8) must be now located to the desidered positions in the complex plane satysfying the transient response characteristics proposed in the design. The objective has been achieved in two steps; in the first one the system (8) by means of the linear transformation:

$$\underline{z}\,(t) = T\,\underline{x}\,(t) \tag{9}$$

is transformed in a system having the following state matrix:

$$A_t = \text{diag}\ [\ (A_{11},\ A_{22})\ \vdots\ A_r\ ]^T \tag{10}$$

where the submatrices A_{11} and A_{22}, in phase variable forms, are respectively the state matrices of the subsystems S_r and S_a and A_r is an additional row resulting from the definition of the transformation matrix T having the same dimension of the state matrix A_d Eq. (8):

$$T = [\ T_1\ \vdots\ T_2\ \vdots\ T_r\ ]^T \quad ; \quad T_1 = C_1 \quad ; \quad T_2 = [\ C_2\ \vdots\ C_2\,A\ ]$$

The row T_r, not influencing the subsystem dynamic, is chosen to be linearly independent from the other rows and avoiding as well the matrix singularity; a subroutine in the computer program will generate the transformation matrix T with such additional row. The structure of the transformed system becomes:

$$\dot{\underline{z}}(t) = A_t\ \underline{z}(t) + B_t\ \underline{r}(t) \qquad (11)$$
$$\underline{y}(t) = C_t\ \underline{z}(t)$$

The linear transformation described in Ref.5 is applied to the system (12) to obtain the subsystems transfer functions in frequency domain making easy task to program the integrator poles shift into the desidered locations in the complex plane. As a result of such computational treatment, including the inverse transformation in the original coordinate $\underline{x}$, the control for the decoupled system satisfying the dynamic requirements will be expressed by the equation:

$$\underline{v}(t) = K_s\ \underline{r}(t) + F_o\ \underline{x}(t) \qquad (12)$$

where the (2x2) gain matrix K_s and the feedback matrix F_o are computed along with the poles positioning numerical process. From Eq.(8) and (13) it is apparent that the mathematical process yielding the regulation of the decoupled system modifies, as depicted in Fig.2, the gain and feedback matrices given in Eq.(7) as follows:

$$G' = [\,g'_{i,j}\,] = K_s\ G \qquad K' = [\,k'_{i,j}\,] = K + K_s\ GF_o \qquad (13)$$

In terms of the new matrices G' and K' the control law for the decoupled and regulated system can be written as:

$$\underline{u}(t) = |u_a(t)\ u_r(t)| = G'\ \underline{r}(t) + K'\ \underline{x}(t) \qquad (14)$$

allowing to keep the same blocks representation given in Fig.1. Eq.(14) can be developed in the scalar form:

$$u_a(t) = \sum_{j=1}^{4} k'_{1,j}\ x_j(t) + \sum_{i=1}^{2} g'_{1,i}\ r_i(t)$$

$$u_r(t) = \sum_{j=1}^{4} k'_{2,j}\ x_j(t) + \sum_{i=1}^{2} g'_{2,i}\ r_i(t) \qquad (15)$$

Eq.(16) indicates that the requested control laws can ben implemented as a sum of the partial products including the constant gains appearing as elements of the computed matrices G' and K', the external forcing functions and the whole set of the feedback state variables. A microprocessor has been employed to generate the control functions (15) processing the feedback and set point data. The constant coefficients k' and g', the numerical values of which for the flight condition considered in this study are indicated in Table 2, are stored in the microprocessor memories.

TABLE 2 - Autopilot gains

Orbiter Shuttle in landing configuration			
Sensor	variable	Subsystem S_a	Subsystem S_r
Lat.Accel.	β	0,00319	2,1545
Roll Rate Gyro	p	2,1611	-6,8768
Yaw Rate Gyro	r	2,2833	11,9183
Vertical Gyro	φ	3,4778	-10,995
Aileron Input Trasd.	r_a	-3,4773	10,995
Rudder Input Trasd.	r_r	-3,0012	-10,3029

3. SYSTEM DESCRIPTION

Three basic sections, the laser package, the autopilot controller and the autopilot aileron and rudder channels, can be recognized in the system block representation in Fig.4. The basic autopilot is configured with the aileron channel regulating the bank angle as the primary lateral state variable with the rudder channel operating fundamentally as a yaw damper unit; the crossfeed gain (K_{cr}), set on the aileron error driving signal, is employed to generate a rudder channel input forcing function required for turn coordination. In the laser implemented version, conceived as a whole digital structure, microprocessors are included in the control loop to carry out the computations required for the laser-doppler signals conditioning and for the generation

of the control laws providing the decoupling and regulating process summarized in the preceding sections. The wind shear control is obtained applying to the subsystem (u_r, r) the reference signal given by the relation:

$$u_r(t) = K_{cr}\, r_a(t) + K_{\beta_t}\, \beta_t \quad (t) \qquad (16)$$

indicating that a portion of the aileron command signal (r_a) controlling the bank angle is fed to the rudder channel in order to satisfy the turn coordination; the other contribution is given by the crosstrack angle measured by the laser system to obtain the wind shear control. When the reference signal (16) is applied to the decoupled lateral control subsystems, the vehicle is forced to track the desidered trajectory in coordinate turns and to perform simultaneuosly sideslip maneuvers to cope with the wind shear effects. In the following sections some of the design details of the overall digital system are described.

4. LASER PACKAGE

Two 10-watts Argon-ion laser trasmitter-receiver coaxial units described in Ref. 1 are employed in a two dimensional laser doppler velocimeter working at 4880 Å coherent light wavelenght for lateral wind velocity component measurements. Computations based on probe volume spatial resolution yielding an acceptable signal to noise ratio in natural contaminated atmosphere, indicate as feasible the value of the front lens radius (6,38 cm.) and the location (35 m.) of the probe volume ahead of the vehicle nose, where the laser package was supposed to be installed. The laser beams angle respect to the reference optical axis was made automatically variant by means of an adaptive servosystem to obtain the best dual mode operations with various seeding particle sizes. In the evaluation of the backscattered radiation efficiency, various atmospheric trasmittance values, ranging from clear air to moderate smoggy situations, were taken into consideration; the corresponding backscattered optical flux originated at the probe illuminated section crossed by 1 μm diameter seeding particle was estimated in order of magnitude of $0,3\ 10^{-3}$ watt. For the assumed values of the optical efficiency (1%) in the collecting light system and considering a 5% quantum efficiency in detection, the current measurable at the output of a photomultiplier with an internal gain of 10^4 was found in the range of $1,5.10^{-3}$ to $6,7.10^{-3}$ Amp., depending on the trasmittance considered; the correspondent number of the observed fringe lines is varying from 20 to 52. These results has been considered, at this stage of the research, acceptable. In the proposed range for the measurable wind velocity magnitude, the resulting doppler frequency assumes values from 0,132 to 2,65 MHz and the total time spent by the particle crossing the probe volume was estimated in the range of 20 ÷ 0,393 μsec.

A digital wind velocity processor performs the computation of the lateral mean wind velocity computation based on zero crossing counting of the pulses generated by a Schmitt trigger excited by the doppler bursts appearing at the photomultipliers output. The sensitivity to the fluctuation existing in the doppler signal can be regulated adjusting the hysteresis trigger voltages to obtain the desidered S/N ratio for accurate measurements. The observation time (1 μ sec.) relative to the counting process was chosen referring to the minimum number of the observed fringes and maximum doppler frequency. The number of pulses counted at each cycle (8) has been established on the ground of the maximum error in counting originated by the asynchronism of the doppler originated and reference pulse trains. The error in time measurements with a clock of 256 MHz correspond to an error of 0,3% in wind velocity computation. Following the blocks sketched in Fig.5, the wind velocity data from the counter are transferred directly into the memory locations of an 8-bits-2 MHz clock microprocessor performing the computation of the mean value of wind velocity based on four data observations. This processor performs also the drift angle computation adding it to the heading error data to obtain the crosstrack angle value requested to implement the wind shear control strategy. The total time requested for computing and I/O operations is in the order of 1,8 msec.; this time, which includes the time for the digital to analog conversion, is considered as the up-dating period for the crosstrack angle informations at the autopilot input.

5. AUTOPILOT DIGITAL CONTROLLER

As mentioned previously, the autopilot controller, treated in this study, is a microprocessor computing the control laws expressed by the Eq. (15) which allows to decouple the original system state variables and regulate the transient response of the resulting decoupled system (5). The autopilot sensors output, together with the reference set-point voltages are applied to a parallel-in-serial-out (8x1) analog multiplexer (MPX). Each of the MPX inputs are enabled to be translated to the 8-bits analog to digital converter under the adressing assignements given by a 3-bits preset counter

working on a clock frequency chosen to satisfy the requirements imposed by the signal reconstruction based on the closed loop autopilot-vehicle bandwidth. In this particular application involving gust and flutter control, the clock frequency for the MPX's counter was established at the value of 160 Hz. The data transfer from the MPX to the analog to digital converter and from the converter to the microprocessor data bus is carried out entirely under the control of the software implemented as a part of the microprocessor interrupt program. Since the total uncertainty in the control laws generation depends predominantly on the uncertainty in the control gains assignement, particular attention was paid in choosing the length of the word representing a coefficient in the control algorithm. The criterion adopted at this regard was refered essentially to the maximum allowable percentage error (1%) in locating the integrator poles in the complex plane as requested in the decoupling and regulating processes; this error was correlated to the minimum number of bits in the numerical representation of the closed loop control gains. For the specific case treated the minimum word length for the requested accuracy was evaluated in 13 bts. The coefficients of the control algorithms are entered in the 8-bits Intel 8080 microprocessor, employed in laboratory applications, as a 16-bits words in two sets of 8 bits each, representing respectively the most and the least significant bits. Since the measured state variables have a direct memory access in the microprocessor as a 8-bits data, the software implementing the control algorithms yields products of 16-bits multiplicand, transferred temporarely in couples of 8-bits registers, by an 8-bits multiplicator; the 8-bits partial products are entered into the accumulator while the multiplicator bits are shifted out. By means of an appropiate use of the memory stack, the sum of the partial products are made available in sequence in the accumulator at the end of each multiplication. The final result is translated to the output port from the accumulator under the program control. The control algorithms requires for each of the two subsystems, 6 multiplications and 6 additions. To perform the arithmetic and miscellaneous operations, the last ones including the interrupt and I/O operations, a total time of 3,9 msec. is required.

This time interval consisting of the acquisition time for a complete set of input data and the above mentioned computing time, defines the sampling time (10.15 msec.) for the digital process considered in this study; it represents the time elapsed to generate the requested control laws based on the laser velocimeter informations.

The control signals governing the decoupled subsystems are translated from the latch register at the microprocessor output to the 8-bits-10 volts full scale voltage digital to analog converter; the conversion is carried out at the rate of its internal clock (10 MHz.) with a resolution compatible with the maximum admissible error in the aerodynamic control surfaces positioning and well within the precision capability of the overall digital system precision.

The autopilot servosystem consists of hydraulic actuators with servovalves regulated by means of variable reluctance stepping motors. The pulse train to the stator windings, is generated by an electronic controller which is essentially a rate multiplier unit working on piecewise constant analog voltages in the range of $10 \div 38\ 10^{-3}$ volts and generating, at its output, pulse trains at a recurrence frequency varying between 100-1000 pulse per second; these pulse trains are properly sequenced, through the control logic unit, to the motor stator windings forcing the stepping motor in the slew range varying from 0,87 to 8,7 rad/sec.

6. SYSTEM SIMULATION

The purpose of the system simulation was essentially to test the process performed by the Intel 8080 microprocessor employed in the laboratory applications and programmed in its assembler language to solve the numerical algorithms proposed to decouple and regulate the system state variables and to obtain the wind velocity informations by means of an hardware emulation of the wind velocity computer. No provisions are made to simulate, at this research stage, the laser velocimeter requiring data from extensive electro-optical laboratory tests. The overall digital system was simulated in a Univac 1100 computer employing a microassembler program allowing the control algorithms to be entered, for the part regarding the microprocessor simulation including all I/O operations, in assembler language while Fortran programming was used for the continuous part of the system. The forcing function for the system was based on the wind shear model considered by the author in a previous work (Ref. 4). The system simulation results are discussed in the next section.

7. DISCUSSION OF THE SIMULATION RESULTS

The time response of the decoupled system, with gains regulated as indicated in Table 2, to r_r step input (r_a=0) is shown in Fig.7, while the response to the r_a (r_r=0) step input is given in Fig.8. From these results is clearly apparent the satisfactory effects of the decoupling process and the acceptable approximation achieved

in the reproduction of the desidered subsystem's dynamical behaviour. In Fig.9 the system rensponse to a step command applied to the r_a input with crossfeed branch closed is shown, indicating that in coordinated turns, the yaw response is dictate only by the crossfeed relation existing between the aileron and rudder forcing functions.

For the evaluation of the system performances under wind shear perturbations, the r_a input command and the heading error were set to zero allowing the rudder command to be proportional to the drift angle computed from laser data. The wind shear perturbation was modelled as linear time function with lateral wind component intensity varying at the rate of 5,23 m/sec^2; this shear model is assumed applied at the probe volume and measured, at the sampling rate of 0,165 HKHz., by the laser velocimeter during the vehicle progression toward it; the correspondent signal at the wind velocity computer input was a sequence of variable frequency doppler bursts. The simulation result shown in Fig.10 indicates that the yaw rate and the drift angle become increasingly larger as the vehicle approaches the probe volume spot reaching, at the time of crossing, 80% of the predicted values for a full correction of the wind shear perturbation. Consider now this result from the point of view of the wind shear predicting capability of the proposed system. A significant parameter at this regard may be the lead margin, defined as the time difference between the vehicle-autopilot reaction time and the time spent to cover at the specified airspeed, the distance from the vehicle present position to the point observed by the laser velocimeter. For the autopilot-vehicle reaction time is intended the sum of the vehicle yaw mode time constant and the time required to generate the control laws. Clearly the defined lead margin must be negative to ensure that the vehicle is capable to react adequately to the wind shear perturbations detected by the laser probe; furthermore greater is its magnitude better will be the operative system capability in correcting the wind shear effects. The lead contribution introduced in the basic feedback control system has been seen to allow the drift angle to reach 80% of the desidered value. This result is specifically referred to an upper limit imposed to the time constant relative to the first order subsystem (u_r,r); in the design this upper limit was set at the value of 0,183 sec.

A larger lead margin can be reached choosing a lower time constant and reducing the control laws computing time; the first solution implies an increase in autopilot gains and rudder travel and the second requires more advanced microprocessor characteristics. Further simulations carried out with different time constants, indicate that a time constant of 0,1 sec. yields an acceptable lead margin with a gain set still realizable from the point of view of hardware implementation; the larger control displacements involved in yaw corrections have been minimized ascribing to the autopilot controller the function of an optimal controller synthetized by the algorithm treated in Ref. 3. Implementing this new configuration, implying some increase in hardware complexity, the resulting lead margin allows the drift angle to reach 90% of the value for full correction at the probe volume spot. It is author's opinion that the choice of a time constant somewhere in between the above considered values, one can satisfy the wind shear requirement with a moderate increase in hardware complexity. Provision were made also using high speed, real time processors where multiplications and additions are carried out in a time more than 50% less of the time required by the present microprocessor generation; considering, as an indication, a multiplication time in the order of 70 μ sec., value indicated as already achieved in current literature, the total computing time would be reduced at the order of a millisecond, that is four time less than the time taken by the laboratory set up used in this study. It is reasonable to say that the use of a microprocessor of a new generation can improve consistently the lead capability of the proposed laser implemented system.

8. CONCLUSION AND AREAS OF FUTURE RESEARCHES

The present study indicates the feasibility of a flight control system made active in controlling the wind shear effects with the contribution of a laser doppler velocimeter which, when judged on the basis of the data available at this phase of the research, looks very promising as a predictor sensor of the airmass dynamics ahead of the vehicle. The decoupling and regulating process implemented by a microprocessor as a computing unit working on the feedback data and reference signals including the laser measurements, becomes essential in controlling simultaneously tracking and wind shear corrective yaw maneuvers during an high speed-high precision approach to land under critical environmental disturbances, problem tipically interesting the terminal phase of the Orbiter Shuttle mission. Further author's works in this research area are in preparation; the subjects treated regard the use of a high speed real time microprocessor to solve the algorithm for model following optimal control applied to the decoupled system and the design of a self-adaptive process optimizing the detection of the laser doppler backscattered quantum efficiency in a atmosphere of low seeding concentration.

REFERENCES

1- Danesi, A.(1981) - Laser implemented active flight control system for reentry Shuttle-XXXII Congress of International Astronautical Federation-Paper IAF-81-29, Rome-6 Sept. 1981

2- Falb, P.L.(1967) - Decoupling in the design and synthesis of multivariable control systems-IEEE Transactions on Automatic Control - VOL.AC-12, pag.651-659, December 1967.

3- Danesi, A. and Curreri, F. (1981) - Aerospace vehicle digital optimal control-Techn. Paper N° 206-Aerospace Research Center, Rome University.

4- Danesi, A. and Curreri, F.(1981) - Wind Shear effects on tracking precision under M.L.S. guidance-Proceeding IV-th A.I.D.A.A. Congress, Rome-15 June 1981.

5- Danesi, A.(1975) - Numerical computation of transfer functions-Techn.Paper N° 200-Aerospace Research Center, Rome University.

AKNOWLEDGMENT

The author would like to express his gratitude to the Staff of the College of Mechanical and Aerospace Engineering of Boston University, Mass., USA, to allow him to carry out experimental activities at the Laser Laboratory during his stay as Visiting Professor. Thanks are due to the M.S.Electronic Engineer Arturo Danesi who assisted in laboratory and in computer programming.

TABLE 1 - SYSTEM MATRICES

Orbiter Shuttle in landing configuration

State, Control and output matrices
for system (1)

$$A = \begin{vmatrix} -0,179 & 0,0 & -1,0 & 0,0,054 \\ -3,723 & -0,785 & 0,266 & 0,0 \\ 0,547 & -0,012 & -0,166 & 0,0 \\ 0,0 & 1,0 & 0,289 & 0,0 \end{vmatrix} \qquad B = \begin{vmatrix} 0,0173 & 0,0398 \\ 1,7368 & -6,4418 \\ -0,2526 & 0,7986 \\ 0,0 & 0,0 \end{vmatrix}$$

$$C = \begin{vmatrix} 0 & 0 & 1 & 0 \\ 0 & 0 & 0 & 1 \end{vmatrix}$$

Gain and feedback matrices
for the decoupled system (Eq.14)

$$K = \begin{vmatrix} 2,15541 & 0,184046 & -0,435162 & 0,0 \\ 0,03184 & -0,072239 & -0,073386 & 0,0 \end{vmatrix}$$

$$G = \begin{vmatrix} -2,06058 & 0,26495 \\ -0,60024 & 0,08385 \end{vmatrix}$$

Gain and feedback matrices
for the decoupled and regulated
system (Eq. 15)

$$K' = \begin{vmatrix} 2,15541 & -6,87675 & 11,9183 & -10,9952 \\ 0,003185 & 2,16111 & 2,2833 & 3,4778 \end{vmatrix}$$

$$G' = \begin{vmatrix} -10,3029 & 10,9952 \\ -3,0012 & -3,4778 \end{vmatrix}$$

State and control matrices
for the decoupled and regulated system

$$A = \begin{vmatrix} 0,14158 & -0,0329 & -0,7029 & -0,00139 \\ 0,894.10^{-7} & -26,65 & 6,2568 & -41,5 \\ 0,745.10^{-8} & 0,406.10^{-7} & -5,0 & 0,89.10^{-7} \\ 0,0 & 1,0 & 0,829 & 0,0 \end{vmatrix} \qquad B = \begin{vmatrix} 0,297 & 0,0518 \\ 1,445 & 41,5 \\ 5,0 & -10^{-7} \\ 0,0 & 0,0 \end{vmatrix}$$

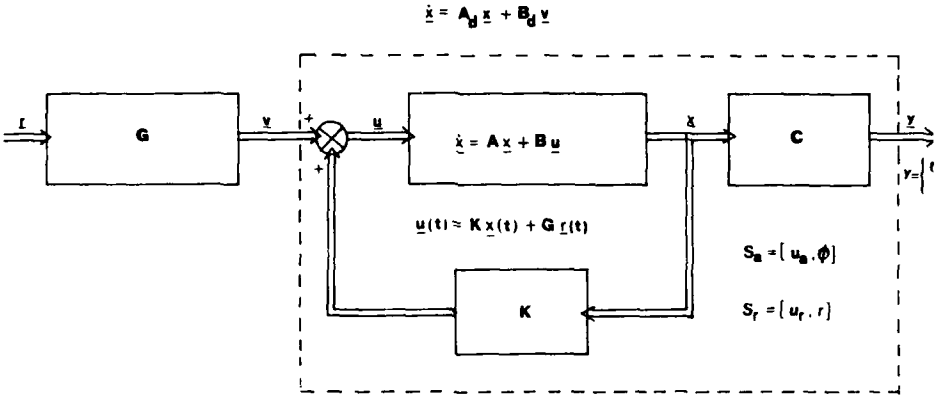

Fig.1 - DECOUPLING PROCESS

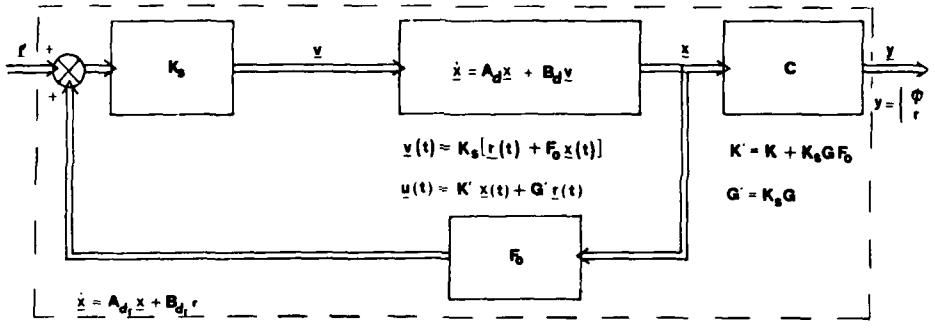

Fig. 2 - REGULATING PROCESS FOR THE DECOUPLED SYSTEM

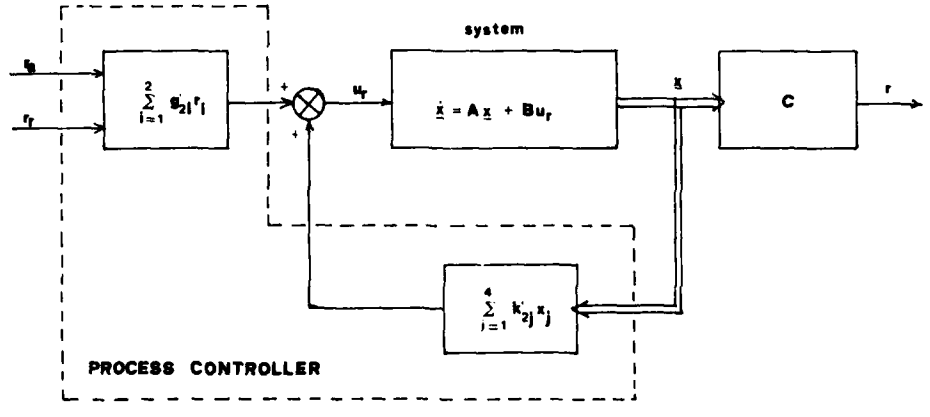

Fig.3 - SYMBOLIC REPRESENTATION OF CONTROL PROCESS FOR THE SUBSYSTEM (u_r, r)

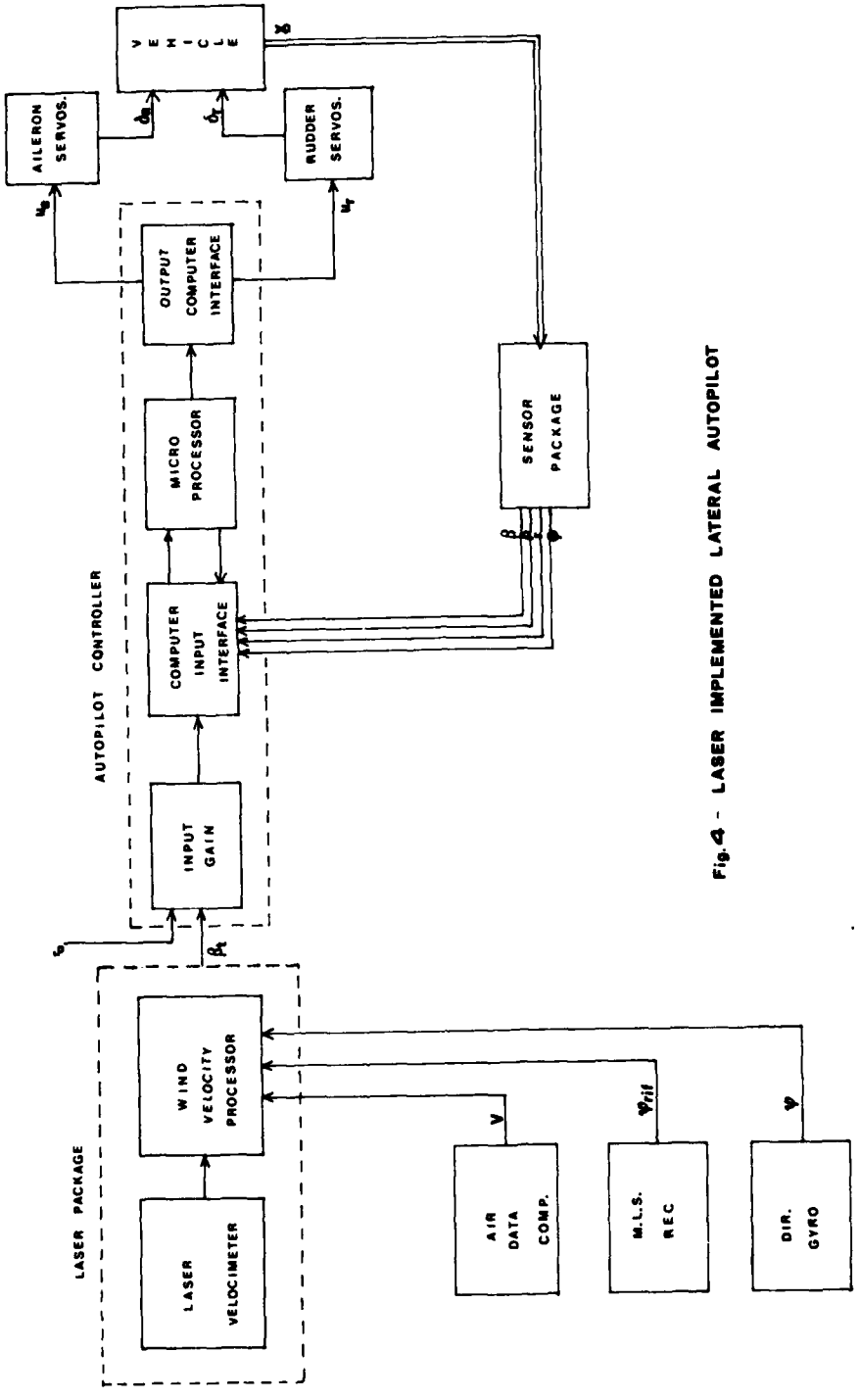

Fig.4 - LASER IMPLEMENTED LATERAL AUTOPILOT

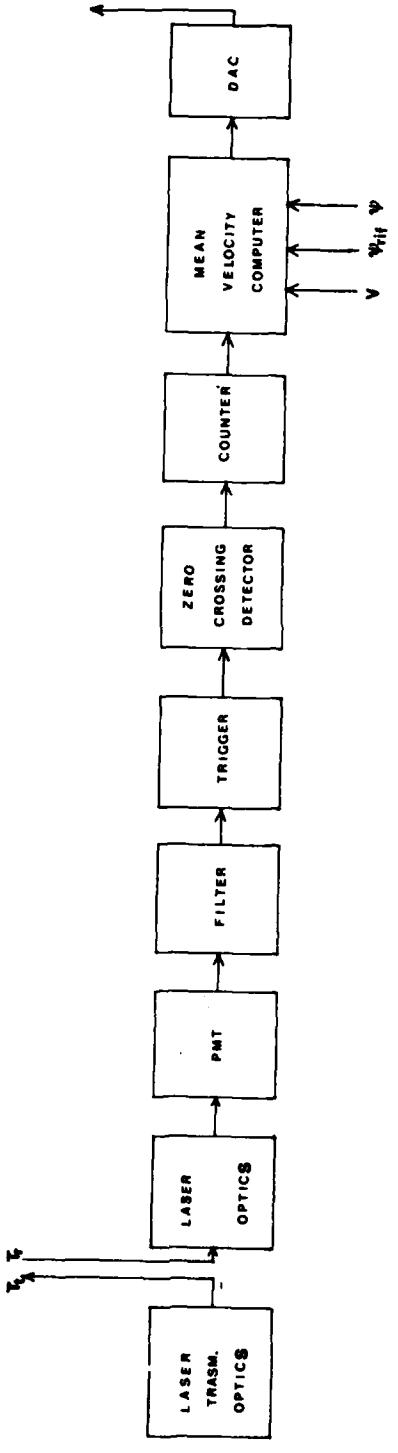

Fig.5 - WIND VELOCITY PROCESSOR

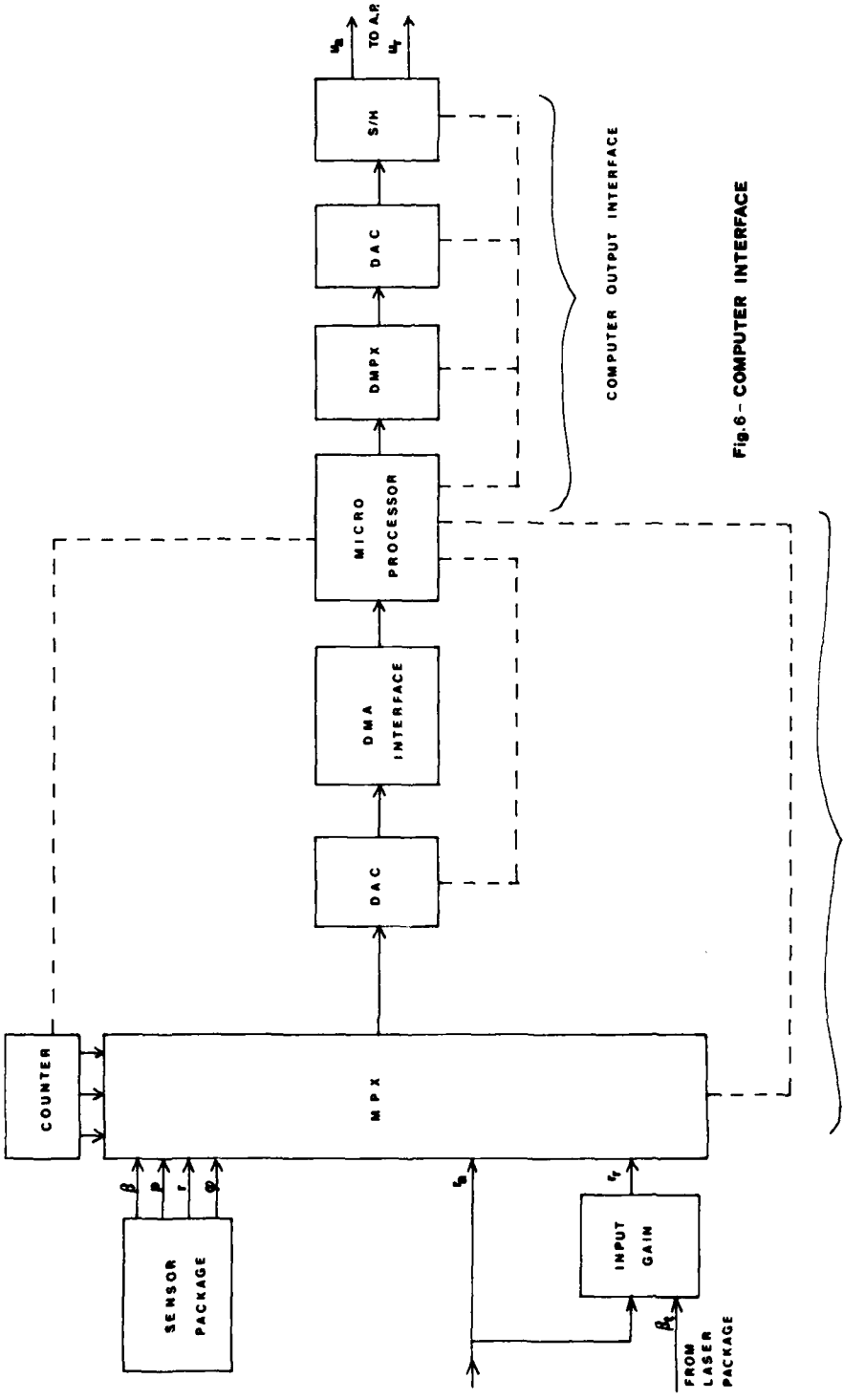

Fig.6 - COMPUTER INTERFACE

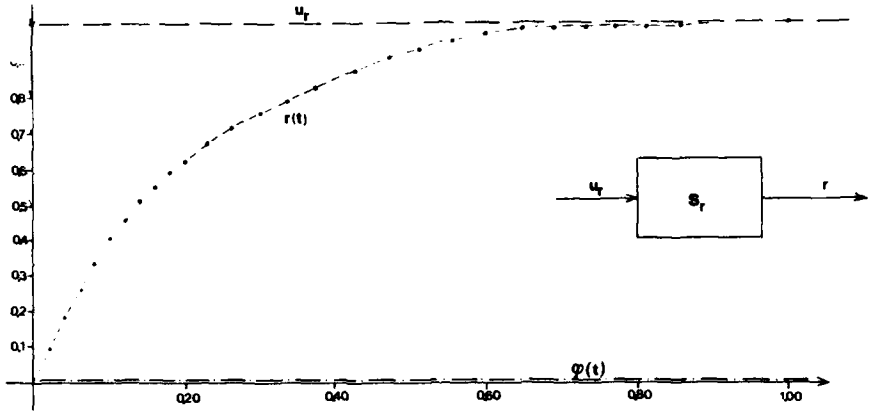

Fig. 7 - DECOUPLED SUBSYSTEM (u_r, r) - TIME RESPONSE

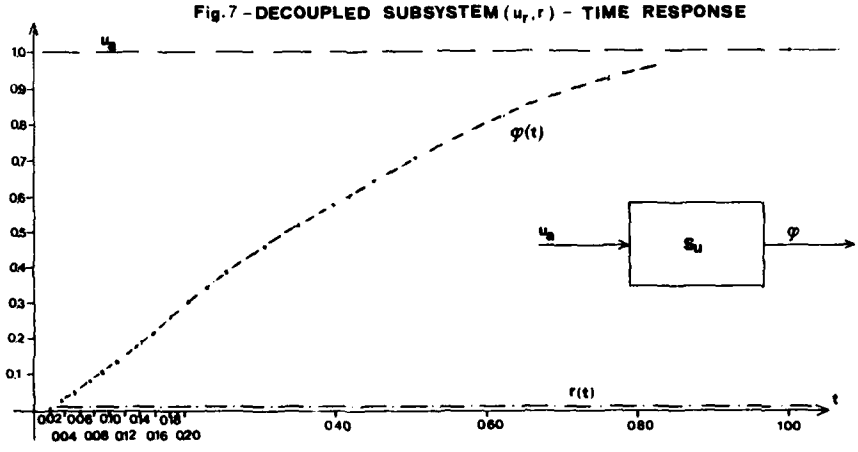

Fig. 8 - DECOUPLED SUBSYSTEM (u_φ, φ) - TIME RESPONSE

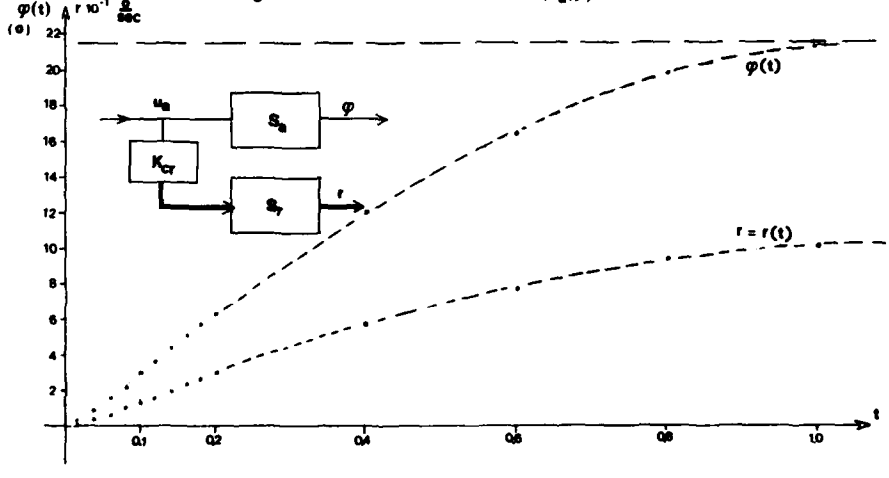

Fig. 9 - DECOUPLED SYSTEM IN COORDINATED TURN MANEUVER

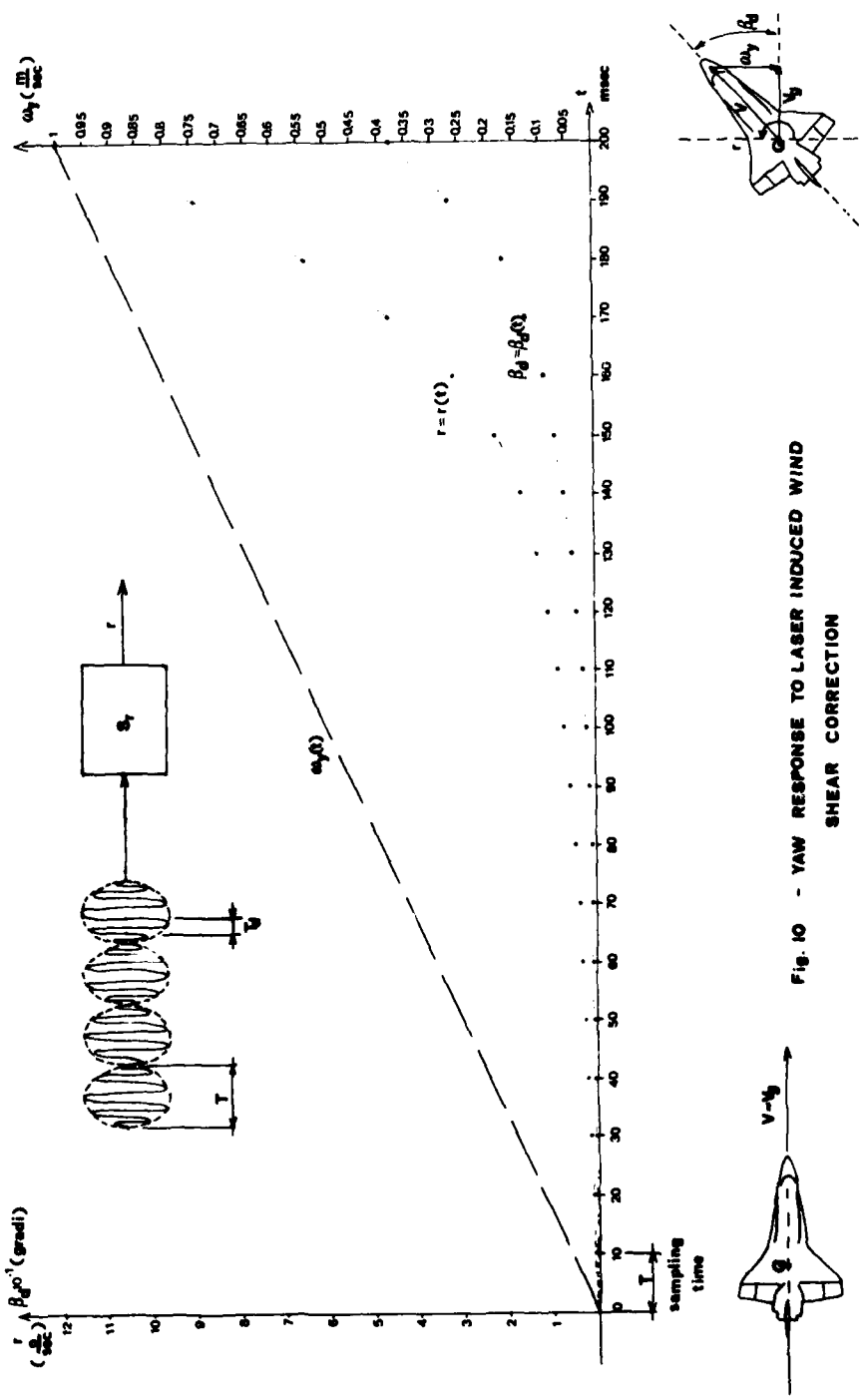

Fig. 10 - YAW RESPONSE TO LASER INDUCED WIND SHEAR CORRECTION

IMAGE SUPPORTED NAVIGATION IN LOW ALTITUDES BASED ON THE DETECTION OF ROADS AND RIVERS

DR. Rolf-Dieter Therburg

Lehrstuhl für Regeltechnik und Elektronik, TU Clausthal
Leibnizstrasse 28
3392 Clausthal-Zellerfeld

Summary

If a flight navigation system has to operate independently of ground stations or satellites, it has to be updated by acquisition of ground data. This paper proposes position-fixing by automated detection of rivers, roads, and other traffic routes in the visual image underneath the aircraft. These patterns, undistorted even if viewed from low altitudes are detected by an electrooptical sensor, which correlates the image with a rotating slit. As this sampling pattern is matched to line-shaped image patterns, traffic routes are detected in highly structured background in spite of weak contrast. For position fixing data of detected traffic routes are fed to a micro computer on board, to be compared with stored map data of traffic routes. This approach forced us to develope a suitable nonlinear filtering method, yielding an optimal estimation of the real position and thereby the position offset of a dead reckoning system.

1. Introduction

Automated image analysis and pattern recognition in production plants as in military equipment is often obstructed by disturbances of the image pattern, noise of its background, lack of contrast, and inhomogeneities of the camera target. Additional difficulties are often found in processing the wealth of pictorial information with reasonable computer power in reasonable time at the site of the industrial or military plant or on board an aircraft. To cope with these problems, the system described in this paper adapts electrooptical scanning to the contours of the image. This yields a novel sensor for detecting weak contours in highly structured background. In the first part of my paper I shall introduce the concept of the so-called contour-sensor. The second part contains its application to image supported navigation. This section will cover:

- The unsupervised acquisition of digital map data from airphotographs or maps by the contour-sensor.
- The in-flight detection of roads and rivers by a contour-sensor of the same type.
- Map matching by a recursive filter, which compresses all information from previous updates into 5 state variables.
- Experimental results of flight-simulations.

2. Acquisition of contour data by a contour sensor

The common procedure for image processing starts by bringing the entire image into a computer after scanning it in a fixed raster. These yields two problems:

- A large amount of information has to be transferred, stored, and processed.

- Sampling noise is generated by any fixed raster converting the smooth contour in fig. 1 into a staircase.

We find rather good examples in newspapers. Who has not seen rastered images from which even our excellent visual system proves unable to extract any essential contour: they have been ruined by noise. A finer sampling raster reduces sampling noise but increases computer workload. It is well known that biological systems can afford highly parallel processing. But even those systems reduces image information before transferring it to the visual cortex.

What can we learn from the biology? It is not very efficient to ask which image data are really needed, after all of them have been brought into the computer. Its much better to think previously, and to control the sensor in such a way, that only really needed information will be selected. The sensor is then adapted to the expected information in the sense of the theorie of optimal-filtering. So we need a controlable preprocessor.

As relevant information for image analysis and classification is mainly contained in image contours, we developed an electrooptical preprocessor, called 'contour-sensor', which adapts the sampling pattern to the image contours. Contours are defined rather simply:

- A contour is a line shaped pattern, formed by the maxima of the gradient of average intensity (or other statistical moments).

Averaging on either side of a contour should cover a wide area to eliminate drop-outs and other local disturbances of the pattern and its background. On the other hand it should not extend to regions outside the homogeneous image area, which might be limited e.g. by the horizontal contour in the upper part of fig. 2.

The sampling or integration area should thus cling to the contour narrowly and should follow the contour as long as possible. Sampling strips F1 and F2 on either side of the contour are each scanned by one scan line of an image-dissector-camera. Averaging of the video signal during the scan of F1 or F2 can be done by analog electronics, reducing computer input data to one value per scan area. The difference between these data yields the gradient of average intensity.

The task is to choose the sampling areas properly, to adapt them to a contour which has yet to be detected. We have to adapt to the contour-parameters

- curvature

- direction and

- position of a contour.

These must be done using as much a-priori-knowledge as available from previous measurements taken of the same image. Hypotheses on the further course of a contour and other contour elements must be based on this knowledge and must be tested by subsequent measurements.

These are the basic principles of our system, as opposed to sampling the entire image in a fixed raster and transmitting all information to the computer:

- Selection of information which is most probably significant reduces computer workload.

- Adaptation to the expected information improves the systems detectivity.

The amount of available a-priori-knowledge will be zero in a pure search process. In this case we vary direction and position of a small rectangular scanning area continuously by shifting a starshaped scanning pattern across the image. For tasks like image supported navigation we use a contour-sensor imaging the pattern onto a mechanical rotating reticle. An integration-lense collects all light penetrating the reticle on a single phototransistor. In this way the contour-sensor performs a two-dimensional correlation with a wedge-shaped slit and computes the tangential component of the correlation-gradient during rotation of the slit. The slit eliminates image defects by averaging many pixles. As only one photoelement is used there are no disturbances by inhomogenious sensitivities of electrooptical targets. After electrooptical conversion the signal is sampled 256 times during one rotation of the slit. This yields an angle resolution of 1.4 degree. When the slit crosses a contour the difference between two samples marks the gradient of the intensity. The moment of crossing yields the orientation of the contour.

Fig. 3 shows an image taken by electron-raster-microscope from monoatomic steps in Fe-mono-cristals, made visible by gold-coating. This preparation technique produces a random pattern which arranges itself in an ordered, though far from continuous straight line at the location of a step. This image has been scanned with a star-distance of 1/2o star radius. In an angular histogram the directions of the bundles of straight lines are prevailing clearly in background noise due to artefacts and accidental line arrangements of gold pixels. This example has been selected to demonstrate the contour-sensors ability to detect very imperfect contours with weak contrast in highly structured background.

3. Image supported navigation

If a flight navigation system has to operate independently of ground stations or satellites, it has to be updated by acquisition of ground data. This paper proposes position-fixing by automated detection of rivers, roads, and other traffic routes in the visual image underneath the aircraft. Flying at low altitudes, perspective distortions will be generated in the region of ground elevations or buildings. This complicates areal-correlation from airframes with maps carried on board. However roads and other lineshaped picture elements are undistorted exactly when the optical axis of the vertical looking contour-sensor crosses them. These patterns, undistorted even if viewed from low altitudes are detected by our sensor system, which correlates the image with a rotating slit. The motion of the scanning star across the visual field results from the flight manoeuvres automatically. As this sampling pattern is matched to line-shaped image patterns, traffic routes are detected in highly structured background in spite of weak contrast. From these measurements the sensor-electronics computes the angular-orientation of traffic routes.

To demonstrate the detectivity of the contour-sensor we follow a continous scan line of the aerial photograph fig. 4. Detected roads are indicated by an arrow. No segmentation problem arises, even if two roads are measured simultaneously by the scanning star. Contours of forests and other area contours are suppressed completely by proper filtering. The continuous scan simulates a flight path. Data on position and direction of several roads are compared with memory data to compute the actual position for navigation updating.

From low altitudes these terrain features will be discernible under most weather conditions by a passive sensor, with electrooptical light amplification for night missions. Dense fogbanks only will interrupt ground-sight for short intervals. Microwave-radiometry promises passive all-weather-navigation capability. In this way the system may be installed in helicopters, aircrafts, or cruise missiles and is specially suitable for flights in low altitudes.

4. Navigation updating

For position fixing, data on detected traffic routes are fed to a micro-computer (LSI 11) on board, to be compared with stored map data of traffic routes. These map data may have been acquired by a ground based sensor of the same type from maps or airphotographs. The flight-path may be presceduled for unmanned missiles or choosen arbitrarily by the pilot during his mission, provided it crosses traffic routes occasionally. As the contour-sensor extracts roads and rivers only, the digital reference map, needed for navigation updating and carried on board, has to contain these patterns only. Their position and orientation is stored as map data from the computer in an index-sequential data-base where the orientation serves as index. This image reduction minimizes storage demand in such a way that the whole area of mission can be memorized for navigation updating in midcourse and terminal guidance.

For in-flight navigation we need a start position and a dead reckoning system. The actual reference map is roughly selected with regard to the dead reckoning position. The unevitable drift error of the navigation system causes a displacement between the real and the dead reckoning position. When the aircraft crosses a traffic route the contour-sensor delivers informations about a lineshaped pattern. The comparison of the detected contour with the reference map yields a position line probably crossed by the aircraft. Due to the drift error this line will not pass through the predicted position. In this way we get a line as hypothesis for the real position in relation to the dead reckoning position.

Taking miamessurements of approximately the width of the traffic route in account we get a line with a gaussian profile, a so-called gaussian-wall. Lets continue the flight. In course of time the position information carried by the position line will get more uncertain, due to the continuing drift. We take this into account by broadening the gaussian-wall continuously. Crossing the next traffic route, the contour-sensor delivers a further gaussian-wall as likelihood-distribution of the momentary real-position. From the last and all former distributions, an a-posteriori-likelihood can be constructed. The compound-distribution arises from a superposition of all gaussian-walls. This can be done by multiplication or logarithmic addition of the single distributions. The basic requirements for the superposition are a translation of all former distributions in cooresponden-dence with the flight progress and a broadening according to the drift error. It can be shown, that the local maximum of this compound-distribution yields an optimal estimation of the real position and thereby the position offset of the dead reckoning system.

The question may arise, why we don't process the measurements with the well proved technique of Kalman-filtering. The profile of the distribution-function is specified by the orientation of the gaussian-wall produced from the traffic route as input signal. Consequently, in our approach, signal and noise are extremely correlated. This violates a critical basic requirement of Kalman-filtering. This forced us to develope a suitable nonlinear filtering method. We succeded in describing the whole history, that means the current compound-distribution by a state-vector with only five scalar, linearly independent components. When the contour-sensor delivers a new measurement the state-vector can be actualized. This yields a recursive presentation of the proposed nonlinear optimal-filtering. Besides position lines point-position data, for example the start position, can be included as the intersection of two orthogonal gaussian-walls. Since we actualise the state-vector for every measurement, it doesn't matter if we include an incorrect gaussian-wall sometimes or if we ignore a traffic route. These mistakes of the contour-sensor, encountered in spite of the optimized contour detection, are suppressed by the nonlinear filtering, described above. With a lot of flight simulations we could demonstrated the efficiency of the algorithms implemented on a microprocessor and the high accuracy of the entire system.

Let me present some performance data of our system to you, finally.

- Single-board-computer PDP 11/23 with 64 KB memory

- Reference map resident in the main-memory

- Position updating in 25o ms

- Simulated flight-velocities up to 28oo km/h

- Updating independently from alterations of illumination and vegetation

- Updating-error less than 2 m.

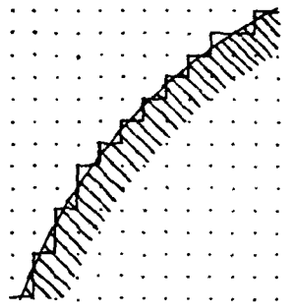

fig.1: A fixed sampling raster would require a great number of pixels to reduce sampling noise.

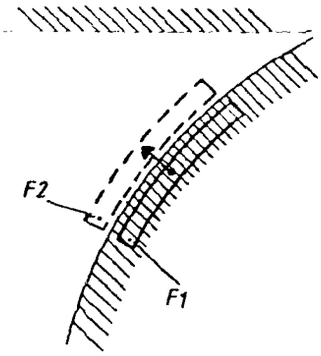

fig.2: One average value of an adapted sampling area is measured by an image-dissector-camera and transmitted to the computer.

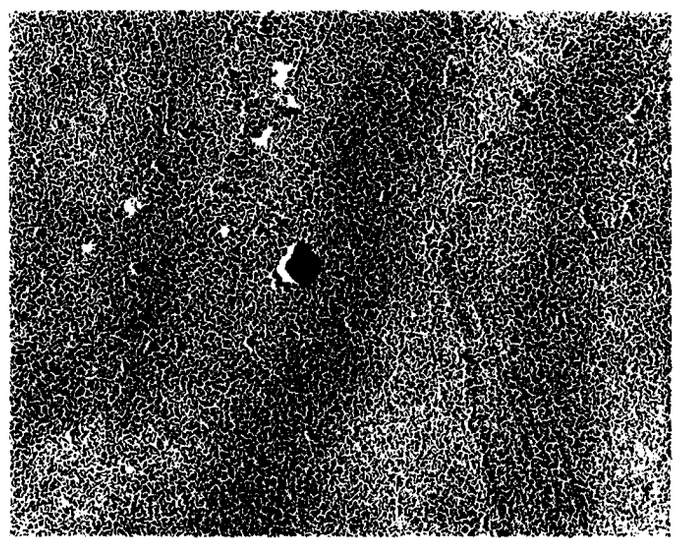

fig.3: The sensor detects position and direction of very imperfect contours with weak contrast in highly strutured background.

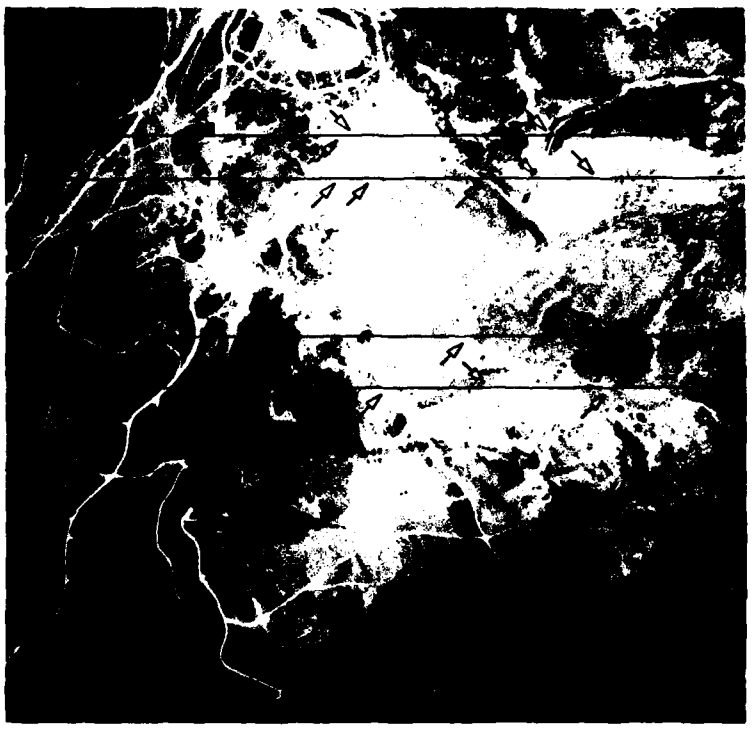

fig 4: 'Flying' accross an aerial photograph along the black lines, the sensor has no segmentation problems when two roads are caught simultaneously by the scanning star.

detected contours

DESIGN AND SIMULATION OF AN INTELLIGENT MISSILE SEEKER

by
J. Hayman
RCA Government Systems Division
Route 38, Building 206-1
Cherry Hill, New Jersey 08358, USA

SUMMARY

An intelligent tracking algorithm for an IR imaging missile seeker and a method of evaluating its performance in simulated flight is described in this paper. The missile is a fire-and-forget, shoulder-launched, anti-tank weapon that lofts to an altitude of approximately 150 meters and then homes toward the target using proportional guidance. A gyro stabilized seeker is precessed to the target by pointing commands. These pointing commands are developed from an imaging sensor by a new tracking algorithm that performs well in a highly cluttered background.

Both the tracking algorithm design and its evaluation in missile flights were accomplished using a digital computer simulation called HUGGER. This program includes a 6 degree-of-freedom missile simulation, a detailed seeker model, a three-dimensional model of the target, a two-dimensional background model, and the intelligent tracking algorithm.

Sensor images of the target as seen from the missile are formed on a 64 x 128 pixel IR-CCD array. The algorithm utilizes three features within the image: intensity, spatial frequency, and internal gradients. A multithresholding technique is also described which enhances target discrimination.

SYMBOLS

B	flux density
C_A, C_{NY}, C_{NP}	aero coefficients for normal forces along the X, Y, Z axes
C_{LD}, C_{MP}, C_{MY}	aero coefficients for moments along the X, Y, Z axes
C_{LP}, C_{MQ}, C_{NR}	aero coefficients for damping moments along the X, Y, Z axes
CG	center of gravity location
d	missile reference length
F	force
$F_T(t)$	missile thrust
H	angular momentum
J	moment of inertia
M	moment
P, Q, R	missile angular body rates about the X, Y, Z axes
s	Laplace operator
S	missile reference area
t	time
T	torque
$[T_{SI}]$	inertial-to-seeker matrix transformation
$[T_{MI}]$	inertial-to-missile matrix transformation
V	missile velocity
V_S	velocity of sound
α	angle of attack
β	sideslip angle
δ	vane deflection
θ_G	pitch gimbal angle
ρ	air density
Ψ_G	yaw gimbal angle
ω	angular rate

SUBSCRIPTS

I	inner gimbal
O	outer gimbal
S	spin axes
X, Y, Z	axes of a right hand coordinate system

INTRODUCTION

Tactical missiles of today have definite operational limitations because seekers are apt to lose track with targets against highly cluttered backgrounds. Such scenarios may be attacks on tanks against a background of roads, foliage, rocks, etc.; attacks on aircraft against a varied cloud background; or attacks from above on aircraft against a terrain background.

The next generation of tactical missiles may use imaging trackers because of the large amount of information in the image that can be utilized by an intelligent tracking algorithm. The algorithm is used to separate (or segment) the target from a cluttered background, and then track this target. With the advent of small, solid state CCD arrays and high speed microprocessors, it is now practical to utilize imaging seekers with intelligent tracking algorithms. Two recent developments by RCA initiated this study. These are the ATMAC microprocessor developed by the Advanced Technology Laboratory (Ref. 1), and the Schottky-barrier IR-CCD array developed by the David Sarnoff Laboratories (Refs. 2, 3, 4 and 5). The latter is a 64 x 128 element staring array which operates in the 3 to 5 micrometer wavelength band with excellent uniformity, sensitivity, and dynamic range. Since it utilizes silicon technology, its potential production economy appears very attractive. A typical image produced by this array is shown in Figure 1.

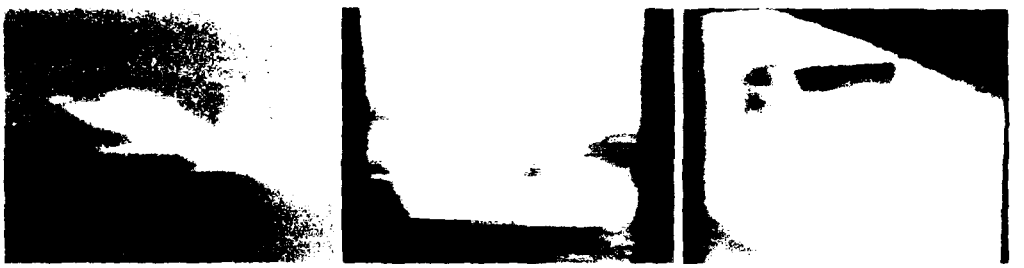

FIGURE 1. AIRCRAFT, TANK AND JEEP IMAGED ON A SCHOTTKY-BARRIER IR-CCD

This paper describes the computer simulation work that verifies successful operation of a missile system containing the IR-CCD array and tracking algorithm. The missile is a fire-and-forget, shoulder-launched, anti-tank weapon that lofts to an altitude of approximately 150 meters and then homes toward the target using proportional guidance. A gyro stabilized seeker is precessed to point at the target by signals developed from the new tracking algorithm. These signals are also used for missile guidance. Both the tracking algorithm design and its evaluation in missile flights were accomplished using a digital computer simulation called HUGGER. Program HUGGER's scenario is illustrated in Figure 2. It includes a 6 degree-of-freedom missile simulation, a detailed seeker model, a three-dimensional model of the target, a two-dimensional background model, and the tracking algorithm. Actual sensor images of the target as seen from the missile are displayed to assist in the algorithm development. HUGGER also provides each corresponding segmented image so that the algorithm's discrimination capability can be evaluated.

The intelligent tracking algorithm encloses the target with an adaptive gate and uses multifeature and multithreshold techniques to achieve superior image segmentation. A rectangular adaptive gate is servoed to enclose only the target vicinity, thereby eliminating most of the extraneous background clutter within the field of view. A background gate is located just around the perimeter of the centroid gate. There are three features extracted from the image: intensity, spatial frequency, and internal gradients. Each of these features is thresholded using the multithreshold technique where up to four thresholds are automatically employed, allowing target pixels to be identified if they are above, below, or in between background value bands. Enhancement is accomplished by changing the intensity value of a pixel if either the spatial frequency or the gradient value is over its respective threshold. The enhanced intensity feature is then finally thresholded to provide the segmented image. Adaptive gate size, seeker pointing commands, as well as missile guidance signals, are all derived from this segmented image.

During terminal navigation, when the target fills the entire field-of-view, the adaptive gate tracker is replaced by a centrally weighted correlation tracker. Correlation is performed along a horizontal strip for yaw and a vertical strip for pitch. These two strips form a cross at the center of the field-of-view. Because of the high rate of range closure and the high line of sight rates during terminal flight, correlation must be done on a frame-to-frame basis. Drift due to the range closure effect is minimized by centrally weighting each correlation strip. This low drift algorithm is used until impact.

The simulations showed that the 64 x 128 CCD array, with the intelligent algorithm, would track targets in high clutter and could be made to consistently impact the upper surface of a tank where armor is at a minimum. Program HUGGER was an excellent tool for evaluating algorithm modifications during development. Algorithms can be compared over the same trajectory, with the same target intensity and background statistics. It would be impossible to do this otherwise, even with actual hardware. HUGGER also allows target tracking with realistic line of sight rates and accelerations, range closure, and changing aspect angle.

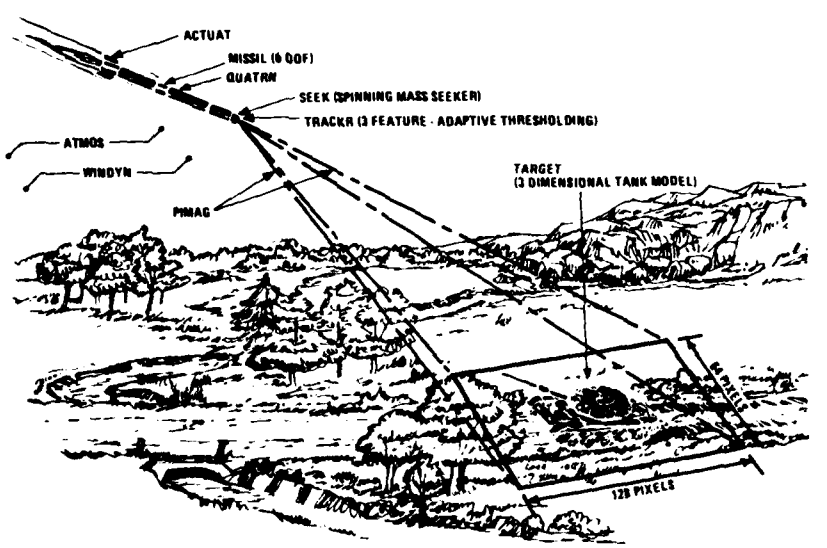

FIGURE 2. PROGRAM HUGGER'S SCENARIO

PROGRAM HUGGER

Program HUGGER is a modularized FORTRAN program consisting of the subroutines listed in Table 1. A flow diagram of the program is given in Figure 3, and a functional block diagram is shown in Figure 4. Output data is provided in the following formats:

1. Printed data, where 56 variables are printed.
2. Striplot (Figure 5), where up to 10 variables are plotted against time.
3. Segmented image plots (Figure 6), indicating target/nontarget pixels as determined by the intelligent algorithm.
4. Image plots (Figure 7), where images formed on a 64 x 128 IR-CCD array are plotted using a gray scale.

Considerable detail is modeled in HUGGER so that many parts of the missile system can be studied during flight. In order to eliminate excessive execution time, the following options are provided:

1. A detailed gyro stabilized seeker with gimbal friction, magnetic torques and input errors, or a simplified seeker model.
2. A three-dimensional target model, the tracking algorithm and image forming, or a simple point target.
3. An optical point spread function, or a simple one-ray-per-pixel projection.
4. Image plots, or no image plots.
5. Steady or gusty wind or both, or no wind.
6. A moving or a static target.

TABLE 1
PROGRAM HUGGER SUBROUTINES

MAIN	CALLS SUBROUTINES AND OUTPUTS DATA
DATA.	INPUTS DATA
MISSIL	SIX DEGREE OF FREEDOM MISSILE SIMULATION
QUATRN .	QUATERNIAN UPDATE OF I/B MATRIX
FUNC1V . .	FUNCTION OF ONE VARIABLE
FUNC2V . .	FUNCTION OF TWO VARIABLES
FUNC3V . .	FUNCTION OF THREE VARIABLES
ATMOS. . .	ATMOSPHERIC MODEL
MAT33 . . .	MULTIPLIES 3 X 3 MATRICES
WINDYN. .	WIND GUST DYNAMICS
RANDOM .	RANDOM NUMBER GENERATOR FOR GUSTS
FILTER . .	AUTOPILOT & ACTUATOR PREFILTERS
GYRODY .	ROLL RATE GYRO DYNAMICS
ACTUAT. .	ACTUATOR DYNAMICS
TARGET. . . .	THREE DIMENSIONAL MODEL OF A TANK
SEEK	TRACKING SERVO & GYRODYNAMICS
TRACKR. . . .	ADAPTIVE GATE & CORRELATION TRACKING ALGORITHMS
PIMAGE	PLOTS THE IMAGES FROM A CCD ARRAY

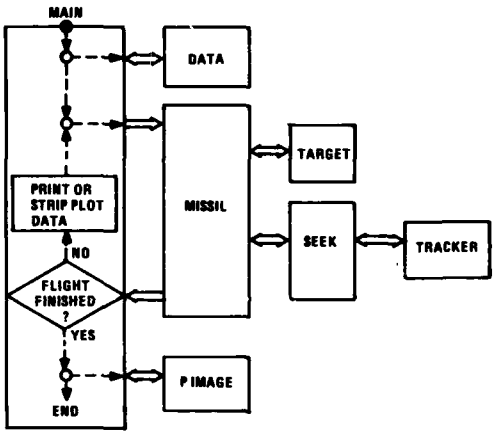

FIGURE 3. SIMPLIFIED FLOW DIAGRAM OF PROGRAM HUGGER

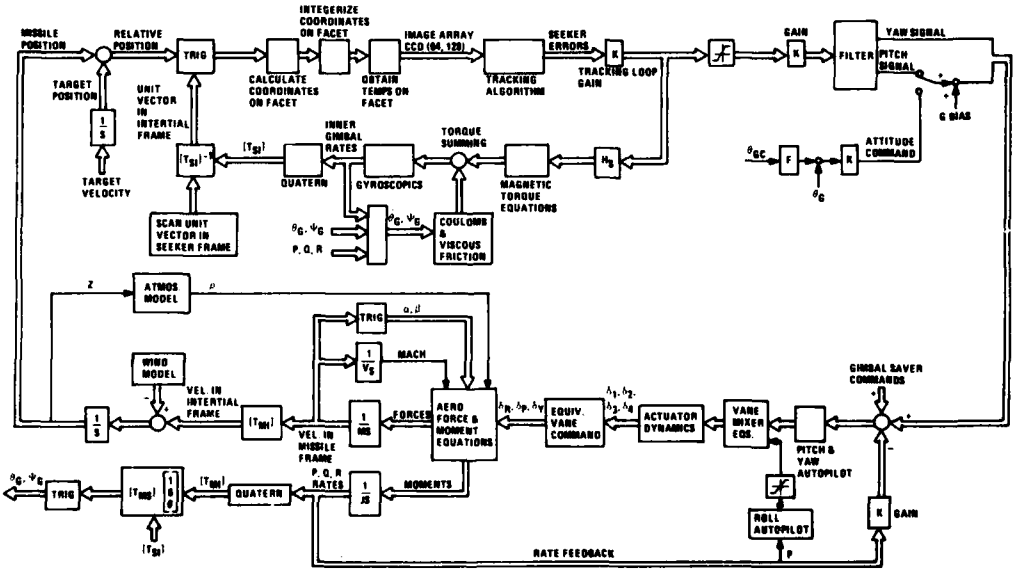

FIGURE 4. FUNCTIONAL BLOCK DIAGRAM OF PROGRAM HUGGER

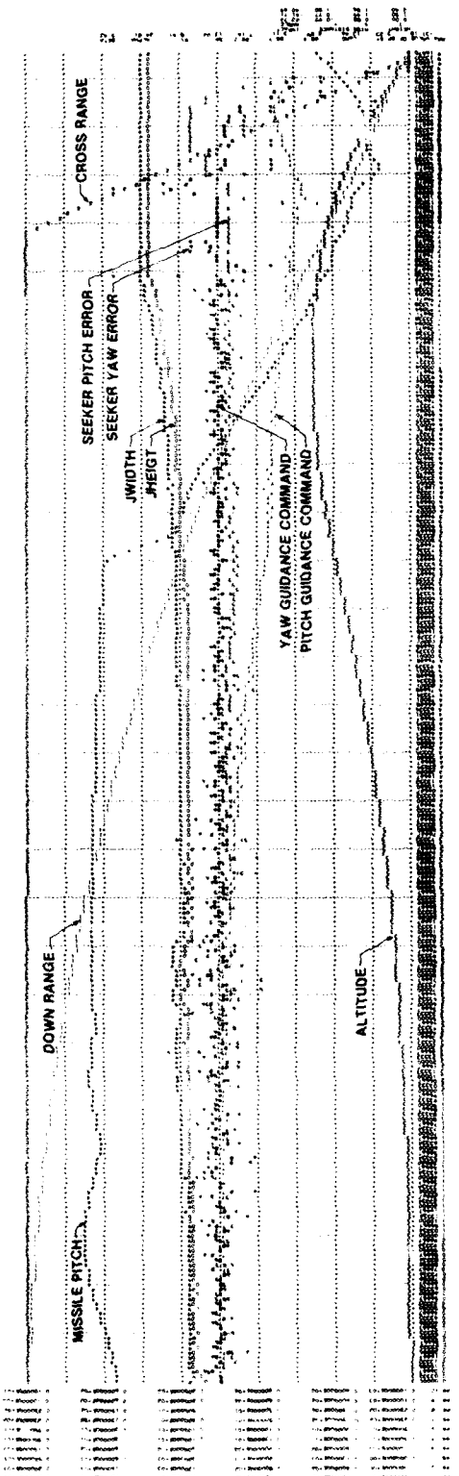

FIGURE 5. STRIP PLOT FROM PROGRAM HUGGER

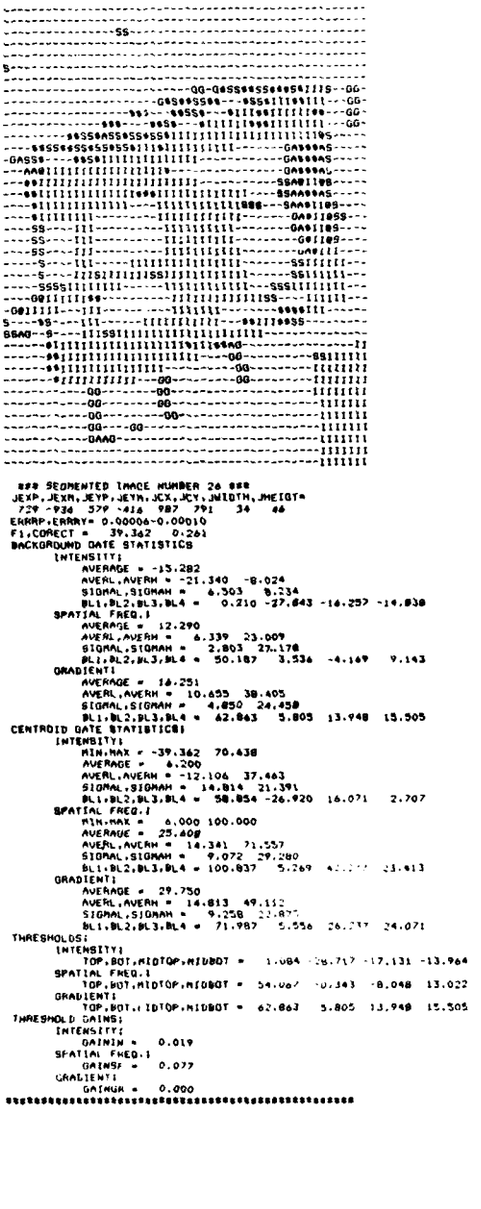

```
  ### SEGMENTED IMAGE NUMBER 26 ###
JEXP,JEXR,JEYP,JEYR,JCX,JCY,JWIDTH,JHEIGT=
 729 -934  379 -416  987  791   34   46
ERRRP,ERRRY= 0.00006-0.00010
F1,CORRECT =  39.342  0.261
BACKGROUND DATE STATISTICS
      INTENSITY:
          AVERAGE = -15.282
          AVERL,AVERH = -21.340  -8.024
          SIGMAL,SIGMAH =  6.503   8.234
          BL1,BL2,BL3,BL4 =   0.210 -27.843 -16.257 -14.838
      SPATIAL FREQ.:
          AVERAGE =  12.290
          AVERL,AVERH =   6.339  23.009
          SIGMAL,SIGMAH =  2.803  27.178
          BL1,BL2,BL3,BL4 =  50.187   3.536   -4.149   9.143
      GRADIENT:
          AVERAGE =  18.251
          AVERL,AVERH =  10.655  38.405
          SIGMAL,SIGMAH =  4.850  24.458
          BL1,BL2,BL3,BL4 =  42.863   5.805  13.948  15.505
CENTROID DATE STATISTICS:
      INTENSITY:
          MIN,MAX = -39.362  70.438
          AVERAGE =   6.200
          AVERL,AVERH = -12.104  37.463
          SIGMAL,SIGMAH =  14.814  21.391
          BL1,BL2,BL3,BL4 =  58.854 -26.920  16.071   2.707
      SPATIAL FREQ.:
          MIN,MAX =   6.000 100.000
          AVERAGE =  25.408
          AVERL,AVERH =  14.341  71.557
          SIGMAL,SIGMAH =   9.072  29.280
          BL1,BL2,BL3,BL4 = 100.837   5.269  [illegible]  23.413
      GRADIENT:
          AVERAGE =  29.750
          AVERL,AVERH =  14.813  49.112
          SIGMAL,SIGMAH =   9.258  [illegible]
          BL1,BL2,BL3,BL4 =  71.987   5.556  26.[illegible]  24.071
THRESHOLDS:
      INTENSITY:
          TOP,BOT,MIDTOP,MIDBOT =   1.084 -26.[illegible] -17.131 -13.964
      SPATIAL FREQ.:
          TOP,BOT,MIDTOP,MIDBOT =  54.067 [illegible] -8.048  13.022
      GRADIENT:
          TOP,BOT,MIDTOP,MIDBOT =  62.863   5.805  13.948  15.505
THRESHOLD GAINS:
      INTENSITY:
          GAININ =   0.019
      SPATIAL FREQ.:
          GAINSF =   0.077
      GRADIENT:
          GAINGR =   0.000
```

FIGURE 6. SEGMENTED IMAGE AND DIAGNOSTICS

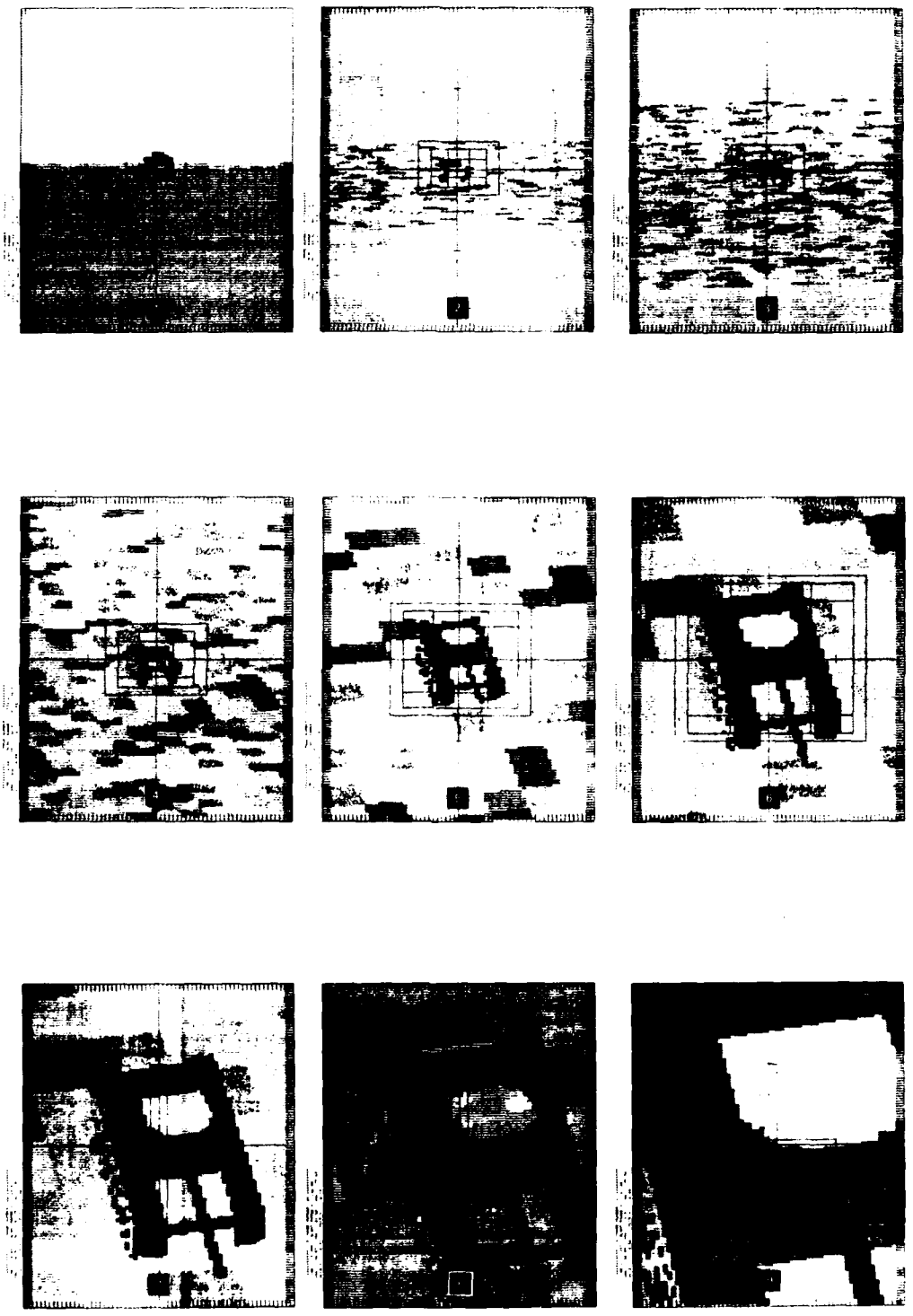

FIGURE 7. TYPICAL IMAGE PLOTS FROM PROGRAM HUGGER

MISSILE MODEL

The missile studied in this paper is a ground-to-ground antitank weapon with its seeker locked on before launch. It is caused to initially loft by commanding a pitch gimbal angle of 17 degrees to an attitude autopilot whose feedback is the pitch gimbal angle. When the pitch line-of-sight rate signal from the seeker increases to 6 deg/sec, the control law is switched to proportional guidance. Proportional guidance is always used for yaw control.

The six-degree-of-freedom missile model is described by the block diagram of Figure 4. This model (Ref. 6) contains the three force equations acting on the missile body:

$$F_X = -C_A(\alpha)\, Q_S + F_T(t)$$

$$F_Y = C_{NY}(\beta, \delta_Y)\, Q_S$$

$$F_Z = -C_{NP}(\alpha, \delta_P)\, Q_S$$

and the three moment equations:

$$M_X = [C_{LD}(M)\,\delta_R + C_{LP}(M)\, D_V P]\, Q_{SD}$$

$$M_Y = [C_{MP}(\alpha, \delta_P) + C_{NP}(\alpha, \delta_Y)\,(CG(t) - CG_R) + C_{MQ}(M)\, D_V Q]\, Q_{SD}$$

$$= [C_{MY}(\beta, \delta_Y) + C_{NY}(\beta, \delta_Y)\,(CG(t) - C_{NR}(M)\, D_V R]\, Q_{SD}$$

where:

$$Q = \tfrac{1}{2}\rho V^2$$

$$Q_S = QS$$

$$Q_{SD} = Q_S d$$

$$D_V = d/2V$$

The aerodynamic coefficients can be functions of one, two or three variables. Linear interpolation is employed between table entries by subroutines FUNC1V, FUNC2V, and FUNC3V.

The required roll, pitch and yaw commands (δ_{RC}, δ_{PC}, δ_{YC}) to the fin actuators are obtained by processing the seeker error signals with the autopilot transfer functions. The individual commands to the four fin actuators are obtained by using the following relations:

$$\delta_{1C} = \delta_{RC} + \delta_{YC} \qquad \delta_{3C} = -\delta_{RC} + \delta_{YC}$$

$$\delta_{2C} = \delta_{PC} \qquad \delta_{4C} = \delta_{PC}$$

These fin commands, when acted upon by the actuator dynamics, result in four actual fin deflections: δ_1, δ_2, δ_3, δ_4. The three equivalent fin deflections required for obtaining the aero forces and moments are:

$$\delta_R = (\delta_1 - \delta_3)/2$$

$$\delta_P = (\delta_2 + \delta_4)/2$$

$$\delta_Y = (\delta_1 + \delta_3)/2$$

The coordinate axis system assumed for the above equations is illustrated in Figure 8.

A quaternian method is used to obtain the inertial-to-missile body coordinate matrix transformation, $[T_{MI}]$, as well as the inertial-to-seeker transformation, $[T_{SI}]$.

TARGET MODEL

A three-dimensional model of a tank is required for a realistic simulation of a missile system with an imaging seeker. The tank model consists of seventeen planes or facets, each 'painted' with the appropriate radiance value to create a tank-like image. The resolution on each facet is 0.10 meters. The tank sets upon a two-dimensional background consisting of a 69 x 69 matrix of radiance values with a resolution of 2 meters. Clutter is simulated by a Gaussian distribution with the mean and standard deviation as program inputs. It is, however, an easy matter to insert a road under the tank or hot objects nearby. An optical point spread function provides more realistic images of the target; however, this feature was made optional because it increases the program run time and does not seem to appreciably affect tracking ability.

The target is modeled by incrementing (pixel-by-pixel) a unit vector, $\underline{U}_S$, in the seeker frame until the entire gate area within the field-of-view is scanned. A transformation to the inertial frame is performed after each pixel increment with matrix equation, $\underline{U}_I = [T_{SI}]^{-1}\,\underline{U}_S$. Use of the appropriate trigometric relations, the unit pointing vector $\underline{U}_I$, and the vector representing the distance between the target and the missile (see Figure 4), yields the location of where a ray impinges on a facet. The resulting two coordinates on the facet are integerized so that the appropriate radiance value can be obtained from a two-dimensional array representing that facet. A 64 x 128 array (called CCD) representing the image is then loaded with these radiance values.

SEEKER MODEL

The gyro stabilized seeker shown in Figure 9 was modeled in considerable detail so that nutation and the effects of various error sources could be evaluated. The gyroscopic equations (Ref. 7) are manipulated so that the torque summing points are located at the gimbal axes, thereby facilitating the input of viscous and coulomb bearing friction. Magnetic torques are generated assuming torquer coils fixed to the missile and a magnet fixed to the spinning inner gimbal. The coordinate systems used in the gyro model derivation is shown in Figure 10.

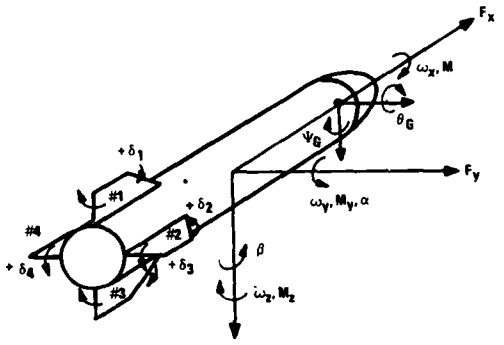

FIGURE 8. MISSILE BODY COORDINATE AXES

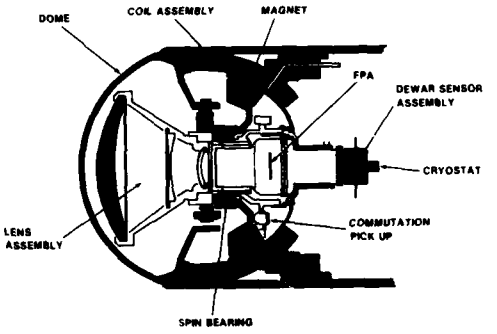

FIGURE 9. GYRO STABILIZED SEEKER

The inner gimbal angular momentum can be expressed as:

$$\underline{H}_I = (J_{IX}\omega_{IX} + H_S)\,\underline{i} + J_{IY}\omega_{IY}\,\underline{j} + J_{IZ}\omega_{IZ}\,\underline{k} \tag{1}$$

and the outer gimbal angular momentum is:

$$\underline{H}_O = J_{OX}\omega_{OX}\,\underline{i} + J_{OY}\omega_{OY}\,\underline{j} + J_{OZ}\omega_{OZ}\,\underline{k} \tag{2}$$

Since the sum of the external torques acting on a body is equal to the time rate of change of its angular momentum, we have for the inner gimbal:

$$\Sigma T = \dot{H}_I = \frac{\partial H_I}{\partial t} + \underline{\omega}_I \times \underline{H}_I$$

$$\dot{\underline{H}}_I = [J_{IX}\dot{\omega}_{IX} + (J_{IZ} - J_{IY})\,\omega_{IY}\,\omega_{IZ}]\,\underline{i}_I + [J_{IY}\dot{\omega}_{IY} + (J_{IX} - J_{IZ})\,\omega_{IX}\,\omega_{IZ} + H_S\omega_{IZ}]\,\underline{j}_I + [J_{IZ}\dot{\omega}_{IZ} + (J_{IY} - J_{IX})\,\omega_{IX}\,\omega_{IY} - H_S\,\omega_{IY}]\,\underline{k}_I \tag{3}$$

Likewise for the outer gimbal:

$$\dot{\underline{H}}_O = [J_{OX}\dot{\omega}_{OX} + (J_{OZ} - J_{OY})\,\omega_{OY}\,\omega_{OZ}]\,\underline{i}_O + [J_{OY}\dot{\omega}_{OY} + (J_{OX} - J_{OZ})\,\omega_{OX}\,\omega_{OZ}]\,\underline{j}_O + [J_{OZ}\dot{\omega}_{OZ} + (J_{OY} - J_{OX})\,\omega_{OX}\,\omega_{OY}]\,\underline{k}_O \tag{4}$$

The torque equations about each gimbal axis are obtained from the following dot products:

$$\Sigma T_{IZ} = \dot{\underline{H}}_I \cdot \underline{K}_I \tag{5}$$

$$\Sigma T_{OY} = (\dot{\underline{H}}_I + \dot{\underline{H}}_O) \cdot \underline{j}_O \tag{6}$$

From Equations (3) and (5),

$$\Sigma T_{IZ} = J_{IZ}\,\dot{\omega}_{IZ} + (J_{IY} - J_{IX})\,\omega_{IX}\,\omega_{IY} - H_S\,\omega_{IY} \tag{7}$$

and from Equations (3), (4) and (6),

$$\Sigma T_{OY} = [J_{IX}\dot{\omega}_{IX} + (J_{IZ} - J_{IY})\,\omega_{IY}\,\omega_{IZ}]\,\text{SIN}\,\Psi_G + [J_{IY}\dot{\omega}_{IY} + (J_{IX} - J_{IZ})\,\omega_{IX}\,\omega_{IZ} + H_S\,\omega_{IZ}]\,\text{COS}\,\Psi_G + [J_{OY}\dot{\omega}_{OY} + (J_{OX} - J_{OZ})\,\omega_{OX}\,\omega_{OZ}] \tag{8}$$

Assuming that terms containing $(J_{IZ} - J_{IY})$, ω_{OX} and ω_{IX} are negligible, Equations (7) and (8) reduce to:

$$\Sigma T_{IZ} = J_{IZ}\,\dot{\omega}_{IZ} - H_S\,\omega_{IY} \tag{9}$$

$$\Sigma T_{OY} = J_{IX}\,\dot{\omega}_{IX}\,\text{SIN}\,\Psi_G + (J_{IY}\,\dot{\omega}_{IY} + H_S\,\omega_{IZ})\,\text{COS}\,\Psi_G + J_{OY}\,\dot{\omega}_{OY} \tag{10}$$

The inner and outer gimbal accelerations are related by the equations:

$$\dot{\omega}_{IX} = \dot{\omega}_{OX}\,\text{COS}\,\Psi_G + \dot{\omega}_{OY}\,\text{SIN}\,\Psi_G$$

$$\dot{\omega}_{IY} = \dot{\omega}_{OX}\,\text{SIN}\,\Psi_G + \dot{\omega}_{OY}\,\text{COS}\,\Psi_G \tag{11}$$

Equation (10) can be further simplified by use of Equations (11) and assuming that $\dot{\omega}_{OX}$ is small,

$$\Sigma T_{OY} = J_Y \dot{\omega}_{OY} + H_S \omega_{IZ} \cos \Psi_G \tag{12}$$

where:

$$J_Y = J_{OY} + J_{IX} \sin^2 \Psi_G + J_{IY} \cos^2 \Psi_G$$

Equations (9) and (12) are used in the seeker model and are shown in the block diagram of Figure 11. Notice that the torque summing points are conveniently located along the gimbal axes.

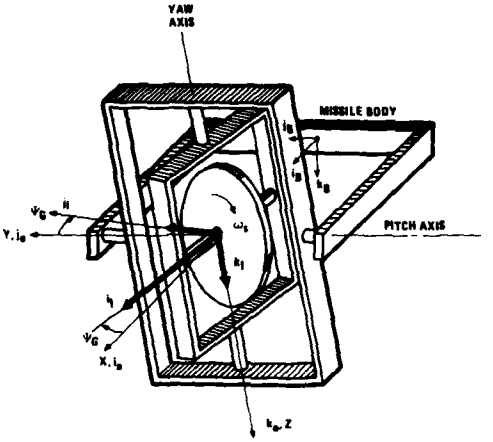

FIGURE 10. COORDINATE SYSTEMS FOR THE TWO DEGREE OF FREEDOM GYRO

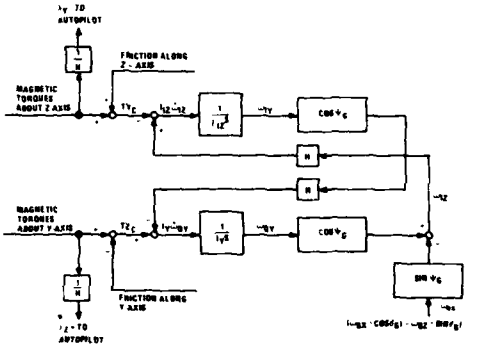

FIGURE 11. BLOCK DIAGRAM OF THE GYRO DYNAMICS

An expression for the magnetic torques (Ref. 8) will be derived with torquer coils fixed to the missile body and a magnet fixed to the inner gimbal. Since the gimbal rotation order used in this analysis is pitch (θ_G), yaw (Ψ_G) followed by roll ($\omega_S t$), the transformation matrix from a body to seeker frame can be obtained.

$$\underline{S} = [T_{SB}]\, \underline{b}$$

where,

$\underline{b}$ = unit vector in the body frame

$\underline{s}$ = unit vector in the seeker frame

$$[T_{SB}] = \begin{bmatrix} (C\Psi_G C\theta_G) & (S\Psi_G) & (-C\Psi_G S\theta_G) \\ (-C\omega_S t\, S\Psi_G C\theta_G + S\omega_S t S\theta_G) & (C\omega_S t C\Psi_G) & (C\omega_S t\, S\Psi_G S\theta_G + S\omega_S t C\theta_G) \\ (S\omega_S t S\Psi_G C\theta_G + C\omega_S t S\theta_G) & (-S\omega_S t C\Psi_G) & (-S\omega_S t S\Psi_G S\theta_G + C\omega_S t C\theta_G) \end{bmatrix}$$

A unit vector in the missile body frame is:

$$\underline{b} = [T_{SB}]^T \underline{s}$$

If a magnet is aligned along the seeker Y-axis, its normalized coordinates in the missile body frame are:

$$\underline{b} = [T_{SB}]^T \begin{bmatrix} 0 \\ 1 \\ 0 \end{bmatrix}$$

$$b = \begin{bmatrix} -C\omega_S t S\Psi_G C\theta_G + S\omega_S t S\theta_G \\ C\omega_S t C\Psi_G \\ C\omega_S t S\Psi_G S\theta_G + S\omega_S t C\theta_G \end{bmatrix}$$

and its projection along the missile X-axis is:

$$b_x = -C\omega_S t S\Psi_G C\theta_G + S\omega_S t S\theta_G \tag{13}$$

A voltage is induced in the coil proportional to the rate of flux lines cut by the coil. The resulting coil current will produce the following induced flux density:

$$B_i = T_i \underline{b}_x \tag{14}$$

where T_i is a constant.

Use of equations (13) and (14) yields:

$$B_i = T_i [S\omega_S t(\omega_S S\Psi_G C\theta_G + C\theta_G \dot{\theta}_G) + C\omega_S t(-C\Psi_G C\theta_G \dot{\Psi}_G + S\Psi_G S\theta_G \dot{\theta}_G + \omega_S S\theta_G)] \quad (15)$$

The flux density produced by the control signals E_y and E_z for pitch and yaw, respectively, is:

$$B_c = T_c (E_y C\omega_S t - E_Z S\omega_S t) \quad (16)$$

and the total flux density vector in the missile frame becomes:

$$\underline{B} + (B_c + B_i)\,\underline{i} \quad (17)$$

The magnetic torque from the two magnet poles is:

$$\underline{T}m = 2t_c (\underline{B} \times \underline{b})$$

$$\underline{T}m = 2t_c \begin{bmatrix} 0 \\ -BbZ \\ BbY \end{bmatrix}$$

$$\underline{T}m = 2t_c \begin{bmatrix} 0 \\ -(B_c + B_i)(C\omega_S t S\Psi_G S\theta_G + S\omega_S t\, C\theta_G) \\ (B_c + B_i)(C\omega_S t C\Psi_G) \end{bmatrix} \quad (18)$$

where t_c is a constant.

The magnetic torque along the missile Y axis (i.e., the pitch gimbal axis) is obtained using Equations (15), (16) and (18):

$$T_{my} = 2t_c [T_c (E_c C\omega_S t - E_Z S\omega_S t) + T_i S\omega_S t (\omega_S S\Psi_G C\theta_G + C\theta_G \dot{\theta}_G) + T_i C\omega_S t (-C\Psi_G C\theta_G \dot{\Psi}_G + S\Psi_G S\theta_G \dot{\theta}_G + \omega_S S\theta_G)] \cdot [C\omega_S t S\Psi_G S\theta_G + S\omega_S t C\theta_G] \quad (19)$$

Equation (19) can be simplified by the following identities and assuming that $2\omega_S$ is beyond the bandwidth of the tracker loop:

$$SIN\omega_S t\ COS\omega_S t = 1/2\ SIN2\omega_S t \sim 0 \qquad SIN^2\omega_S t = 1/2\ COS2\omega_S t \sim 1/2 \qquad COS^2\omega_S t = 1/2 + 1/2\ COS2\omega_S t \sim 1/2$$

$$T_{MY} = t_c [-T_C E_Y S\Psi_G S\theta_G + T_C E_Z C\theta_G - T_i \omega_S S\Psi_G + T_i \dot{\Psi}_G (C\Psi_G C\theta_G S\Psi_G S\theta_G) - T_i \dot{\theta}_G (C^2\theta_G + S^2\Psi_G S^2\theta_G)] \quad (20)$$

Equation (20) can be further simplified by neglecting terms containing $\dot{\theta}_G$ and $\dot{\Psi}_G$ since they are much smaller than ω_S.

$$T_{MY} = t_C (T_C E_Z COS\theta_G - T_C E_Y SIN\Psi_G SIN\theta_G - T_i \omega_S SIN\Psi_G) \quad (21)$$

Equation (21) provides the magnetic torque about the Y-gimbal axis. The torque along the Z missile axis is obtained using Equations (15), (16) and (18):

$$T_{MZ} = 2t_C [T_C (E_Y C\omega_S t - E_Z S\omega_S t) + T_i S\omega_S t (\omega_S S\Psi_G C\theta_G + C\theta_G \dot{\theta}_G) + T_i C\omega_S t (S\Psi_G S\theta_G \dot{\theta}_G - C\Psi_G C\theta_G \Psi_G + \omega_S S\theta_G)] [C\omega_S t C\Psi_G]$$

Simplifying as before yields:

$$T_{MZ} = t_C (T_C E_Y COS\Psi_G + T_i \omega_S SIN\theta_G COS\Psi_G) \quad (22)$$

Since the torque about the Z-gimbal axis is:

$$T_{GZ} = T_{MZ} COS\theta_G$$

$$T_{GZ} = t_C (T_C E_Y COS\Psi_G COS\theta_G + T_i \omega_S SIN\theta_G COS\theta_G COS\Psi_G) \quad (23)$$

Equations (21) and (23) are put in the following forms for convenience:

$$T_{GY} = T_Z COS\theta_G - T_Y SIN\Psi_G SIN\theta_G - \frac{H}{\tau_A} SIN\Psi_G \quad (24)$$

$$T_{GZ} = T_Y COS\Psi_G COS\theta_G + \frac{H}{\tau_A} SIN\theta_G COS\theta_G COS\Psi_G \quad (25)$$

where,

$T_Z = t_c T_c E_Z$, torque command about the Y-axis

$T_Y = t_c T_c E_Y$, torque command about the X-axis

$H = J_s \omega_s$, gyro angular momentum

τ_A = autoerection time constant.

These are the magnetic torque equations used in Program HUGGER.

Gimbal angles are obtained from the inertial-to-missile and the inertial-to-seeker matrix transformations, $[T_{MI}]$ and $[T_{SI}]$. These two matrices are obtained using a quaternian method. The seeker-to-missile transformation, $[T_{MS}]$ becomes:

$$[T_{MS}] = [T_{MI}]\,[T_{SI}]^T$$

The three components in the missile frame of a unit vector which lies along the seeker X-axis are:

$$\begin{bmatrix} T_{X1} \\ T_{X2} \\ T_{X3} \end{bmatrix} = [T_{MI}]\,[T_{SI}] \begin{bmatrix} 1 \\ 0 \\ 0 \end{bmatrix}$$

from which the gimbal angles are obtained:

$$\theta_G = \text{TAN}^{-1}(-T_{X3}/T_{X1})$$

$$\Psi_G = \text{SIN}^{-1}(T_{X2})$$

An electrical nutation damping loop was effective, easily adjusted, and economical to implement. A gimbal angle signal is merely passed through two filters and then fed back and summed with the voltage precession commands, as illustrated in Figure 12. The filters consist of a differentiator followed by a bandpass filter. Only a single feedback loop, in either pitch or yaw, is necessary. Also, either sinusoidal or square wave commutating signals can be used.

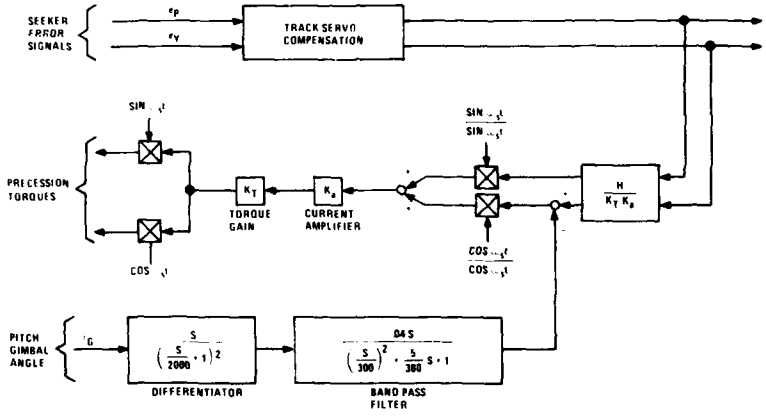

FIGURE 12. BLOCK DIAGRAM OF NUTATION DAMPING LOOP

INTELLIGENT TRACKING ALGORITHM

A major purpose of this paper is to emphasize the advantages of using an intelligent tracking algorithm in a homing missile. The significant features of the algorithm will therefore be described. An overall block diagram showing the sequence of operations is given in Figure 13.

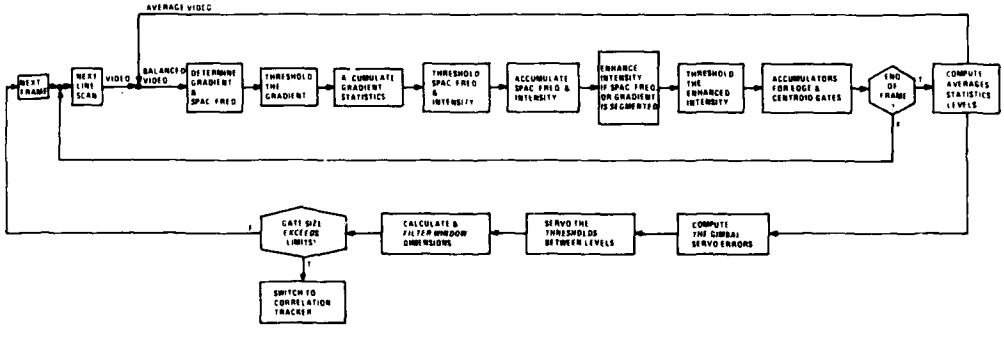

FIGURE 13. BLOCK DIAGRAM OF TRACKING ALGORITHM

A prime consideration during development of this algorithm was its implementation in real time with a minimum of electronics. The algorithm was therefore made one-dimensional to minimize execution time and memory requirements.

An adaptive gate is used by the tracker to enclose only the target area, thereby eliminating the processing of extraneous clutter some distance from the target. This gate adaptively changes in size to enclose the target, while the target is kept centered in the field-of-view by the gimbal servos. The gate arrangement is shown in Figure 14. Four edge gates are located along each side of a rectangular shaped centroid gate. A narrow background gate is placed around the perimeter of the centroid gate.

Simplified one-dimensional operation of the tracker is illustrated in Figure 15. If the target grows in size, the edge gates expand, thereby increasing the size of the centroid gate. The signal to spread or contract the edge gates is obtained by an area balance technique (target/non-target) within each pair of edge gates (right/left, top/bottom). The signals to move the gimbals are developed within the centroid gate. Again, an area balance technique (target/non-target) is used within each half of the centroid gate (right/left, top/bottom). The centroid gate continually adapts to enclose only the target region and thereby eliminates most of the clutter within the FOV.

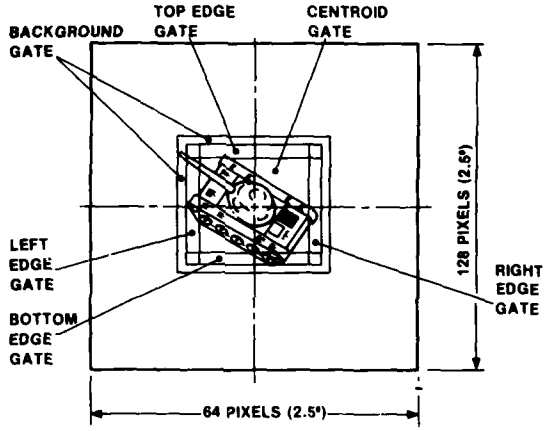

FIGURE 14. GATE ARRANGEMENT FOR THE ADAPTIVE GATE TRACKER

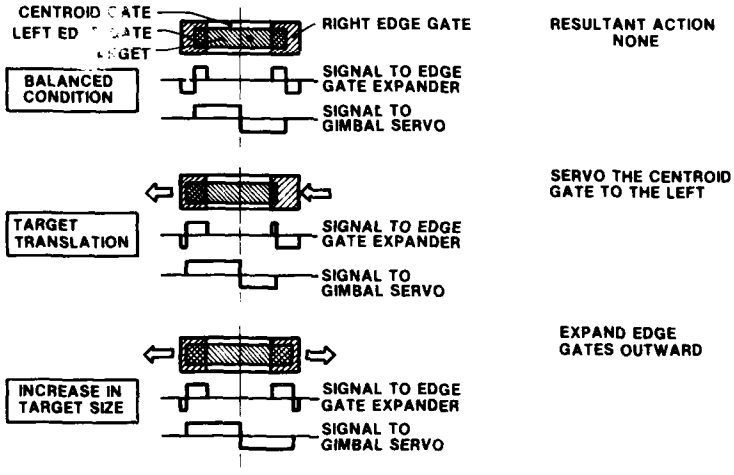

FIGURE 15. OPERATION OF THE ADAPTIVE GATE TRACKER

The tracking servo must be designed (Ref. 9) to complement the tracking algorithm. A type-one servo was not used because it develops excessive error signals, particularly during terminal flight when line-of-sight rates and accelerations are high. An offset target results in a larger gate which encloses more cluttered background and degrades tracking. A type-two tracking servo, shown by the simplified block diagram of Figure 16, eliminates this problem.

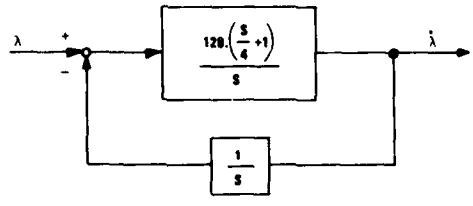

FIGURE 16. SIMPLIFIED TRACKING SERVO

Three features of the image – intensity, spatial frequency, and gradient – are determined for every pixel within the gate areas. The three feature values for each pixel of a line are all determined during the scan of that line. Figure 17 shows how values are assigned to a line of pixels. It also illustrates the uncorrelated nature of the three features.

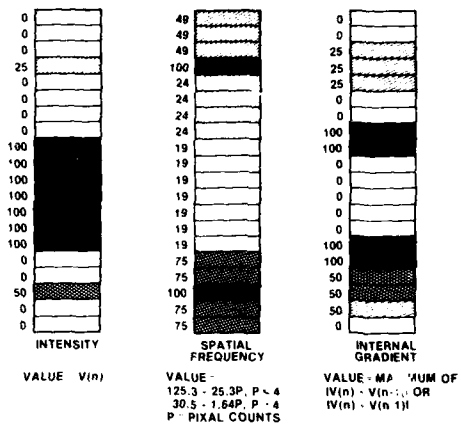

FIGURE 17. ASSIGNMENT OF FEATURE VALUES

The spatial frequency and gradient features are first thresholded. The intensity feature is then increased with a multiplying factor each time the spatial frequency or gradient is above threshold. Finally, the enhanced feature is thresholded for each pixel, yielding the segmented (target/non-target) image.

A tracker with conventional thresholding suffers from a disadvantage, as illustrated by Figure 18.

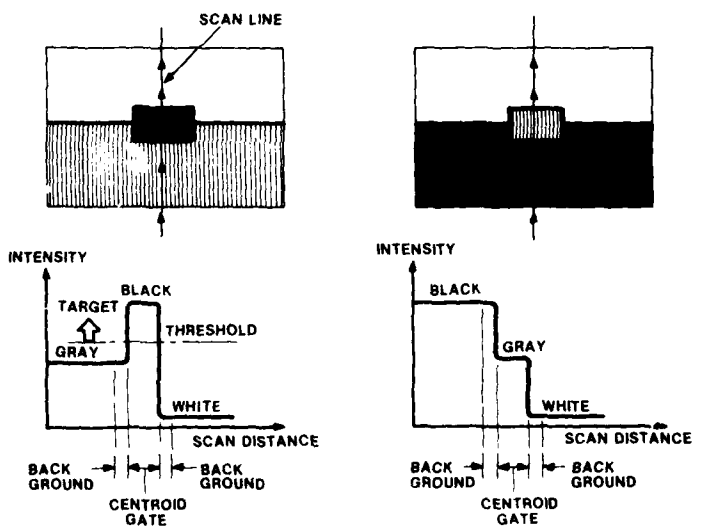

a. THIS TARGET CAN BE THRESHOLDED b. THIS TARGET CANNOT BE THRESHOLDED

FIGURE 18. CONVENTIONAL THRESHOLDING

A black target against a white and gray background is shown in Figure 18-a. In this case, the average background level is between gray and white, and a threshold level can easily be established somewhat above the background. The scene in Figure 18-b, with a gray target against a white and black background, cannot be thresholded even though the target is easily discernible by eye. In this case, the average background level is gray (between black and white), as is the target. Multithresholding eliminates this problem.

The *multithresholding* technique requires the use of the background and centroid gate statistics for each feature. In general these statistics are scene dependent, non-Gaussian, and skewed. Figure 19 shows a plot of intensity values for each pixel along a scan line and illustrates how multithresholding is accomplished. Because of the irregular statistics, the following computational steps are required. First, the background and centroid window averages (W_B, W_C) are calculated. Then, two local averages are obtained for each window, one for pixel values above, and one for pixel values below each window average. These are shown in Figure 19 as B_H, B_L for the background gate and C_H, C_L for the centroid gate. The standard deviation is next calculated for pixel values above and below each window average. These are shown in Figure 19 as σ_{CH}, σ_{CL} for the centroid gate. The six signal levels, L_1 through L_6, are obtained by using the local averages and the standard deviations. Four threshold levels, T_1, T_2, T_3, and T_4 are calculated from

$$T_1 = L_2 + \Delta, \quad T_2 = L_3 - \Delta, \quad T_3 = L_4 + \Delta \quad \text{and} \quad T_4 = L_5 + \Delta,$$

AD-A125 887 ADVANCES IN GUIDANCE AND CONTROL SYSTEMS(U) ADVISORY GROUP FOR AEROSPACE RESEARCH AND DEVELOPMENT NEUILLY-SUR-SEINE (FRANCE) JAN 83 AGARD-CP-321 2/3

UNCLASSIFIED F/G 17/7 NL

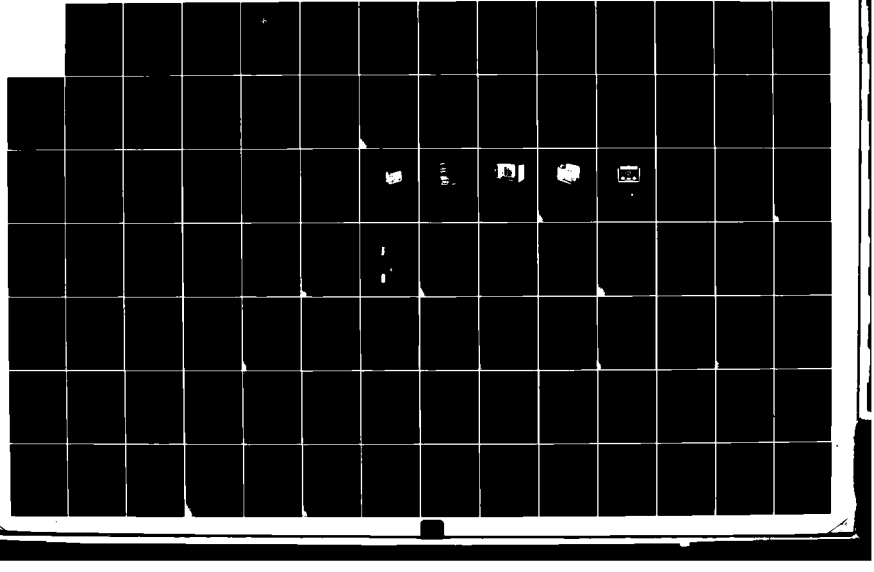

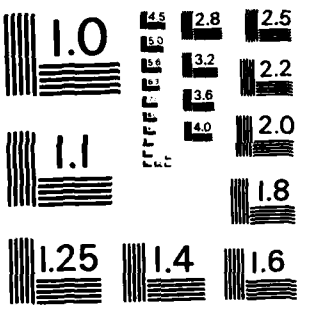

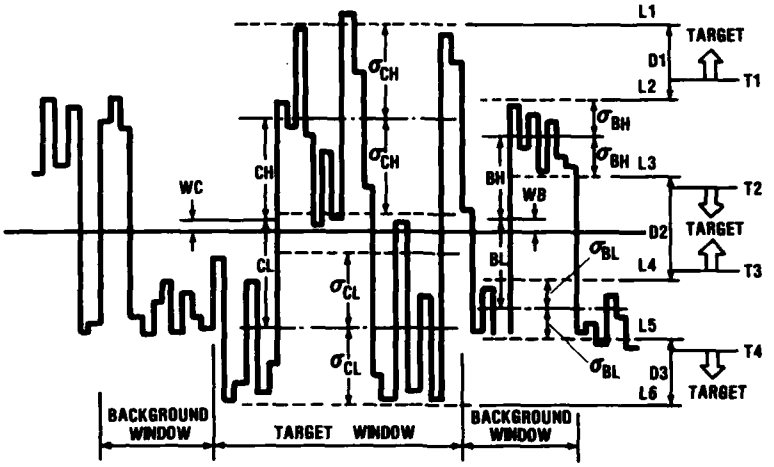

FIGURE 19. SEGMENTATION USING MULTITHRESHOLDING (FOR THE INTENSITY FEATURE)

where

$$\Delta = \text{GAIN}\,[\text{MAX}\,(D_1, -D_2, D_3)].$$

The value of GAIN is determined by servos (one for each feature), which forces an acceptable, five percent of background pixels to be misclassified as target pixels. A flow diagram for thresholding the intensity feature is given in Figure 20. Thresholding for spatial frequency and gradient is identical. It should be noted that the current video intensity signal (BAL) is compared to the four threshold signals (T_1, T_2, T_3, T_4) which were determined from the previous frame. If a particular pixel is classified as target, then INT = 1; if non-target, then INT = 0. A significant improvement in segmentation was obtained using this multithresholding technique.

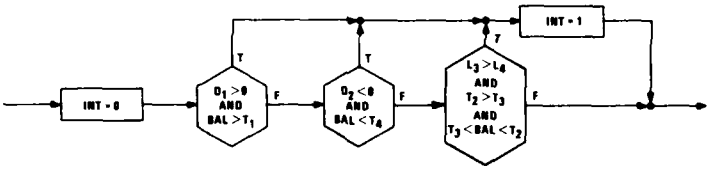

FIGURE 20. THRESHOLDING FOR THE INTENSITY FEATURE

Gate size and servo error signals are determined from the segmented image, as indicated in the block diagram of Figure 21. Most calculations are performed during the line scan. End-of-frame computations are thereby minimized, so that the total processing time is small. The weighting factors W_1 and W_2 have values of +2 and -1, respectively. The weighting factor W_f is given a value equal to the distance (in pixels) from the center of the field of view, and the factor K is used for converting pixels to radians.

The signals which determine the width and height of the centroid gate are processed with digital filters. It is desirable to have low bandwidth, type-2 servos controlling the gate size. The low bandwidth prevents gate jitter, and the type-2 servo allows the gate to expand at a high rate during the terminal portion of the missile trajectory. It was therefore desired to have a gate servo whose open loop Laplace transfer function is:

$$G(s) = \frac{.4(S/.4 + 1)}{S^2} \tag{26}$$

The equivalent Z-transform (Ref. 10) can be obtained by using a bilinear transformation:

$$S = \frac{2}{T}\,\frac{1 - Z^{-1}}{1 + Z^{-1}} \tag{27}$$

Substitution of Equation (27) into (26) yields:

$$G(Z) = .008\,\frac{1 + .00665Z^{-1} - .99335Z^{-2}}{1 - 2Z^{-1} + Z^{-2}}$$

This difference equation is shown implemented in the block diagram of Figure 22.

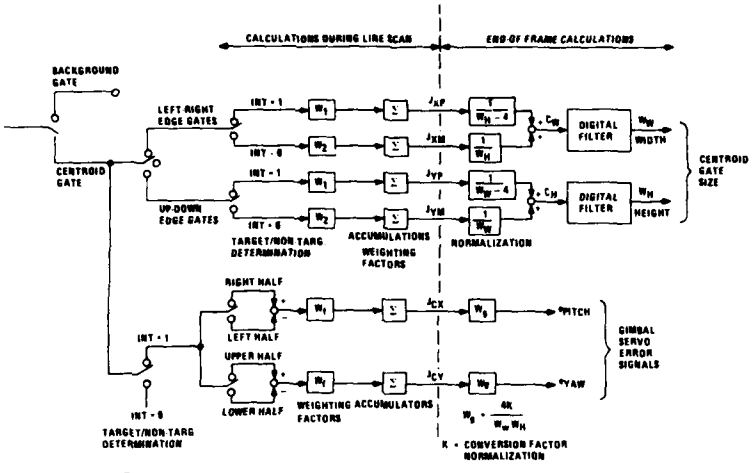

FIGURE 21. GATE SIZE AND SERVO ERROR DETERMINATION

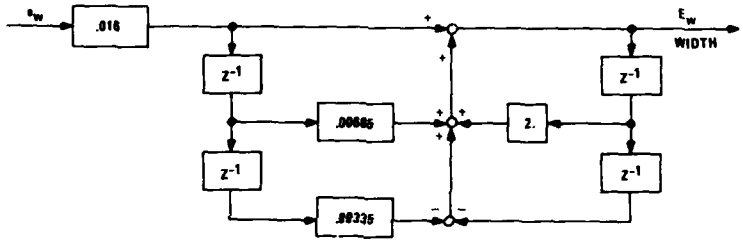

FIGURE 22. DIGITAL FILTER FOR WINDOW SIZE

During terminal guidance, the image of the tank becomes large and eventually fills the entire field-of-view. When this happens, the adaptive gate algorithm will not work because the gates cannot function. A simple correlation tracker is therefore switched into use when the centroid gate exceeds approximately 80% of the field-of-view. The vertical and horizontal correlation strips (see Figure 23) are used to generate the pitch and yaw servo error signals. These strips are four pixels wide, to reduce sensitivity to missile roll. Each set of four pixels is averaged to obtain a single signature along the strip. This results in a horizontal signature 1 x 40 pixels and a vertical signature 1 x 72 pixels. A flow diagram for the correlation tracker is shown in Figure 24. A slice is taken through both signatures at a level of the last signature's average value. The two signatures are then digitized, i.e., given a value of +1 or −1, depending on whether its signal is above or below the slice. Because of the large amount of target expansion during terminal guidance, a frame-to-frame correlation is required. The last digitized signature therefore becomes the current digitized reference signature. Correlation is done by shifting the live signature four pixels to the left and four pixels to the right with respect to the reference signature. This procedure is illustrated in Figure 25. During each shift, each of the aligned pixels is compared. If the aligned pixel of the live signature is the same as that of the reference signature, a value of WGHT is accumulated. If they are different, a value of -WGHT is accumulated. The value of WGHT increases linearly as the center of the field-of-view is approached. It ranges from 1. to ±4.1 for the horizontal correlation and from 1. to ±7.3 for the vertical correlator. This center weighted correlation significantly reduced the drift due to range closure.

In order to find the pitch and yaw error signals, the shift with the greatest correlation value is determined. Shift number 0 indicates a zero error condition (Figure 25). The shift number (in pixels) is converted to the offset error (from shift number 0 in radians. This offset error is accumulated for implementation of a type-one servo. If a no-correlation condition occurs, the last offset error is used. A sequence of images during the terminal trajectory is given in Figure 7. Notice that the correlation strips stay locked on to the same point on the tank in spite of a large image expansion rate and high line of sight rates.

CONCLUSIONS

Recent military events have vividly shown that precision guided missiles are so effective they have changed concepts of modern warfare. With the advent of small, high speed microprocessors and solid state staring arrays, this trend will continue. Imaging seekers which utilize considerably more information concerning the target area are now possible. The recently-developed Schottky-barrier IR-CCD sensor array has the potential for being economically produced since it is fabricated using conventional silicon technology. Intelligent tracking algorithms can be implemented economically with software using presently available digital processors.

Development of intelligent algorithms can be accomplished efficiently by using computer simulations of the entire missile-target system. All the variables of the algorithm and missile are observable, and both the target intensity and the background statistics are controllable.

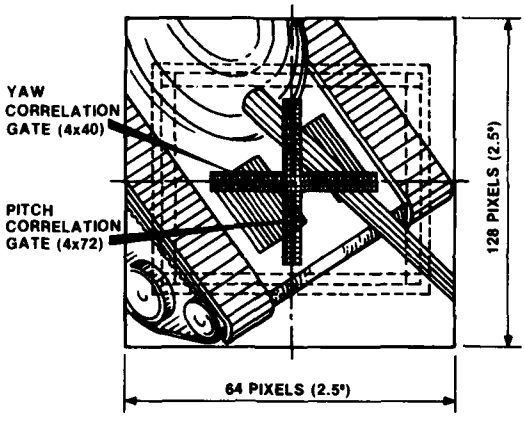

FIGURE 23. CORRELATION TRACKER FOR TERMINAL GUIDANCE

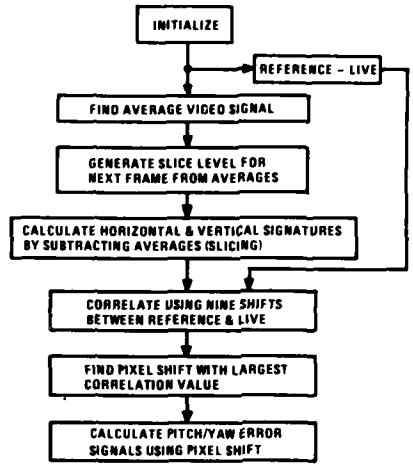

FIGURE 24. FLOW DIAGRAM FOR CORRELATION TRACKER

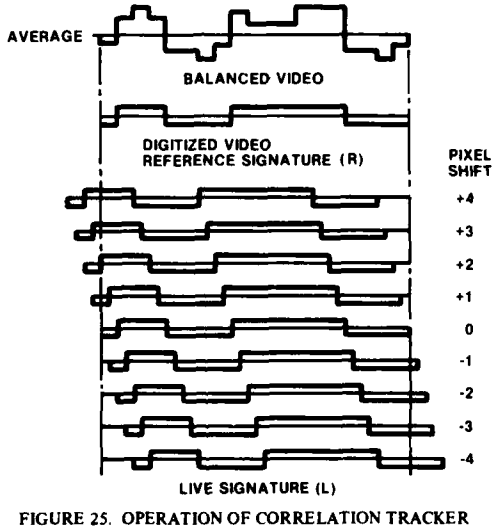

FIGURE 25. OPERATION OF CORRELATION TRACKER

REFERENCES

1. Helbig, W. A., W. J. Davis and A. D. Feigenbaum, "ATMAC Microprocessor," *RCA Engineer*, V23N1, 1977, p. 33.
2. Kosonocky, W. F., H. Elabd et al, RCA Laboratories, Princeton, NJ 08540; and Cantella, M. J., et al, RCA Automated Systems, Burlington, MA 01803, "Design and Performance of a 64 x 128 – Element PtSi Schottky-Barrier IR-CCD Focal Plane Array," SPIE Technical Symposium East, 1982, Arlington, VA, May 3-7, 1982.
3. Taylor, R., L. Skolnik, et al, "Improved Platinum Silicide IRCCD Focal Plane," SPIE Technical Symposium, Advances in Focal Plane Technology, Los Angeles, CA, 217, 103, February 4-5, 1980.
4. Shephard, F D., R. W. Taylor, et al, "Schottky IRCCD Thermal Imaging," Advances in Electronics and Electron Physics, Vol. 52, 7th Symposium on Photo-Electronic Image Devices, 495, 1979.
5. Tegnelia, J. A., "DARPA Unveils Staring Focal Plane Array," *Defense Electronics*, 12, 101, 1980.
6. Blakelock, J. H., *Automatic Control of Aircraft and Missiles* (John Wiley & Sons, Inc., 1965).
7. Thomson, W. T., *Introduction to Space Dynamics* (John Wiley & Sons, Inc., 1963).
8. White, S. A., "Dynamics of a Solenoidal-Torqued Gyro-Stabilized Seeker Assembly for Guidance and Tracking," IEEE Transactions on Aerospace and Electronic Systems, Vol. AED-10, No. 1, January 1974.
9. Kuo, B. C., *Automatic Control Systems* (Prentice-Hall, Inc. 1962).
10. Ragazzini, J. R. and G. F. Franklin, *Sampled-Data Control Systems* (McGraw-Hill Book Co., Inc., 1958), p. 298.
11. Barbe, D. F., "Imaging Devices Using the Charge-Coupled Concept," Proceedings of the IEEE, Vol. 63, No. 1, Jan., 1975.
12. Beynon, J. D. E. and D. R. Lamb, *Charge-Coupled Devices and Their Applications* (McGraw-Hill Book Co., Inc., 1980).
13. Sequin, C. H. and M. F. Tompsett, *Charge Transfer Devices* (Academic Press, Inc., 1975).

SYSTEMES ANEMOBAROMETRIQUES POUR AVIONS DE LA PROCHAINE GENERATION

J. MANDLE

CROUZET DIVISION "AEROSPATIAL"

F26027 VALENCE CEDEX

RESUME

Le but de cet exposé est de présenter les grandes lignes et les résultats significatifs d'une étude générale concernant les moyens anémobarométriques des avions de la prochaine génération, étude soutenue par le Service Technique des Télécommunications et Equipements (STTE) Français.

On examine l'évolution des équipements dans le passé et on présente les nouvelles tendances. Deux architectures typiques sont présentées, représentatives de deux conceptions différentes (Système Intégré ou Spécifique). Une enquête menée en 1980 auprès de nombreux organismes, tant en France qu'aux Etats-Unis, a montré que la deuxième solution avait de plus nombreux partisans.

INTRODUCTION

L'importance des systèmes anémobarométriques s'est considérablement accrue au cours du temps. De simples indicateurs pneumatiques, ils sont devenus des éléments importants de l'équipement des avions.

L'apparition de systèmes d'armes de plus en plus sophistiqués et des commandes de vol électriques est pour une grande part responsables de cet état de fait.

Le Service Technique de l'Aéronautique (STAé) puis le Service Technique des Télécommunications et des Equipements Aéronautiques (STTE) ont soutenu une étude générale des moyens anémobarométriques pour avions de la prochaine génération, étude menée par notre société. Cette étude comportait plusieurs volets :

- recensement des besoins en fonctions anémobarométriques,
- analyse des méthodes et moyens envisageables pour répondre à ces besoins,
- diverses études ponctuelles pour étayer les choix précédemment faits.

La synthèse de ce travail a permis d'approcher les spécifications préliminaires des principaux constituants des architectures de systèmes anémobarométriques possibles dans l'avenir ainsi que leur relative complexité. Une enquête auprès des constructeurs d'avions et des Services Officiels en France et aux Etats-Unis a permis d'étayer cette démarche.

EVOLUTION DU BESOIN

L'apparition de systèmes d'armes de plus en plus sophistiqués ainsi que des commandes de vol électriques sont les raisons majeures de l'existence de deux spécifications concernant les systèmes anémobarométriques :

- Spécification de sécurité : la perte de certaines informations de ce type imposerait au mieux l'arrêt de la mission. Au pire, elle peut être catastrophique pour l'avion et son équipage.

- Spécification de rapidité : l'accroissement des bandes passantes des commandes de gouverne et de la manoeuvrabilité en découlant ont des répercussions sur les systèmes anémobarométriques qui devront avoir de meilleures bandes passantes.

L'introduction de calculateurs de plus en plus petits, intégrés et efficaces a permis (référence 1) :

- une miniaturisation de l'avionique et corrélativement une diminution importante du poids, du volume et de la consommation. Par exemple : 38 kg, 200 VA pour la centrale anémométrique du F105, 8 kg et 90 VA pour celle du F15,

- une complexité croissante caractérisée par l'augmentation du nombre d'entrées/sorties. Par exemple 63 E/S pour la centrale anémométrique du F15, 198 pour celle du F18,

- une augmentation importante de la fiabilité de ces systèmes. Le taux de couverture des tests intégrés atteint en effet maintenant 95 à 98 %.

Les résultats d'une enquête effectuée en France et aux Etats-Unis auprès de Services Officiels et d'avionneurs montrent que ces tendances vont se maintenir dans l'avenir.

- La technologie du contrôle actif ("CAG" ou "CCV" et l'utilisation de commandes de forces directes imposent l'emploi de commandes de vol électriques (référence 2 et 3). Il est donc probable que les exigences de fiabilité et de sécurité vont devenir de plus en plus critiques.

L'incidence et le dérapage seront sûrement des informations primordiales pour ce genre de système, puisqu'utilisées systématiquement dans les boucles primaires des commandes de vol. Le nombre de Mach et la pression cinétique resteront des paramètres critiques.

Enfin, l'utilisation intensive de systèmes numériques peut conduire à imposer des sorties numériques ou facilement numérisables pour les capteurs et sondes (sorties fréquences) et même à devenir un critère de choix pour un nouveau principe physique.

- L'accroissement des performances et de la manoeuvrabilité des avions pourra conduire à spécifier :

- Un accroissement de bande passante pour :

  - l'incidence et le dérapage, principalement pour des raisons de sécurité,

  - la température d'arrêt, pour améliorer à la fois les performances de navigation dans le plan vertical et celles des contrôles des moteurs et des entrées d'air. La précision sur ce paramètre devra, par ailleurs, être augmentée.

- Un élargissement de la gamme de mesure de l'incidence et du dérapage.

- Une réduction à la fois du nombre et de la taille des protubérances situées à l'extérieur de la peau de l'avion et susceptibles de perturber l'écoulement aérodynamique autour de l'avion.

- Voler en transsonique, à basse altitude et dans le contexte de guerre nucléaire imposera :

- L'utilisation d'un détecteur de rafale (si un système en "boucle ouverte" est retenu).

- Le durcissement aux radiations nucléaires et aux champs électromagnétiques associés aux explosions ou à la foudre.

- Enfin, les problèmes de coût de cycle de vie sont de plus en plus aigus pour les systèmes d'armes. Cette exigence peut être prise en compte par :

- réduction de la masse et du volume pour tous les équipements, calculateurs, sondes et capteurs ,

- réduction des coûts d'acquisition,

- amélioration de la fiabilité,

- amélioration de la maintenabilité des composants et du système lui-même, et cela par une prise en compte de ces contraintes dès le début du projet.

EVOLUTION DES ARCHITECTURES

Le but de cette démarche était uniquement d'obtenir un certain nombre d'indications sur la complexité relative de différentes solutions d'organisation des composants susceptibles d'entrer dans la composition d'un système anémobarométrique. Il ne se veut pas exhaustif, l'organisation étant très liée à la configuration finale de l'avion : il n'existe probablement pas d'architecture disponible a priori pour tout type d'avion de combat.

On a donc essayé de prendre en compte les besoins recensés précédemment dans deux architectures typiques. Ces architectures sont elles-mêmes représentatives de deux concepts généraux concernant les systèmes spécifiques et intégrés (références 4-5-6).

Un certain nombre d'hypothèses communes aux deux architectures ont été faites :

- Redondance d'ordre trois pour les informations à destination des commandes de vol (y compris l'incidence et le dérapage).

- Source pneumatique pour l'incidence et le dérapage (sondes multiorifices ou prises de pression statique latérales). Cette solution a l'avantage de minimiser le nombre de protubérances sur le fuselage de l'avion.

- Redondance d'ordre deux pour les informations à destination du système d'arme, des moteurs et des entrées d'air. Pour ces deux derniers types de paramètres, fourniture sous forme numérique (liaison point à point ARINC 429 par exemple).

SYSTEME INTEGRE

Ce système (Figure 1) est très voisin de celui décrit dans les références (7 et 8).

L'idée directrice consiste à distribuer dans l'avion un certain nombre de capteurs effectuant des mesures primaires. Une telle organisation doit se comprendre dans un cadre plus large, prenant en compte d'autres paramètres, par exemple de nature inertielle. On ne s'intéresse ici qu'aux paramètres de nature anémobarométrique, c'est-à-dire pressions et températures.

Ces informations de pression et température sont pré-traitées localement, à proximité immédiate des capteurs.

L'acquisition, l'échantillonnage et les corrections d'effets locaux (température) une fois effectués, les valeurs numériques des paramètres sont émises sur un bus numérique multiplexé tri-redondant (électrique ou optique). La redondance d'ordre trois est nécessaire pour les commandes de vol électriques.

Le calcul des paramètres dits élaborés, tels que le nombre de Mach, la vitesse air, les corrections globales (telles que les corrections d'antennes), les tests et les comparaisons à des fins de vérifications de cohérences sont tous effectués en dehors du sous-système proprement dit. On suppose qu'il existe un système extérieur capable d'effectuer ces [illegible]s, suffisamment robuste et fiable pour fournir à tous les sous-systèmes utilisateurs avec les performances requises l'information qui leur est nécessaire. Ce système gère par ailleurs les bus numériques.

Les composants de cette architecture sont :

- Une sonde pneumatique multifonction, située au nez de l'appareil. Elle fournit des informations de pression concernant la pression d'arrêt, la pression statique, les angles d'incidence et de dérapage.

- Deux sondes multifonction "en L" situées sur les côtés du fuselage. Elles fournissent des informations de pression concernant la pression génératrice, la pression statique et l'incidence.

- Deux sondes de température, bi-élément et dégivrées.

- Deux paires de prises de pression statique fournissant une information de dérapage.

- Trois modules électroniques identiques comprenant :

  - un capteur de pression absolue,

  - trois capteurs de pression différentielle

  (ces quatre capteurs sont de bonne précision relative : quelques centièmes de pour cent).

- quatre circuits de mesure des informations délivrées par ces capteurs de pression (mesure de fréquence),

- un microcalculateur (de classe 8 bits) qui calcule les corrections locales de température, élabore les informations de pression brute, assure une surveillance élémentaire des capteurs et gère les entrées/sorties,

- un interface électronique simple pour la logique et de redondance d'ordre trois pour les circuits d'émission et de réception,

- pour deux d'entre eux, deux circuits de mesure de résistances (température d'arrêt).

Rien d'autre n'est nécessaire, les bus étant gérés par ailleurs dans le système de calculateurs centraux.

Une telle architecture présente les avantages suivants :

- Extensibilité : le nombre de capteurs dialoguant sur le bus peut être modifié assez aisément au cours de l'évolution du projet.

- Standardisation possible au niveau matériel, ce qui peut amener des diminutions importantes du coût de cycle de vie.

- Faible vulnérabilité : le sous-système proprement dit peut être dispersé donc peu vulnérable aux impacts de projectiles. La vulnérabilité du système complet dépend de l'agencement du calculateur central.

- Minimisation du nombre d'unités de calcul.

Elle présente aussi les inconvénients suivants :

- Validation du logiciel : à chaque étape du projet et à chaque modification, la validation du logiciel principal est relativement difficile, de même que les démonstrations de sécurité.

- Gestion du logiciel : elle est lourde dans les unités de calcul centralisées du fait des interactions multiples.

- Fraîcheur de l'information : elle n'est pas accessible aisément.

- Coordination difficile : la coordination du programme entre les Services Officiels, les avionneurs et les équipes de projet peut être problématique en cas d'extension à des mesures de nature inertielle.

SYSTEME SPECIFIQUE

Ce système, du point de vue de sa philosophie de conception, se rapproche des systèmes actuels (Figure 2). Néanmoins, l'ensemble des besoins énumérés plus haut a été pris en compte, en particulier les problèmes de sécurité et l'utilisation intensive de techniques digitales.

L'idée principale est d'effectuer l'ensemble des calculs de paramètres anémobarométriques dans un ou deux boîtiers spécifiques. Ces boîtiers possèdent éventuellement eux-mêmes des capteurs ou des circuits de mesure de capteurs et reçoivent des informations d'autres boîtiers. Un certain nombre de vérifications de validité et de tests de cohérence sont effectués dans le sous-système qui fournit donc les paramètres anémobarométriques requis et l'information de validité associée.

Toutes les corrections sont faites dans le sous-système :

- Corrections locales (température) près des capteurs,

- Corrections d'ordre global (incidence, dérapage, nombre de Mach, corrections dites d'antenne).

Le sous-système élabore donc toutes les informations nécessaires aux utilisateurs et les leur fournit sous la forme la mieux adaptée (bus numérique multiplexé électrique ou optique, bus unidirectionnel type ARINC 429 ou autre). La gestion des bus se fait toujours en dehors du sous-système lui-même.

Les composants de l'architecture sont :

- Une sonde pneumatique multifonction située au nez de l'appareil. Elle fournit des informations de pression concernant la pression d'arrêt, la pression statique, les angles d'incidence et de dérapage.

- Deux sondes multifonction "en L" disposées sur les côtés du fuselage. Elles fournissent des informations de pression concernant la pression d'arrêt, la pression statique et l'incidence.

- Deux sondes de température bi-élément et dégivrées.

- Deux paires de prises de pression statique.

- Deux modules électroniques identiques comprenant :

  - un capteur de pression absolue,

  - trois capteurs de pression différentielle,

  - quatre circuits de mesure des informations délivrées par ces capteurs (mesures de fréquences),

  - un microcalculateur (de classe 8 bits) qui calcule les corrections locales de température, élabore les informations de pression brute, assure une surveillance élémentaire des capteurs, gère les entrées/sorties et effectue des comparaisons grossières avec les autres sources d'information anémobarométrique,

  - un interface électronique simple pour la logique et de redondance d'ordre trois pour les circuits d'émission et de réception.

- Un module électronique comprenant :

  - un capteur de pression absolue,

  - trois capteurs de pression différentielle,

  - quatre circuits d'acquisition pour ces capteurs,

  - quatre circuits de mesure de résistances (température d'arrêt),

  - deux microprocesseurs de taille moyenne (de classe 16 bits) avec approximativement 10 kilomots de mémoire. Ils calculent les paramètres élaborés (nombre de Mach, vitesse air,...), toutes les corrections nécessaires (y compris les corrections d'antenne), effectuent la surveillance des capteurs et les tests de validation de toutes les informations.

  - un circuit d'interface tri-redondant (pour le bus tri-redondant),

  - deux circuits d'interface bi-redondant,

  - deux circuits d'interface pour liaisons unidirectionnelles (type ARINC 429).

Une telle organisation possède les avantages suivants :

- une certaine standardisation des différents modules,

- gestion assez aisée des modifications au niveau du système,

- modifications du logiciel possibles sans interactions multiples,

- fourniture d'informations spécifiques aisée, sous une forme non standard pour des utilisateurs isolés,

- bonne connaissance de la fraîcheur et des caractéristiques dynamiques de l'information,

- démonstration relativement aisée des niveaux de sécurité au niveau du système.

Elle a par contre les inconvénients suivants :

- nombre élevé de microprocesseurs,

- matériel plus important.

COMPARAISON DES DEUX SYSTEMES

Du point de vue du matériel, la seconde architecture est plus lourde (1 microcalculateur, plusieurs circuits d'interfaces et de mémoires supplémentaires). Les avantages et inconvénients comparés sont a priori équilibrés. Cependant, on doit noter que les deux architectures ne fournissent pas du tout la même nature d'information : la première fournit des informations brutes et non validées ; la deuxième est capable de fournir à la fois les informations brutes et les paramètres élaborés ainsi que leur validité.

Pour pouvoir faire des comparaisons exactes, il faut donc prendre en compte la part de calculateur central mobilisée pour l'anémobarométrie. Cela est aussi valable pour le logiciel et la complexité du logiciel intégré n'est pas facile à appréhender.

L'enquête menée aux Etats-Unis et en France auprès des Services Officiels et des avionneurs de ces pays, en 1980, a indiqué qu'une majorité semblait se dégager pour la solution à calculateurs spécifiques. L'importance donnée à la démonstration de la sécurité d'un logiciel serait donc déterminante. Il faut noter cependant que le concept d'architecture intégrée pourrait être utilisé dans certains projets où la complexité globale est très élevée, et une proportion non négligeable d'utilisateurs est en sa faveur.

Il est très probable que le choix dépendra généralement du type d'appareil.

CONCLUSION

L'étude générale des moyens anémobarométriques pour avions de la prochaine génération a permis d'identifier les tendances des besoins à venir pour les paramètres anémobarométriques.

Ces paramètres auront dans l'avenir une importance grandissante par rapport à l'époque actuelle.

Enfin, la prise en compte de l'ensemble des problèmes conduit une majorité de personnes compétentes à choisir une architecture spécialisée pour le traitement de ces paramètres, par opposition à une architecture intégrée (ou centralisée), bien qu'un tel concept semble viable pour certains programmes spécifiques. Ce choix semble être dicté par des questions de gestion de développement de systèmes.

REFERENCES

(1) TJ DICKMAN

A standard air data computer. Proceedings of Air Data Symposium Conference 1976.

(2) P. Poisson-Quinton

Aerodynamic controls for CCV aircraft. VKI lecture studies on CCV 12/4-8/1978.

(3) P. Poisson-Quinton

Evolution de la conception des avions grâce aux commandes automatiques généralisées.
Proceedings of S.E.E., GRENOBLE (France)
09/20-24/1977.

(4) WR Richter

Air Data system redundancy required for F 16 fly-by-wire flight controls.
Proceedings of Air Data Symposium Conference 1978.

(5) CJ Sheets

Air data sensors or air data computers. The system's integration question.
Proceedings of Air Data Symposium Conference 1976.

(6) CR Abrams - D. Gertz - K. Grobert

Present and future naval aircraft air data systems.
Proceedings of Air Data Symposium Conference 1976.

(7) CR Abrams - D. Gertz - H. Grobert

An integrated air data sensory subsystem.
Proceedings of Air Data Symposium Conference 1980.

(8) J.D. Chang

Optimum design approach for air data systems for 1980 CTOL aircraft.
Proceedings of Air Data Symposium Conference 1978.

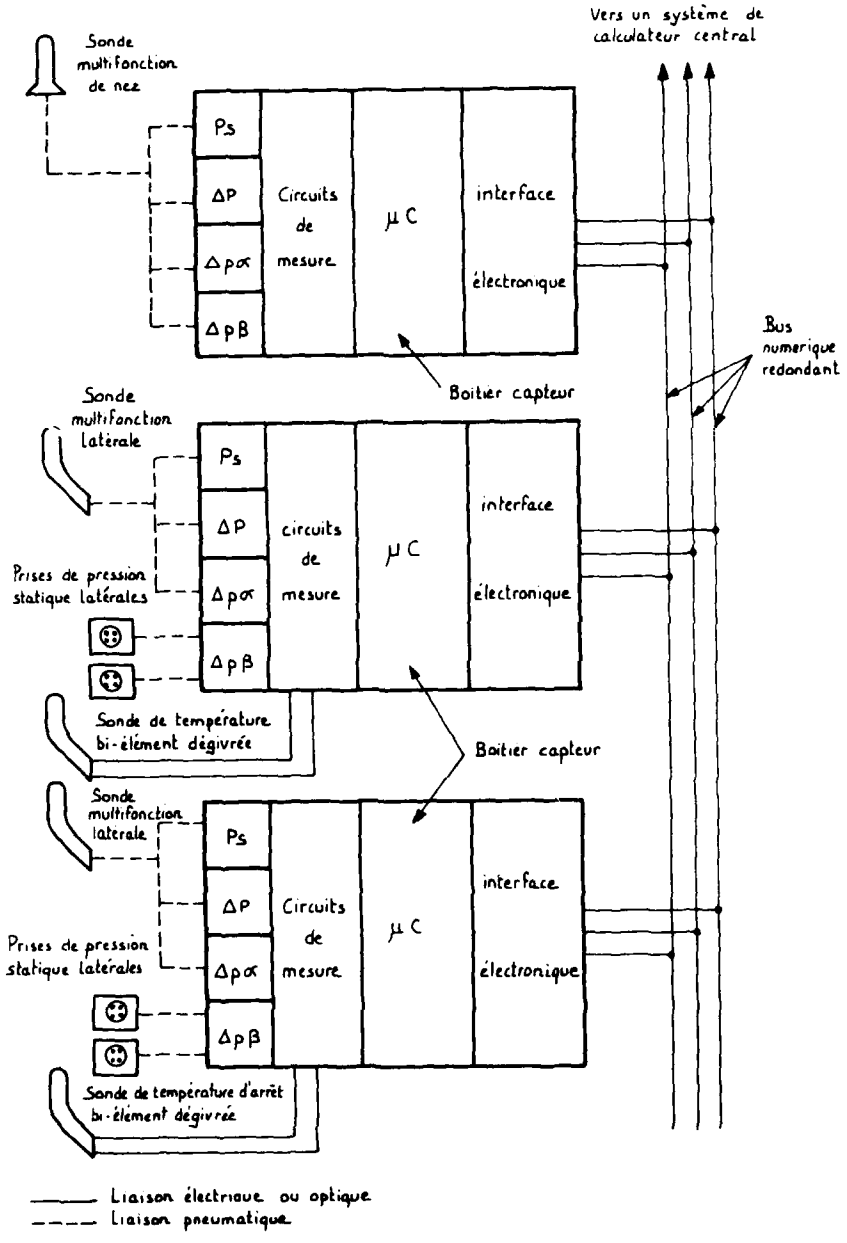

figure 1 : ARCHITECTURE 1

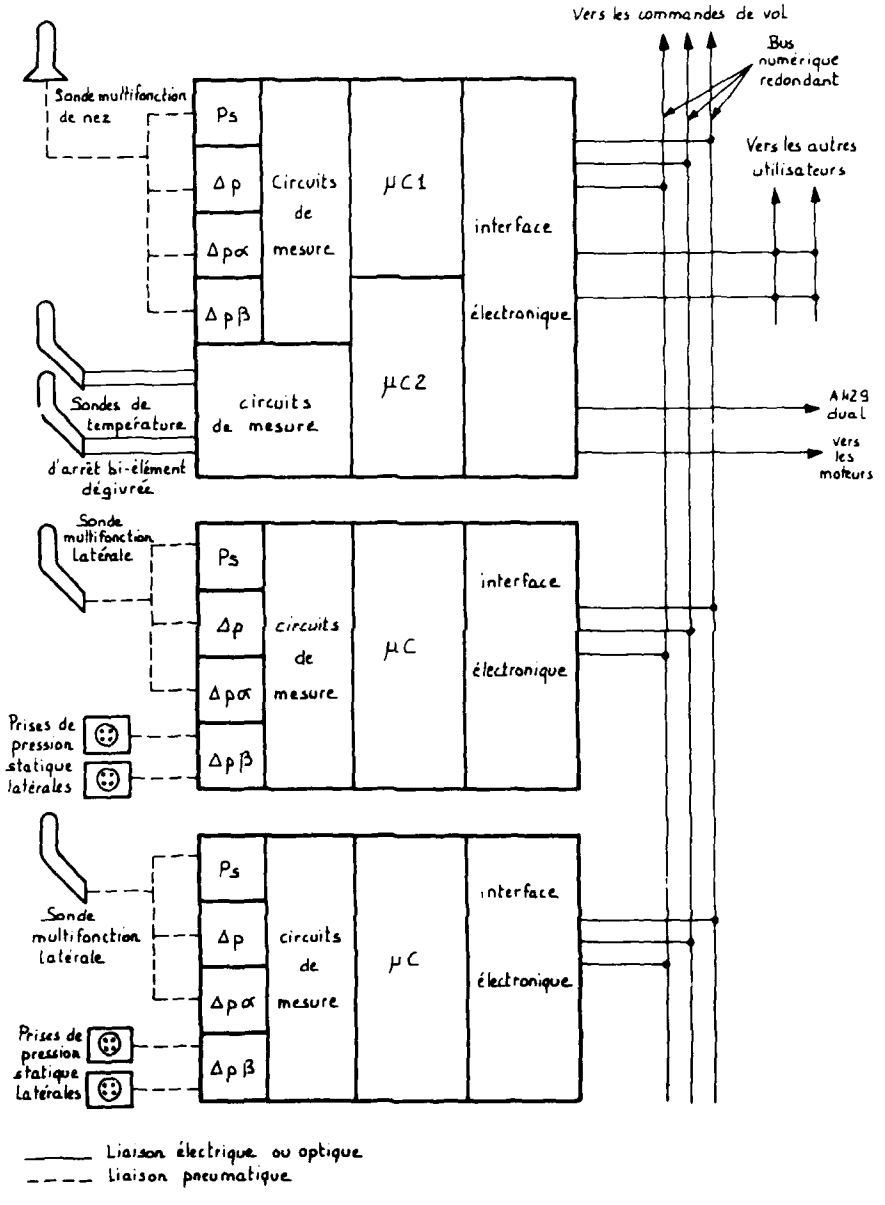

figure 2 : ARCHITECTURE N°2

THE USE OF MULTIPLEX DATA BUSES IN A HIGH INTEGRITY SYSTEM

P. Crouch
Smiths Industries Aerospace & Defence Systems Company,
Cheltenham Division,
Evesham Road,
Bishops Cleeve,
Cheltenham,
Gloucestershire. GL52 4SF
England.

and

A.G. Seabridge
British Aerospace,
Aircraft Group,
Warton Division,
Warton Aerodrome,
Preston,
Lancashire. PR4 1AX
England.

SUMMARY

The Utility Systems of an aircraft have been analysed and shown to benefit considerably from integration into a connected system with shared processing resources. The MIL-STD-1553B data bus has been selected as the most cost effective tool for integration but raises problems connected with ensuring the safety of the aircraft.

Careful design of the data bus components and controllers with particular attention being paid to Built-In-Test techniques and in the functional segregation of the interfaces, subsystems and computing facilities has allowed a sufficiently reliable system to be designed and this is now entering full scale development.

1. INTRODUCTION

High integrity applications of Data Bus technology in recent years have usually postulated the use of specially modified or newly designed signalling formats or architectures, or have been restricted to the use of straightforward serial point-to-point links.

With this paper we hope to show the practical work which has been done and to show analytically that, for some applications, it is possible to use the now widespread MIL-STD-1553B Serial Time Division Multiplex Data Bus as the data transfer medium in a safety critical system.

The components used are those designed purely to meet the standard, but some of the techniques used are necessarily specific to the application and its particular integrity requirements.

The systems description is presented here to enable other users to benefit from our experiences and to appreciate the reasons behind the design decisions.

2. APPLICATION

The particular application which will be used as an example of the Multiplex Data Bus in a High Integrity System is that of an Integrated System for control of aircraft Utility Systems. The Utility Systems are those subsystems that perform the basic mechanical functions of the aircraft and contain an element of logical or closed loop electronic control.

These functions have, in the past, been controlled by separate, independent items of hardware. Typically the functions are included in the following major subsystems:

- Powerplant
- Hydraulic
- Fuel
- Environmental Control
- Secondary Power
- Electrical Power

In all, these major headings may encompass some 30 to 40 minor subsystems which are listed in Table 1. In a typical aircraft these subsystems require a large number of inputs and outputs, examples of which can be observed in Table 2. The aircraft may depend on the correct functioning of many of these subsystems for safe, continued operation.

In the context of modern aircraft projects using advanced cockpits and data transmission systems a method of integrating Utility Systems into the overall Avionic architecture has been proposed (1) which takes the general form shown in Figure 1.

This design allows Utility Systems to be integrated with the aircraft Data Transmission Systems and enables the mechanical systems to be interfaced with advanced cockpits.

The use of a data bus for interconnection of a small number of units performing the tasks of data acquisition, load power control and the performance of control algorithms allows significant benefits to be obtained in hardware weight, volume and numbers.

TABLE 1 - UTILITY SYSTEMS LIST

A. POWERPLANT SYSTEMS

1. Engine Start
2. Ignition Mangement
3. Engine Speed Switch
4. Thrust Reverse Control
5. Fire Detection
6. Fire Suppression
7. Ice Detection
8. Intake De-Icing

B. HYDRAULIC SYSTEMS

1. Hydraulic Control
2. Hydraulic Utilities
3. Hydraulic Depressurisation
4. Undercarriage Control
5. Undercarriage Indication
6. Brakes and AntiSkid
7. Nosewheel Steering

C. FUEL SYSTEM

1. Fuel Gauging
2. Fuel Management
3. Fuel Feed Control
4. Flight Refuelling Probe
5. Fuel Indications
6. Hit Detection

D. ENVIRONMENTAL CONTROL

1. Cabin Temperature Control
2. Equipment Bay Cooling
3. Coolant Control System
4. On Board Oxygen Generation
5. Air System Protection
6. Air System Indications
7. Nuclear/Biological Protection

E. SECONDARY POWER SYSTEMS

1. Auxiliary Power Unit
2. Emergency Power Control
3. Gearbox Control
4. Secondary Power Cooling

F. ELECTRICAL POWER

1. Power Generation Control
2. Power Distribution

G. MISCELLANEOUS

1. External Lights
2. Internal Lighting
3. Probes Heating
4. Windscreen Heating
5. Canopy Control
6. Canopy Demist
7. Arrestor Hook
8. Brake Parachute
9. Rain Dispersal

TABLE 2 - TYPICAL INPUT/OUTPUT TYPES

	Type	Quantity
INPUTS	Discrete Data	123
	Pulse Probes	4
	Analogue Sensors	65
	Level Sensors	25
OUTPUTS	Discrete Data	26
	Power Control	93
	Analogue	17
	Excitation	56

3. SYSTEM OBJECTIVES

The main objectives of integration are to obtain benefits in some or all of the following:

Reduced Systems Mass
Reduced Overall System Volume
Reduced System Cost
Improved Maintainability
Improved Fault Tolerance
Consistency in Design
Commonality of Equipment
Flexibility in Development
Increased Reliability
Reduced Pilot Workload
Improved Systems Performance

Some of these benefits have been quantified in early Utility Systems Studies (2). In addition to the easily quantifiable, physical benefits, the increasing complexity of aircraft projects demands more automation and less pilot intervention in low level tasks. Thus the Utility Systems are heading toward more complex control tasks, using the power of digital processing to achieve system objectives. Opportunities for reduction in pilot workload are limited but some reductions in tasks under emergency conditions have been estimated (3).

The work conducted in the study of Utility Systems management at British Aerospace, Warton found that the majority of these objectives could be achieved. The major problem was associated with the safety of the system, with particular emphasis on the behaviour of the system, and the effect on the aircraft, of a total data bus failure. Suitable design of the external system circuitry, and the specification of a minimum set of requirements that must be met in order to safely continue to operate the aircraft allowed a safe system to be designed. However, some sacrifices had to be made in the overall systems design and the resulting system did not make full use of the potential savings offered by maximum use of the data bus for inter-system data communication.

4. UNIQUE FEATURES OF UTILITY SYSTEMS

The Utility Systems display certain characteristics that require a different approach to integration compared to that used, for example, on Avionic or Flight Control Systems.

(a) The subsystems are essential for the continued and safe operation of the aircraft - they are safety critical rather than merely mission critical, for example Engine Relight, Brakes and Fuel Management.

(b) The externally connected components of the systems are essentially simplex in nature and the systems do not lend themselves to multiple redundant control methods.

(c) There are a large number of dependent and independent variables within the total system leading to a large number of connected devices as illustrated in Table 2.

(d) The characteristics of the systems are such that considered separately their independent integrity requirements are low, but in an integrated system the possibility of multiple systems loss tends to raise the required integrity. For example the Arrestor Hook is a relatively unimportant item considered in isolation. However, following a combined brakes and thrust reverse failure the continued operation of the arrestor hook is extremely important.

In order to meet the individual system safety requirements care is needed in the design of the externally connected subsystem components and in the subsystem design philosophy to enable reversionary modes to be incorporated to absorb a number of faults without endangering the aircraft.

To this end a policy of functional segregation has been applied. Subsystem functions can be separated at the gross level by splitting them between Systems Management Processors (SMP). Within the SMPs further isolation can be obtained by the use of multiple but separate Central Processor Units (CPU). Additionally, the interface with a particular subsystem can be physically separated even if the control task is time-multiplexed with others in a single CPU.

The isolation of software into specific memory areas with the least possible interaction between program modules is another segregation principle applied, and the feasibility of managing segregation principles within the assembler program is being actively pursued. It is, of course, not wholly possible to separate the programs entirely and recovery routines can be written into the executive program, which queues the tasks, to prevent any single software failure in a control task causing a total processor loss. Reversionary data values can be preprogrammed or statistically calculated should real data not be available for any reason.

The possibility of a failure within a CPU causing simultaneous loss of control of a number of subsystems has added another dimension to the segregation task and the example of Brakes, Arrestor Hook and Thrust Reverse has already been mentioned.

In particular the system needs to be capable of withstanding the following failures:

(a) Total loss of a single processor. (Battle Damage).

(b) Combinations of dissimilar failures in the total system.

(c) Total loss of the Utilities Data Bus.

(d) Total loss of the Avionics Data Bus.

The ability to tolerate these two latter failures with the system configured as in Figure 1 using a dual redundant mode of operation is important. The studies so far conducted indicate that many of the physical benefits of Integration in Utility Systems may be eroded if triple redundant bus operation is used with its higher equipment overhead at today's standard of technology.

Thus the control of Utility systems, many of which are critical for safe operation of the aircraft, requires a high degree of fault tolerance of the Multiplex Data Bus in order to achieve an acceptable failure rate for the total system.

5. PRACTICAL APPLICATION

In the application of Utility Systems Management to a project it became clear as a result of analysis that the probability of a double bus failure could be regarded as a potential hazard and therefore a minimum set of requirements was established for the systems that would enable the aircraft to be flown safely back to base and landed (the "Get You Home" philosophy). Methods of attaining these conditions were then investigated using a variety of techniques. Typical examples are:

(a) Tolerating the loss of the system, for example the engine starting system is not required once the engines are running.

(b) Providing a method of recognising the loss of bus-borne data and substituting fixed values for variable data and for output states to allow continued safe operation.

(c) Avoiding the use of the data bus for safety critical data, such as brake pedal position, the sensors being hardwired into the Utility Processors.

(d) Providing an alternative means of systems operation, for example emergency undercarriage operation using a nitrogen bottle.

(e) Bypassing Utility Systems Management altogether as in the case of the arrestor hook, which will be hardwired.

Consideration of the minimum set of requirements allowed a design philosophy to be developed which had a fundamental impact on the design of the total system.

The resulting architecture can be seen in Figure 2 and it can be seen that the correct operation of the total system is critically dependent on the continued operation of the data bus.

6. MULTIPLEX BUS CHARACTERISTICS

The Multiplex Data Bus which has gained wide acceptance within the international community as a system integration tool for aircraft mission systems is that defined by MIL-STD-1553B in the US and DEF-STAN 00-18 Part 2 in the UK. Features developed for its application also make it well suited for use in Utility Systems Management (USM) Data integration, although the higher integrity constraints imposed on USM require that special care be taken over its implementation.

Figure 3 shows a typical multiplex bus implementation for Utility Systems Management. For high integrity systems Electro-Magnetic Interference susceptibility is minimised by the use of transformer isolated stubs to improve common mode noise rejection, the use of connectors with 360^0 screen termination rather than pig-tailed screens and the use of double screened cable. The exact bit error rate (BER) for the bus is dependent on many factors, however the Multiplex Applications Handbook (4) suggests that a BER of 10^{-12} is commensurate with noise test levels which correspond to a detected word error rate of 10^{-7}. Consequently the probability of corrupting a single subsystem data item is unlikely to exceed 5×10^{-6} per hour. It is possible to improve on this figure by transmitting critical data items two or more times, although in practice it is felt that hardware failure rate will dominate system reliability.

The multiplex bus protocol provides sufficient checks to ensure that in-line failures of the bus will be detected with high probability. Of greater concern are the failures which merely degrade performance, for example high impedance in-line connections and loss of screen terminations. Advantage can be taken of the wide difference between detected and undetected error rates to enable the bus controller to isolate a faulty bus by noting an increase in message rejection rate before BER becomes significant.

Battle damage could represent a significant threat to multiplex data bus systems as severance of the bus terminates all information transfer. However, the bus is much smaller in volume than the cable looms it replaces, and is thus less likely to be damaged. By carefully routing dual redundant busses in the airframe to maximise separation the probability of losing both busses will be made very small. The use of transformer isolated stubs is made mandatory by battle damage considerations, as without the protection they afford against short circuits, remote terminal units would represent single point failure hazards.

Experience with the implementation of remote terminal units (R/Ts) has led to the following features being incorporated to improve integrity:

(a) The 1553 protocol forms a good basis for checking the functionality of R/Ts. Wrap-around addresses are designated in each R/T to allow complete test messages to be routed via the subsystem back to the bus controller for verification, thus providing a high degree of confidence in the main data paths.

(b) The responses of R/Ts to invalid, illegal or illogical commands are well defined in order to provide system integrity, although it may prove difficult to test for compliance in flight. The UK has defined a set of preferred responses to these conditions in the Guide to the UK Defence Standard definition of the Multiplex Data Bus, DEF-STAN 00-18. (5).

(c) Every effort should be made in R/T design to provide robustness. In addition to the preferred responses, terminals also provide freedom from latch-up and perform reasonability checks on bus commands by implementing the following features:

  (i) Mode code reset is made as near to power-up reset as possible (for enhanced error recovery).

  (ii) A no-response timeout for R/T to R/T transfers (to prevent erroneous data capture).

  (iii) Parity on R/T address lines.

  (iv) End of Transmission check prior to sending the status word.

  (v) Validity checks on T/R bit, sub-address, and word count (to ensure that messages comply with subsystem formats).

(d) The R/T is a potential single-point failure hazard, both for the multiplex bus and the subsystem. A watch-dog timer is implemented to prevent a "chattering" R/T from disabling the bus, provision being made to periodically check its functionality. Although the bus itself may be dual redundant, the R/T is implemented simplex behind the immediate wire interface, which has previously been noted as a potential problem in high integrity systems (4). For high reliability systems dual redundancy is propagated right through to the subsystem at the cost of a few extra integrated circuits.

7. BUS CONTROL

The multiplex data bus operates under a command-response protocol, requiring that one unit act as a Bus Controller issuing a sequence of commands to order data transmission. Consequently the Bus Controller is a single-point failure hazard, and redundancy must be provided to ensure system reliability. In order to provide adequate reliability the failure modes of bus control have been analysed. These may be summarised as:

* Total Failure
* Partial Failure (e.g. Short cycling or command corruption).
* Recurring intermittent failures.
* Transient disturbance.
* Pattern sensitive failures.

Additionally, to ensure operating integrity, certain mode codes are avoided, particularly dynamic bus control hand-over (because of noise induced errors) and broadcast of data to all terminals (as there is no confirmatory response from R/Ts).

A number of different structures for the Bus Control function have been considered with various methods of fault detection, fault analysis and fault recovery.

These range from straightforward simplex controllers to complex self-monitored or externally monitored duplex or triplex configurations. It was quickly recognised that the simplex unit would prove unacceptable because its failure rate was worse than the required probability of a complete bus failure.

When a dual redundant Bus Control function is considered it is necessary to decide how the stand-by Bus Controller should operate:

(a) It may be in a pure stand-by mode, where it is executing self-test procedures until called upon to take over Bus Control.

(b) It may split the task of Bus Control with the other unit on a time-share basis.

(c) It may monitor the bus transactions being conducted by the other controller.

These modes of operation are not mutually exclusive and a combination of them may be considered desirable.

The use of a triplex Bus Controller was found to be impractical because of the large overhead of providing the three independent processors with their associated stores, peripherals and power supplies. The difficulties of transferring control between the three controllers were also compounded by the characteristics of the data bus and the need for cross-checking.

From this study, two strong contenders emerged. The first of these was the Bus Voter-Monitor architecture shown in Figure 4. The third element, the Voter-Monitor, is intended to resolve disputes between the two Bus Controllers when they disagree over their respective serviceabilities. In order to achieve this task the Votor-Monitor was necessarily complex, amounting almost to a third Bus Controller.

The second, and eventually the preferred, option was to provide two Bus Controllers with a high level of Built-In-Test (BIT) coverage, Figure 5. It was determined that, provided careful attention was paid to BIT coverage and the design of circuits to transfer control in the event of a failure, a viable Bus Control function could be designed to meet the reliability criteria.

The use of BIT as the fault detection medium can be shown to provide considerable improvements in overall reliability of the system. Small improvements in detection capability provide dramatic improvements in the overall reliability of the system. This is shown graphically in Figure 6.

The time required to execute some of the BIT software routines could make self testing impractical as a background exercise. In order to overcome this difficulty a switching arrangement was introduced to allow each bus controller to generate word commands on the bus for one major cycle (about 1 second) before passing control to the other unit. This allowed extensive self testing to be carried out during the non-active period and also prevented latent faults in the stand-by processor causing a problem.

The switching circuit itself was a dual purpose design which allowed switch-over under failure conditions and also carried out the major cycle switching. It operated via a pair of dedicated links between the Bus Controllers and its correct functioning under fault conditions was the subject of extensive analysis. It was designed to provide unambiguous indications to the primary Bus Controller even when a link was open or short circuit or any single component failure occurred including the power supply.

In order to overcome some of the limitations of BIT and also to provide the Utilities System with some capability when aircraft or ground power was not available, for example for re-fuelling or maintenance purposes, a dual power supply unit was found to be necessary. This had the incidental benefit of improving overall reliability because power supply faults are notoriously difficult to accurately detect.

The system to be installed in a new project at British Aerospace, Warton uses such a dual power supply, control switched bus controller arrangement and can be shown to exhibit sufficient reliability to ensure that a message will be correctly transmitted and received with a probability of $1-10^{-6}$ per hour excluding the effects of noise on the signal.

8. SYSTEM INTEGRITY ANALYSIS

The reliability block diagram, Figure 7, shows the contributory factors affecting the use of the data bus in this application. The use of Large Scale Integration (LSI) in the Remote Terminals significantly improves reliability in this area but the ultimate success of the Data Bus always depends on the correct operation of the Bus Controller.

The design to be used in a future project at British Aerospace, Warton has a calculated Mean Time Between Defects (λ) of just under 5000 hours and an estimated BIT efficiency (m) of 95%.

The primary Bus Controller will therefore contribute $(1-m)\ \lambda$ to the overall failure rate because 5%, (1-m) faults will be undetected and therefore lead to complete failures.

The switching circuit has been designed to operate under all failure conditions of the Bus Controller, including Power Supply dropouts so that it will switch in the stand-by controller for all detected faults. The secondary Bus Controller is identical to the primary so that the overall failure rate of the function is:

$$(1-m)\ \lambda + m\lambda^2$$

For large m this expression is dominated by the first term and is shown graphically in Figure 6.

The probability of total loss of bus traffic for dual redundant system with a modest BIT system can therefore be shown to be better than 10^{-5} per hour.

The Systems Management Processor block diagram, Figure 8, shows how the six separate processing elements have the interfaces distributed between them. Each interface is duplicated and also has direct access to the bus via a Remote Terminal should the controlling Processor fail.

The fully functional system therefore passes processed data between elements and into the Avionics Data Bus under normal control. Should internal processing elements fail the Systems Management Processor has the capability to re-configure such that raw interface data is passed to the bus and can be processed in a redundant CPU. Subsystem interface failure can be tolerated because the interfaces are duplicated in other Systems Management Processors with consideration being given to those naturally redundant systems within the aircraft to ensure that no common mode failure hazards are introduced.

9. CONCLUSION

With this paper we have shown the principles by which a particular system can be designed to meet a specific reliability target with an existing data bus standard and currently available components. It is necessarily not a general approach to high integrity data bus applications but some of the techniques can be applied to other systems.

The limitations of the data bus have been highlighted and some methods of overcoming them have been demonstrated with particular attention being focussed on the maintenance of the bus controller integrity.

The ultimate limitation of the data bus has been indicated to be an undetected word error rate of 5×10^{-6} per hour but at current levels of technology this is swamped by the probability of total bus controller failure. The aim for high integrity applications therefore must be to improve the reliability or BIT efficiency of the bus controller either by further integration, such as custom components, or by improved Built-In-Test.

Work conducted to compare this method of design with that used for a contemporary aircraft showed the following benefits:

Mass reduction	47%
Volume reduction	52%
Cost reduction	50%

Additionally improvements are anticipated in areas such as Reliability, Pilot Workload, Flexibility and Design Commonality and Consistency.

REFERENCES

1. Seabridge, A.G. M.Phil Thesis, University of Lancaster, 1982.

2. Wilcock, G.W., Moxey, C. and Lancaster, P.A. "Integrated Control of Mechanical Systems for Future Combat Aircraft."

   AGARD CP 303 Tactical Airborne Distributed Computing and Networks, June 1981.

3. Moir, I., Lancaster, P.A. and Moxey, C. "Command-Response Data Transmission Applied to Mechanical Systems Management - The Effect on the Crew-System Interface."

   AGARD CP 312 The Impact of New Guidance and Control Systems on the Military Aircraft Cockpit Design, May 1981.

4. Seabridge, A.G. and Lancaster, P.A. "The Dual Redundant Remote Terminal in High Integrity 1553 Based Systems."

   Electronic Engineering, January 1982.

5. Crossgrove, W.A. et.al. Multiplex Applications Handbook, 1979.

6. UK Defence Standard 00-18 Part 2, 1982.

ACKNOWLEDGEMENTS

The authors wish to acknowledge the valuable assistance of Mr. L.R. Collingbourne of RAE Farnborough and the engineers at British Aerospace, Warton and Smiths Industries Aerospace & Defence Systems Company, Cheltenham Division engaged in this project.

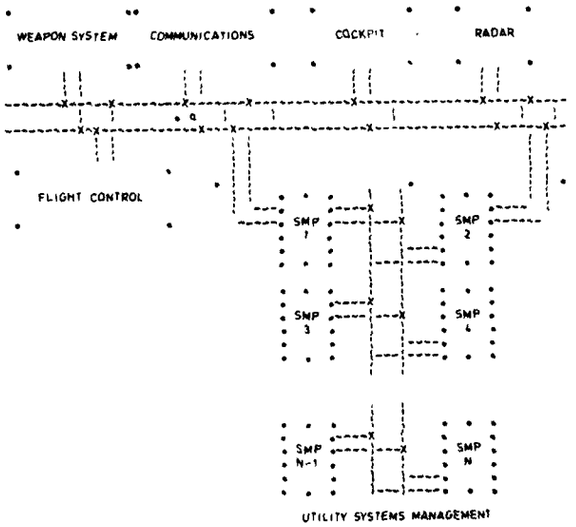

FIG.1 UTILITY SYSTEMS MANAGEMENT IN THE AVIONIC ARCHITECTURE

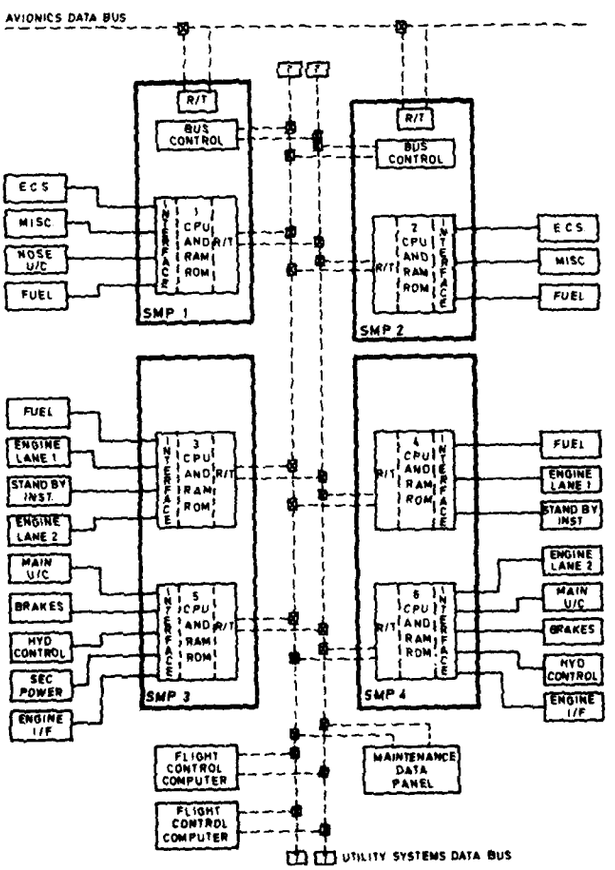

FIG.2 UTILITIES SYSTEM GENERAL ARRANGEMENT

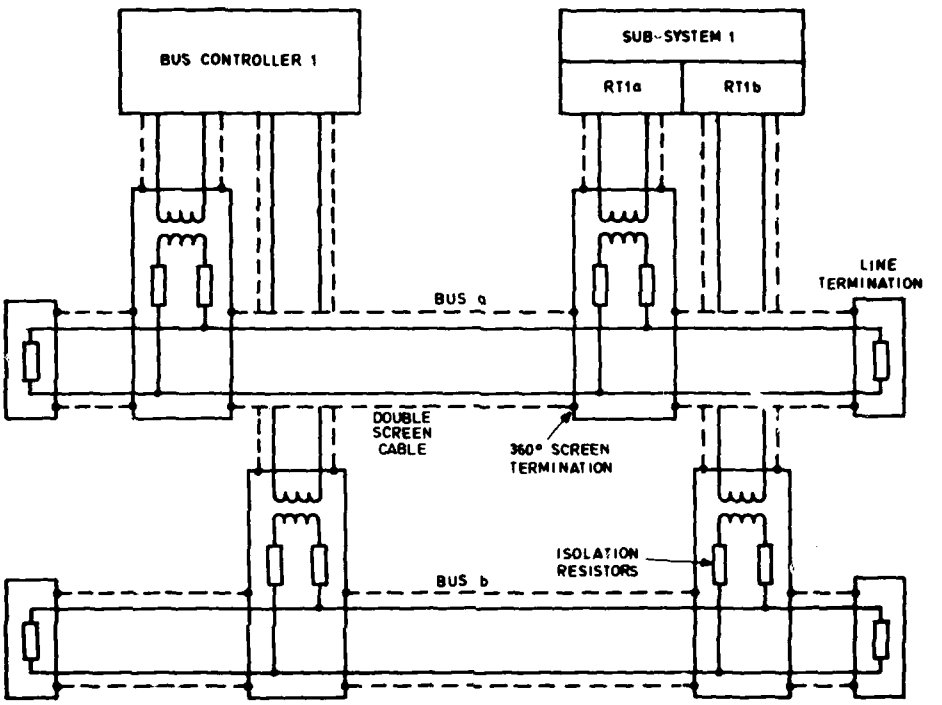

FIG.3 UTILITY SYSTEM MULTIPLEX BUS IMPLEMENTATION

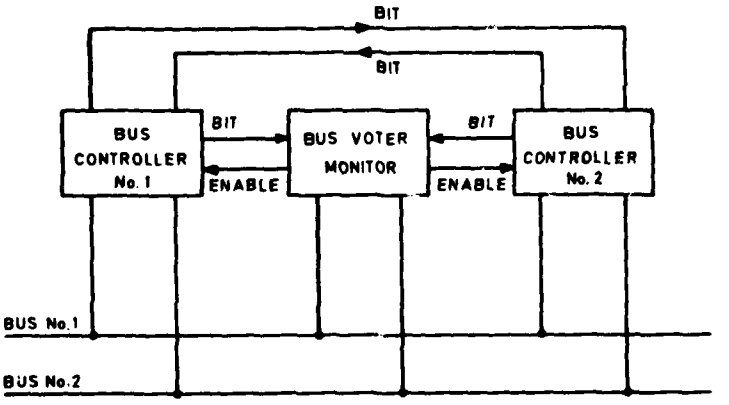

FIG.4 BUS VOTER MONITOR

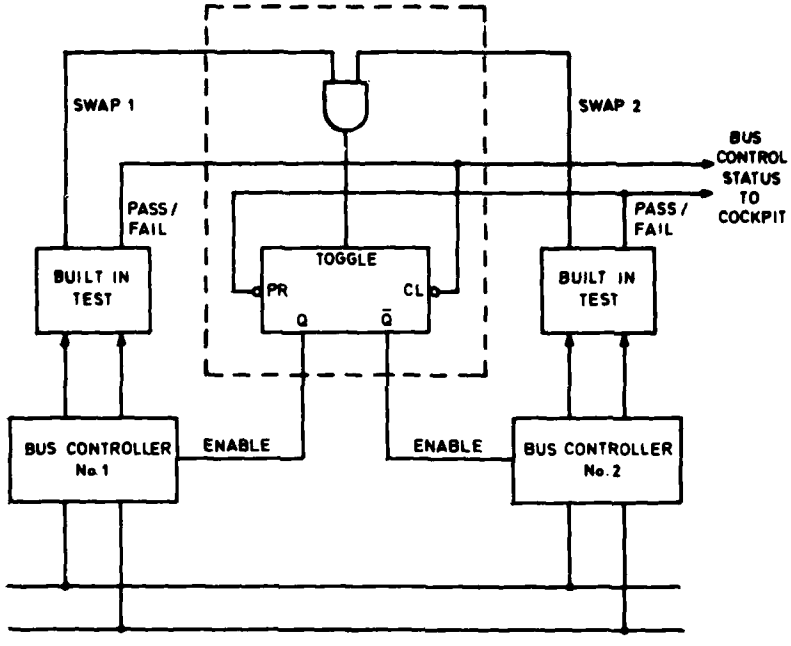

FIG.5 TIME SHARED BUS CONTROL

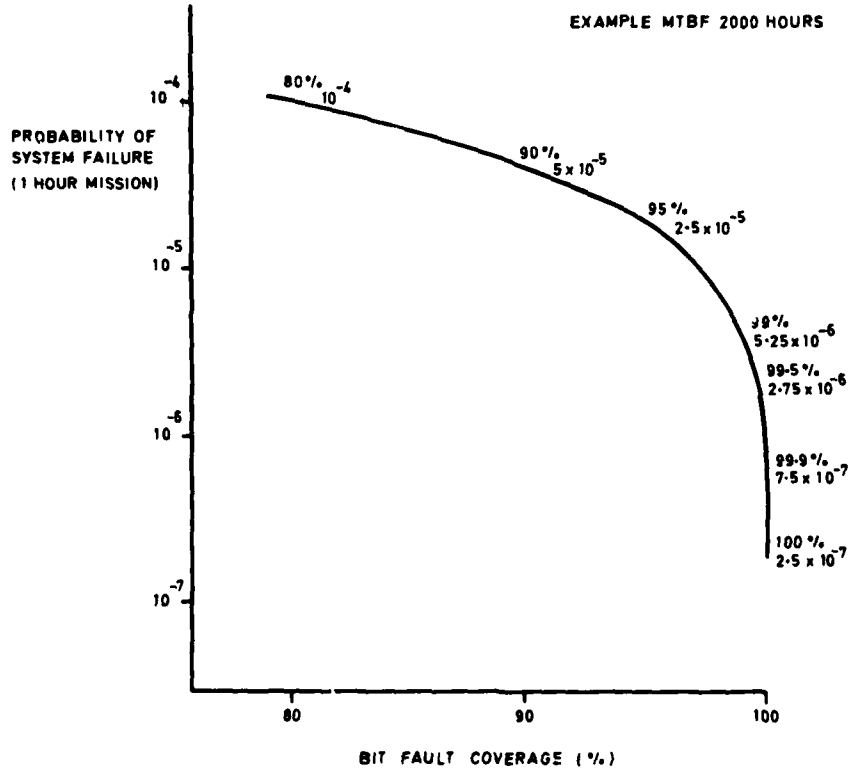

FIG.6 EFFECT OF BIT FAULT COVERAGE ON SYSTEM RELIABILITY

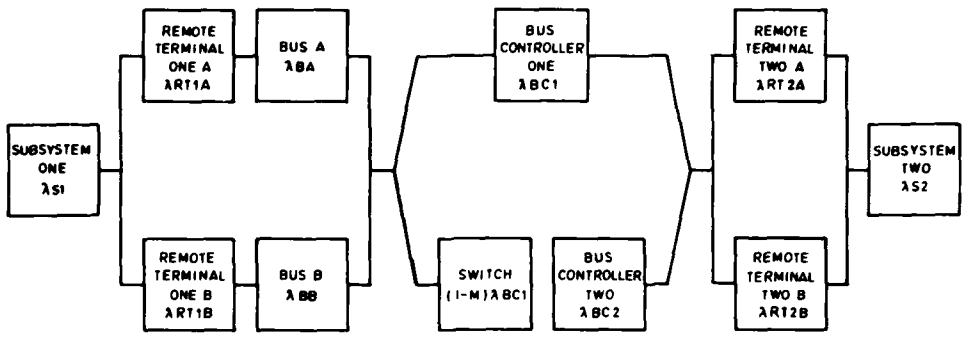

FIG.7 RELIABILITY BLOCK DIAGRAM FOR DUAL BUS CONTROLLER

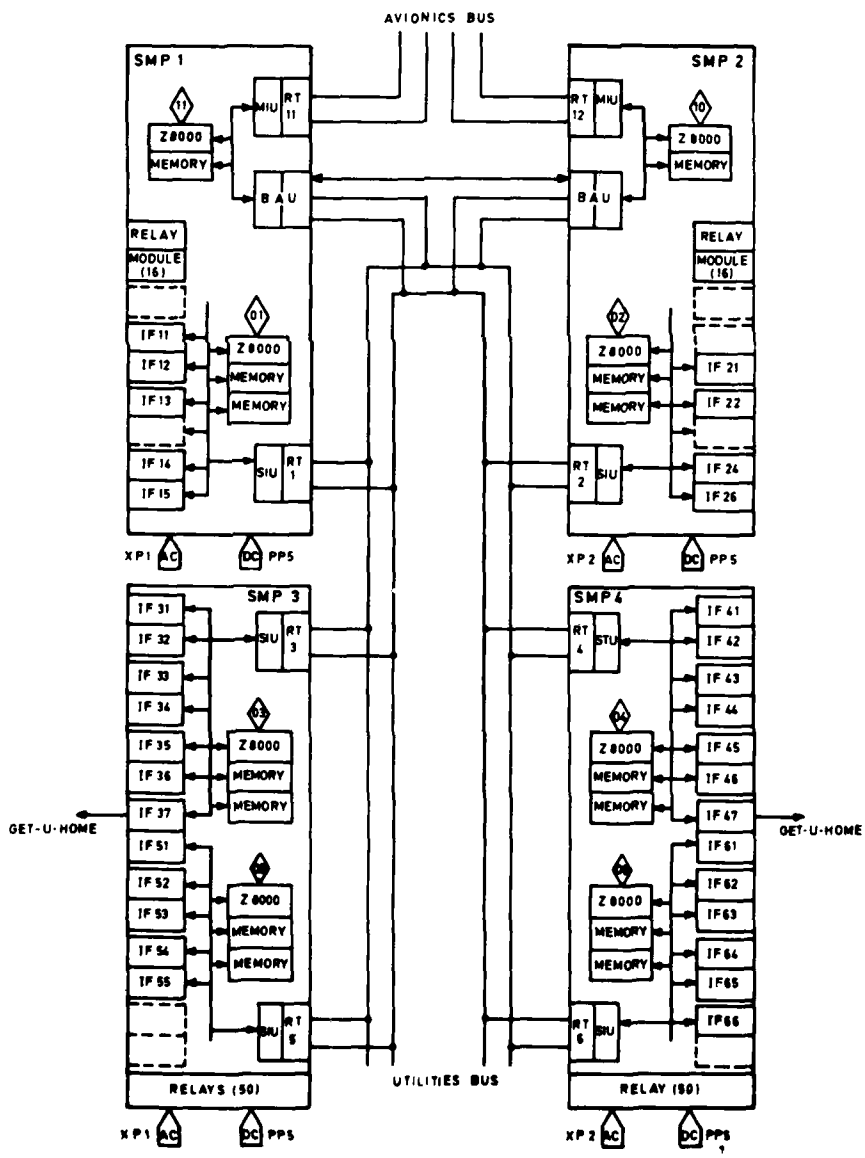

FIG.8 SYSTEMS MANAGEMENT PROCESSORS

ADVANCED DESIGN AND PERFORMANCE OPTIMIZATION TECHNIQUES UTILIZED TO DEVELOP THE F-111 WEAPONS/NAVIGATION COMPUTER (WNC)

by

Albert J. Shapiro

The Singer Company
Kearfott Division
150 Totowa Road
Wayne, NJ 07470
USA

1. SUMMARY

In September 1981 The Singer Company, Kearfott Division was awarded a contract to develop a new Weapons Navigation Computer (AN/AYK-18) to provide the F-111 with an upgraded central computer to serve through the 1990's. The goals for this computer were increased computational capability, increased reliability, operability with existing (CP-2/CP-2 EX) and future (MIL-STD-1750) Instruction Set Architectures (ISA's), and form, fit and function compatibility with its AN/AYK-6 predecessor. By the systematic application of design, performance and cost trade-offs described in the paper, all essential goals have been achieved and USAF flight tests have commenced one year after contract award.

Computational capability improvement was achieved by using a 32-bit Central Processor Unit (CPU), memory and local bus and a 16-bit bus and architecture for the remainder of the computer. Reliability was improved by employing Kearfott's hollow card cooling concept and thereby keeping all components well below their critical temperatures. The ISA's for both AN/AYK-6 and AN/AYK-18 were embedded in microcode and selectable by software. The resultant WNC has an affordable production cost, can emulate the required ISA's, has a predicted reliability of over 3000 hours, a throughput of 462 KOPS, Built-In Test (BIT) to the card (SRU) level and is interchangeable with the AN/AYK-6.

2. INTRODUCTION

The present day multi-mission aircraft, containing sophisticated avionics for fire control and navigation, has created a need for compact, highly efficient, and reliable Central Digital Computers. This paper describes the USAF F-111 WNC (AN/AYK-18) and the design methodology and some of the performance optimization techniques utilized in its development.

3. F-111 WNC GOALS

The computer avionics currently in the F-111 aircraft are of a mid-to-late 1960's design vintage and are not representative of today's technology in either performance, reliability or cost. Based on the need to update the performance capability of the F-111 fleet in light of the continued use of this aircraft well into the 1990's, the US Air Force defined a set of demanding improvement goals for the F-111 WNC (AN/AYK-18). These goals include the following:

- A throughput increase to 450 KOPS, at least a factor of three improvement over the original AN/AYK-6 machine.
- A memory size increase of four-fold, from 16K to 64K words. This growth will allow room for program expansion to enhance operational capability.
- A five-fold increase in Mean Time Between Failure (MTBF) to a minimum of 2,000 hours while operating in the same environment.
- An extended ISA, CP-2 EX* to provide floating point and integer arithmetic for higher order language capability. At the same time an effective emulation/translation capability was required for AN/AYK-6 instructions to permit low risk conversion of current flight software. In addition, the computer must achieve a simple conversion to the MIL-STD-1750A ISA, since a transition of operational flight programs to the Air Force Standard ISA is required.
- An Input-Output (I/O) which maintains the parallel bus structure of the AN/AYK-6 and in addition contains a dual redundant MIL-STD-1553B MUX. The addition of MIL-STD-1553B capability allows the computer to interface with future equipment having a MIL-STD-1553B capability.
- An enhanced BIT capable of providing a probability of 0.90 that a failure will be isolated to an SRU. To facilitate maintainability and identification of the faulty SRU a latched mechanical indicator display must be provided.

These goals were to be implemented in a form/fit replaceable Line Replaceable Unit (LRU) providing for minimum impact on current operational readiness of aircraft in use when installation is performed. No modification to aircraft wiring or structure was to be be necessary, thus requiring little or no aircraft downtime for retrofit.

The above mentioned improvements were to be achieved in a computer configuration producibile at a low enough recurring cost for the quantity of 525 units to justify the program on a Life Cycle Cost (LCC) basis.

*CP-2 extended; CP-2 is the ISA of the AN/AYK-6

4. DESIGN APPROACH

In September 1981, The Singer Company, Kearfott Division was awarded a contract for the design, development and production of the AN/AYK-18 Computer (Figure 1).

The design process commenced with a detailed examination of the customer requirements by a team of designers and support personnel to devise a series of design approaches or goals that would satisfy the specifications and the underlying customer need.

Some of the more significant tasks faced by the design team that required approach resolution were to:

- Minimize the MIL-STD-1750A retrofit program
- Minimize Intermediate Level Automatic Ground Equipment (AGE) and AGE data
- Modify the SKC-3132 multitarget emulator for CP-2 EX and 1750A architectures
- Examine and select production techniques best suited to this program
- Minimize recurring cost
- Substantially improve MTBF without compromising cost, maintainability and ability for retrofit
- Make or buy core memories to the required cost, configuration and performance.

Following is a brief discussion of each of the above issues and the approach selected. Trade-offs are discussed in Section 5.

Retrofit Program for MIL-STD-1750A ISA

Although the F-111 WNC had required operation only with the CP-2 EX ISA, the Air Force planned and required that a switchover be made to the MIL-STD-1750A ISA at some later date. They envisioned that the retrofit switchover would consist of replacing one or more cards in the CPU and performing an acceptance test procedure after the kits were installed in the field. A cost-effective approach of having both ISA's coresident in microcode, developed by Kearfott, eliminated the entire retrofit program requirement.

Minimization of Intermediate Level Test Equipment and its Supporting Data

Intermediate level test equipment to isolate a malfunctioning SRU in the field usually requires considerable expenditures for test stations, fixtures and supporting software. If the computer is properly designed, particularly with respect to partitioning and by the selective addition of BIT circuitry, an internal SRU fault isolation capability can be achieved. The cost in BIT hardware, not counting some utilization of microcode and core memory assets should be significantly less than $1000 per production unit to be cost-effective. This technique was successfully adopted for the WNC, thereby eliminating the need for Intermediate Level Test Equipment.

Multitarget Emulator

The development of a computer for Kearfott in-house programs and forthcoming procurements like the F-111 WNC resulted in a versatile processor with the ability to emulate other computers. This emulator offered an excellent response to this requirement. To be performed efficiently, emulation of computers (in addition to microcode format) requires a flexibility of data paths and sufficient hardware in the form of registers, shifters, multipliers, etc. This approach required that additional hardware be provided, but the cost was relatively low when compared to the flexibility achieved. The Kearfott SKC-3132 CPU designed as a multi-target emulator for our in-house JTIDS program with the Kearfott ISA has successfully emulated other ISA's, including the IBM CP-2 EX and the USAF MIL-STD-1750A, Notice 1.

Examination of Production Techniques

The predominant factor in the cost of the F-111 WNC program was the recurring cost to build and test 525 production systems. As a direct result the material and labor costs required careful scrutiny. Various modes of fabrication were examined to ascertain the optimum approach. Dual In-line Integrated Circuit (IC) Packages (DIP's), presently cheaper than flatpacks or chip carriers, automatically inserted and wave soldered provided the most cost effective fabrication technique.

Design To Cost (DTC)

A rigorous DTC activity was invoked and adhered to. Trade-offs with respect to circuit design, assembly and test were weighed against production cost. In some cases additional hardware was allowed to be added, e.g., SRU Built-In Test Equipment (BITE), because the increased cost of hardware was far less than the eliminated Intermediate Level AGE. The resulting low recurring per unit cost was the direct result of this activity.

Substantial Improvement in MTBF

The importance of achieving major improvement in reliability was a driving force in the trade-off decisions relating to the mechanical configuration of the AN/AYK-18. Particular emphasis was placed on cooling since the MTBF of an Integrated Circuit (IC) is influenced in a major way by its operating temperature. A reduction of 20°C in the operating temperature of an IC will almost double its MTBF. If conductive heat removal methods are used, they become less effective as card size increases. On the other hand, a large card means fewer intercard connections which improves reliability. The trade-offs were made among cooling method, card size, mechanical stiffness, soldering method, ease of inspection, etc., to maximize MTBF.

The MTBF for the F-111 WNC is calculated to be in excess of 3000 hours. A similarly constructed unit, the F-111 Advanced Microelectronic Converter (AMC) has actually surpassed its calculated MTBF of 1200 hours in the field; its operational MTBF is over 1400 hours.

Core Memory Modules

Although Kearfott has designed and built memory modules, it was decided for reasons of non-recurring and recurring cost savings to use militarized, multisourced 32 K word by 18-bit modules which fulfill this requirement. Such modules are available from EM&M, Quadri, and Fabritek.

5. DESIGN TRADE-OFFS

In the preceding section we reviewed a number of critical items requiring unique design approaches to develop the optimum computer configuration and discussed in a summary manner the approach selected. In the following section we have selected a limited number of significant subjects for discussion of the technical trade-offs conducted by the designer in arriving at a final configuration.

5.1 CPU ARCHITECTURE TRADE-OFFS

The design of the CPU was driven by three major requirements; performance, self-test and fault isolation, and the ability to emulate three architectures. All of the above, while essentially independent, exhibited a significant interrelationship during the trade-off activity.

The most fundamental performance requirement which was addressed was that of throughput. It is generally accepted that an arithmetic unit, memory, and data bus, each 32 bits wide, will result in higher speed execution for double length instructions such as floating point and double precision. It is equally recognized that such an architecture will be more costly and complex, and not cost-effective in the areas of I/O and AGE interfaces which are not usually required to operate at the highest word rate. The resulting architecture was a compromise employing a 32-bit CPU, memory, and local bus with the remaining elements of the computer employing a 16-bit bus and architecture.

Other speed enhancement techniques, such as pipelining and look-ahead memories, were rejected because their added cost and complexity were considered unwarranted for the specified performance and cost targets.

The design of the microprogram control section was critical to the successful achievement of the performance, emulation and self-test goals. An extra wide format was selected to provide optimized solutions to each of these three requirements. The broad parallel organization permitted all essential logical decisions to be performed simultaneously, thereby meeting the emulator goal with no degradation in computer performance. A microcode memory capacity of 4096 words was selected which provided sufficient memory for both required architectures and built-in test and fault isolation.

Another concern was the method to be employed to "select" the particular architecture in which the machine was to operate. Candidate solutions included a protected front panel switch, a unique jumper in the chassis which could be removed to accomplish the architecture transition, or a software switch transparent to the hardware. The latter approach was selected and implemented through a microcode test of a word in the software load module which indicated to the microcode which architecture was to be executed. This technique makes all computers interchangeable and reversible with regard to the selected architecture.

In addition, the requirements for dual architecture imposed significant constraints on the design of the I/O channels. The differences between the two architectures required that any logic operated in conjunction with the CPU be capable of accommodating the same basic I/O instructions in both architectures.

The goal of fault isolation to an SRU was addressed during early stages of design in the partitioning of the logic to be placed on each circuit card. It was identified early in the program that if the goal of fault isolation was to be truly met, each SRU must be carefully partitioned so that its function is uniquely located on, and limited to, one SRU. Upon satisfying this requirement, faults were categorized into those which could be detected by software and those which would disable the CPU/memory relationship, making normal operation impossible. The latter category of fault was assigned to the microcode for fault isolation. One of the first tasks of the microcode at computer turn-on is to ensure that the CPU and memory are operating properly enough to guarantee that the subsequent software self-test would be effective and accurate.

5.2 MEMORY ARCHITECTURE TRADE-OFFS

The F-111 WNC memory requirement was to provide a non-volatile core memory of 65,536 words, 18 bits per word (16 data bits plus 1 parity bit and 1 write protection bit). Several factors were considered in the design of the memory organization:

- The memory access and cycle times were specified to be 350 and 900 nanoseconds maximum, respectively, which is typical of available hardware. This speed limitation, unless circumvented architecturally, would preclude meeting the throughput specification.
- A 32-bit bus permits two memories to be operated concurrently such that one memory access provides two words of data/instruction in 350 nanoseconds. The double word data is particularly important when performing floating point or double precision fixed point operations.

The above factors were considered and resolved in the following fashion. Although 64 K x 18 modules offered a reduced cost approach, their use did not permit meeting the throughput specification of 450 KOPS. Performance could have been increased by additional changes in the processor, either look-ahead or faster clock speed but the increased complexity of the hardware in the processor negated this approach. The use of two 32 K x 18 modules and the 32-bit bus was the selected approach. With the one word look-ahead instruction capability of the 32-bit memory access, plus the availability of double precision data for floating point and fixed point operations, the performance increased to 462 KOPS, meeting the specification requirement, while using multisourced available memories. This permitted competition among several suppliers and a lower cost product was the direct result.

5.3 BIT TRADE-OFFS

A major element of cost in the F-111 WNC program was the requirement to provide a Support Equipment (SE) capability at the Intermediate Level (I-Level) of maintenance where the SE was required to verify computer malfunctions and to identify the failed SRU. The non-recurring cost to design the SE plus the recurring cost to fabricate eleven sets of hardware and data would have cost several million dollars. Comprehensive trade-off reviews resulted in a design approach on the F-111 WNC, whereby the SRU fault isolation was internal to the LRU thereby eliminating the requirements for SE, an approach which to our knowledge had never been applied to an airborne digital computer.

5.4 SOFTWARE

The software trade-off and decision process was more a user task. It is included here for the sake of completeness.

On the system level, the principal software task was the adaptation of existing flight proven software, which runs on the original AN/AYK-6 computer, to run on a new enhanced computer. It was also desired that the upgrade and expansion of the program be performed using the JOVIAL (J73) high order language to enhance the maintainability of the flight software. All this was to be achieved without compromising any delivery commitments for flight software in the various operational F-111 aircraft. Toward that end, the Air Force devised a clever plan for achieving the desired goals in a gradual manner, minimizing schedule risks.

The enhanced flight computer AN/AYK-18 provides the Air Force with a MIL-STD-1750A ISA capability. To facilitate the software transition, the new computer also provides a bridge ISA, CP-2 EX, which retains substantial compatibility with the CP-2 ISA but which also included several new features found in the MIL-STD-1750A ISA. As mentioned earlier, Kearfott designed the computer's microcode to be switchable between these two ISA's under the control of a single word in the computer's main memory.

Using these design concepts, the software conversion would proceed in the following manner:

1) Convert all existing flight programs from CP-2 Assembler code to CP-2 EX, largely via the use of an automatic translator program. Kearfott developed a translator via its general purpose macroprocessor program which achieved 98% effectiveness.

2) Flight test the new programs and release them to operational use as required.

3) In a gradual manner (usually as part of the normal update cycle), convert modules in the existing flight programs to the JOVIAL (J73) language. Kearfott and Proprietary Software Systems are developing a J73 compiler which generates CP-2 EX Assembler code for this purpose.

4) Once a major portion of an F-111 flight program has been converted to the JOVIAL language, recompile the J73 code, rewrite the few remaining CP-2 EX modules into MIL-STD-1750A language, retest and release the complete 1750A flight programs.

This process provides both immediate capability via the CP-2 EX ISA and eventually full Air Force Standard capability (using MIL-STD-1750A and JOVIAL) with essentially no schedule risk for interim releases of the F-111 flight programs.

5.5 ELECTRONIC PACKAGING TRADE-OFFS

Specification requirements, reliability, cost and maintainability represent the major factors to be considered in selecting the features that are to be incorporated in the mechanical design of an avionics package. In addition, schedule requirements, tooling needs, and the capabilities of the manufacturing facility must be evaluated before a final decision is made.

The above considerations plus the extensive design and manufacturing experience with a variety of packaging philosophies employed in Kearfott's varied product mix, coupled with continuing research and development in advanced packaging techniques, provided a sound basis for the trade-offs.

The most significant trade-off factor in determining system reliability is component operating temperature. A 10°C decrease in component temperature may raise the MTBF by 15 to 30%. The type of component case used, i.e., a flatpack or DIP, has a significant effect on system cost. The use of the DIP in preference to flatpacks results in component procurement and assembly cost savings in excess of 20%, however, a concomitant volume penalty of as much as 50% may have to be absorbed. The method used for interconnection between the circuit card modules, and between the backplane and external connectors, also affects cost and reliability. The use of large cards reduces the number of connector pins, which in turn enhances reliability and reduces cost. In the dynamic environment experienced by avionic equipment, a rigid card and chassis construction is preferred in order to limit card displacement. Soft construction and subsequent large card displacements lead to solder joint failures and connector pin wear.

The F-111 WNC volume and weight constraints permitted the use of DIP's. The desire to use large cards and simultaneously achieve optimum cooling of DIP cards having appropriate structural characteristics presented a significant challenge. In order to exploit the advantages afforded by the use of cost-effective DIP's and large cards, one has to overcome the problems of structural rigidity and cooling associated with this combination.

These problems could be solved by two basic construction techniques which have been extensively used at Kearfott. One utilizes sidewall heat exchangers while the other employs the integrally cooled card (i.e., the hollow card). The two techniques are illustrated in Figure 2.

The DIP solid card is a somewhat more conventional card construction employing the sidewall heat exchangers. The circuit card contains an aluminum heat sink to conduct heat from the power dissipating devices to the heat exchanger. Wedge clamps are employed at the card edge to minimize the contact resistance. One can appreciate the fact that as the card length (L) increases, the thermal path length and total power on the card increases, producing a higher temperature drop from the components to the heat exchanger. Essentially the temperature rise to the center of the card varies as the square of the card length.

For typical power densities of about 270 mW/in^2, the temperature for a solid core full ATR card (9.0 inches long) will be approximately 15 to 20°C higher than that of a 3/4 ATR card (6.0 inches long). Therefore, using large, solid core cards would compromise system reliability.

Thus, a card configuration is desired wherein component temperatures are independent of card length. The desired high reliability and the cost savings associated with a large card can then be achieved. The Kearfott-patented integrally cooled card module or hollow card incorporates these desirable features. By circulating cooling air directly through the

module as shown in the illustration of the DIP hollow card (Figure 2), the long conductive path along the card length is eliminated and component temperatures become essentially independent of card size. The hollow card module offers other advantages in that component temperatures are not affected by card location within the chassis. Also, cooling air can be allocated to each card in proportion to the power dissipated.

The module construction consists of two card mounted to each side of a module frame, which provides for the structural support and the physical separation of the cards. The cooling air circulates in the channel between the cards. The back side of the cards can be considered a planar heat exchanger that provides direct cooling of the cards. Relative cooling characteristics of the two card designs, illustrated in Figure 2, are tabulated in Table 1 which clearly illustrates the merit of the hollow card module as the card size increases.

TABLE 1.
THERMAL CHARACTERISTICS OF INTEGRALLY COOLED CARDS VS
SIDE WALL COOLED CARDS OF VARIOUS LENGTHS

	3/4 ATR CARD 6" LENGTH			FULL ATR CARD 9" LENGTH		
CARD TYPE	POWER DISSIP.	AVG. COMP. CASE TEMP.	RELATIVE MTBF*	POWER DISSIP.	AVG. COMP. CASE TEMP.	RELATIVE MTBF*
WAVE SOLDERED DIP HOLLOW CARD	8.0 W/ SIDE	70°C	1.07	11.3 W/ SIDE	72°C	1.00
WAVE SOLDERED DIP SOLID CORE	8.0 W	89°C (82°C)	0.56	11.3 W	106°C (92°C)	0.26

*ELECTRONICS ONLY, AIRBORNE, UNINHABITED FIGHTER ENVIRONMENT, SAME COMPONENT QUANTITY AND MIX USED THROUGHOUT

NOTE: 1. COOLING AIR TEMP t_{in} = 27°C, t_{out} = 71°C, or 3#/min/kW

2. NORMALLY THE CARDS CONTAIN ALUMINUM HEAT SINKS. TEMPERATURES IN ( ) INDICATE TEMPERATURES FOR CARDS WITH COPPER HEAT SINKS.

In summary, the trade-off study indicated that a cost effective and reliable design should maximize card size, optimize the component cooling technique, use a rigid card/chassis construction technique, and utilize DIP's. Details of the implementation are in Section 6.1.

6. F-111 WNC HARDWARE DESCRIPTION

The F-111 Advanced Avionics Digital Computer Complex (DCC) consists of two Kearfott WNC's and a Kearfott AMC. This arrangement, shown in Figure 3, provides selective functional redundancy to enhance the probability of mission success and flexibility to accommodate mechanization changes. Figure 1 is a photograph of the WNC alone. Its salient physical and performance characteristics are given in Table 2.

TABLE 2.
PERFORMANCE AND PHYSICAL CHARACTERISTICS

The F-111 WNC, a high performance central processor class computer in a single LRU, contains:

- CPU microcoded for CP-2 EX and MIL-STD-1750A ISA's
- Microcode memory of 4096 words (30% spare)
- Two 16-bit processor sections extend performance capability that exceeds 450 KOPS (CP-2 EX mix)
- Fast hardware multiply provided for fixed and floating point operations
- 64 K x 18 core memory
- Two dual MIL-STD-1553B RT/BC MUX
- Two bi-directional parallel channels
- Eight external interrupts
- 24 input/16 output discretes
- Timers, real time clock, time out counter
- AGE interface
- Power supply in accordance with MIL-STD-704.

Reliability
- Calculated MTBF is 3026 h vs spec requirement of 2000 h

BITE
- Self tests exceeds 95% capability and identifies the failed SRU

Input Power
- 400 W

Size
- 7.62 x 10.125 x 18.56 in

Weight
- 48.5 lb

6.1 PHYSICAL DETAILS

The internal arrangement of the WNC is depicted in Figures 4 and 5. There are eight SRU's which are plugged into a connector plate on the main chassis. Each of the two cards associated with a module (SRU) frame has independent functional connectors and separate test connectors to permit card testing prior to assembly to the module frame. Once plugged in, these SRU's are clamped in place between the front and rear panels by four longitudinal bars which are located at each edge of the main chassis (see Figure 4). This construction contains features that lead to a low cost, readily maintainable and structurally sound chassis assembly. By clamping the cards along their four edges with a set of upper and lower bars, a rugged box-beam-like structure is formed that is ideally suited for large cards exposed to high-g dynamic environments.

The hollow-card construction of the SRU's is shown in Figures 6 and 7. The annular openings located at the sides of the frame (see Figure 6) form the system entrance and exit cooling air plenums when the cards are clamped in position. Cooling air is passed into the air plenum formed by these openings at the left edge of the card frames. Each card frame conducts some of that air to its opposite edge. Here the air is collected and exits through the plenum formed by the elongated holes on the right side of the frames. Thus each card independently receives cooling air at the entrance temperature, which is in intimate contact with its interior surfaces.

Figure 5 shows the LRU frame with SRU's removed. The connector plate and clamping bars are clearly shown in this photo. The set of lower bars serves as a subchassis by retaining the connector plate and harnessing system. Chassis maintainability and assembly is optimized by having front and rear panels with harnesses that plug into the central connector plate. Elimination of cumbersome chassis side walls minimizes cost and permits complete visibility of the interconnection system.

This construction increased the MTBF by:

- Lower operating temperature due to hollow card cooling
- Reduced number of connectors due to large card size
- Mechanical ruggedness due to clamping of all SRU's
- Ease of inspection of all cards
- Wave soldering of all SRU's
- Wire wrap of connector plane.

Based on experience with the AMC which used the same type of construction, a high degree of confidence exists that the MTBF predicted for the WNC will be exceeded.

6.2 FUNCTIONAL DETAILS

The block diagram of the WNC is shown in Figure 8. Of the eight SRU's, two are identical MUX and Controller cards. The types and quantities are:

QTY.	SRU TYPE
1	Parallel Channels
2	Dual Redundant MIL-STD-1553B MUX and Controller
1	CPU #1 (timing and control)
1	CPU #2 (arithmetic and memory interface)
1	Core Memory Module (64 K x 18)
1	AGE port, discretes, timers and miscellaneous I/O
1	Power Supply.

Figure 8 indicates the major signal flow internal to the computer and at the interfaces. Each of the major elements are interconnected on the internal computer bus. The externally-controlled parallel channels, the two MUX channels, the AGE, and the CPU are capable of becoming master of the internal bus. The CPU has the lowest priority, while the externally-controlled parallel channels have the highest priority. Program-controlled I/O is performed at the CPU priority level on the bus.

6.3 PARTITIONING

The physical partitioning of the functional elements was accomplished with a careful eye toward isolation of the SRU from the BIT perspective. The CPU is partitioned into two SRU's in a way that sorts timing/control from register/data paths. The MUX channels are independent identical SRU's. Both parallel channels are contained within the same SRU. The power supply is packaged in a single SRU. The discretes and AGE port share an SRU.

6.4 CPU DESCRIPTION

The SKC-3132 provides a capability that is unique as evidenced by the following salient features. It has a throughput of 462 KOPS with core memory using the CP-2 EX mix. (For the DAIS mix the throughput is 509 KOPS.) Two 16-bit processor sections are included to extend its performance capability at a minimum hardware cost. A hardware multiply is provided for fixed and floating point operations. A 20 MHz fast shift register is used to speed shift instructions and for automatic floating point normalization. A one-word look-ahead memory is included, as well as additional data paths to eliminate waiting times that would be incurred by multiplexing.

6.5 CORE MEMORY

The core memory consists of two SEMS-16 type militarized modules that are mounted in a common assembly to improve their cooling characteristics. Each module is 32 K x 18 and is identified as having an odd or even address. Each

memory access may read or write both memory modules simultaneously on the 32-bit bus. This approach effectively reduces the memory access per instruction by 1/2.

All of these memories are physically and functionally interchangeable. All meet the performance of Table 3 and have the characteristics shown herein. As mentioned earlier the SEMS-16 type modules are available from EM&M, Fabritek (MMS32), Quadri (Q32), and others. The availability of multiple suppliers, and the fact that all three units are mature designs reduces potential production schedule and cost risk while significantly improving the spares support requirements when the computers are fielded.

All of the above memories have conventional three-wire 3D organizations. They use 13- or 14-mil wide-temperature cores with X-Y selection of 32 K words and sense/inhibit loops in 16 K-word blocks. All make extensive used of monolithic core drivers and sense amplifiers.

TABLE 3.
CORE MEMORY MODULE CHARACTERISTICS

Storage Capacity	32,768 words x 18 bits
Storage Elements	Wide temperature magnetic cores
Cycle Time	900 ns
Access Time	350 ns
Operating Modes	Read-Restore Read-Modify-Write Clear-Write
Interface	TTL
Size	9.0" x 6.4" x 1.4"
Weight	4.0 lb
Power (Typical)	35-60 W, depending on operating conditions

6.6 MUX BUS CONTROLLER/REMOTE TERMINAL (BC/RT)

The BC/RT consists of the Multiplexer Transmitter/Receiver Module (MTRM) and the Control Interface Module (CIM) packaged on a single SRU. Each BC/RT contains two independent transmitter/receiver channels.

The two-part architecture provides a flexible and universal bus type structure, having the ability to organize all the invariant MIL-STD-1553 functions into a set of high density circuit elements on the MTRM. The bus-oriented architecture of CIM provides rapid data transfer and manipulation between itself and the host CPU and memory module.

6.7 BITE

The BITE is capable of detecting over 95% of all component faults. In addition, it will identify the faulty SRU on the front panel indicators (see Figure 9). To achieve this BIT capability, the following elements were required to perform an LRU validation and to isolate malfunctions to an SRU:

- Partitioning of functional elements to a unique SRU
- An end-around test capability of I/O channels
- There should be no signals other than the internal bus signals and power between SRU's
- The CPU is essential to BIT and presents the initial self-test task
- The Real Time Clock timers and counters must be both loadable and readable to self-test their operation
- Power supply BIT test is required
- There must be a method to test and verify the NO/GO logic
- Indicators must be provided to identify the failed SRU.

All of the above are accomplished in the F-111 WNC.

The BIT concept, as implemented in the AN/AYK-18, is composed of three major elements: Hardware Error Detection Circuits, Software Test Routines and Microcode Test Routine.

The self-test and fault isolation routines are initiated by a programmed routine or upon the detection of a NO-GO condition.

The first step in the self-test routine is to verify that the CPU is functioning. Since the CPU is divided between two SRU's, the microcontroller SRU must be given the kernel capability for BIT execution. In addition to BIT microcode, it is desirable to have local macroinstruction sequence capability for BIT so that independence from core memory is obtained for isolation.

This BIT microcode and macrocode may be used to test the arithmetic SRU of the CPU. CPU arithmetic tests include the execution of instructions and validation of data. Memory tests are conducted by the CPU. These tests include sum tests and verification of the ability to read and write into areas of unprotected memory.

Each MUX SRU is practically self-sufficient with respect to BIT. MUX self-test has been incorporated in the existing hardware and has been proven to be very effective. In addition the MUX microcode can check the internal bus/memory interface redundantly with the CPU and the other MUX SRU.

The parallel channels and discretes are tested in an end-around mode.

Power supply self-check includes the monitoring of the four dc voltages that are generated, to determine whether they are within specified tolerances.

Each of the individual SRU BIT detectors is summed in a BIT register. The CPU monitors this register and may cause a self-test procedure to be initiated when a BIT error is detected. The CPU or the MUX microprocessor may

initiate the test, depending on the specific failure. If the failure is verified, the computer NO-GO is generated and the specific SRU failure is identified on the front panel coded and latched failure indicator. Figure 9 is a photo of the WNC front panel, showing the seven electromechanical BIT indicators. When all indicators are black, system operation is normal. A decal, mounted directly above these indicators, informs the maintenance man how to interpret the indicators to determine whether the LRU is in good working order, or which SRU of the LRU is at fault. Each time the power is turned on, these indicators are reset. A pushbutton directly below the displays will permit the maintenance man to reset the indicators, assuming power is on. When power is removed from the LRU, the indicators continue to hold their last setting until power is reapplied. The indicators are controlled entirely by the CPU's microcode through the BIT register and in no way by the software. Thus, memory faults leading to apparent software errors cannot cause these indicators to be set incorrectly.

As a result of this unqiue capability, the I-Level SE requirement was eliminated and several other by-products accrued, namely:

- The skill level of the maintenance personnel was reduced
- Turn-around time was cut in half
- Unexplained or non-reproducible failures will be minimized.

6.8 DESIGN TOOLS

A discussion of the design techniques for modern digital electronics would be incomplete without some discussion of Computer Aided Design (CAD).

6.8.1 CAD

One of a number of CAD techniques used in the development of the WNC was the use of our CRT-based interactive graphics system, in conjunction with a computer having special placement, routing and verification programs to design the printed wiring boards. This system is used to accomplish automatic parts placement and automatic routing of virtually all of the connections. Once completed, the result is edited on a CRT design console for correctness and for conformance with preset design rules. After final editing a paper tape is prepared for subsequent use in a Slosyn Film Generator to produce the PCB artwork and for the numerically controlled PCB drilling.

In addition to the above, a Microsim Simulator is another form of CAD used in the design of the AYK-18. It is a four-state logic simulator with assignable propagation delays which is used for design verification. It is also utilized for fault simulation to determine testability of digital circuits.

6.8.2 LABORATORY SUPPORT EQUIPMENT (LSE)

The LSE (see Figure 10) is a multi-usage, user-oriented, modular, integrated hardware/software computer testing tool. Kearfott uses variations of this device to perform:

- Computer SRU (card level) testing and development
- LRU (box level) testing
- Software development of programs
- System integration.

The LSE is a computer controlled unit, either a PDP-11-24 or -34, that controls the operation via a keyboard entry and supports a variety of user-selectable operating modes that include:

- Interaction with the computer during program execution. This includes the capability to examine and load memory so as to modify programs on-line.
- Monitoring and debugging of software either in real-time or off-line.
- Loading and verification of programs by use of floppy discs which are an integral part of the LSE.
- Programs listing on a line printer.
- Comprehensive diagnostic procedures to separate hardware and software faults, and to troubleshoot hardware faults in the computer as well as the full system which is controlled by the computer via its I/O.
- Unlimited break point capability.
- Performance measurements on the computer.

The data logging capability includes the ability to store the last 2000 instructions that were executed and print out the data on hard copy. Units that are delivered for operation at Air Force maintenance depots are militarized versions of the LSE.

6.9 STATUS

The F-111 WNC contract was awarded to Kearfott on 15 September 1981. This is a multi-year contract for 525 computers, support software, LSE, Data and AGE equipment.

The first computer delivery, a brassboard with its LSE, was made three months ARO, 1-1/2 months ahead of contract schedule. The first two preproduction computers were delivered 7-1/2 months ARO. To date (30 August 1982), six preproduction computers and six LSE units plus data have been delivered.

The U.S. Air Force has validated flight software with the new computers and flight testing commenced in September 1982.

7. GROWTH CAPABILITY

The AN/AYK-18 architecture has built-in growth capability in a number of areas without major redesign. It has a high degree of functional and physical modularity which permits upgrading individual modules (cards) without changing architecture, internal electrical interfaces or mechanical design as new memories, IC and VLSI devices become available. This growth potential is facilitated by the use of a standardized high speed parallel bus to interconnect the various modules.

7.1 MEMORY

The CPU has an addressing and memory management growth capability range of 1,048 K words, and thus can handle larger size memories. The present magnetic core memory modules can be directly replaced by double density magnetic core modules to increase capacity from 64 K to 128 K words with the same module dimensions.

In addition to core memories, the variety of solid state memory devices available also offers substantial performance trade-offs and improvement, including increased speed, lower power (CMOS RAM's) and greater density, although not at the same time. Solid state RAM memory can be combined with core to provide higher speed scratch pad memory while retaining core for program storage.

If a mass memory is considered such as disk or bubble memory, a high speed RAM can then be introduced for all of main memory to increase execution speed. The combination of UVEPROM or bi-polar PROM/ROM for program storage and RAM for data can be considered for applications in which program changes are unlikely.

7.2 CPU

CPU performance can be upgraded in several ways. The logic is capable of running at an increased clock rate to directly speed up execution. An instruction look-ahead cache memory can be incorporated to provide a queue of instructions which eliminates instruction fetch times as a contribution to execution times, particularly with core memories.

7.3 I/O GROWTH

A high degree of I/O customizing to application requirements is feasible without affecting overall architecture. Individual I/O modules can be configured as "Smart" processors to further minimize CPU time loading. Standard I/O modules are available, e.g., MIL-STD-1553 Dual Bus Controller, parallel DMA channels, etc., to accommodate this expansion capability.

8. CONCLUSION

By the optimum utilization of digital signal processing, computer architecture, and mechanical trade-offs, strict adherence (from inception) to design-to-cost methodology, and the utilization of modern CAD techniques, the dual ISA Computer described has fully achieved its performance and LCC goals.

The computer, to quote a recent Air Force report, will have approximately four times the memory, five times the *reliability, and twice the speed at one half the cost of the original.*[1]

[1] 3rd Annual USAF Avionics Master Plan (AMP).

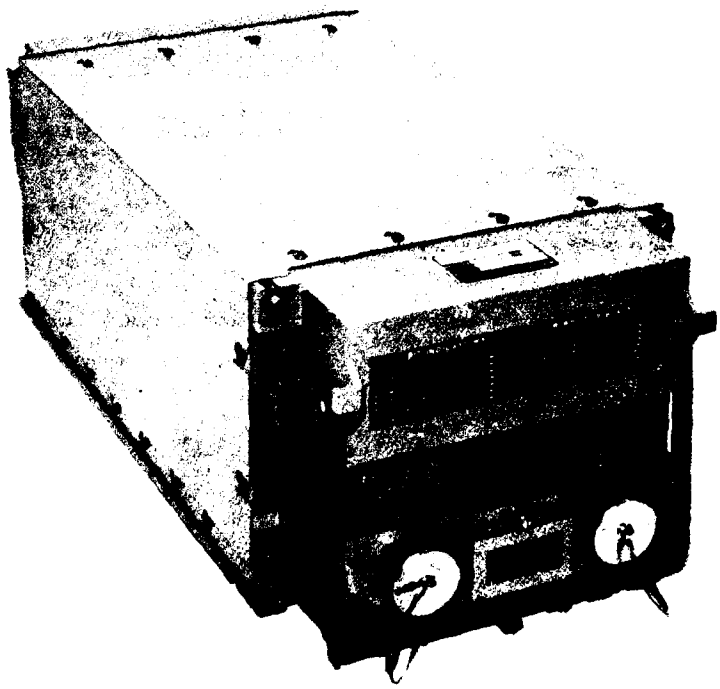

F-111 WNC COMPUTER (AN/AYK-18)
FIGURE 1

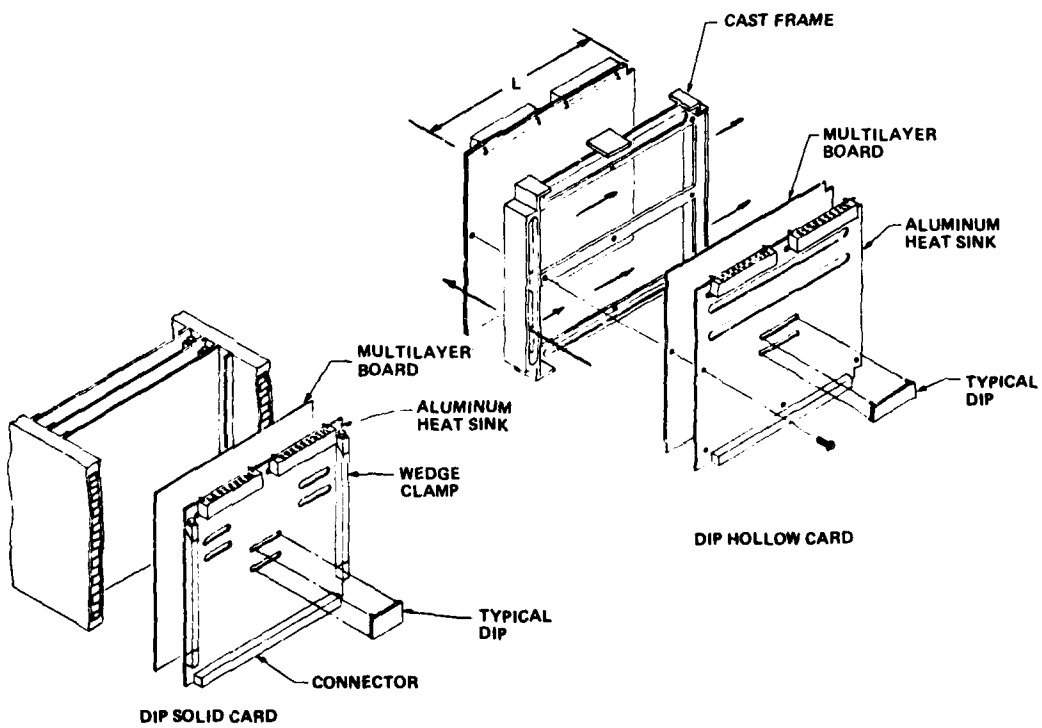

MODULE FEATURES
FIGURE 2

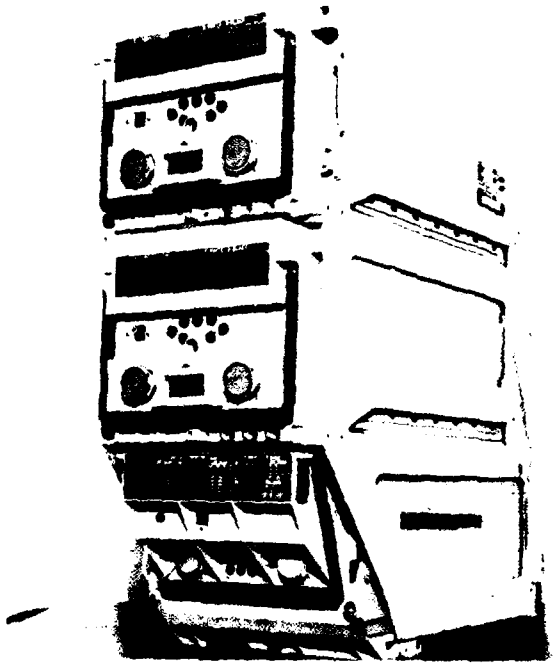

DIGITAL COMPUTER COMPLEX (DCC)
FIGURE 3

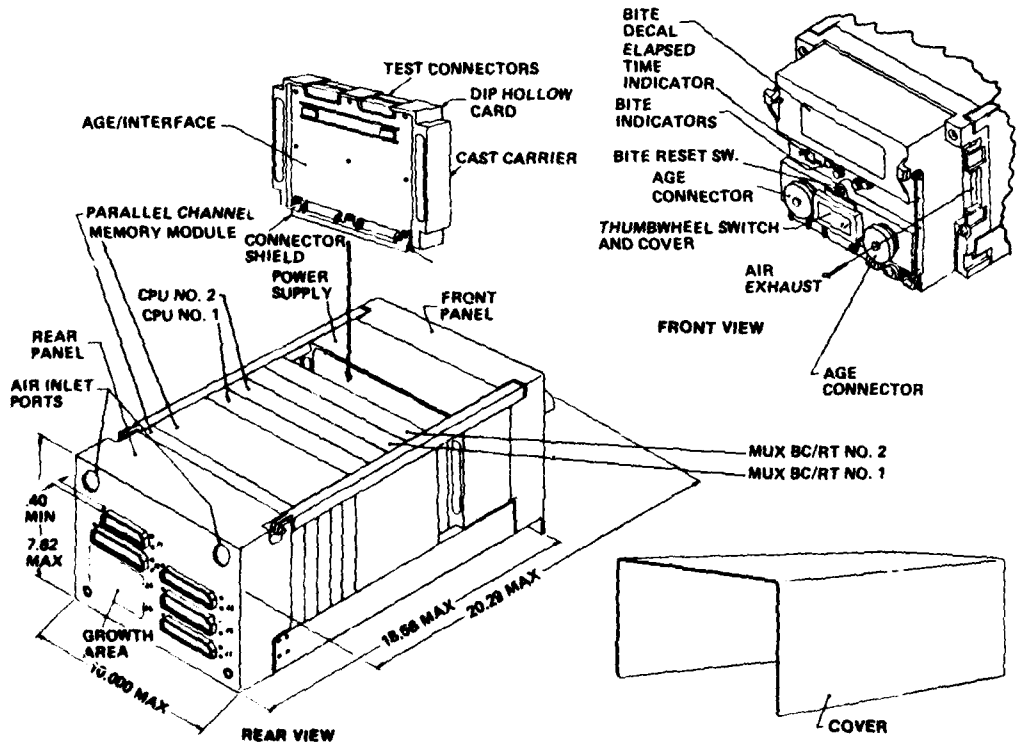

F-111 WNC COMPUTER
FIGURE 4

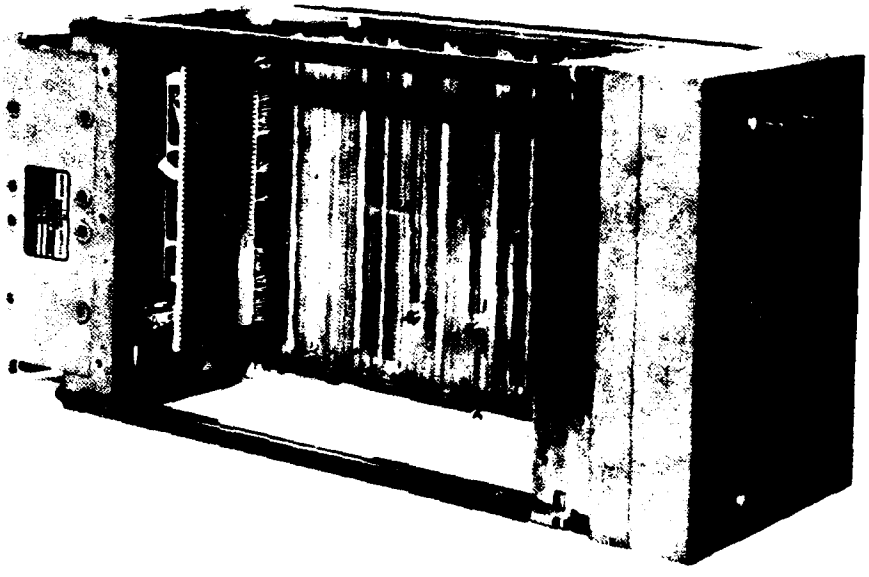

F-111 CHASSIS SHOWING CONNECTOR PLATE
FIGURE 5

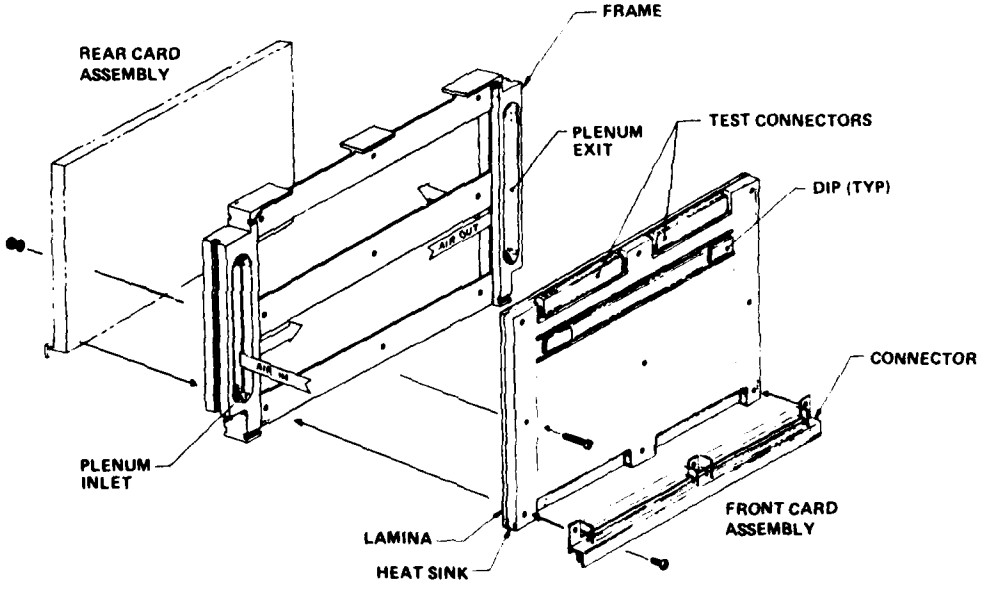

F-111 COMPUTER HOLLOW CARD CONCEPT
FIGURE 6

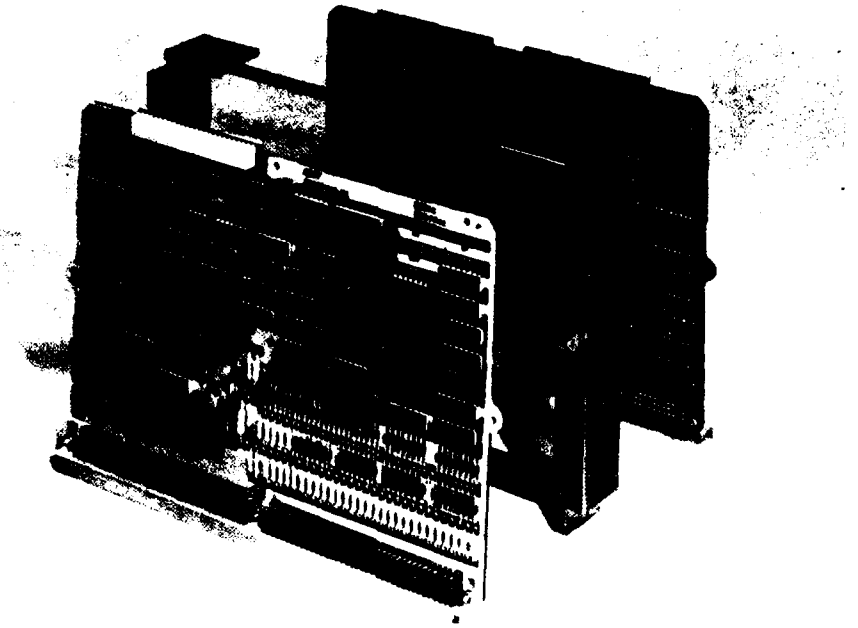

PHOTOGRAPH OF DIP HOLLOW CARD
FIGURE 7

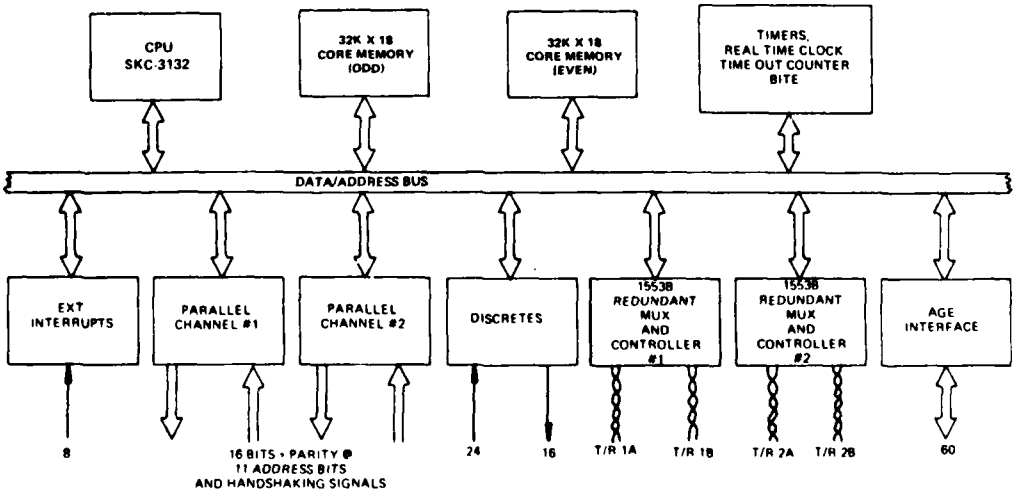

F-111 WNC BLOCK DIAGRAM
FIGURE 8

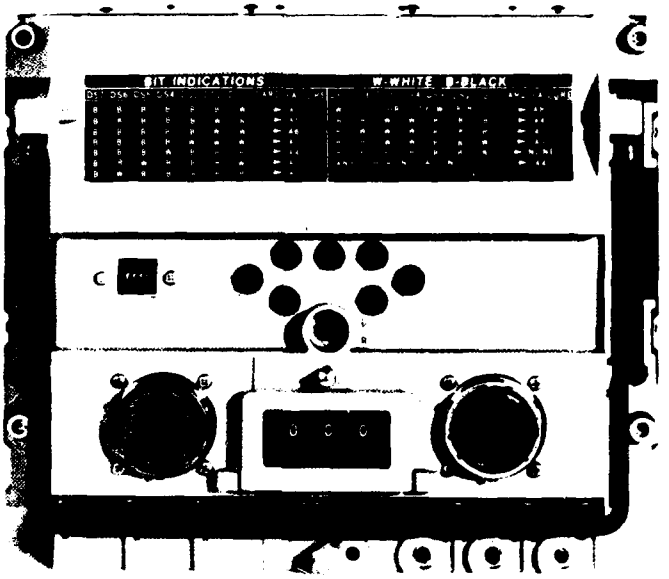

F-111 WNC FRONT PANEL
FIGURE 9

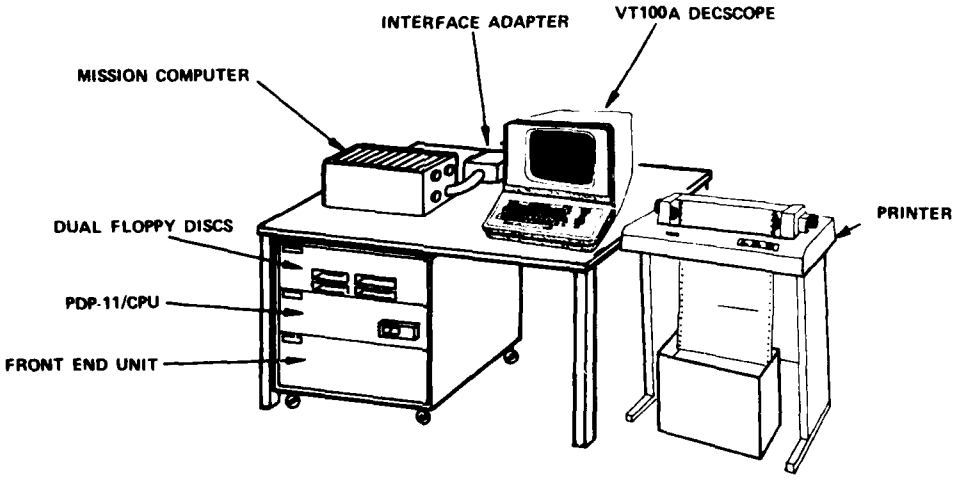

AN INEXPENSIVE USER - ORIENTED, HARDWARE/SOFTWARE TESTING SYSTEM PROVIDING THE ABILITY TO

- LOAD, MODIFY AND EXAMINE MEMORY CONTENTS FROM DISC, TAPE, OR CONSOLE PANEL
- DEBUG SOFTWARE
- OPERATE AS A DATA LOGGER
- LIST PROGRAMS ON A LINE PRINTER
- TROUBLESHOOT HARDWARE FAULTS
- MINI-ASSEMBLER

LABORATORY SUPPORT EQUIPMENT (LSE)
FIGURE 10

A modular approach to high reliability software generation with application to non linear control

S M WRIGHT
Section Leader
ACT Design group

J S WINTER
Flight Systems Department
Royal Aircraft Establishment
Farnborough

Summary

This paper describes an interlocking set of techniques covering control law and control system architecture design, documentation and validation. These address the problems experienced by the airframe manufacturer in proving the integrity of a digital control system (hardware and software) in such a way that the undoubted power and flexibility of digital techniques can be fully exploited. An idealised processor architecture and instruction set is presented and its application illustrated by reference to a set of non linear control laws. This shows how the control law coding and verification can be eliminated as a separate step in the design process. Finally the beneficial effect of the control law structure on the process of failure identification and subsequent failure management is described.

1. Introduction

Flight control systems are required by modern combat aircraft to provide acceptable response characteristics for a wide range of flight conditions and tasks. In recent years, the rapid development of digital control techniques has provided the means of fulfilling such requirements, not only through the greater sophistication that these allow, but also through implementation advantages of reduced noise problems, improved self-test capability, function modification by reprogramming and an inherent function repeatability from one unit to the next. As experience with this type of system has accumulated, it has become clear that advances in software production techniques have not kept pace with advances in hardware. In particular, there are problems in quantifying the integrity, and this has left the problem of common mode software failures unresolved.

The principal problem of ensuring safe software is related to maintaining visibility of the algorithms. This requires identifiable logic paths and partitioning of control laws into functional blocks. Attempts to improve visibility include the use of high level languages in which logic paths can be easily checked, but this shifts the problem of ensuring safe software since it is now the compiler integrity that must be resolved, an equally if not more difficult task.

Ensuring safe software is time consuming, and costly. If the control program is contained in a single processor, any modification to part of the control algorithms will result in the need to reverify the whole software package. Use of a distributed processor system, in which control algorithms are physically partioned, alleviates the situation but the need for high rates of throughput limits the degree of partitioning if the processors are connected by a data bus.

The ramifications of the problem are widely felt. Experimental research aircraft, development flying of prototype aircraft or variations in production aircraft to meet different customer specifications, all currently need substantial effort to verify control law software. Failure to alleviate the situation places constraints on the range of applications of active control, and detracts from its use as a cost effective method of improving pilot in the loop efficiency.

This paper describes an approach to this problem. It is directed towards the use of asynchronous processors which are programmed through a limited but highly flexible instruction set. The system architecture is appropriate to complete functional partitioning of the control algorithms and has implications on the complexity (and hence integrity) of flight control computer performance monitors. The approach described eliminates the need to treat coding of flight control algorithms as a separate phase, since the code is developed as an integral part of any non-real time simulation undertaken by the system designers. The documentation of the resulting code is essentially diagrammatic and hence very concise and easily understandable, particularly since it uses conventions which would be familiar to most engineers.

2. A Simple Safe Software System

This approach uses an assumed common characteristic of all control tasks in order to achieve simple specification, documentation and code.

All control algorithms can be represented as a continuous signal flow diagram which can be decomposed into a small number of component elements; viz Add, Subtract, Load, conditional load, Multiply, Divide, Look-up, Integrate, etc. Fig.1 shows the original Laplace transform specification of a control function and Fig.2 illustrates a corresponding pseudo-analogue representation. It is this diagram which forms the basis for subsequent simulation and coding. Fig.3 gives the decomposition of this into a specification file using an idealised instruction set.

The use of the pseudo-analogue diagram (Fig.2) allows explicit diagrammatic representation of all intermediate points in the calculation, and this clearly identifies possible scaling problems. It is a very convenient and rigorous program specification document requiring very few types of instruction to completely describe its operation (say 16 compared with 128 for common microprocessors). This eases the task of proving the correct operation of those instructions in hardware. It also minimises the effort involved in learning to use, or check the use of, the instruction set.

The instruction set is limited to that set of operations which have a one to one equivalence with a feature in the pseudo analogue diagram, so the set can grow, but not in any way which would detract from the inherent simplicity of specification and documentation. See Table 1 for the present suggested instruction set.

This idealised instruction set can now be used in one of two ways. It can be used as a specification language with a translation team or program used to convert the code to target machine code, together with the incorporation of whatever timing and synchronisation is necessary. (A good example of this approach is LUCOL $ Ref 1). Alternatively, since the idealised instruction set is so small and simple it can be executed directly by a suitable processor. This is of considerable benefit when it comes to proving the integrity of the code implemented on the machine since a translator approach will considerably expand and complicate this final code.

If the target processor is fast enough to execute all program statements every program pass, the need for separate executive functions within the program is removed. If the program iteration rate can then be made sufficiently fast, further simplifications are possible since the digital implementation of the control function can be considered as continuous. This removes the need to consider any timing or synchronization problems other than those implicit in the control function being executed, and also simplifies the control function design stage by eliminating the need to perform a Z transform analysis.

3. Hardware Implications

Software is becoming relatively more important than hardware in determining the costs of ownership of many digital systems. Therefore for this class of system it may become advantageous to trade off an increase in processor speed for a reduction in software complexity. (See Fig.4)

For any particular application the Safe Software System described above would require an increase in processor speed of approximately two orders of magnitude when compared with a more conventional approach. When considered in conjunction with the fact that the function being executed will naturally become ever more complicated*, then this approach presents a formidable hardware requirement.

This processing speed requirement will be at least partially met by increasingly dense integrated circuit techniques, such as those being developed in the USA's VHSIC (Very High Speed Integrated Circuit) or the UK's VHPIC (Very High Performance Integrated Circuit) programmes.

In addition the use of a multiprocessor configuration ensures that sufficient processing power is available as well as allowing the control task to be partitioned into convenient modules. The communication between modules is now important since if the Safe Software benefits outlined above are not to be lost then the interface between processors must be rigorously controlled. The standard multi processor communication techniques of shared memory or common data bus would restrict either the number of processors which could be linked or the rate at which data could be exchanged or both. Also in the event of faulty operation of one processor either through a hardware fault or program error, it would be difficult to predict the effect on the other processors. If a network approach is adopted with one variable being transmitted per physical link in a continuous manner, the number of processors can be extended indefinitely and no handshake routines or protocols are needed. The propagation of failures between processors is entirely predictable and the interface between processors can be rigorously controlled by a single patching function which can use standard analogue drawing and inspection techniques for design, documentation, and change control. (Ref 2 describes early development of these asynchronous multiprocessor concepts)

An idealised processor module specification has been suggested based on our experience with hardware concept proving exercises (See Table 2). The interfacing and instruction set is as outlined above with all input/output memory mapped and the maximum program size determined empirically from the size of functional design tasks which would normally be allocated to a single individual. All data storage is assumed to be of the same type, 32 bit real. This outline hardware specification has been derived from the requirement to operate high integrity control systems with no reference to the limitations of current technology. As such it could alleviate a number of hardware support problems. In particular it would insulate the system designer and system owner from changes in technology since the benefits in terms of reduced module cost, size, weight, power requirement or improved EMI performance could be capitalised on without changing the essential form and fit of the processor module.

The highly modular nature of this type of processor and the ease with which it can be configured to a wide range of control requirements would also lead to what would be, in military terms, a relatively large volume application and this would justify the highest levels of integration.

4. Program development

One of the major benefits anticipated from the adoption of a Safe Software System such as that described above is that the control system design engineers generate their own code. The software development procedures therefore become an integral part of the control design, simulation and validation procedures.

In particular the simulation language TSIM developed by the RAE at Farnborough (see ref 3) is used to optimise a control system design, taking into account the non linearities both within the controlled, and the control system.

* Flight control functions are becoming more comprehensive and complicated as task oriented control and carefree manoeuvering modes are more fully exploited.

$ LUCOL is a registered trade mark of Lucas Industries Ltd.

The simulation of the control system using this software package is documented within BAe using a pseudo-analogue diagram identical to that already described.

Normally the code to implement this function is written in a specification language which is then translated into a Fortran program for subsequent compilation and execution. It would only be a small step to make the TSIM specification language used for the simulation of the control program identical to the idealised instruction set already described. Thus the development of the function and the proof of its correct operation would inherently develop the target machine code and prove its correct operation. The resulting code from the final approved control design would only then require a very simple assembler and down loading operation. Change control on this software development system would be based on the established procedure of automatically updating the version number of a file after any edit.

5. Application to control algorithm design

In respect of control system design the most attractive aspect of the software/hardware concept described above is that the control algorithms may be easily physically partioned into functional blocks. This is a more cost effective method of introducing additional control algorithm options since implementation will not affect already existing proven controllers. Different control algorithms may be switched in manually through some pilot selectable cockpit switch (eg in the case of task oriented control), or automatically through some prespecified switching criteria. The latter approach may be used to yield a class of non linear control laws which revolve around switching between essentially linear sub-controllers (see Fig.5). This has the attraction that the design rules and stability criteria for each sub-controller are well established, and the non linear control problem is reduced to one of determining the piloting and stability implications of the switching action. An additional attribute is that in partitioning control laws in this manner, the designer does not have to compromise designs of controllers for different tasks.

Examples are provided below for two aspects of a fighter aircraft longitudinal control. Firstly, a pitch rate manoeuvre demand system which switches to an incidence demand system at high angles of attack. This provides the pilot with good control when at the edge of a manoeuvre boundary without sacrificing control characteristics in normal operation. The second example demonstrates a pitch rate manoeuvre demand system in which the response bandwidth varies with amplitude of error signal. This provides a means of achieving rapid response to pilot demand without compromising the need for noise rejection.

5.1 Angle of attack limiting

Angle of attack limiting has long been recognised as an important part of a carefree manoeuvring system in which the pilot does not have to continually monitor the state of the aircraft in order that it does not enter an unstable portion of the flight envelope. In this approach to designing such a system (based on an extension to those described in Ref 4), the control laws are partioned into two, a pitch rate manoeuvre demand controller and an angle of attack demand system. The two controllers are then modified so that, with the switching algorithm included, the overall system takes the form shown in fig 1, in which measures of pilot demand are input to each loop. The elevator actuator demand is then derived from the more nose down signal from either of the two controllers. In normal operation, the angle of attack controller demands an incidence higher than that demanded by the pitch rate controller, and thus the latter loop remains engaged. As the angle of attack increases towards the boundary, the angle of attack controller takes over, with the maximum angle of attack achieved when the pilot stick is fully aft.

This system was applied to the mathematical model of the RAE fly-by-wire Hunter (See Ref 5). The system performance has been demonstrated in both off-line studies and in piloted simulation and has received favourable pilot comment. An example of the response is shown in fig 6. Fig.7 illustrates the stick versus angle of attack relationship produced by this system.

As an extension to such a system, the relationships between demanded angle of attack and stick position could be varied with forward speed, and used as a method of blending response modes (Ref 8). For example if an angle of attack controller were deemed appropriate for the landing phase, it would only be necessary to vary the relationship between stick position and angle of attack demand with forward speed in order to effectively disengage the pitch rate controller.

5.2 Non-linear pitch rate manoeuvre demand system

One of the problems in control system design is the need to generate a high gain control system with rapid removal of any closed loop steady state errors whilst preserving adequate noise rejection. These requirements are in conflict and have, in the past, compromised control system design. To resolve this conflict, recent work has been aimed at varying system bandwidth so that for small closed loop error signals, a narrow bandwidth exists (thus fulfilling noise rejection criteria), whilst, in response to pilot demand, the bandwidth increases temporarily to provide a rapid response. (See Ref 6)

The switched linear system approach to resolving the conflict in design criteria is based on a number of pitch rate manoeuvre demand loops of progressively increasing loop gain/bandwidth. The individual loops are linked together as shown in Fig.8. Taking a linearised aircraft model the responses of the individual loops to pitch rate gyro noise are shown in Fig.9. As seen in Fig.10, although the bandwidth/loop gain changes are discrete, there appears to be a 'pseudo continuous' change in degree of sensor noise reaching the actuator as the closed loop error signal reduces to zero. Effects of dominant aircraft parameter changes are shown in Figs.11 and 12.

6. Performance monitoring

The partitioning of the control laws in the manner described above provides a more appropriate system architecture for the use of flight control computer performance monitors. Monitors dedicated to specific controller functions may be included, and in view of their resultant simplicity, their integrity may be more easily quantified. Simple algorithms can be derived on the basis of generation and cross-comparison of band-limited signals from dissimilar sources, and their algorithms can be designed for one controller with only limited change required if any gain scheduling exists in the control algorithms. (See Ref 7)

7. Current applications

The work described in this note was developed in the course of the joint BAE/RAE Farnborough control laws research program on the FBW Hunter. This was prematurely curtailed by the recent loss of the aircraft following engine failure on take off.

It is now intended to continue this work using rig studies pending the location of a suitable flight vehicle to replace the Hunter. These rig studies will give the opportunity to develop a system engineered in a manner representative of future project aircraft, and to investigate the most appropriate level of integration with other avionics equipment connected by the 1553 data bus.

8. Final Comments

A complementary set of design techniques have been developed which attain high confidence in their operating techniques through reliance on simple established good practice within a module. The sophistication and power of the control action is then achieved by suitable linking of modules. The two techniques described in this paper of "switched linear control" and "asynchronous multiprocessor" show how this linking can be achieved with a minimum of additional problems. This approach is ideally suited to the use of dissimilar redundancy both in the control law design and its implementation and could well be extended to a gracefully degrading system configuration due to the ease with which failure propagation through the system can be analysed.

The original intent of this work was to ease the task of developing and proving high integrity systems, but as experience has accumulated, various potential hardware and logistic support benefits have become apparent.

These techniques have been implemented to date using commercially available processors, and their application has been considered only in the context of inner loop control tasks where the speed and integrity requirements are at their most severe. A more representative engineering implementation and application to a wider range of control tasks are now being investigated both within BAe and in the Avionics industry principally at Lucas Aerospace. If successful this work could allow the considerable benefits of active control to be applied to a wider range of aircraft types both by reducing the non recurring system design and verification task, and by reducing the recurring system costs of hardware provision and support.

9. Acknowledgements

The authors are indebted to British Aerospace and to the Royal Aircraft Establishment for their support of the above work. The views presented however are entirely their own.

10. References

1. Dolman W.C. and Parkes J.P. — An approach to software for high integrity applications. American Society of Mechanical Engineers Conference (1982)
2. Wright S.M. and Brown J.G. — The development of asynchronous multiprocessor concepts for flight control system applications AGARD CP 303 (1981)
3. Corbin M.J. and Winter J.S. — 'TSIM' - A combined analysis package for the design of flight control systems RAE Tech Memo FS 256 (1979).
4. Hartman G.L., Hauge J.A. and Hendrick R.C. — F8 Digital CCV Flight Control Laws NASA CR2626 (1976).
5. Wright S.M. — Longitudinal Control Law design for phase three flying on ACT Hunter XE531 BAe Tech Note YED 6939 (April 1980).
6. Winter J.S. and Murphy L.M. — Description of a non linear flight control system. RAE Tech Memo FS 414 (July 81).
7. Jones J.G. — Analytical Redundancy using band limiting filters. Part one, basic principles. RAE Tech Memo FSF 458 (Feb 82).
8. Wright S.M. — V.S.T.O.L. Control Law Options (a progress report). BAe Tech Memo YED 7001. (Nov 1980).

LDK.X, K	MUL. Z, Y, X
LD. Y, X, C*	DIV. Z, Y, X
LOOKUP. Y, X, T	INTEG. Y, X
ADD. Z, Y, X	LIM. Y, X, A, B
SUB. Z, Y, X	

* Instruction executed if contents of c are positive

X = DESTINATION	I = INDEX	T = TABLE NUMBER
Y = FIRST OPERAND	A = UPPER LIM	B = LOWER LIM
Z = SECOND OPERAND	K = CONSTANT	

Table 1:- Idealised processor module, Instruction Set

- 256 x 32 bit program store
- 256 x 32 bit R.A.M.
- Program interation rate 0.5 ms
- Sequential instruction execution
- "Analogue" saturate on overflow
- 16 bit by 16 bit hardware multiply
- 8 pseudo analogue inputs } memory mapped
- 4 pseudo analogue outputs }
- 1 serial I/O port for test purposes (1553B)
- Up to 32K words for lookup table

Table 2:- Idealised processor module Hardware Specification

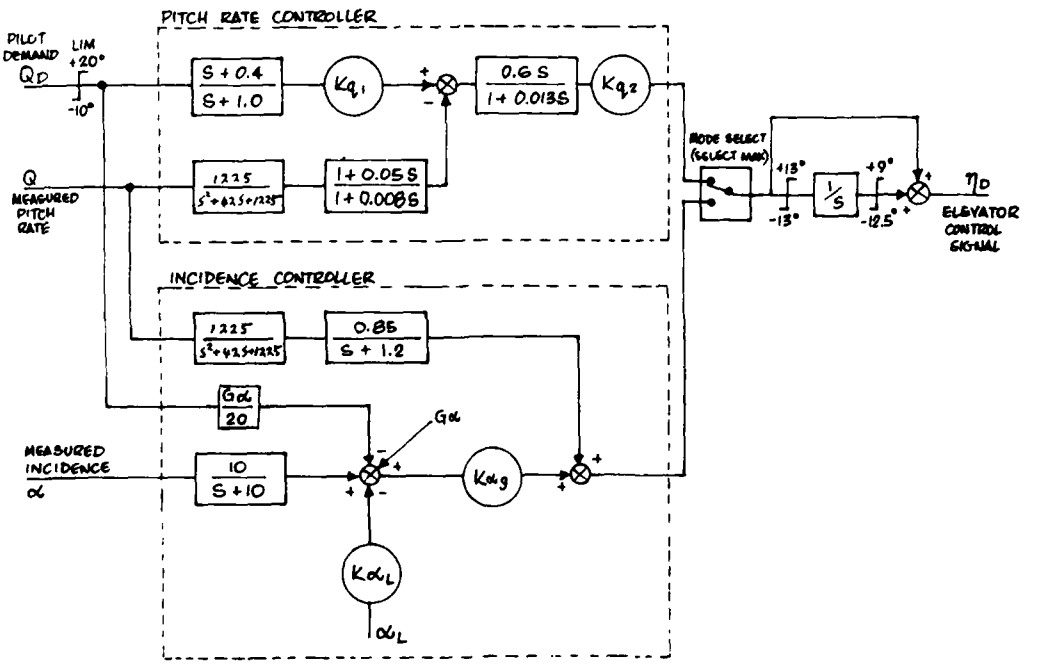

FIG. 1 PITCH RATE CONTROL LAW WITH INCIDENCE LIMITING

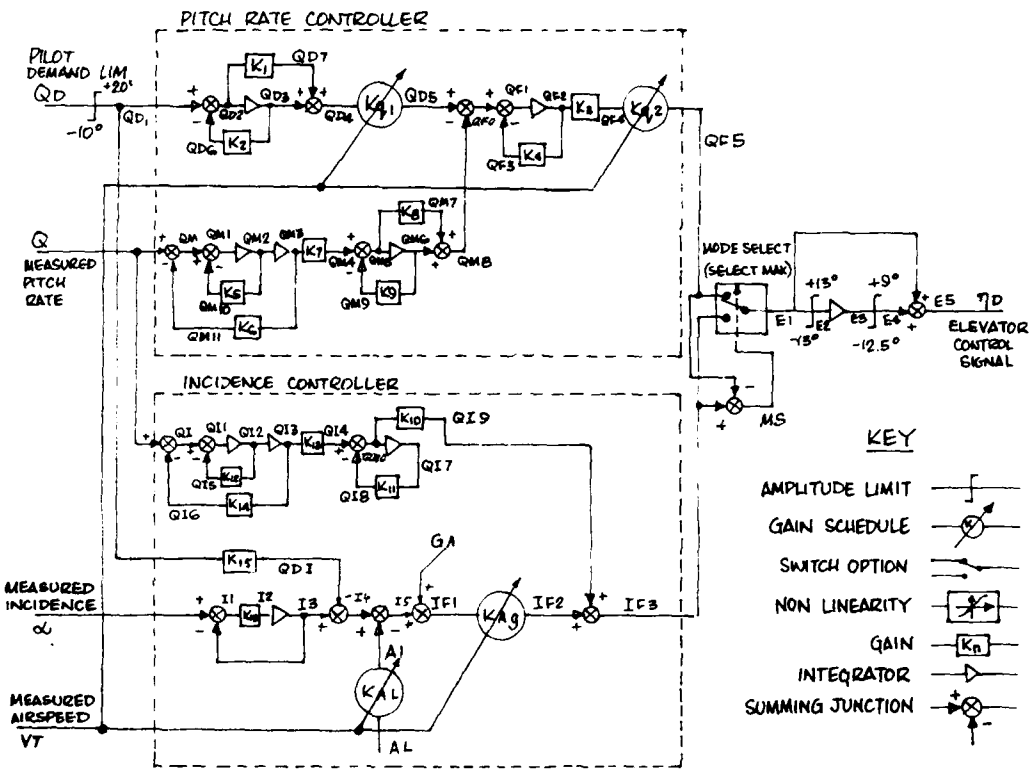

FIG. 2 PITCH RATE CONTROL LAW WITH INCIDENCE LIMITING (PSEUDO ANALOGUE REPRESENTATION)

```
LIM QD, QD1, +20, -10
SUB QD1, QD6, QD2
INTEG QD2, QD3
MUL QD2, K1, QD7
MUL QD3, K2, QD6
ADD QD7, QD3, QD4
LOOKUP KQ1, V, TABLE 1
MUL QD4, KQ1, QD5
SUB Q, QM11, QM
SUB QM, QM10, QM1
INTEG QM1, QM2
INTEG QM2, QM3
MUL QM2, K5, QM10
MUL QM3, K6, QM11
MUL QM3, K7, QM4
SUB QM4, QM9, QM5
INTEG QM5, QM6
MUL QM5, K8, QM7
MUL QM6, K9, QM9
ADD QM7, QM6, QM8
SUB Q, Q16, QI
SUB QI, Q15, Q11
INTEG Q11, QI2
INTEG QI2, QI3
MUL Q12, KI3, QI5
MUL QI3, KI4, QI6
MUL QI3, KI3, QI4
SUB QI4, QI8, QI10
INTEG QI10, QI7
MUL QI7, QI8
MUL QI10, K10, QI9
MUL QD1, K16, QD1
SUB I, I3, I1
MUL I1, K15, I2
INTEG I2, I3
SUB I3, QD1, I4
LOOKUP KAL, VT, TABLE 3
MUL AL, KAL, AI
SUB I4, AI, I5
ADD GA, I5, IF1
LOOKUP KAG, VT, TABLE 4
MUL IF1, KAG, IF2
ADD IF2, QI9, IF3
SUB QD5, QM8, QF0
SUB QF0, QF3, QF1
INTEG QF1, QF2
MUL QF2, K4, QF3
MUL QF2, K3, QF4
LOOKUP KQ2, VT, TABLE 2
MUL QF4, KQ2, QF5
LD E1, QF5, UNCONDITIONAL
SUB QF5, IF3, MS
LD E1, IF3, MS
LIM E1, E2, +13, -13
INTEG E2, E3
LIM E3, E4, +9, -12.5
ADD E4, E1, E5
```

Pitch input filter
Pitch input gain Schedule
Pitch rate noise filter (Q)
Pitch feedback compensation
Pitch rate noise filter (I)
Pitch rate wash out
Incidence control input gain
Incidence noise filter
Incidence scheduling and feedback summing junction
Pitch feedback summing junction
Pitch forward loop compensation
Pitch loop gain schedule
Mode select
Proport, lus integral term

NB: This excludes the listing of constants, lookup tables, and the hex code all of which would appear in a full assembler file.

FIG.3 IDEALISED ASSEMBLER LISTING FOR FIG.2

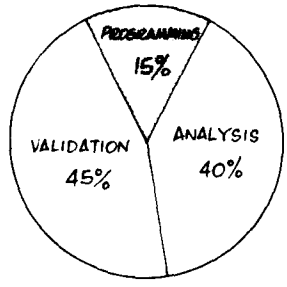

TOTAL COST OF GENERATING A PROGRAM

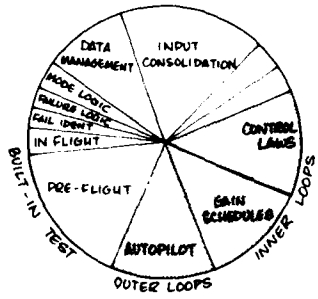

BREAKDOWN OF PROGRAM TASKS

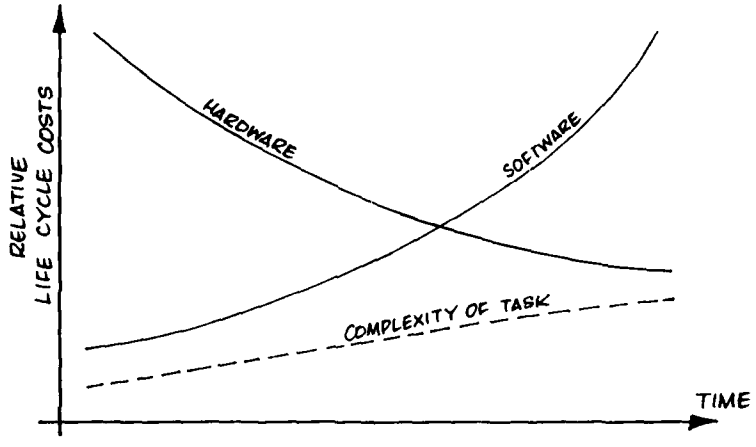

FIG. 4 SOFTWARE COSTS IN PERSPECTIVE

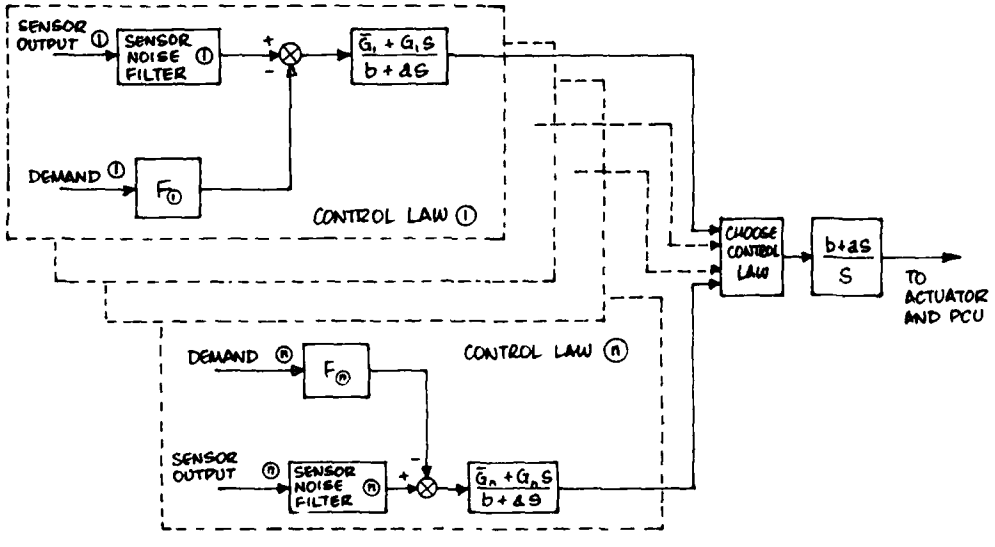

FIG. 5 BLOCK SCHEMATIC ILLUSTRATING GENERAL STRUCTURE OF NON LINEAR FLIGHT CONTROL LAWS INVOLVING SWITCHING BETWEEN DIFFERENT ERROR SIGNALS

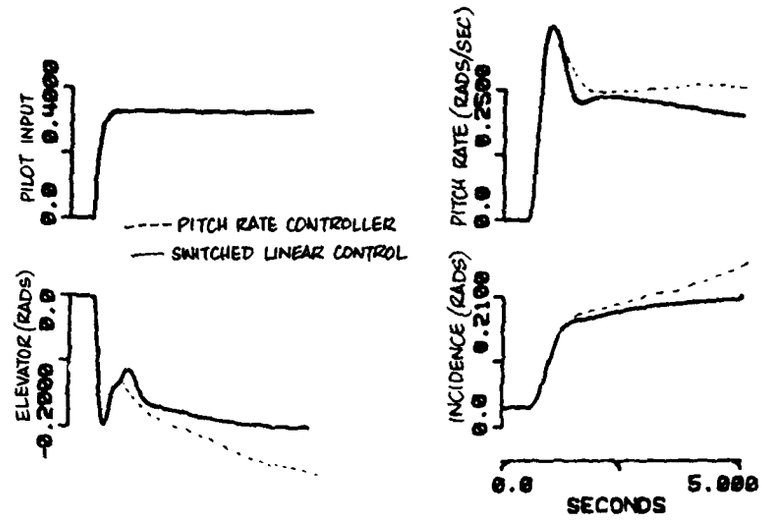

FIG. 6 TRANSIENT RESPONSE OF THE CONTROL SYSTEM SHOWN IN FIG. 1

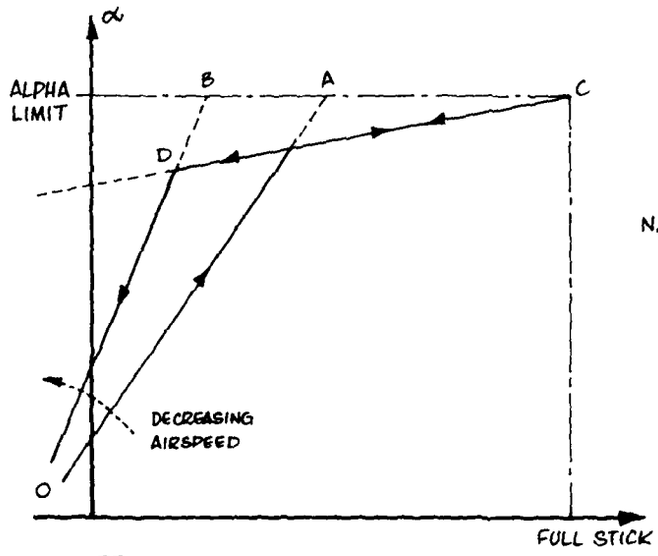

N.B. THE ARROWS DENOTE THE APPROXIMATE STICK/α LOCUS TRACED DURING A SHORT DURATION FULL STICK DEMAND AND RETURN TO STICK CENTRE

$\overline{OA}$, $\overline{OB}$ } Q CONTROLLER LINES

$\overline{CD}$ α CONTROLLER LINE

FIG. 7 STICK/α CHARACTERISTICS OF LONGITUDINAL CONTROL SYSTEM (DEFINED IN FIG. 1)

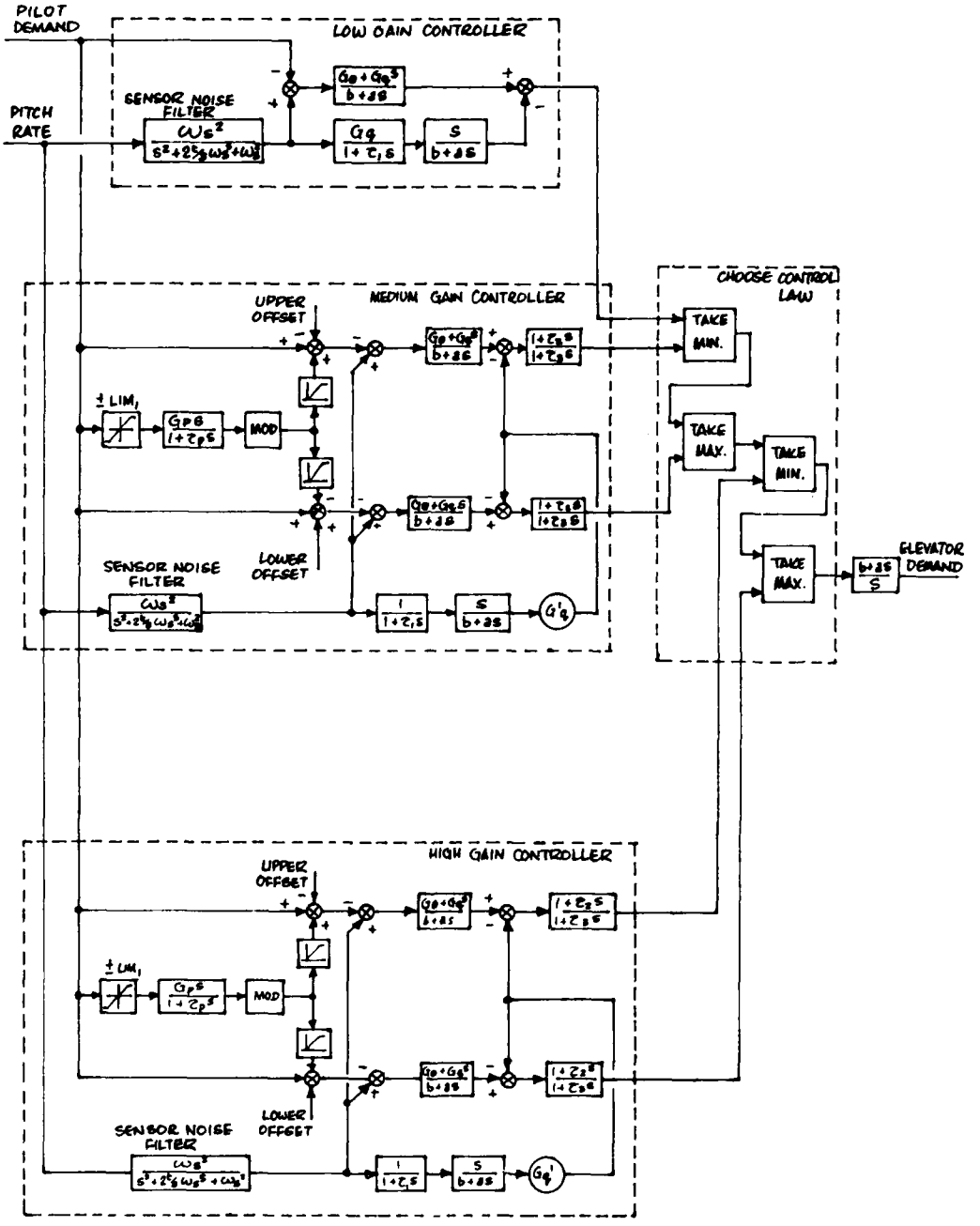

FIG. 8 BLOCK SCHEMATIC OF NON LINEAR PITCH RATE MANOEUVRE DEMAND SYSTEM

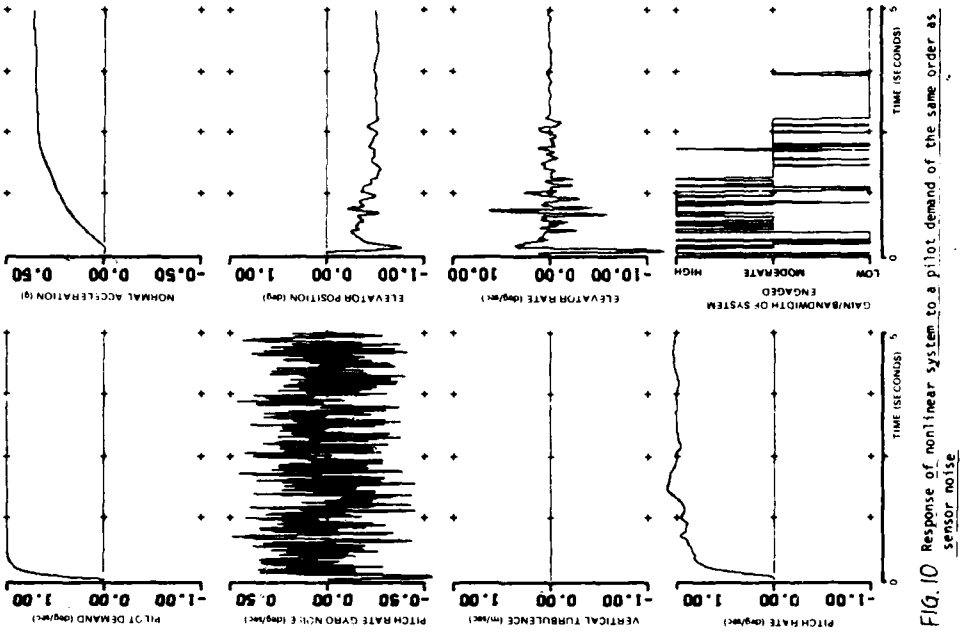

FIG. 10 Response of nonlinear system to a pilot demand of the same order as sensor noise

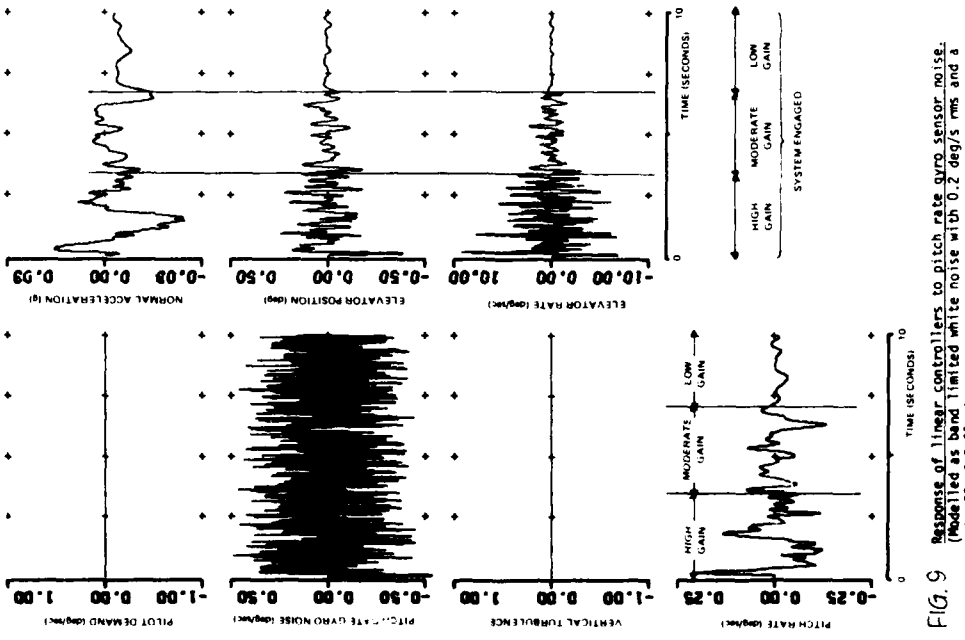

FIG. 9 Response of linear controllers to pitch rate gyro sensor noise. (Modelled as band limited white noise with 0.2 deg/s rms and a cut off of 0.01 s)

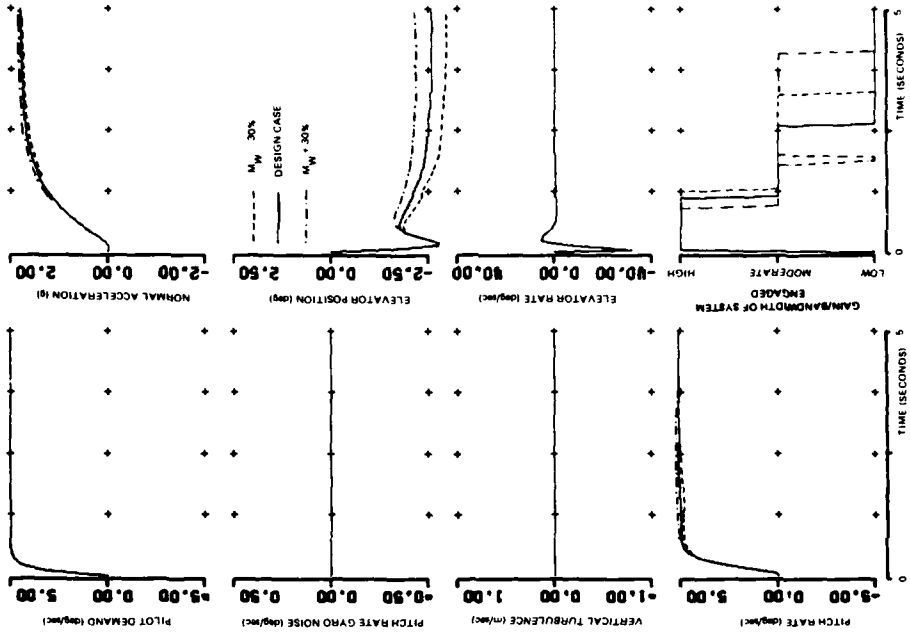

FIG. 12 Variation in response characteristics of nonlinear system for ±30% variation in static margin (M_w)

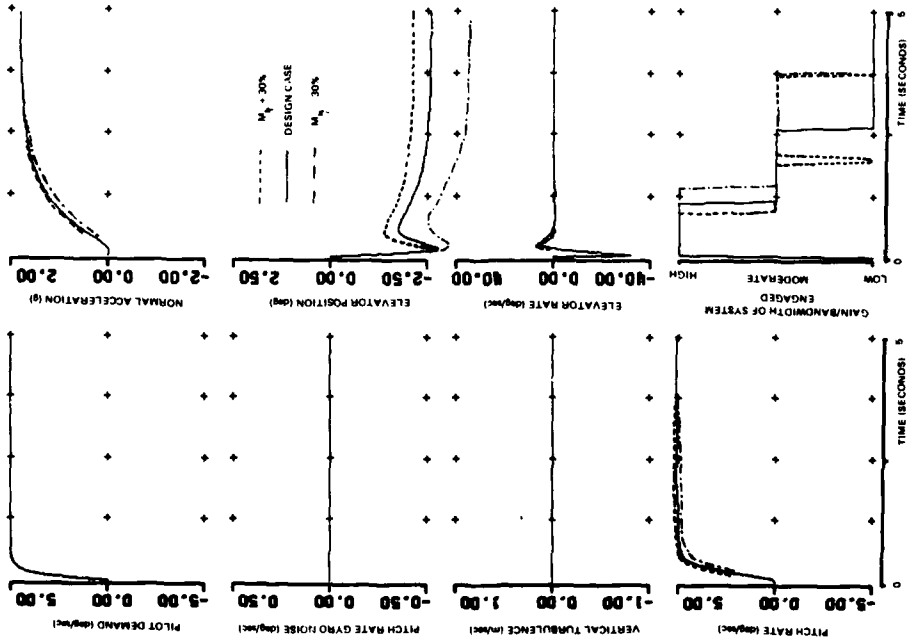

FIG. 11 Variation in response characteristics of nonlinear system for ±30% variation in elevator effectiveness (M_{δ_e})

FLIGHT CONTROL SYSTEM DESIGN USING ROBUST OUTPUT OBSERVERS

E. G. Rynaski
Staff Engineer
Arvin/Calspan Advanced Technology Center
Buffalo, New York 14225

Summary

An investigation was made of the application of robust output observer theory to the design of flight control systems for advanced aircraft configurations. Observer theory constitutes a natural design tool because the resulting observers are in themselves unobservable and do not increase the order of the closed-loop response, thereby more closely satisfying flying qualities requirements. Examples are presented to show that the observer configuration is not unique in either the observer poles or the output sensors, and many different control system configurations using a variety of sensors can be designed to yield identical closed-loop dynamic behavior. In this way, considerable analytic and physical redundancy can be incorporated into nearly any flight control system.

Introduction

Advanced control concepts for aircraft almost always involve new ways of generating forces and moments on the vehicle, thereby implying a potential for enhanced maneuverability and precision of flight with augmented performance through weight and drag reduction. Conventional control system design theory is not really adequate for multicontroller flight control system design so the tendency is towards the use of the more modern control theories, such as optimal control, that can conceptually generate acceptable designs quickly and efficiently.

The systems that result from the application of modern control theory are generally complex, requiring feedback from each of the states to all of the controllers. In an attempt to avoid or sidestep the requirement that all states be measured, state estimator or observer systems have been devised in an attempt to reduce the number of required sensors or to improve the accuracy of the state measurements. This has led to a totally new crop of problems, including reduced robustness through reduction of gain and phase margins as compared to state feedback systems, inability to guarantee stability and a closed-loop system characterized by response delays and lags that almost always degrade the flying qualities of the vehicle itself.

This paper describes the theory and presents applications of robust output observers. The motivation for this research stems from a desire to reduce the number of sensors required to implement a multivariable system control law without reducing the robustness of the system as compared to state feedback, It is based upon the accurate premise that most sensors used in flight control system design, such as rate and attitude gyros, linear accelerometers and even angle of attack sensors are essentially noise-free in themselves.

Critical to the design of an observer system is the selection of the observer poles. As shown below, proper selection of these poles can lead to the achievement of a number of desirable control system properties, including:

- Synthesis of the optimal system with fewer sensors than states.
- Preservation of the robustness of the system as defined by state feedback.
- Elimination of the higher order response lags that degrade flying qualities associated with most estimator systems.
- Elimination, in many cases, of the need to measure the inputs or control surface deflections of the vehicle.
- Enhancement of system observability as measured by decreased feedback gains required to achieve a particular closed-loop dynamic response.

Observer Theory

The original observer theory by Luenberger[1] was developed as a state reconstruction technique, in which the output of the observer system approached, as time increased, the state that is to be reconstructed. The theory developed by Luenberger described deterministic observers which are in themselves unobservable and do not contribute to an increase in the order of the response of the system. In general, the poles of the observer can be chosen arbitrarily, but this choice generally results in a requirement that the control input to the aircraft also is a control input to the observer system. A recognition of the interactions involved in observer design can result in considerable observer design simplifications. This paper explores and defines some of the freedom allowed the designer in deterministic observer choices that can result in simplified systems that still meet the objectives of the flight control system.

Consider the linearized, small perturbation equations of vehicle motion

$$\dot{x} = Fx + Gu \qquad (1)$$
$$y = Hx$$

where x is the state vector, u the control input vector and y the output vector, the measurement set such as a pitch rate gyro and accelerometer sensor. The observer is of the form

$$\dot{z} = Az + By + Du$$

subject to the conditions:

1. The matrix A is chosen such that the observer is stable.

2. A transformation T can be found such that $TF-AT = BH$.

3. $TG = D$

where F, G and H are defined above.

A robust output observer must satisfy, in addition to the above conditions:

4. The observer poles, defined from $|Is-A| = 0$ are chosen from the transmission zeros of the system, defined by $|H(Is-F)^{-1}G| = 0$, i.e. when the number of sensors equals the number of controllers.

5. $TG = D = 0$.

6. The matrices H and T constitute a transformation M

$$\begin{bmatrix} y \\ z \end{bmatrix} = Mx \tag{3}$$

such that the equivalent output and observer control law is given by

$$u = -Kx = -KM^{-1}\begin{bmatrix} y \\ z \end{bmatrix} \tag{4}$$

The condition that $TG = D = 0$ is automatically satisfied if the observer poles are chosen from among the system transmission zeros. Not only does this simplify the observer network but also reduces the number of required measurements of the vehicle dynamics.

Example 1

Observers can often be used to enhance the observability of the system in the sense that much lower feedback gains are often required to obtain the same closed-loop dynamic behavior as compared to state feedback. This comes about because the feedback through the observers is shaped as a function of frequency and this can often be used to the advantage of the designer. Consider the system

$$\begin{bmatrix} \dot{x}_1 \\ \dot{x}_2 \\ \dot{x}_3 \end{bmatrix} = \begin{bmatrix} 0 & 2 & -1 \\ 1 & 6 & -12 \\ 1 & 6 & -11 \end{bmatrix}\begin{bmatrix} x_1 \\ x_2 \\ x_3 \end{bmatrix} + \begin{bmatrix} 1 \\ 0 \\ 0 \end{bmatrix} u \tag{5}$$

with a single measurement $y = x_1 - 2x_2 + 3x_3$.

If it is assumed that it is for some reason desirable to alter the open-loop characteristic polynomial $D(s) = |Is-F| = s^3 + 5s^2 + 5s + 2$ to a closed-loop characteristic polynomial $\Delta(s) = |Is-F+GK| = s^3 + 5s^2 + 6s + 7$, then the state feedback control law is given by

$$u = 5x_2 - 6x_3 \tag{6}$$

According to condition (4), the poles of the observers can be chosen from among the system transmission zeros which, for this example, are the zeros of the transfer function

$$y/u(s) = \frac{s^2+6s+8}{s^3+5s^2+5s+2} = \frac{(s+2)(s+4)}{s^3+5s^2+5s+2} \tag{7}$$

This output transfer function represents a minimum phase, completely observable measurement so two output observers can be constructed with observer poles equal to the zeros of the output transfer function; i.e. $s_1 = -2$, $s_2 = -4$. The observers can then be chosen automatically as

$$\begin{aligned} \dot{z}_1 &= -4z_1 + y \\ \dot{z}_2 &= -2z_1 + y \end{aligned} \tag{8}$$

The matrix M of condition (6) listed above and the control law is most easily obtained by first transforming into the phase variable form

$$\begin{aligned} \dot{w} &= F_O w + G_O u \\ x &= Nw \end{aligned} \tag{9}$$

where

$$F_O = \begin{bmatrix} 0 & 1 & 0 \\ 0 & 0 & 1 \\ -2 & -5 & -5 \end{bmatrix} \quad G_O = \begin{bmatrix} 0 \\ 0 \\ 1 \end{bmatrix} \quad N = \begin{bmatrix} 6 & 5 & 1 \\ -1 & 1 & 0 \\ 0 & 1 & 0 \end{bmatrix}$$

The transformation $\begin{bmatrix} y \\ z \end{bmatrix} = Mx$ can then be determined as follows[2]:

a) The elements of the first row of the matrix M are made up of the coefficients of the numerator polynomial of the output transfer function, i.e.

$$m_1 = [8 \quad 6 \quad 1]$$

b) The second row of the matrix is made up from the coefficients that result when $s+4$ has been factored out of the numerator polynomial of the output transfer function, i.e.

$$m_2(s) = \frac{s^2+6s+8}{s+4} = s+2$$

so

$$m_2 = [2 \quad 1 \quad 0]$$

c) Similarly, the third row is formed from the coefficients that result when the factor $s+2$ has been factored out of the numerator polynomial

$$m_3(s) = \frac{s^2+6s+8}{s+2} = s+4$$

so

$$m_3 = [4 \quad 1 \quad 0]$$

This process is exactly the same as defining the matrix T in the equation

$$TF - AT = BH$$

when F and H are defined in the phase variable form.

The observer control law is then given by

$$u = -KM^{-1}\begin{bmatrix} y \\ z \end{bmatrix} = \frac{1}{2} z_1 - \frac{3}{2} z_2 \tag{11}$$

and the closed-loop system is shown in Figure 1. The system shown in Figure 1 has the same robustness or gain and phase margins as the state feedback system, but the system employing observers uses only one output or sensor, the feedback gains are much lower and the observers constitute low pass filters, useful for structural mode stabilization or noise suppression.

Multivariable System

In the previous section, it was shown that if the observer poles were chosen from among the zeros of the transfer functions, no plant input measurements were required in the observer synthesis for systems that were completely observable. For multi-controller systems, exactly the same principle holds except that the observer poles are chosen from the transmission zeros of the system defined as the roots of the polynomials

$$|H(Is-F)^{-1}G| = 0 \tag{12}$$

when the system is defined by the standard equations of motion

$$\dot{x}(t) = Fx(t) + Gu(t)$$
$$y(t) = Hx(t)$$

As indicated by Equation (12), the transmission zeros are a function of the sensors or outputs as well as the controller inputs. In general, a robust output observer can be obtained if the system is completely controllable and observable with the chosen sensors and if the number of non-minimum phase transmission zeros is equal to $n-m$, where m is the number of sensors used. For an nth order system with m independent output measurements and p independent inputs, the maximum number of transmission zeros is given by

$$N = (n-p)\frac{m!}{(m-p)!\,p!} \tag{13}$$

Ordinarily, the number of transmission zeros exceeds the number of observers to be constructed so there is design freedom, as shown by the following example.

Consider the 4th order system given by

$$\begin{bmatrix} \dot{x}_1 \\ \dot{x}_2 \\ \dot{x}_3 \\ \dot{x}_4 \end{bmatrix} = \begin{bmatrix} -1 & 0 & 1 & 0 \\ 0 & -2 & 0 & 1 \\ 1 & 0 & -2 & 0 \\ 0 & 1 & 0 & -4 \end{bmatrix} \begin{bmatrix} x_1 \\ x_2 \\ x_3 \\ x_4 \end{bmatrix} + \begin{bmatrix} 1 & 1 \\ 0 & -1 \\ -1 & 0 \\ 0 & 1 \end{bmatrix} \begin{bmatrix} u_1 \\ u_2 \end{bmatrix}$$

$$\begin{bmatrix} y_1 \\ y_2 \\ y_3 \end{bmatrix} = \begin{bmatrix} 1 & 0 & -1 & 0 \\ 1 & 1 & 0 & 1 \\ 0 & 1 & 0 & 1 \end{bmatrix} \begin{bmatrix} x_1 \\ x_2 \\ x_3 \\ x_4 \end{bmatrix} \tag{14}$$

According to Equation (13), the maximum number of transmission zeros of this system is

$$N = (n-p)\left[\frac{m!}{(m-p)!\ p!}\right] = (4-2)\left[\frac{3!}{1!\ 2!}\right] = 6 \tag{15}$$

A maximum of two of a possible six transmission zeros must be minimum phase in order to be able to construct a stable output observer system. There are three sets of transmission zeros that can be used in the selection of the output observer poles. These three sets involve the outputs $(y_1 y_2)$, $(y_1 y_3)$ and $(y_2 y_3)$ and produce the transmission zeros

$$\begin{aligned} (y_1\ y_2) \quad & -s^3 - 7s^2 - 20s - 21 = -(s+2.45)(s+4.215) \\ (y_1\ y_3) \quad & 3s^2 - 3s + 6 = 3\left(s - \frac{1}{2} \pm \frac{j}{2}\sqrt{7}\right) \\ (y_2\ y_3) \quad & 2s + 6 = 2(s+3) \end{aligned} \tag{16}$$

The system possesses five of a possible six transmission zeros and three are non-minimum phase. Any two can be chosen for the system design. The obvious choice is to design an output observer using the two measurements y_1 and y_2. The third measurement y_3 is not required. In fact, an observer set for the measurement pair $y_1 y_2$ is given by

$$\begin{bmatrix} \dot{z}_1 \\ \dot{z}_2 \end{bmatrix} = \begin{bmatrix} -2.45 & \\ & -4.215 \end{bmatrix} \begin{bmatrix} z_1 \\ z_2 \end{bmatrix} + \begin{bmatrix} -1.8 & 1.45 \\ 1.215 & -0.45 \end{bmatrix} \begin{bmatrix} y_1 \\ y_2 \end{bmatrix} \tag{17}$$

Figure 2 shows the observer system that can be used in feedback control to produce a control law equivalent in every sense to a state feedback control law. Two simple filters serve the same purpose as additional sensors. If the feedback control system had been designed originally with three sensors and sensor #3 failed, a reversion to the observer system shown in Figure 2 would yield exactly the same closed-loop dynamic response. Therefore, the use of output observers, even if not used to mechanize the system originally, produces a method of obtaining analytic redundancy with no loss in performance or dynamic behavior.

Flight Control Application

The fundamental purpose of a flight control system is to enhance the flying qualities of the vehicle. Flying qualities in turn state that an increase in the order of the response of the system will amost always degrade the flying qualities of the vehicle. This means that prefilters, compensation networks and the like are inadmissible unless the inclusion of these dynamic elements does not increase the order of the response of the system. However, because dynamic elements are an integral part of closed-loop system design technology, they must be chosen as observers to satisfy stringent flying qualities requirements. As it turns out and as shown by the flight control system designs below, the requirement that the filters be observers is not much of a disadvantage and, in fact, can simplify the design procedure considerably. The examples below show several different observer configurations, all of which produce the same closed-loop dynamic behavior and satisfy flying qualities requirements without increasing the order of the system response.

The example aircraft is a linearized approximation to the AFTI-16 on landing approach with V = 139 knots. The objective will be to design feedback configurations using both an angle of attack sensor and a rate gyro, a rate gyro alone and an angle of attack sensor alone. Because all the control system configurations yield the same closed-loop dynamics, they constitute a level of redundancy that can allow for a failure of either sensor without change in the dynamic behavior of the vehicle.

The small perturbation longitudinal-vertical equations of motion are given by

$$\begin{bmatrix} \dot{q} \\ \dot{V} \\ \dot{\alpha} \\ \dot{\theta} \end{bmatrix} = \begin{bmatrix} -0.4932 & 0.000129 & 1.4168 & 0.0 \\ 0.0 & -0.0507 & -3.861 & -32.17 \\ 1.000 & -0.00117 & -0.5164 & 0.0 \\ 1.000 & 0.0 & 0.00 & 0.0 \end{bmatrix} \begin{bmatrix} q \\ \Delta V \\ \Delta\alpha \\ \Delta\theta \end{bmatrix} + \begin{bmatrix} -1.648 \\ 0 \\ -0.0717 \\ 0 \end{bmatrix} \begin{bmatrix} \delta_e \end{bmatrix} \tag{18}$$

with transfer functions

$$\frac{\dot{\theta}}{\delta_e}(s) = \frac{-1.644s^3-1.032s^2-.0407s}{D(s)} = \frac{-1.644s(s+.587)(s+.0422)}{D(s)}$$

$$\frac{\alpha}{\delta_e}(s) = \frac{-0.0717s^3-1.683s^2-.0852s-.0622}{D(s)} = \frac{-.0717(s+23.44)(s^2+.0471s+.037)}{D(s)} \tag{19}$$

and $$D(s) = (s+0.724)(s-1.705)[s^2+.38(.204)s+.204^2]$$

The aircraft is typical of a statically unstable aircraft with a left half and right half plane roots and a stable "3rd mode." Satisfactory and acceptable flying qualities for this aircraft would result if the airplane were augmented to produce the following short period and phugoid mode characteristics:

$$\omega_{sp} = 2.5 \text{ rad/sec} \quad \zeta_{sp} = 0.5$$
$$\omega_{ph} = 0.1 \text{ rad/sec} \quad \zeta_{ph} = 0.1$$

which defines the desired closed-loop characteristic polynomial of the closed-loop response.

$$\Delta(s) = s^4+2.52s^3+6.31s^2+0.150s+0.0625 \tag{20}$$

Figure 3 shows the response of the augmented or closed-loop aircraft to a step command pilot input. As specified by the flying qualities requirements, the short term response in angle of attack is primarily defined by the short period mode characteristics of the augmented aircraft, allowing for precision control of the flight path, which is the primary control task during the landing phase of flight. The responses of Figure 3 define the response of all of the observer configurations, for the residue of the responses of all the observer modes are zero and do not add to the output response of the vehicle.

Observer Designs

As defined by Equation (9), the feedback control law in the phase variable form is found simply by the difference of the coefficients of the powers of the Laplace transform variable s of the closed-loop and open-loop characteristic polynomials. In this form the control law is simply

$$\begin{aligned}\delta_e &= -(\Delta-D)\omega \\ &= -[.0625+.0512, .150+.0365, .631+1.216, 2.52-1.06]\omega \\ &= [\ 0.1137 \quad .2065 \quad 1.747 \quad 1.46]\omega\end{aligned} \tag{21}$$

The problem then simply becomes one of defining transformation $x = T\omega$ that will yield control laws that can be mechanized. As shown by Equation (10), the transformations are obtained from the numerator polynomials of the α/δ_e and $\dot{\theta}/\delta_e$ transfer functions. Using measurements of angle of attack and pitch rate and the pitch rate numerator polynomial root at $s = -0.587$ as one observer and the angle of attack numerator factor $(s^2+.0471s+.037)$ as the second observer, the resulting transformation is

$$M_1 = \begin{bmatrix} -0.0622 & -.0852 & -1.683 & -0.0717 \\ 0 & -0.0407 & -1.032 & -1.644 \\ 0 & -0.0694 & -1.644 & 0 \\ -1.6906 & -0.0717 & 0 & 0 \end{bmatrix} \tag{22}$$

which yields the feedback control law

$$\delta_e(s) = -(\Delta-D)M^{-1}\begin{bmatrix} y(s) \\ z(s) \end{bmatrix} \tag{23}$$

$$= 0.268\alpha(s)-1.60\dot{\theta}(s)-10.02\frac{\dot{\theta}(s)}{s+0.587} - 0.3[illegible]\frac{\alpha(s)}{s^2+.04[illegible]s+.037} \tag{24}$$

and the system is shown in the block diagram of Figure 4.

Because the pitch rate transfer function is minimum phase, a control law can be obtained using only a pitch rate sensor and each of the three numerator polynomial roots as observers. The resulting feedback control law is given by

$$\delta_e(s) = -1.5210-2.75\frac{\dot{\theta}}{s}(s) -.904\frac{\dot{\theta}(s)}{s+0.587} + \frac{1.650\dot{\theta}(s)}{(s+.587)(s+.0422)}$$

and the resulting system is shown in Figure 5.

The integrator in the control loop is required to obtain complete observability of the system, but a measurement of the control input can serve just as well, as shown by the configuration of Figure 6.

Angle of attack can be used instead of the rate gyro to produce a feedback control law yielding the same flying qualities. The observers selected in this case are centered around the factor $s^2+.[illegible]s+.[illegible]$ of the $\alpha/\delta_e(s)$ transfer function. The resulting system has the control law

$$\delta_e(s) = -2.[illegible]\,\alpha(s) - \frac{4.35\,\alpha(s)}{s^2+.[illegible]s+.[illegible]} + \frac{[illegible]}{s^2+.[illegible]s+.[illegible]} + \frac{[illegible]}{s+.[illegible]}\left[\alpha(s)+\delta_e(s)\right]$$

$$\delta_e(s) = -2.[illegible]\,\alpha(s) + \frac{[illegible]}{s^2+.[illegible]s+.[illegible]}\,\alpha(s) + \frac{[illegible]}{s+.[illegible]}\left[\delta_e(s)+\alpha(s)\right] \tag{26}$$

The configuration is shown in the block diagram of Figure 7a.

With the exception of the direct angle of attack path, the observers generally constitute low pass filters in the feedback path. This would be important for an angle of attack feedback configuration, as shown in Figure 7a, to not increase the gust sensitivity of the aircraft if the angle of attack is obtained from an air data measurement.

Because the block diagram of the observers can be manipulated at will, the block diagrams shown in the figures would not necessarily represent a final flight control system configuration. However, it would occasionally be difficult to change the mechanization by incorporating some of the dynamic elements in the feedforward rather than the feedback path. As shown in Figure 7b, mathematically equivalent to 7a, the mechanization would require an unstable feedforward loop, and is, therefore, unrealizable.

Control Law Approximations

The control computation shown in Equation (23) requires the inverse of the transformation matrix M. Each row of the matrix is associated with the output of a sensor or observer and if, for some reason, the feedback path is lost, a new control law can be instantly calculated that would result in a best approximation. For instance, in Figure 4, assume the feedback path represented by the observer output $\frac{[illegible]}{s^2+.[illegible]s+.[illegible]}$ was lost. The best approaximation would then be obtained by the control law

$$\delta_e = -(I-D)(M_{11}^T M_{11})^{-1} M_{11}^T \begin{bmatrix} [illegible] \\ z \end{bmatrix} \tag{27}$$

where the superscript T represents the matrix transpose and M_{11} is M_1 of Equation (21) but with the 4th row of the matrix deleted

$$M_{11} = \begin{bmatrix} -.0622 & -.0852 & -1.683 & -0.0717 \\ 0 & -0.0407 & -1.032 & -1.644 \\ 0 & -.0694 & -1.044 & 0 \end{bmatrix}$$

The resulting control law becomes

$$\delta_e(s) = -.[illegible]\,\alpha(s) - [illegible]\,\dot{\theta}(s) - \frac{[illegible]}{s+0.[illegible]} \tag{28}$$

which yields the closed-loop response characteristic polynomial

$$\Delta(s) = (s+.044)(s+2.72)\left[s^2+2(.25)(.778)s + .[illegible]^2\right]$$

Stability is preserved but the flying qualities have deteriorated considerably, with a dominant mode damping ratio of $\zeta = .25$ and natural frequency $\omega = .78$ rad/sec. A conclusion is that it would be better to switch to an alternate observer network if an observer path is lost.

Concluding Remarks

Output observers have the significant advantage in control system synthesis of yielding feedback control system designs using fewer sensors than states without increasing the order of the response of the system to a command input. The observers in themselves are unobservable. Using the methods outlined in this paper, the observer theory can be very effectively used to quickly obtain feedback control system configurations using a variety of sensors that satisfy the same flying qualities requirements. Because all the configurations yield the same closed-loop dynamics, they constitute a collection of analytically

and physically redundant control laws.

References

1. Luenberger, D. G.: "Observers for Multivariable Systems," IEEE Transactions on Automatic Control, Vol. AC-11, April 1966.

2. Rynaski, E. G., Whitbeck, R. F. and Wierwille, W. W.: "Optimal Control of a Flexible Launch Vehicle," Calspan Report No. IH-2089-F-1, July 1966.

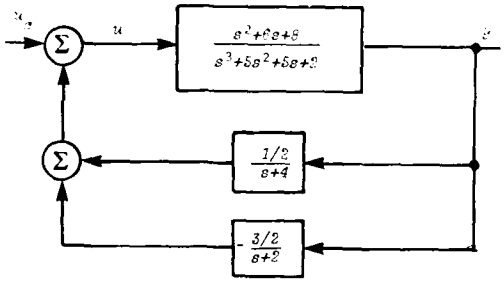

Fig. 1 Observer Control System

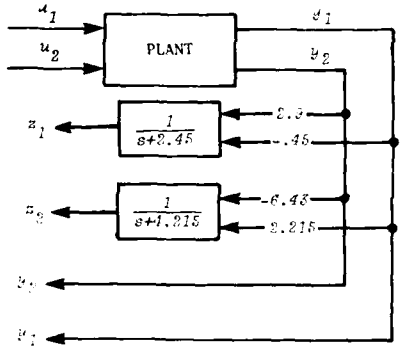

Fig. 2 Multivariable Observer

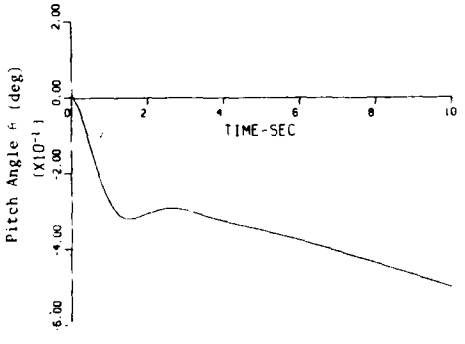

Fig. 3a Pitch Attitude Response to Step Command

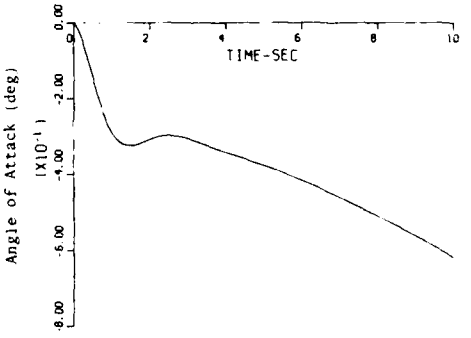

Fig. 3b Angle of Attack Response to Step Command

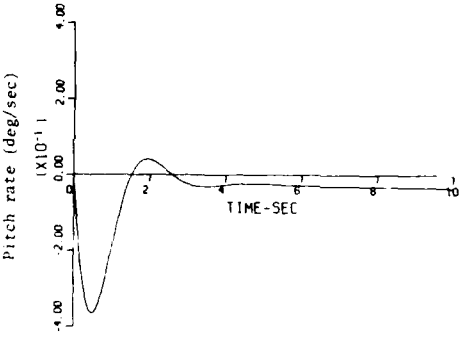

Fig. 3c Pitch Rate Response to Step Command

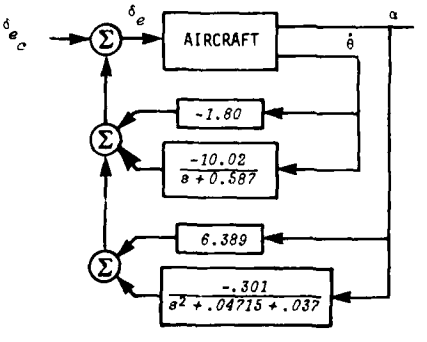

Fig. 4 Observer System Using Pitch Rate and Angle of Attack Measurements

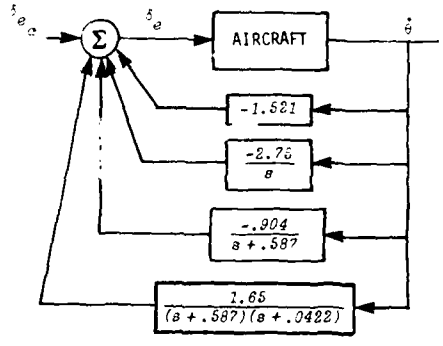

Fig. 5 Feedback Control Using Only Pitch Rate Gyro

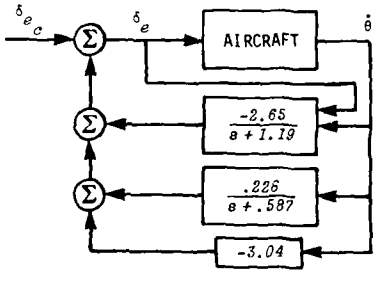

Fig. 6 Alternate Pitch Rate System

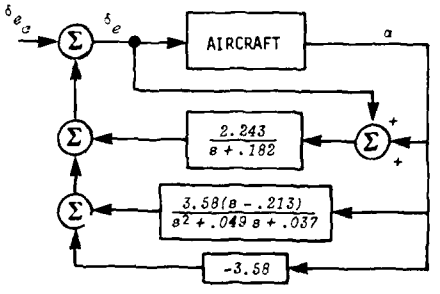

Fig. 7a Feedback Control Using Angle of Attack Sensor

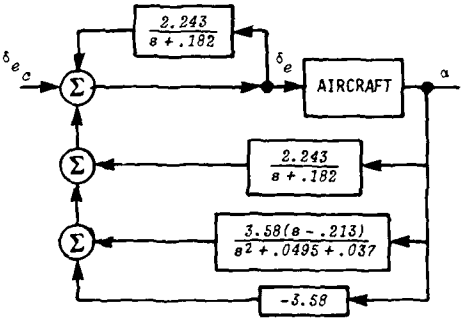

Fig. 7b Unrealizable Mechanization of Angle of Attack System

ON VALIDATION OF MISSION-SOFTWARE BY CLOSED-LOOP TESTING IN REALTIME

by
Hermann Neubauer
MBB GmbH
Dynamics Division, D 8000 München 80

SUMMARY

This contribution is intended to provide both some basic considerations on validation techniques for simulations and their application to a real-time digital computer simulation with hardware-in-the-loop (HWIL).

1. GENERAL REMARKS ON VALIDATION

1.1 The Problem of Validation

Validation in general refers to the assessment of the quality of match of the computational results of simulation models with

- actual data from similar real systems
- independent theoretical data

and the assessment of the correspondence with the

- hypotheses and assumptions of the conceptual model.

1.2 HWIL-Simulations

The purpose of HWIL-simulations is the improvement of the simulation performance level comparable with that expected from the hardware and the validation of the operational software and hardware at system level. This can be accomplished by

- using (open-loop) hardware test results to update and validate the subsystem models
- substitution of (flight-) hardware for subsystem models.

Especially the lack of experimental data from not yet existing systems requires the substitution of available subsystem hardware for subsystem models to gain confidence that the model adequately represents the overall system.

1.3 Overview of Validation-Techniques

Quantitative measurement of coincidence: (objective techniques)

- Point fit tests: Measurement of point by point coincidence
  (Theil's coefficent, regression analysis, etc.)
- Comparison of aggregated measures:
  Agreement of means, variances
  (Analysis of variance schemes)
- Test of properties of time-series:
  Examination of shape of amplitude-distributions, spectral-densities, cross-spectral analysis

Qualitative analysis: (subjective techniques)

This form of testing is important, when the model is used to investigate a system, for which exists a lack of data for use in validation. It is based on:

- Pattern recognition of human eye:
  (comparison of time structure, amplitude fluctuation between sets of output)
- Expert critic due to a priori knowledge about the system or empirical evidence:
  recognition of discrepancies between model output and underlying hypotheses.

To ground this "common sense" validation, it is necessary to point out the major difficulties in selecting appropriate quantitative techniques:

- No appropriate data available for following reasons:

  Historical or theoretical data are not available for comparison in the case of validating non-existing systems.

  The available data are not appropriate for use in validation.
  (Data have no significance with respect to the objective of the modelling exercise or have low accuracy)

  Data have been used in model development.

- Formal techniques are difficult to apply and costly:

  They prove less insight than direct examination (The structure in time is destroyed).

  They require a large number of observations (Sufficient samples for use of spectral techniques).

  Assumptions are necessary for statistical tests (Normality, common variance, stationarity).

  The problem of setting a level for deciding, when model and system output are close enough for the purpose, for which the model is intended requires particular insight, and it is difficult to pick out specific aspects of the output.

2. AN INDUCTIVE APPROACH TO QUALITATIVE VALIDATION PROCEDURES

Since the basic experiment for the validation described herein is justifying the model by interpretation of its output, the procedure is inductive and focuses on the question:

Does the simulation model's output agree within "acceptable errors" with

- empirical evidence
  (replication of "real world" observations from similar systems - retrospective method)
- the analyst's theory of the real system described in the theoretical definition of the model
  (the expert attempts to forecast the model behaviour - prospective method)

This approach requires the examination of three questions:

1. What are the main system output variables over a variety of test-cases, that check all relevant aspects of the simulation model?
2. How ought one compare the model output with "real world" results resp. assumptions about the system behaviour?
3. What coincidence criteria should be used to assess the coincidence?

2.1 Selection of Appropriate Output Variables

If dynamic data are available from

- a previous hardware experiment
- analytical solutions of a mathematical model
- a theoretical model in the case of substitution of hardware subsystems for their simulated counterparts

the emphasis is put on the generation of corresponding simulation data.

If no previous data are available, the emphasis is put on the generation of significant logical and physical variables, which record the past history or relevant properties and characteristics of the (sub-) system to be validated.

The following criteria are proposed for the selection:

- Variables which reflect static resp. dynamic properties of the system:

  Appropriate variables, to recognize initial status, transients (phaseshift properties and amplitude attenuation),

- Variables which reflect nonlinear properties of the system:

  Selected variables, to allow "handchecking" of wanted discontinuities (are amplitudes/ slopes inside specified limits?).

- Variables to monitor the logical flow of the system:

  Main control variables, to check the correct implementation of control-logic and system variables which are effected by the execution of the control logic for traceback.

- Variables which are effected by neglecting of dynamics, errors and relationships:
  To check, if the conceptual approximations are satisfied.

- Variables which reflect interconnections between subsystems:
  To recognize the amount of coupling and the propagation of disturbances.

- "Performance"-Variables:
  To determine, that the system meets the requirements established by the specifications.

2.2 Selection of Appropriate Test-Conditions

In a first step, the simulation model is tested under "soft" conditions.

The provided input should yield:

- a minimum of coupling between logically independent subsystems (excite only parts of the system, to allow isolation of errors)
- small deviations from a nominal state of the system to recognize principal errors in the relevant relationships and to determine principal characteristics of the model.

Processing to the following steps, the system should be tested under "harder" conditions (hereby the objective of the modelling exercise is emphasized) to check the relevant aspects of the simulation study:

- are the goals achieved?
- are the constraints being met?

A coverage of the specified performance is to be achieved.

2.3 Comparison Procedure

The comparison procedure consists of the match of selected test results with available data and a priori knowledge about the system.

Match with available data:

- Graphical testing of analog output (strip-charts) by use of overlays:

  The first step is to verify the "overall" correspondence of the curves in time-structure, amplitude-fluctuations, and frequency content.

  The next step is to pick out these aspects of the output considered to be important. The examination is centered on points (amplitude and timing) and closed time intervalls (rise-times, asymptotic bounds, mean values)

- "Read outs" from digital output

  This allows to check the exact matching of key variables at selected points and over closed intervals and the log of the magnitude of critical values.

- "Log" of control logic

  Monitoring of timing and sequencing of major events for comparison with flow-charts resp. decision-tables.

Match of a priori knowledge with selected test-results.

The model must exhibit general characteristics of dynamic systems:

- Continuity of state variables
- Amplitude attenuation and phase shift properties must be in accordance with the bandwidth of the system
- The frequency content of linear systems remains unchanged
- Asymptotic stability

Special properties of feedback systems can be checked like:

- Tracking performance
- Achievement of a predetermined steady state
- Estimation of true values from disturbed data

For a particular model, the overall integrity has to be demonstrated:

- The generated results must be "linked" with the associated assumptions
- The results must be in accordance with other test data (laboratory tests)
- The performance data must be achieved and constraints are being met.

2.4 Coincidence Criteria

If corresponding time series are given, at selected points considered to be important the deviation can be read out and viewed relative to the emphasis on the match of certain data. To assure that specified limits are not exceeded, an allowable performance tolerance bound can be applied.

If no data records for comparison are available, it is the engineer's job to take the model output and to determine that it meets prespecified requirements within acceptable limits. Irregularities will have a specific meaning to the expert in most cases. The major drawback of the procedure is, that it does not quantify the degree of coincidence, the judgement is based on a "data transformation model" that is not made explicit.

3. SAMPLE APPLICATION

3.1 Subject of Validation

Subject of the validation procedure described in this section is the HWIL-simulation for the flight test planning of a solid ram-jet-powered missile development program. The flight hardware under consideration is the onboard-computer, the mission software to be validated is depicted in fig. 1.

The system-level test is necessary to certify

- the performance of the onboard-computer in its operational environment
- the satisfaction of requirements.

In the special case of missile development no inflight observations are available and the validation procedure focuses on the correspondence between the computational results of the HWIL-simulation and theoretical data.

For the purpose of validating HWIL the required data for comparison are obtained by independently simulating with the validated theoretical model of the overall system.

Since the assessment of the quality of match and the examination of differences between the data records requires a lot of engineering judgement, it is necessary to have

- an indepth understanding about the functional and desired operating characteristics of the hardware in its operational environment

- knowledge about the goals for the actual flight test, to assess the satisfaction of requirements.

Thus it is possible to determine the specific aspects, where the emphasis of the validation procedure is put on in accordance with the available turnaround time and validation technique. To develop the necessary understanding of the requirements, it is necessary to attempt a forecast of the general model behaviour, as for example a timing diagramm of the intended flight test.

3.2 Basic Software Requirements for the Validation Procedure

A basic requirements is a validated theoretical model of the overall system, which consists of the following submodels for

Airframe/Kinematics
Aerodynamic/Propulsion
Guidance/Control
Missile Instruments with Follow-up A/D-Conversion
Servos.

The results taken from this 6-DOF simulation are used as a standard benchmark for the hardware under consideration.

The model must have the following properties:

- Realtime simulation capability to exercise the operational software in realtime by simulating its operational environment.

- A simulation performance level commensurate with that of the hardware.

  The parts assigned to the operational software are modeled in great detail. They are implemented with scaled equations in 16-bit wordlength. The other simulation characteristics are close enough to the actual systems characteristics to be able to predict the system performance.

- For the purpose of partitioning the theoretical model must be subdivided into submodels representing the available subsystem hardware and allow subsystems to be bypassed and the corresponding hardware inserted in their place. The required simulation system is depicted in fig. 2.

A verification of the operational software in open-loop tests has to be performed to assure that it is functionally equivalent to the represented algorithms.

3.3 Hardware Requirements

To assure, that the system will perform reliably in its operational environment as well as in the computer system test bed, the configuration must allow the validation of the flight hardware and software in the same manner as during actual operation.

This means:

- Identical software for test cases and operational conditions.
  As seen from fig. 4 the input from actual hardware or main computer is buffered in memory. Either of them is identical zero depending on the origin of the data and an addition is performed between the registers. Unnecessary test-output is discarded during actual operation. This technique requires additional software residence in memory but no modification for the purpose of validation.

- This configuration allows as far as possible identical interfacing to simulation computer resp. hardware subsystems, i.e. most functions necessary for providing data streams to and from the onboard-computer are accomplished with the operational interface.

- In addition, the data transfer from a peripheral device or main-computer to memory and vice-versa is initiated at the same prespecified, identical fixed time-intervalls for test cases as under operational conditions. Thus it is verified that equivalent models for hardware subsystems yield equivalent simulated results (ref. to fig. 5).

A schematic of the interconnections between the main-computer and the onboard-computer is shown in fig. 3 resp. fig. 4. This configuration allows the validation of the flight software in a test bed which is a realistic representation of the operational environment.

3.4 Simulation Facility

The hardware and simulation facility required to validate the HWIL-simulation is depicted in fig. 6. It employs the following major functional elements

- Main Computer
- Interface
- Hardware System
- Peripheral Device

and allows optionally to interface the onboard-computer to the system model implemented on the main-computer and substitute it for its simulated counterpart. The E25-Interface is a direct memory access digital interface to the onboard-computer, that buffers real-time data in 16-bit word lenght and transfers them in blocks. The data transfer from the onboard computer or main computer to the interface occurs via a program call after completion of the current computation, the data transfer from the interface to either computers is initiated by the real-time clock at the beginning of the basic intervall. Each request can be synchronously handled.

3.5 Validation through Substitution of Hardware Subsystems

In a first step, the validation procedure focuses on the identification of "elementary errors" like

- Software errors
  wrong equations, wrong control of switching or branching logic, wrong parameter values
  wrong interprogram linkages, code/data allocation errors

- Hardware errors
  real-time requirements not fullfilled, data ranges insufficient

Those errors are at first to be removed, before further analysis of the test data is attempted.

Apart from that, the output cannot be expected to agree exactly because "high order" errors introduced due to different representation of basic external functions or different numerical approximations. Since no subjective assessment of "high order" errors can be made, quantitative methods are necessary that characterize the degree of similarity. In a second step, it may be necessary to modify the mission-software to match the theoretical results to some level of goodness-of-fit.

There are three test-activities:

1. The validation procedure starts with the substitution of certain logically independent parts of the mission-software for subsystem models.
   Performance-resp. time-critical modules like strap-down algorithms or control algorithms are chosen, because of their greater impact on the system-performance.
   The great advantage of the stepwise substitution lies in the isolation of errors to particular sections, which allows easy correction.

2. In the second step, previously tested modules which are sequentially bound, put together in groups and substituted for their simulated counterparts. Thus the connections between the modules are checked in their operational environment.

3. This leads in the last step to the insertion of the whole subsystem hardware and the validation of the overall HWIL-simulation. In each step the later described tests are performed.

3.6 Test-Cases and Test-Techniques

The test runs started with "soft-trajectories" to demonstrate the "reasonableness" of the simulation:

- ballistic trajectories with soft single plane maneuvers to study the controllability over the trajectory. This simplifies the error analysis for autopilot axis, autopilot modes and strapdown algorithms performance.
  The next step is advancing to combined plane maneuvers within specified limits, to check if system performance data are achieved and constraints are met:

- flight conditions according to the preprogrammed flight tests to check the influence of nonlinear effects and the logic flow especially in the case of malfunctions of subsystems. This allows the synthesis of the intended flight test trajectory.

The output variables are chosen to exhibit significant information about the processing of the system inputs. This particular simulation analysis concentrated on output variables, which are related directly to the onboard computations: e.g.:

- Inertial reference data for the strap-down-calculations
- Missile latax along the trajectory and lateral displacement for the guidance performance
- Autopilot axes response
- Log of autopilot modes resp. guidance logic

The analysis starts with highly aggregated data. For a detailed examination of discrepancies one will resort to less aggregated data, e.g.

elements of the transformation matrix to check computationally introduced errors in strap-down calculations
internal variables of the autopilot to check mode switching

The tests performed focus on the comparison of the simulated variables with the corresponding results from the theoretical model. The records were either superimposed (data output in analog form) or digital records of point pairs where examined.

Points or time-segments of major interest are:

- Starting values/initial slope of time series
  They are verified for proper initialization (discovery of scale-errors, bias)

- Discontinuities
  This check is a useful aid for the logical analysis and the analysis of the transient behaviour of the system. It allows to trace through the logic of the system and to visually verify the interconnections between the subsystems.

It includes the check, if switching criterias are fullfilled or unexpected discontinuities occur, the discovery of time-lags between corresponding curves and the analysis of certain nonlinear effects (saturations etc.)

The switching condition in most cases yields a change of the inputs or parameters of the system. This allows to assess the transient behaviour of the closed loop system and to trace back, if the effects of abrupt changes are supported by the underlying model assumptions.

- Asymptotic behaviour of the system
  The agreement of the time series, when the dynamics have slowed down ensures that the statistic relations are equivalent and numeric perturbations have no signifigant effect.

- Other significant points: extremal values, turning points, zero crossings
  A discrepancy in timing resp. amplitude of these points between corresponding time series points out possible errors due to numerical techniques (introduced phase-shift, gain errors) or different equations (error in differential equations, not similar implemented limits)

3.7 Difficulties with a Quantitative Judgement of the Validity

The validation procedure is based on a graphical approach and therefore subjective.

A desired quantitative measurement of point to point fit is restricted to appropriate time-series and in this case is misleading.

Due to switching operations major time-lags are introduced into the system. Small deviations in the state of the system can mean that the switching occurs one time step later, which results in different time histories but common properties of trajectories. The same happens, if variables exhibit a limit cycle behaviour. Samples can differ by a large amount, if the variables are slightly out of phase. A measurement of point by point accuracy would be improper.

Comparisons based on aggregated measures have provided less insight than careful examination at selected sampling points.

4. CONCLUDING REMARKS

During the validation procedure was learned that the HWIL-simulation is most important for the dynamic testing of flight hardware. Laboratory tests, which have been performed before, are strictly open-loop and therefore failed to test the important closed-loop feature of the onboard-computer.

The HWIL-simulation results indicated that significant aspects of the hardware subsystem had not been adressed by open-loop tests, e.g.

- proper execution of the program's branching logic
- proper implementation of parameter values
- real-time requirements
- sufficient data ranges

Finally,

the HWIL-simulation has proved to be more representative of the system and much more confidence can be placed in its simulation results.

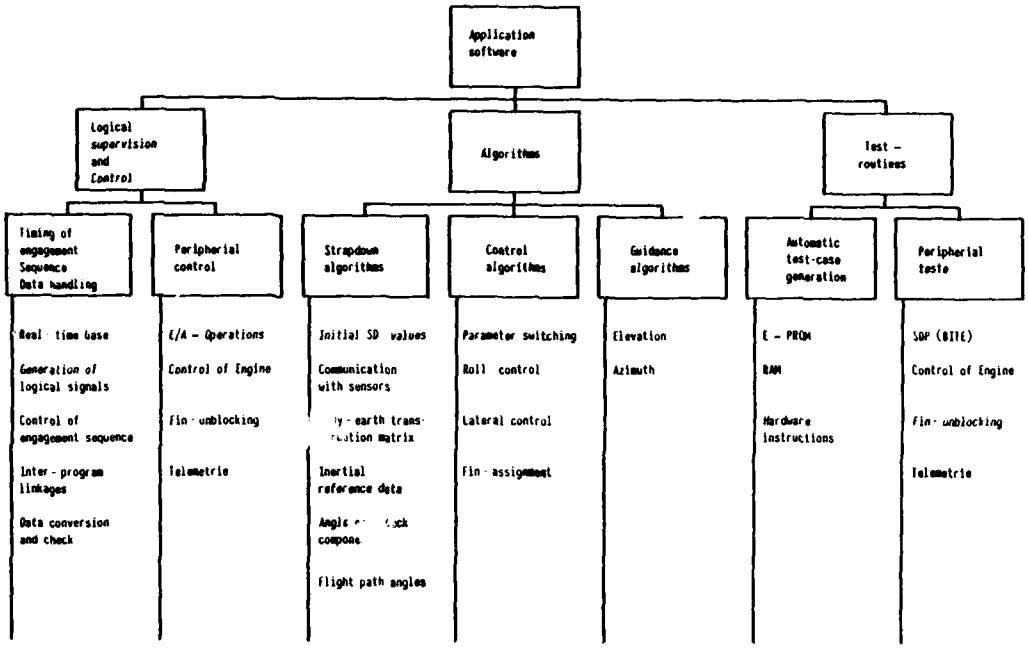

FIG. 1 APPLICATION-SOFTWARE

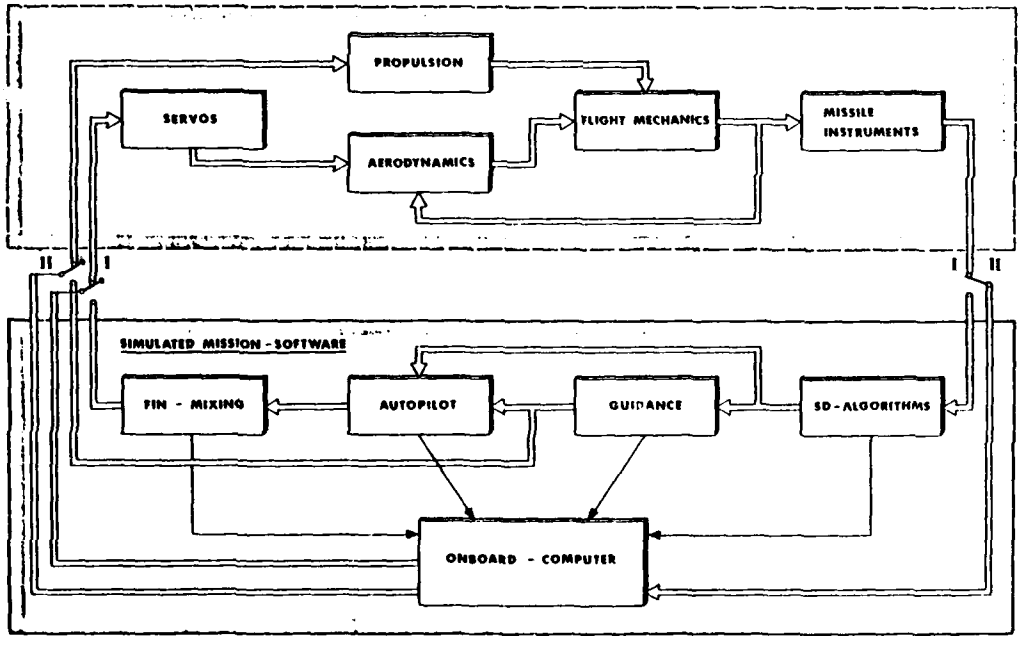

FIG. 2 SIMULATION SYSTEM

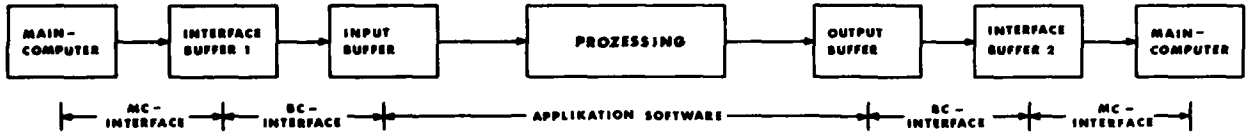

BLOCK-DIAGRAM OF THE INFORMATION FLOW

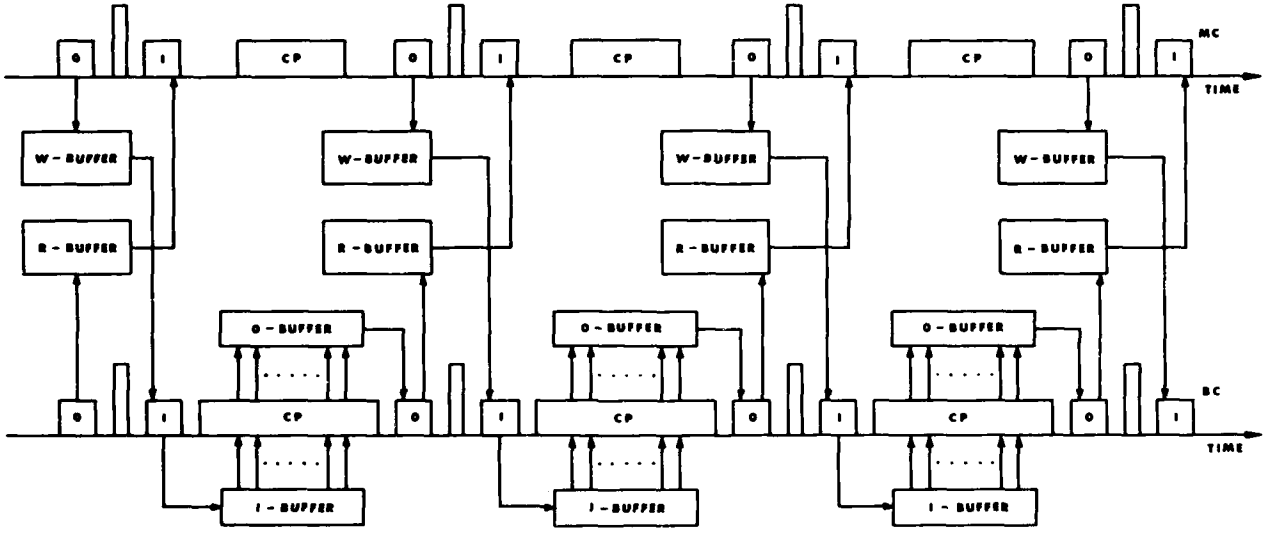

FIG. 3 TIMING-DIAGRAM

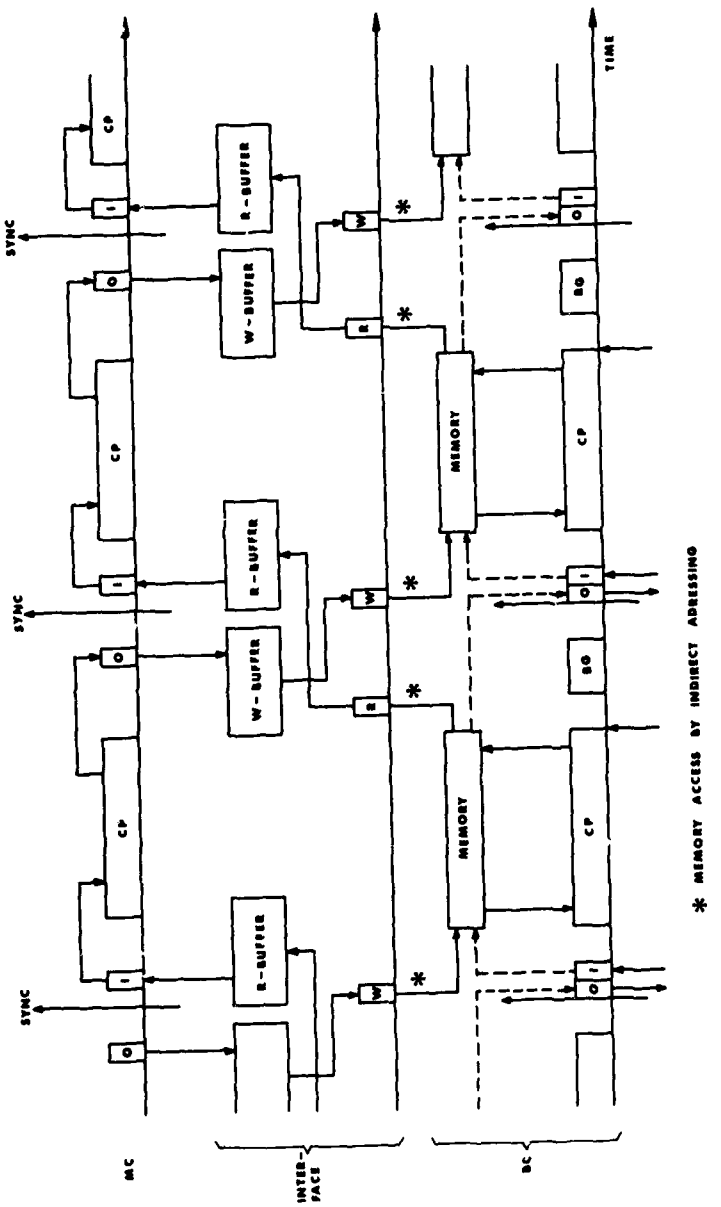

FIG.4 TIMING DIAGRAM OF THE INFORMATION FLOW

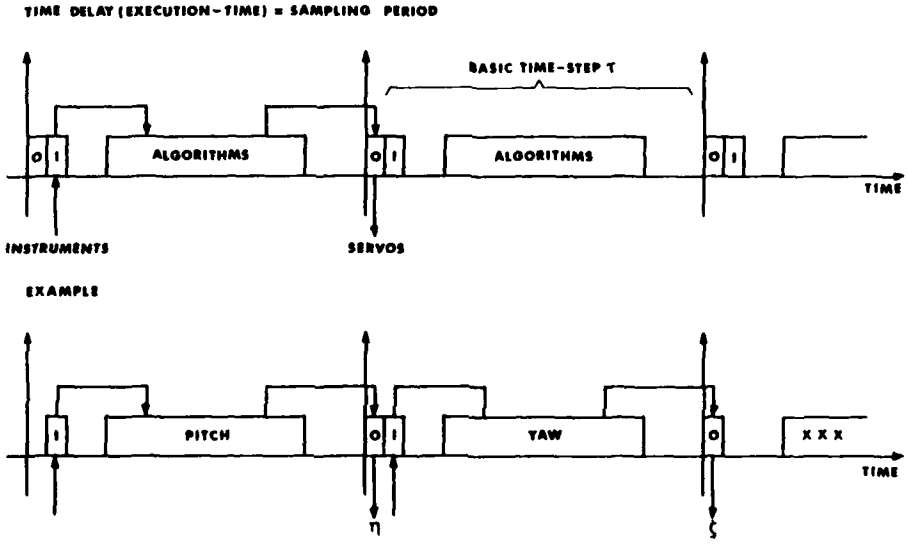

FIG. 5 CONDITIONS FOR CONTROL SYSTEMS DESIGN

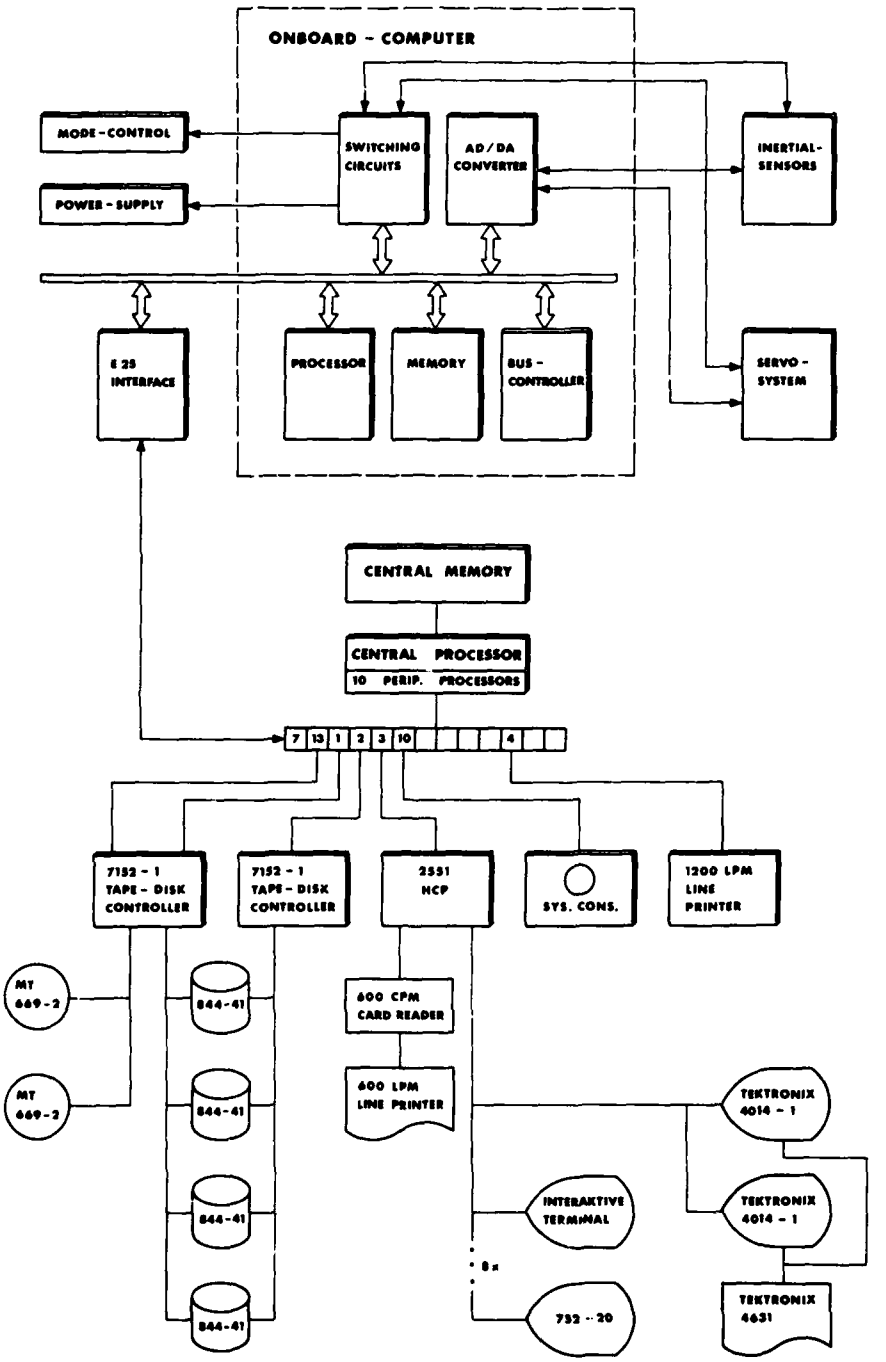

FIG. 6 SIMULATION - FACILITY

BUILDING IN INTEGRITY TO A HIGHER ORDER LANGUAGE

DR. N.J.B. YOUNG
DOWTY ELECTRONICS LTD.
MANSFIELD ROAD
WESTERN AVENUE
ACTON
LONDON W3 ORT
UNITED KINGDOM
FORMERLY ULTRA ELECTRONIC CONTROLS LTD

SUMMARY

Despite potential advantages the use of High Order Languages (HOL's) in high integrity systems remains inadvisable. HOL compilers are complex and difficult to validate and even when correct may produce unexpected results. Methods are discussed for simplifying HOL's so that high visibility is maintained from HOL code through the process of translation down to machine code level. These methods can be applied to standard HOL's or a new HOL can be designed around them. The methods are particularly useful in embedded systems (such as engine controllers) of low cost relative to the facility to which they are applied and which require considerable modification during trials or in service.

Introduction

The advent of low cost relatively powerful microcomputing components capable of meeting the demanding environmental and quality specifications of military applications, especially airborne applications, has led to a revolution in the design of embedded systems for the industry. Whilst previous designs were achieved purely by hardware means the new computerised systems rely heavily on software. This poses a number of challenges to the system designer. Not only must the new systems match or exceed the old in performance and integrity, they must also achieve high visibility of design for validation or certification purposes, and they must also be modifiable as conveniently as the old systems and without compromising the other objectives.

In early products the software was implemented in low order languages such as assembly codes. This was largely because mature High Order Language compilers for the new microprocessors were not available, or did not provide the necessary real time facilities. This demanded highly disciplined procedures for software design, documentation and testing to ensure not only reliable software performance in applications which are largely safety critical, but also that maintainable software would be produced.

By comparison, much software outside the specialised safety critical area of embedded airborne applications has long been written in High Order Languages. It is widely recognised that this has considerable benefits in terms of cost, ease of testing, documentation and maintainability. Unfortunately the use of compilers for producing software in safety critical applications remains inadvisable. Validation of compilers, which are often highly complex, is an extremely difficult and daunting task. Further, even a fully validated compiler may produce results which are unexpected or counter intuitive in some circumstances, because the transformations involved in the compilation process may be complex and not fully understood by the programmer. Therefore, although the use of High Order Languages tends to increase software visibility, the use of compilers tends to reduce it.

Various methods have been employed to overcome these problems, including the use of High Order Language - like pseudocodes to specify software designs and low order languages to implement them. However, these do not of themselves provide the convenience of modification with which final users became accustomed before the advent of software - based systems. This problem has often been tackled by resort to direct modification at the machine code level - the so-called "midnight patch" - which most certainly compromises integrity, visibility and maintainability.

Characteristics and Requirements

The characteristics of software for airborne embedded systems may be summarised as:

1) Small to medium size. For example an embedded system may perform one or a few functions associated with engine control, each requiring 1/2K to 5K words of program memory.

2) Designed to satisfy memory and run-time constraints.

3) Produced by a development team which is large in comparison with the program size but not large in absolute terms.

4) Short preparation times.

5) Extremely high integrity and reliability requirements.

6) Extremely long software lifetimes (perhaps more than 20 years).

7) Maintenance requirements commensurate with long software lifetimes.

8) Often implemented in low order languages at present

9) High complexity relative to program size.

10) Very often modified during development or trials of the overall facility to which the embedded system is applied (such as an aircraft engine) - see figure 1.

11) The embedded system may be of low cost relative to the facility to which it is applied and to the daily cost of trials of such a facility.

Some requirements for embedded systems are therefore:

i) High integrity, even during a phase of frequent modification.

ii) Low cost and very fast and convenient modification capability. In the extreme this might include the capability of modification while a trial is in progress to avoid the need to halt and restart.

iii) High visibility of design.

iv) Strict configuration control.

v) Validation or certification capability.

vi) Speed and memory efficiency (perhaps becoming less important).

vii) Low cost initial development.

Clearly these are not readily reconciled

High Order Languages (HOL's)

It is useful to consider the characteristics of HOL's which make it difficult to meet these requirements. As stated above, the validation of complex compilers is an extremely difficult - daunting

task, and even valid compilers may produce unexpected results. This is particularly so with current generation microprocessors and short word length arithmetic. Intermediate transformations performed by compiler generated code and intended by the compiler writer to protect against overflow or preserve accuracy may produce unexpected results for even the simplest of operations. While it may be acceptable (if undesirable) that this should occur in a HOL at the extremes of value ranges, this phenomenon is not limited in that way. A single example will suffice (Figure 2). Although this shows a result which is unexpected, it is not an "error". At least if is consistent with the language specification, and the compiler which produces this result is approved by the relevant Government authority. Further, the intermediate transformations which give rise to this result are not standard between compilers for different processors nor even necessarily between different issues of the same compiler. The "visibility" of the object code generation process has been lost.

Approaches

Three types of approach have been followed in trying to overcome these problems.

i) Validation

There is continuing interest in methods to validate complex compilers, or to validate particular compiled code against its source. While some progress has been made, this is not yet a solution.

ii) Standardisation

On a well-designed general purpose language and development support tools. It is hoped that when the use of one language becomes enforced to the exclusion of others then it will rapidly acquire a pedigree of successful applications. But a general purpose language which really is suitable for a wide range of applications must necessarily be complex and involve the use of a complex compiler. It is by no means certain that it would be acceptable in high integrity applications.

iii) Simplification

This is an alternative approach which is explored in this paper. If the system for translating from a HOL into object code can be simplified and made transparent then the above requirements can be met, and in this sense integrity has been built in to the HOL. Of course such simplifications are likely to involve loss of general applicability. The simplications should therefore be chosen so as not to restrict the usefulness of the HOL for airborne embedded systems.

Simplication Concepts

A HOL and software system can be conceptually broken down as follows:

Software system = Real time executive + User software

User software = Data items + Permissible Operators + Format to express these.

For the purposes of this paper, the real time executive will be assumed to be well-proven, common between systems, and not affected by frequent user software modifications. It is not considered to detract significantly from integrity therefore.

To simplify the software system it is proposed to restrict the data types to the minimum necessary, predefine the total numbers of entities of each type, and define all Permissible Operations to have

i) A known meaning

ii) An obvious, visible meaning

iii) A least unsafe (or fault tolerant) meaning to optimise integrity even during phases of rapid user software modification.

iv) A standardised implementation, for checking and portability.

The format should be easily read and understood and the translation to object code should also be performed in a standard way.

Minimum set of data types

What is an appropriate minimum set of data types? Clearly this will depend on the application. For example a minimum set for real time control of aircraft engines would not be appropriate for payroll calculations or financial reporting. The intention is therefore to choose a minimum set appropriate for a class of applications such as real-time control and capable of meeting the requirements (accuracy, run-time efficiency, direct mapping to hardware signals in the external world) of this class.

An example of such a minimum set includes only 3 types, namely:

Single word integer

Single word (16,8) fixed point real

Single bit on/off switch

It is recognised of course that this is highly restrictive. In this approach this restriction is accepted for the benefits that it implies and which are to be assessed, and an extension of this set is not desired.

Predefined totality of data items

Whereas the minimum set of data types is defined for a class of applications, the number of items of each tyupe available, e.g. the number of integers, any vary within this class. But it is intended that the totality of data items of each type available should not vary even during the phases of frequent modification during development. In this way the effects of user software changes are restricted to the operations performed on the data items, but the data framework itself is stable.

Permissible Operations

Permissible Operations are either

i) A single arithmetic or comparison operation, e.g. multiplication, with overflow protection and clearly stated accuracy and other appropriate characteristics.

ii) A single input or output operation to external hardware.

iii) A single dedicated albebraic or control orientated operation, e.g. square root or minimum, with the necessary protections. This group is likely to vary for different classes of application.

Note that for example an arithmetic operation with the desired characteristics will not normally be available as a single machine code instruction. Nor, except by chance, will it be implemented exactly by a compiler. It is therefore necessary to enforce particular interpretations of arithmetic and other operations.

The method used to do this is to perform Permissible Operations by means of "primitive" subroutines. A primitive is a very small single purpose module to perform one operation according to a predefined schedule. Primitives are themselves written in low order languages, but they rapidly acquire a pedigree from use in a primitive library and it is not considered that they detract significantly from integrity. They can be tested satisfactorily using conventional techniques.

Permissible Operations are only defined for certain combinations of data items and all others are rejected. For example integer - integer and real-real arithmetic are both defined but mixed mode arithmetic is forbidden. In this way the class of Permissible Operations is simplified and the exact meaning of each one is immediately clear.

In the event of an arithmetic overflow the result of a Permissible Operation is held at the maximum positive or negative value respectively and the occurrence of the overflow is logged for future debugging purposes. This is considered to be the safest and most acceptable option available, and corresponds to the familiar saturation of an amplifier in an analog system. It is an appropriate option to provide some measure of fault-tolerant protection for example during a trials programme which does not allow sufficient time for full software validation of numbers of software modifications.

HOL Translation to Object Code

In order to meet the requirements for visibility, simplicity and integrity, it is intended that the process of translation uses a very strongly structured, one-to-one mapping process to convert a line of HOL code effectively into a data table which will link the predefined primitives to perform Permitted Operations on the predefined data items. Each elemental block of converted code consists only of:

i) Instructions to fetch data items, which are themselves predefined, and place them in a standard transfer area.

ii) A call to a standard primitive.

iii) Instructions to return values from the standard transfer area to the data items.

Because the form of the translated code is so restricted it is practical to check it by means of a de-translator program or by inspection of the translated object code. This does depend on the one-to-one mapping between the HOL statements and the blocks of converted code. It is preferred that this mapping is independent of other HOL statements, i.e. there is no "optimisation" as with a conventional compiler which is why the term "translation" is used. Indeed for integrity the translation should be similar to a macro-assembler.

The Permitted Operations and their exact characteristics are not only fully defined but also highly simplified. Therefore it becomes relatively simple to perform a static analysis of the numerical properties of an entire user program and thus determine the effective accuracy and permissible data value ranges for this program.

Implementation - standard HOL

The techniques described in this paper can be used to best advantage within an environment of specially designed HOL, host computer and target high integrity device. However, for defence projects it is often necessary to use a defence standard language such as CORAL 66 in the U.K. (reference 1) or ADA. When the techniques described in this paper are used with a standard language the task of limiting the use of the language facilities becomes a software management or quality assurance problem. This could, for example, involve the use of a pre-processor to highlight the use of data types or operations which are not permitted. This is no different in principle, but much easier in practice, to the familiar restriction in high integrity software on the use of iteration loops unless they can be proven to terminate. With a specially designed HOL, of course only permitted constructs can be part of a valid program.

The simplification concepts are implemented in a standard HOL as follows

i) Data types. A minimum set of data types is used.

ii) Totality of data items. The number of data item of each type is chosen to be sufficiently large for the requirements of the system and should not vary even during phases of frequent modification of the system. In a typical control system performing several tasks at different recursion rates it is preferred that all data items be common at least to all modules above the level of primitive within a task, i.e. there is no local data below the level of task.

iii) Permissible Operations. The requirement is to replace the use of operations available within the HOL by the use of Permissible Operations with the desired characteristics. For operations which are not available as standard within the HOL this presents no problem. For example operations such as taking a square root or implementing a lag-lead control network are performed by primitives which are accessed as subroutine procedures. However, for arithmetic operations it it necessary both to prevent the use of the standard operation and to enforce the use of the Permissible Operation. For example, an addition of fixed point variables

may be written:

```
x : = ADDF (y,z)
```

but may not be written

```
x : = y + z
```

The run-time efficiency depends on the method of parameter passing enforced by the compiler, which will not normally be optimised for programs configured in this way. Benchmark tests of a CORAL 66 compiler for the U.K. defence standard Ferranti F100-L microprocessor indicate a 10% run time overhead due solely to the parameter passing method used.

The main disadvantage of this method of writing the Permissible Operations is the loss of visibility at the HOL level of code. For example, the statement.

```
x : = y + z - b * c
```

might become

```
x : = ADDF (y, SUBF (z, MULF (b,c)))
```

It is preferable to redefine the arithmetic symbols to have the desired meanings where this facility is provided by the HOL. For example, the "overloading" facilities of ADA might be employed in this way (reference 2,3).

Note that when more than one operation is called up in a single HOL line the structure of the generated object code will not accord precisely with that of the elemental block defined above since instructions to transfer values to or from a standard transfer area will not be generated by the compiler. It is possible to regard these values as existing within an "implicit register", but this is likely to complicate any de-translation for validation procedure according to the characteristics of the compiler and the target hardware. Therefore it is considered to be a higher integrity solution to permit only one operation per HOL line, although it is recognised that this reduces program visibility and comprehensibility.

Implementation - ZICOL (c)

The techniques described in this paper have been incorporated into an environment of a specially designed HOL called ZICOL (c) (ZEUS Integrated Control Oriented Language), a range of host computers from small desktop to supermini sizes and the ZEUS (c) range of high integrity target units using the Zilog Z8000 or Ferranti F100-L microprocessors. Most of the target units have been general purpose controllers designed for use with the system, but it has also been possible to adapt existing controllers which were originally programmed in assembly code.

The minimum ZICOL instruction set is given in table 1. For most applications this is extended to include additional libraries of Permissible Operations and corresponding primitives. Examples are data validation (rate and range checking and scaling), interfacing with special busses, and control law implementations. Note in particular that operations of passing monitored information to the host computer are provided in the minimum set.

Modification - The High Order Patch

The technique of translation to blocks of object code which act as a linking table for primitive routines is capable of very high integrity but is not particularly convenient to use during the phase of rapid program modification. To overcome this the independence of the elemental blocks is exploited in a novel way. During development of a user program the converted code is augmented by additional code interleaved between the elemental blocks. This additional code is transparent to the application program but enables a user to affect its operation, for example making alterations to the ZICOL program and activating or de-activating these changes in real time. (See figure 3). Because of the extreme rapidity with which an unsatisfactory change can be de-activated and because of the fault tolerance built in to the primitives it becomes as acceptable to make modifications with digital units as it was with analog equipments. At the end of development these features may be removed and the high integrity linking table alone recovered.

An alteration to a program consists of one or more elemental blocks which may either be additional to or replace existing elemental blocks. Such an alteration is not limited to a parameter change and can be a structural change (an example is shown in figure 4). Since one elemental block corresponds to one ZICOL line this modification process does not compromise the integrity, visibility or maintainability of the software development process. This can be said to be a "High Order Patch".

Performance

These techniques have been used in a wide range of application areas including aircraft control systems, gas turbine engine controls, weapon launchers, torpedo controls and a combined engine and transmission control for the U.K. Challenger tank. The last application has been implemented both in ZICOL and in CORAL 66, configured as described above. Measured overheads compared with assembly codes are shown below, the lower figures corresponding to more complex systems.

Overhead	Memory	Speed
ZICOL	20-40%	0-20
CORAL (optimised with code inserts.	30-40%	10-30%
CORAL (unoptimised)	40-60%	50-80%

Conclusion

By restricting High Order Languages for ranges of applications there can be considerable increases in visibility of the process of generation of object code from highly visible source code. If these restrictions are built into a High Order Language then these advantages can be utilized to accelerate the software modification process without unacceptable loss of integrity.

REFERENCES

1. HMSO Official Definition of CORAL 66, London, 1970.

2. Association for Computing Machinery, Inc.
Preliminary ADA reference manual, New York June 1979 Sigplan notices volume 14, No. 6.

3. Association for Computing Machinery, Inc.
Rationale for the Design of the ADA Programming Language, New York June 1979, Sigplan notices Volume 14, No. 6.

Software error correction	10%
(In initial code 4% During parameter changes 3.5% During system function and self-check changes 2.5%.	
Datum & control law parameter changes:	66%
Sensor and actuator parameter changes.	1%
System self-check changes in software.	1%(?)
Minor system function additions	2%
Major system function changes.	2%
Hardware changes.	18%
	100%

= 700 changes

Figure 1 Projected modification breakdown for full-authority engine controller over 16 years (based on experience of current digital systems and last generation analog systems).

```
FIXED (16,6) a,x,y,z;
a : = (value);
x : = a;
y : = a * a;
z : = a * a * a;
```

a	1.0	2.0	4.0
x	1.0	2.0	4.0
y	1.0	4.0	16.0
z	0.0	0.0	64.0

Figure 2 Simple CORAL-66 program and equivalent multiplication table for particular compiler.

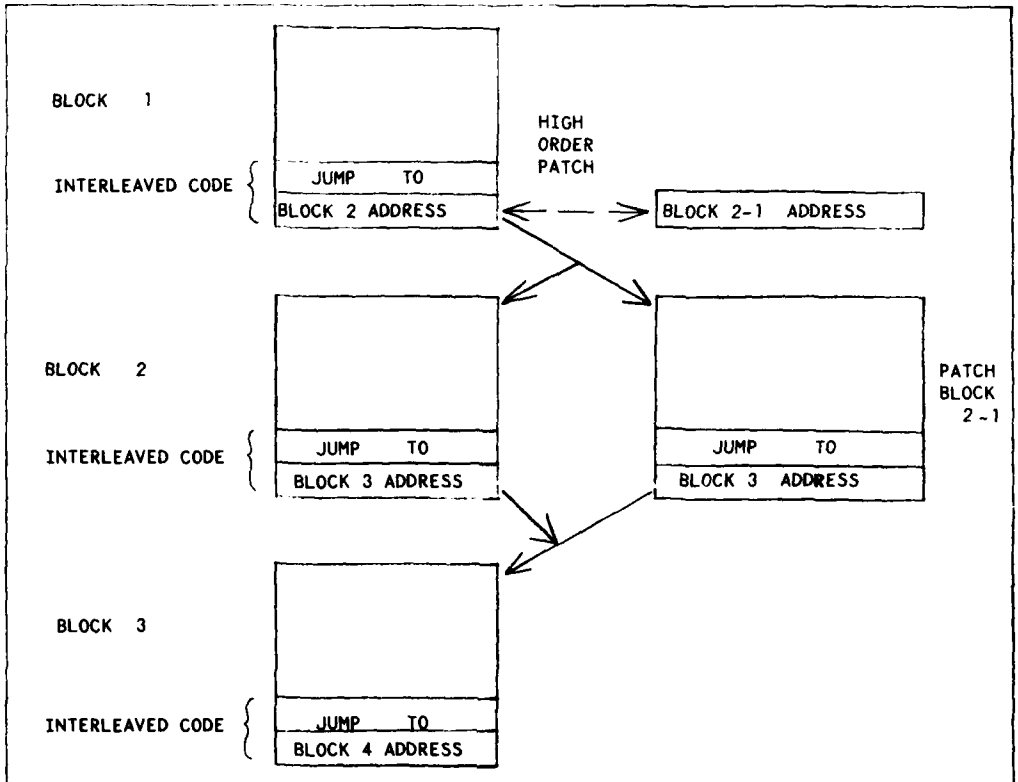

Figure 3 Use of interleaved code to permit High Order Patches.

EXAMPLE LAG-LEAD NETWORK

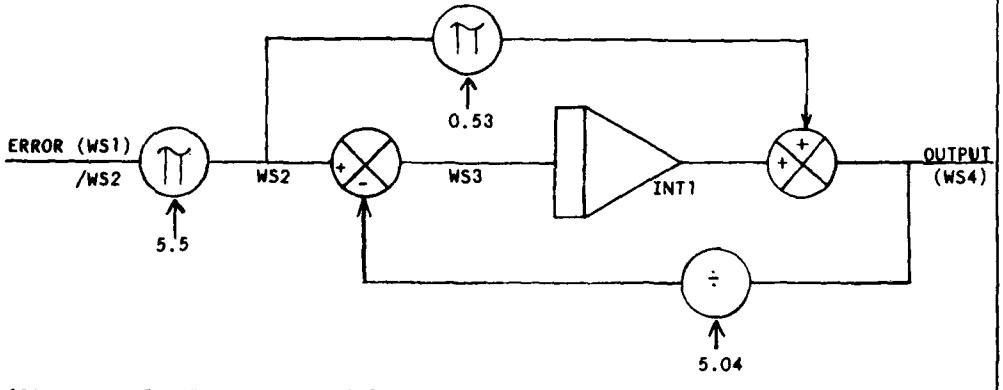


```
100         DEFINE      WS1 = ERROR
110         DEFINE      WS4 = OUTPUT

120         WS2 = 5.5 * ERROR
120-1       OUTPUT = 0.99 * OUTPUT + 3.193 * ERROR - 2.918 * WS2
130         WS3 = WS2 - OUTPUT/5.04

140         OUTPUT = INT1 (WS3) + WS2 * 0.53
140-1       WS2 = ERROR
```

Figure 4 Example of use of ZICOL to implement lag-lead network in s-plane and as High Order Patch in z-plane.

TABLE 1. INSTRUCTION SET

Type	Format	Example
Assignment	Variable=Arithmetic Expression	X=A+B*(C-D)
Integration	Variable=INT_n (Variable)	X=INT1(A)
Differentiation	Variable=DIF_n(Variable)	X=DIF2(A)
Highest Wins	Variable=MAX(Variable)	X=MAX(A,B,C,D,etc)
Lowest Wins	Variable=MIN(Variable)	X=MIN(A,B,C,D,etc)
Look-Up Table	Variable=LOOKUP n(Variable) (n is the Look-Up table No.)	X=LOOKUP3(A)
Loop Initialize	FOR IN=Int. Value to Final Value	FOR I=1 to 10
Loop Terminate	NEXT In	NEXT I9
Program Jump	GOTO Line Number	GOTO 25(line No.25)
Conditional Jump	IF Conditional GOTO Line No.	IF X=5 GOTO 95
Subroutine Call	GOSUB Line Number	GOSUB 200
Conditional Subroutine Call	IF condition GOSUB Line No.	IF X > Y, GOSUB 45
Return Subroutine	RETURN	RETURN
Rename Variable	DEFINE Variable=Defined Name	DEFINE AOUT3=DRIVE1
Initialize Constant	SETKn=Numeric Value	SET K1=0.45
Initialize Look-Up Table	Set LnX=Numeric Value; Initialize the Math. Co-ordinate	SET L2X=0.4,0.6,0.8,...
Initialize Look-Up Table	SET LnY(m)=Numeric Value; Pair Of The nth. Table	SET L2Y=0.3,0.9,1.7,...
Set Timer	TIMEn=Time In Seconds, n is The Timer Number	TIME3=27 (seconds)
Debug Trace	TRACE Variable, Variable;Outputs Variable Values on Trace Cycle	TRACE X,Y,X
Monitor	MONITOR 'Text', Variable; Continuous Variable Output	MONITOR 'SIX', X
Program Termination	STOP	STOP
End of Program	END	END

TABLE 1. *Notes*

The following symbols perform the function of Conditional Operators:

a. Equal to =
b Not equal to < >
c Greater than >
d Less than <

DEVELOPMENT AND APPLICATION OF DIGITAL CONTROL FOR TACTICAL AIRCRAFT FLUTTER SUPPRESSION

Dr. Dinesh S. Joshi, Engineering Specialist and Don F. Kesler, Senior Technical Specialist
Flight Control Research
and
Dr. Erwin H. Johnson, Engineering Specialist
Structural Dynamics Research
Northrop Corporation, Aircraft Division
One Northrop Avenue
Hawthorne, California 90250

SUMMARY

Active control methods have been applied to synthesize and mechanize digital control laws for tactical aircraft flutter suppression. Several methods to digitize analog control laws have been compared. The State Space Method with Jordan Canonical Transformation offers a systematic and efficient digital flutter control design for multivariable systems. A transonic wind tunnel test conducted under a U.S. Air Force contract conclusively demonstrated the feasibility of digital implementation.

INTRODUCTION

Flutter is an explosive phenomenon in which the aerodynamic forces feed energy into the aircraft structural system through interacting natural modes. If uncontrolled, flutter can destroy the structure through divergent oscillations in a fraction of a second. Passive means to control flutter require expensive structural modification or the imposition of speed placards which reduce the aircraft speed capability and, thus, decrease its survivability. Active flutter suppression has shown promise of preventing wing/store flutter, with potential for providing significant improvements in aircraft operation and mission effectiveness.

For the past nine years, Northrop has been researching flutter suppression technology and has investigated its applications to tactical aircraft (References 1, 2, and 3). In these research programs, analog control laws were synthesized via least square and optimal control techniques. To demonstrate the effectiveness of these control laws in flutter suppression, several wind tunnel tests were conducted on a half span YF-17 wing/store scale model. The results show a 70 percent improvement in the flutter dynamic pressure through active control. Although the analog mechanization of these control laws was highly successful, a transition to digital control is desirable because of the advances in digital fly-by-wire technology. The use of a digital computer to perform control tasks is in line with general transition of aircraft control systems from analog to digital devices. In addition to the microprocessor technology applications, the advantages of digital logic are accuracy, flexibility and the ease of multiplexing a given computer on a time shared basis.

The primary objective of this paper is to compare methods to mechanize digital control laws from their analog counterparts. The methods include:

1. Generalized State Space Method
2. State Space with Jordan Canonical Transform
3. Phase Variable Canonical Transform (Z-Transform)
4. Prewarped Tustin Transform.

Although the end results, a set of difference equations providing control, are similar, each of the methods is numerically different. This paper presents the results of digital simulations of several YF-17 flutter configurations stabilized by digital control laws. In addition, the results of a recent wind tunnel test to demonstrate the feasibility of digital flutter control have been summarized and included in this paper.

CONTROL LAW SYNTHESIS

The flutter suppression control laws were synthesized by least square (Reference 3) and optimal control techniques (Reference 4). Table 1 summarizes the salient features of the three selected control laws used on a YF-17 flutter configuration.

Least Square Synthesis. The essence of the least square synthesis technique described in Reference 3 is to take outputs from specified sensors and to blend them in such a way that the total signal closely approximates that of the following equation:

$$d(s) = \frac{s\omega_f^2}{s^2 + 2\zeta\omega_f s + \omega_f^2} \qquad (1)$$

where d(s) is the desired signal, s is the Laplace operator, ω_f is the frequency of the flutter mode, and ζ is a damping parameter. The transfer functions of each of the sensor responses can be generated analytically or experimentally. If the transfer functions from n sensors are denoted by $h_i(s)$ (i = 1, 2, ... n),

the least squares technique determines the complex weights, R_i which minimize the error between the desired signal and the signal that is to be fed back. For a continuously defined transform, the error term between the desired and the blended signal is

$$e(s) = d(s) - \sum_{i=1}^{n} R_i h_i(s) \tag{2}$$

TABLE 1. SELECTED YF-17 FLUTTER CONTROL LAWS

CONTROL LAWS	CONTROL SURFACE		ACCELEROMETERS				SYNTHESIS TECHNIQUE
	LEADING EDGE	TRAILING EDGE	A1	A2	A3	A4	
N1	X				X	X	LEAST SQUARE
N3	X		X		X	X	LEAST SQUARE
N4	X	X	X	X	X	X	OPTIMAL CONTROL

For a practical application, the transfer functions are evaluated at r discrete frequencies and a mean square error is formed.

$$E^2 = \sum_{k=1}^{r} \left| \epsilon_k \right|^2 = (D^T - R^T H)\ (\bar{D} - \bar{H}^T \bar{R}) \tag{3}$$

where D, R, and H are matrix representations of the scalar terms given in Eq. (2) with dimensions: r x 1, n x 1, and n x r respectively. The superscript ($\bar{}$) denotes complex conjugate, while the T superscript signifies the transpose. The 'R' vector can be determined by setting the derivatives of E^2 with respect to 'R' to zero and solving the resulting system of simultaneous, linear complex equations. The resulting maxtrix equation for 'R' has the following simple form:

$$(\bar{H} H^T) R = \bar{H} D \tag{4}$$

This least square synthesis procedure provides a simple, effective means of synthesizing an arbitrary number of transfer functions into a robust feedback signal. The block diagrams of the specific control laws N1, N2, and N3 are shown in Figures 1, 2, and 3. G and H for all the block diagrams are given below.

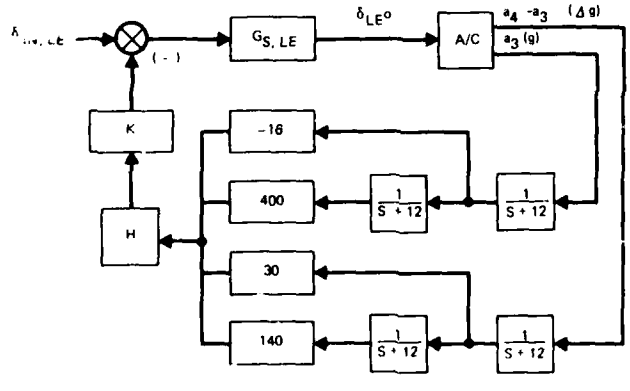

FIGURE 1. CONTROL LAW N1

$$G_{s,LE} = \frac{94 \cdot 28{,}900}{(s + 94)(s^2 + 204s + 28{,}900)}$$

$$G_{s,\,TE} = \frac{124 \cdot 19{,}044}{(s + 124)(s^2 + 138s + 19{,}044)}$$

$$H = \frac{S^2 + 45590}{S^2 + 213S + 45590} \cdot \frac{S}{(0.03S + 1)(0.01\,5S + 1)} \cdot \frac{69700}{S^2 + 264S + 69700} \cdot \frac{S}{S + 10}$$

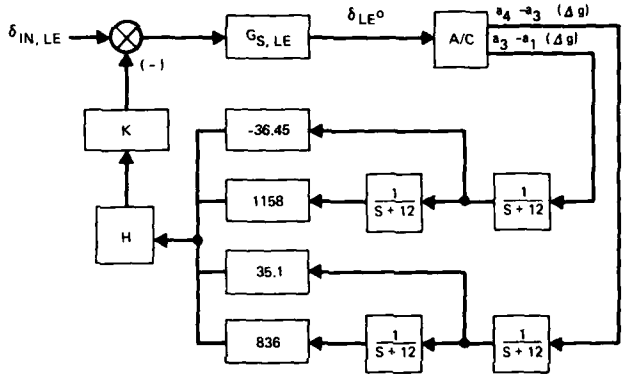

FIGURE 2. THE THREE TRANSDUCER CONTROL LAW N3

Optimal Control Synthesis. The performance and effectiveness of single-surface control laws can be significantly improved by the use of multisurface optimal control laws. Reference 4 details an optimal control approach to aircraft flutter suppression and load alleviation. Primarily, this design involves the determination of three gain matrices in the feedback network. A fixed format introduces a number of judiciously selected poles in the feedback transfer function which augments the optimization procedure. Once the controller function is determined, the complete closed-loop system is examined for stability margins. The controller is synthesized through the minimization of a performance index. Figure 3 shows the results of this procedure applied to YF-17 flutter control. The significance of this multivariable controls design is the utilization of two surfaces and four accelerometers.

DIGITAL CONTROL LAW MECHANIZATION

Theoretical background and the application of four methods to digitize the control laws synthesized in the previous section are presented in the following discussion.

Generalized State Space Method. The generalized state space method for digitizing analog control laws transforms a continuous system

$$\dot{x} = Ax + Bu$$

$$y = Cx \qquad (5)$$

into a discrete system.

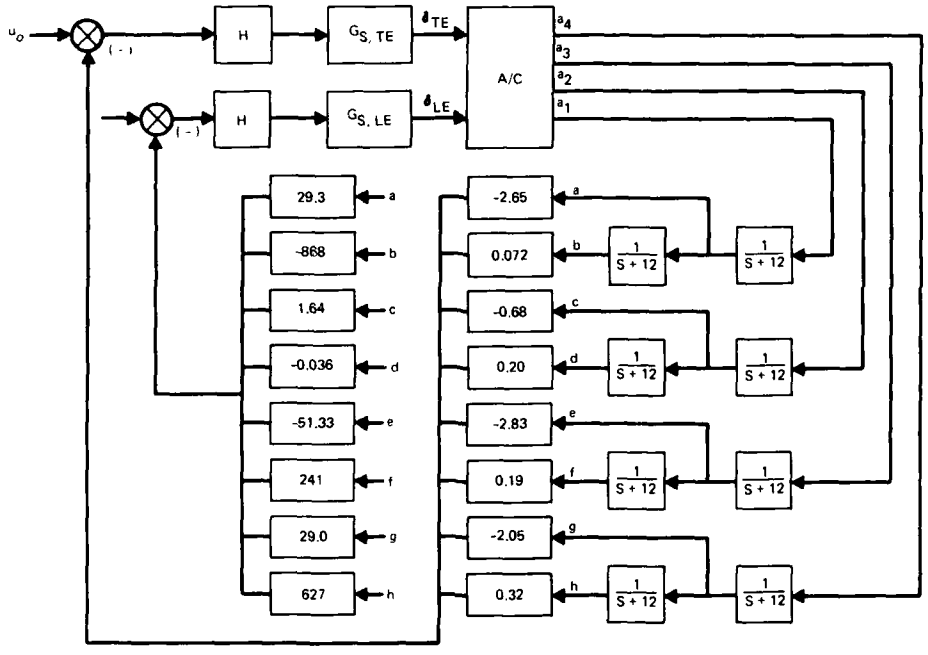

FIGURE 3. A TWO-SURFACE CONTROL LAW N4

The exact solution of Eq. (5) is

$$x(t) = x(t_0)e^{A(t - t_0)} + \int_{t_0}^{t} e^{A(t - \tau)}Bu(\tau)d\tau \tag{6}$$

Consider the situation in which the state and the output variables are sampled periodically in time, so that their values are available every T seconds at t = kT. When t = kT is substituted in Eq. (6), we obtain:

$$x(kT) = e^{A(kT - t_0)}\, x(t_0) + \int_{t_0}^{kT} e^{A(kT - \tau)}Bu(\tau)d\tau \tag{7}$$

Similarly, at t = (k + 1)T, we have:

$$x[(k + 1)T] = e^{A[(k + 1)T - t_0]}x(t_0) + \int_{t_0}^{(k + 1)T} e^{A[(k + 1)T - \tau]}Bu(\tau)d\tau \tag{8}$$

Multiplying Eq. (7) by e^{AT} and subtracting from Eq. (8):

$$x[(k + 1)T] = e^{AT}x(kT) + \int_{kT}^{(k + 1)T} e^{A[(k + 1)T - \tau]}Bu(\tau)d\tau \tag{9a}$$

and

$$y\,[(k+1)T] = Cx[(k+1)T] \tag{9b}$$

To further simplify Eq. (9) let $u(t) = u(kT)$, $kT \leq t \leq (k+1)T$. This is analogous to a sampled-data model with a zero order hold as shown in Figure 4.

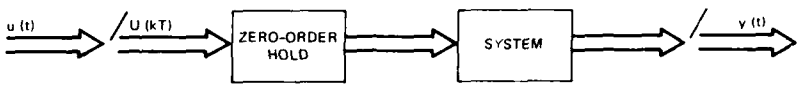

FIGURE 4. SAMPLED DATA SYSTEM

Thus, Eq. (9) can be rewritten as:

$$x[(k+1)T] = e^{AT}x(kT) + \int_{kT}^{(k+1)T} e^{A[(k+1)T-\tau]}Bu(kT)d\tau \tag{10a}$$

Since this is a stationary system:

$$\int_{kT}^{(k+1)T} e^{A[(k+1)T-\tau]}d\tau = \int_{0}^{T} e^{A(T-\tau)}d\tau = \int_{0}^{T} e^{A\tau}d\tau \tag{10b}$$

Finally, the discrete system equations can be written as:

$$x[(k+1)T] = e^{AT}x(kT) + Bu(kT)\int_{0}^{T} e^{A\tau}d\tau \tag{11}$$

or

$$x[(k+1)T] = F\,x(kT) + G\,u(kT) \tag{12a}$$

$$y[(k+1)T] = C\,x[(k+1)T] \tag{12b}$$

By forming an approximate sampled-data model, it is possible to obtain the states and outputs of a continuous linear system at discrete instants in time. These equations can easily be programmed on a digital computer to provide the digitally simulated system responses. The computer algorithm which generates the F and G matrixes uses a series expansion for the exponential:

$$F = e^{AT} \cong \sum_{i=0}^{36} \frac{T^i A^i}{i!} \tag{13}$$

$$G = \int_{0}^{T} e^{A\tau}d\tau \cong \sum_{i=0}^{36} \frac{T^{i+1} A^i}{(i+1)!} \tag{14}$$

One of the important considerations in mechanizing digital control laws is their real time operation on microprocessor-based computers. Because the flutter suppression control laws are high order systems (e.g. N1 and N3 are of 11th order and N4 is of 15th order), the generalized state space method will require N^2 (order) multiplications for real time operation. This could not be achieved in real time on the SEL-32/55 digital computer selected for the control law mechanization. To minimize the number of multiplies a canonical transformation was used to diagonalize the characteristic matrix A.

State Space with Jordan Canonical Transformation. The basic state space Eq. (5) can be transformed to a Jordan canonical form. The transformed system improves the computational efficiency by reducing the number of multiplications from N^2 to about 3N. It is possible to find a nonsingular matrix P that will transform a square matrix into the Jordan canonical form.

Define $x = PZ$ so that,

$$\dot{Z} = P^{-1}APZ + P^{-1}Bu$$

$$Y = CPZ \text{ and } Z(0) = P^{-1}x(0) \qquad (15)$$

Note that $P^{-1}AP = DIAG\ (\lambda_1, \lambda_2 \ldots \lambda_n)$ and the columns of P are the Eigenvectors of A, where the λ_1, $\lambda_2 \ldots \lambda_n$ are the Eigenvalues of matrix A. In this mechanization some numerical problems were encountered for repeated Eigenvalues for each of the three control laws ($\lambda = -12$). This was overcome by slightly separating the poles at $s = -12$ (i.e. $s = -12.1, -11.9$, etc.). Once the diagonalization is achieved, the generalized state space method can be used to discretize the continuous system. Control laws N1, N3, and N4 were mechanized by this technique and the results are shown in Figures 5, 6, and 7. In all the time history figures, the flutter is allowed to build up with the loop open, and then the loop is closed. The effectiveness of the control can be measured by the envelope damping after the loop is closed. In each case, the digital control law stabilized a YF-17 flutter configuration. It should be noted that state space law can be used for both multi-input/single-output (MISO) (N1 and N3) as well as multi-input/multi-output (MIMO) (N4) systems. The important asset of this mechanization is the ability to mechanize multi-input/multi-output control laws often encountered in flutter suppression applications.

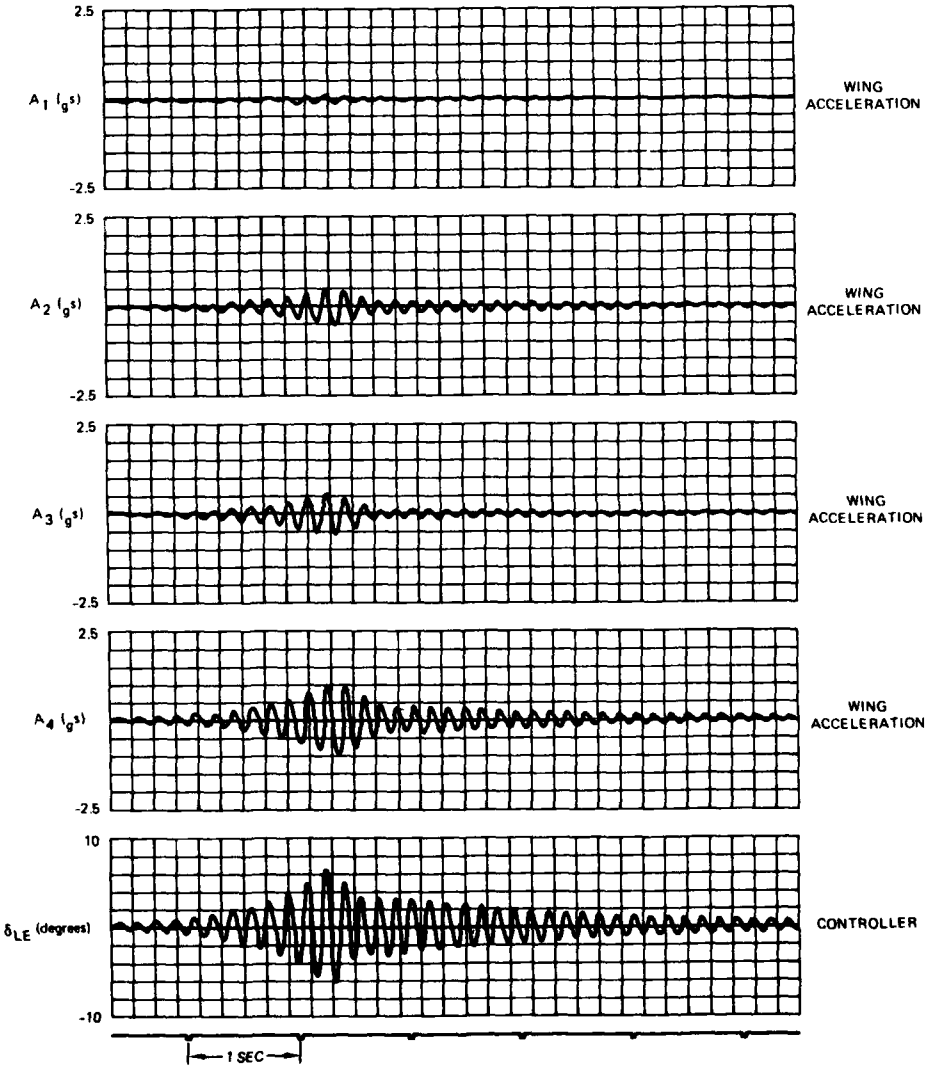

FIGURE 5. STATE SPACE MECHANIZATION OF N1 CONTROL LAW (SAMPLE TIME 10 MSEC)

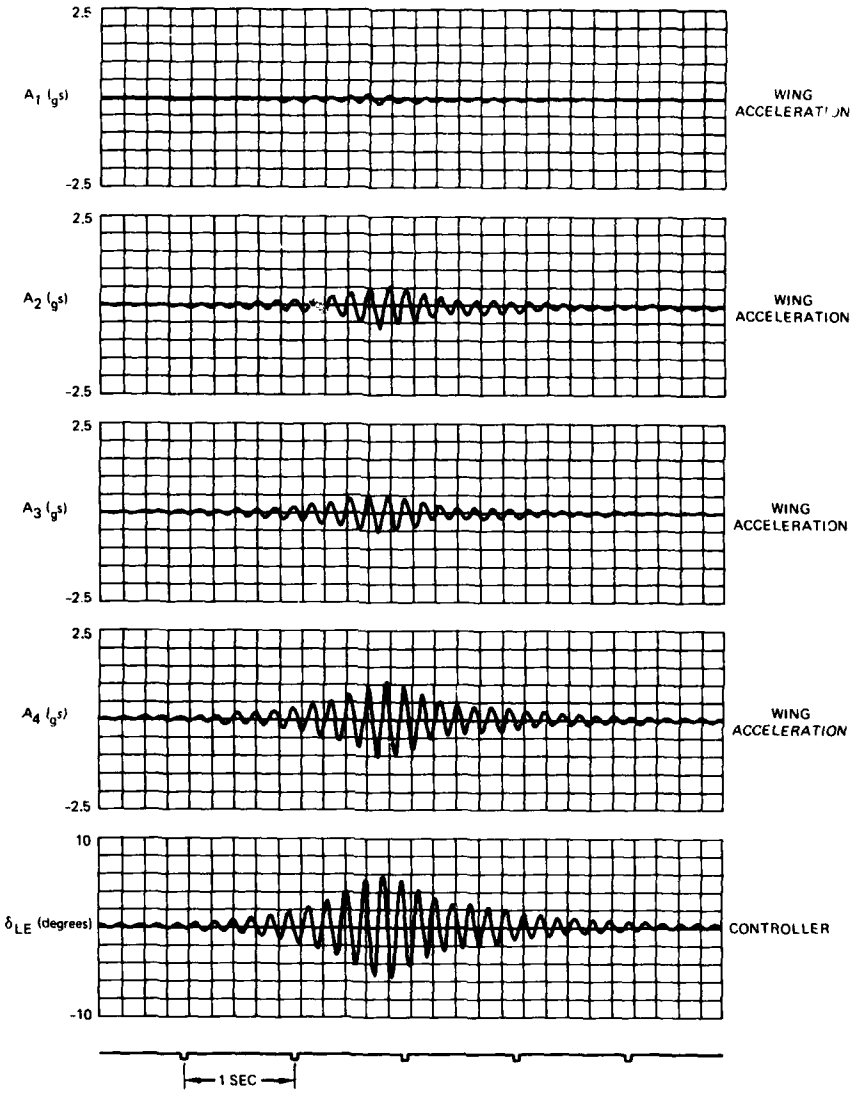

FIGURE 6. STATE SPACE MECHANIZATION OF N3 CONTROL LAW (SAMPLE TIME 2.5 MSEC)

Phase Variable Canonical Transform. A transformation to the Phase Variable Canonical Form (Reference 5) yields a minimum implementation which is the same as a true Z transform. The form of the result looks exactly like a transfer function in state variable representation.

Let P be the transformation matrix:

$$z = Px, \; x = P^{-1}z \tag{16}$$

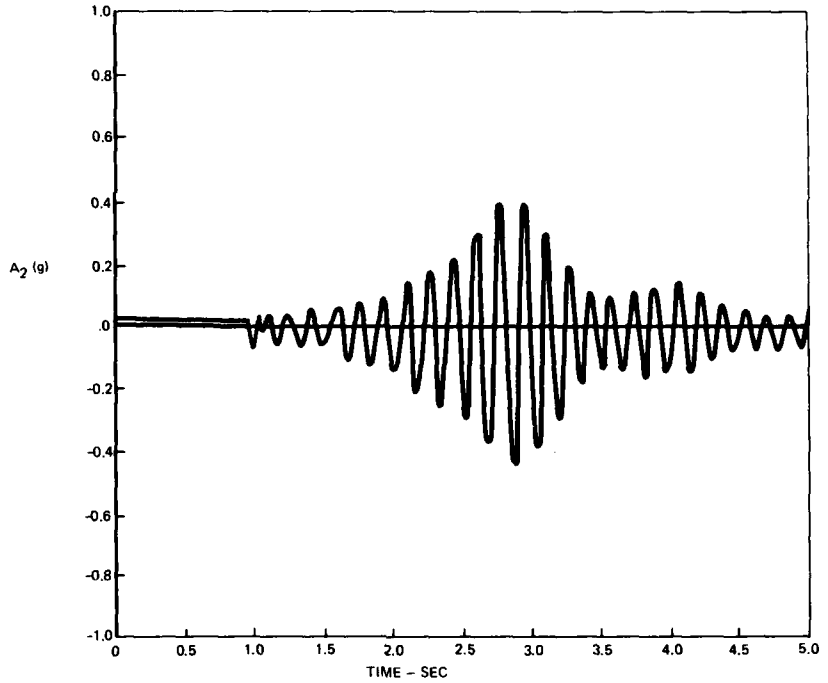

FIGURE 7. STATE SPACE MECHANIZATION OF N4 CONTROL LAW (SAMPLE TIME 10 MSEC)

Then Eq. (12a and 12b) become (using $\phi(z) \approx F$ and $\Gamma(\tau) = G$)

$$P^{-1}z\ (t+\tau) = \phi(\tau)\ P^{-1}\ z(t) + \Gamma(\tau)Bu(t)$$

$$z(t+\tau) = P\phi(\tau)\ P^{-1}\ z(t) + P\Gamma(\tau)Bu(t)$$

$$y = CP^{-1}z \tag{17}$$

The transform P is such that the state equation takes the form (for a fourth order system with a single input)

$$\begin{bmatrix} z(t+\tau) \end{bmatrix} = \begin{bmatrix} 0 & 1 & 0 & 0 \\ 0 & 0 & 1 & 0 \\ 0 & 0 & 0 & 1 \\ C_1 & C_2 & C_3 & C_4 \end{bmatrix} \begin{bmatrix} z(\tau) \end{bmatrix} + \begin{bmatrix} 0 \\ 0 \\ 0 \\ 1 \end{bmatrix} u \tag{18}$$

It is seen that the implementation takes the form:

$$z_1(t+\tau) = z_2(t)$$

$$z_2(t+\tau) = z_3(t)$$

$$z_3(t+\tau) = z_4(t)$$

$$z_4(t+\tau) = C_1z_1(t) + C_2z_2(t) + C_3z_3(t) + C_4z_4(t) + u$$

$$y = D_1z_1(t+\tau) + D_2z_2(t+\tau) + D_3z_3(t+\tau) + D_4z_4(t+\tau) \tag{19}$$

where $D = IIP^{-1}$

This form takes 2N multiplies and N delays. Multiple outputs are formed by using more rows in the H matrix. Multiple inputs can be used; however, only one input satisfies the phase variable canonical form. The state transition matrix remains the same, but the input matrix no longer has only one nonzero term. The other columns multiplying u are general. The disadvantages of this form is its transfer function nature. This causes the C terms to have a high dynamic range of numbers. The numbers range from one to the product of the roots. Because of these numerical problems, this method was not further investigated.

Prewarped Tustin Transform. The most commonly used implementation of analog control laws in a digital computer is the Tustin transform. The main reason for this popularity is the ability to cascade the filters and thus insert nonlinear elements and gain changes. In systems where these elements are necessary, state variable methods have serious shortcomings. Prewarping (Reference 6) is used to correct the frequency distortion that occurs with the Tustin transform. A step-by-step set of rules for filter design via bilinear transformation is presented in Reference 6. Following the prewarping it can be shown that Tustin transformation maps roots from the S-plane to the Z-plane such that a real root located at $s = -\beta$ will map to a real root located at $z = e^{-\beta T}$, and a pair of complex conjugate roots with the characteristic polynomial $(s + c)^2 + d^2$ will map to a pair of complex conjugate roots with the characteristic polynomial $z^2 - 2e^{-cT} \cos dT\, z + e^{-2cT}$. Band-limited transforms, such as low-pass filters with more poles than zeros have additional zeros inserted at $z = -1$ such that the orders of the denominator and the numerator of G(z) are the same. The effect of these zeros at $z = -1$ (for low-pass filter forms) is to introduce a "notch" characteristic in the frequency response of the digital filter at the half-sample frequency. This is in addition to the desired low-pass characteristic for which the filter was designed and may be regarded as a "free" noise rejection capability of the digital filter at frequencies near the half-sample frequency.

The complete algorithm can be stated as follows: Given a continuous transfer function,

$$\frac{Y}{u} = G(s) = \frac{K' \prod_{i=1}^{m} (s + \alpha_i) \prod_{i=1}^{n} \left((s + a_i)^2 + b_i^2\right)}{\prod_{i=1}^{r} (s + \beta_i) \prod_{i=1}^{t} \left((s + c_i)^2 + d_i^2\right)} \tag{20a}$$

a digital filter approximating G(s) is given by

$$\frac{Y}{u} = G(z) = \frac{K''(z + 1)^k \prod_{i=1}^{m} \left(z - e^{-\alpha_i T}\right) \prod_{i=1}^{n} \left(z^2 - 2e^{-a_i T} \cos b_i T z + e^{-2a_i T}\right)}{\prod_{i=1}^{r} \left(z - e^{-\beta_i T}\right) \prod_{i=1}^{t} \left(z^2 - 2e^{-c_i T} \cos d_i T z + e^{-2c_i T}\right)} \tag{20b}$$

where $k = r + 2t - m - 2n$ and K" is determined by the condition $G(z)\Big|_{z=+1} = G(s)\Big|_{s=0}$. The difference equations were programmed so that $z^{-n}\, Y(k) = Y(k-n)$ and $z^{-n}\, u(k) = u(k-n)$.

The results of this mechanization for control laws N1 and N3 are shown in Figures 8 and 9. It should be noted that the Tustin mechanization of the N4 control law was not attempted because of its MIMO nature and the resultant complexity of this mechanization. The advantage of this method is its ease of implementation for single input/single output systems as well as its ability to accommodate nonlinearities.

WIND TUNNEL TEST

Under a U.S. Air Force Contract, Northrop conducted a wind tunnel test to demonstrate the feasibility of digital control for flutter suppression (Reference 7). Figure 10 shows the configuration of the model. Several control laws were mechanized by the State Space Jordan Canonical Transformation method. In this test, the feasibility and the effectiveness of digital control were conclusively demonstrated. Figures 11 and 12 show the salient results of this wind tunnel test.

Figure 11 shows that the digital laws performed comparably to the analog laws where zero damping parameter represents a flutter condition. By using digital control, the YF-17 flutter dynamic pressure was improved by 100 percent ($Q/Q_f = 2.0$) of the open loop dynamic pressure. Figure 12 shows the effect of sampling time on the digital control law. The digital control law performed adequately up to T = 10 msec. As the sampling frequency was decreased further, a significant degradation was observed at T = 15 msec. Adequate performance at 10 msec is an important result, because this time is typical of the sample time employed in aircraft digital control systems.

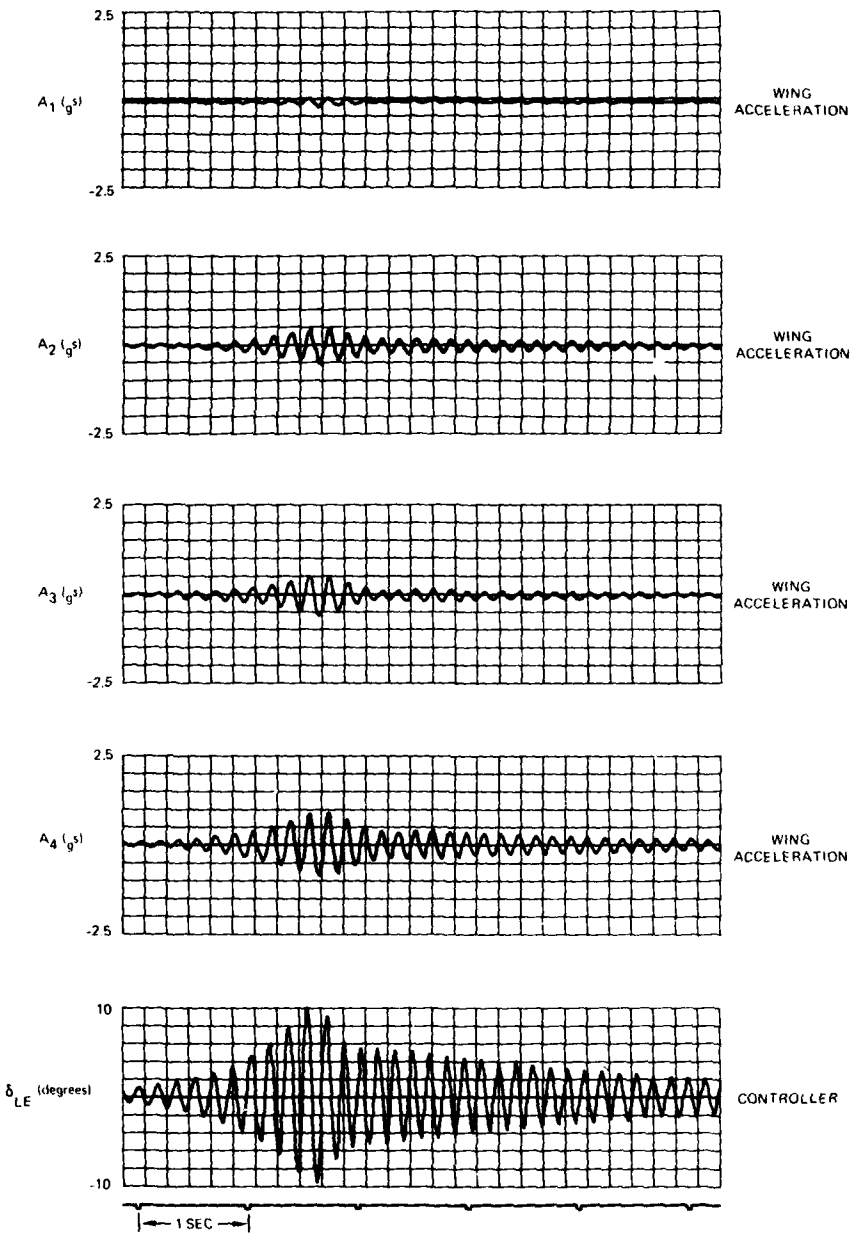

FIGURE 8. TUSTIN MECHANIZATION OF N1 CONTROL LAW (SAMPLE TIME 10 MSEC)

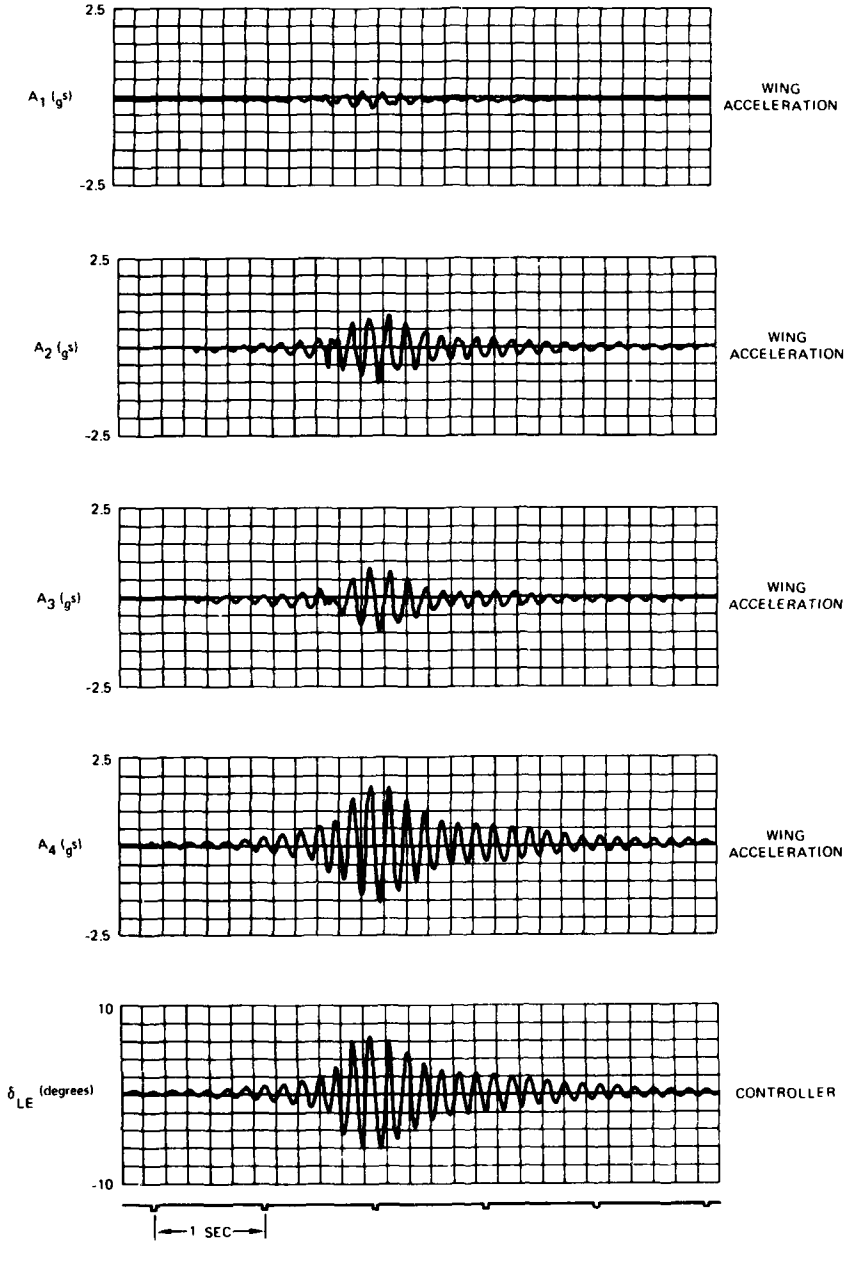

FIGURE 9. TUSTIN MECHANIZATION OF N3 CONTROL LAW (SAMPLE TIME 2.5 MSEC)

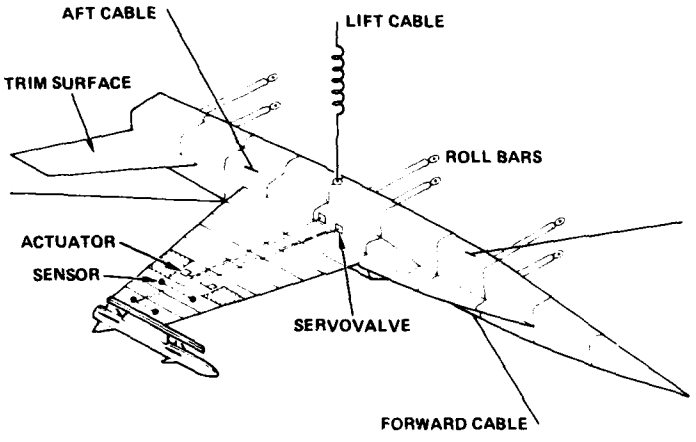

FIGURE 10. YF-17 WING/STORE FLUTTER SUPPRESSION MODEL, CONFIGURATION B.

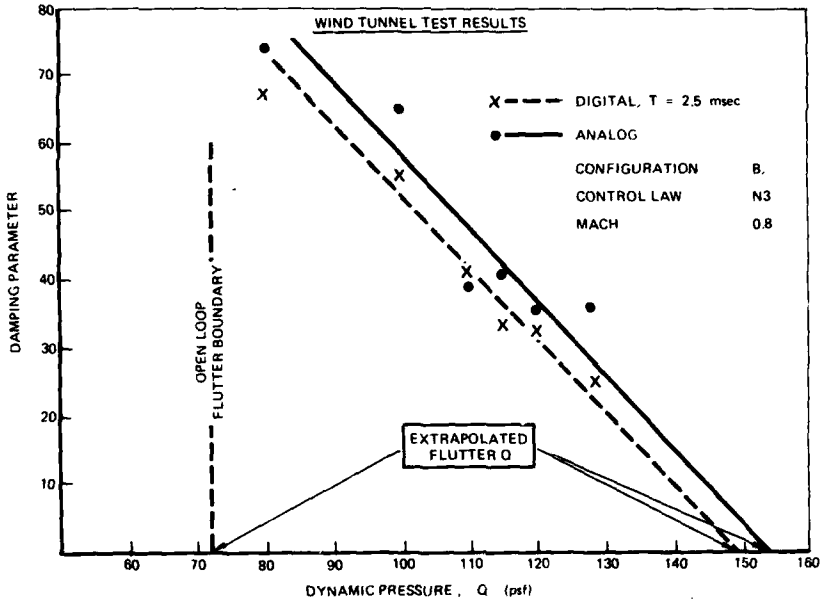

FIGURE 11. DAMPING VS. DYNAMIC PRESSURE FOR ANALOG CONTROL LAW AND ITS DIGITAL VERSION

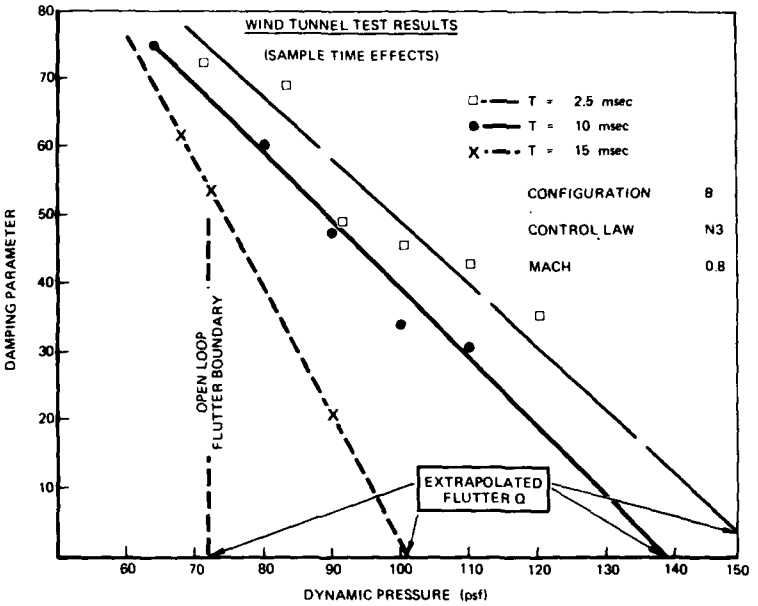

FIGURE 12. EFFECTS OF SAMPLE TIME ON DIGITAL CONTROL LAW PERFORMANCE

CONCLUDING REMARKS

The successful development and application of digital control for tactical aircraft flutter suppression has been conclusively demonstrated, both analytically and experimentally. The key conclusions are summarized in the following discussion:

1. The optimal control synthesis of flutter suppression control laws are often MIMO systems. Thus, they require input from several sensors and the multi-surface actuation (output) to effectively control flutter instability.

2. Of the four mechanization methods discussed in this paper, Tustin Transform and diagonalized State Space methods show the most promise for flutter applications. The Tustin Transform is best where nonlinearities exist and the system is single input/single output. For MIMO systems, the State Space method provides a systematic and computationally efficient mechanization. A Jordan canonical diagonalization is necessary because the flutter control laws are generally high order systems (e.g. N4 is 15th order).

3. For control laws N1 and N3, the prewarped Tustin Transform and State Space mechanization provide identical results.

4. Wind tunnel test results indicate that the performance of a digital control law is comparable to its analog counterpart.

5. Despite its complexity, the digital flutter control system mechanization and sample time frame are compatible with other aircraft digital control systems.

REFERENCES

1. Hwang, C., Johnson, E.H., Mills, G.R., and Pi, W.S., "Additional Demonstration of Active Wing/Store Flutter Suppression Systems," AFWAL-TR-80-3093, August 1980.

2. Collection of papers, "Report on a Cooperative Program on Active Flutter Suppression," AGARD Report 689, August 1980.

3. Johnson, E.H., "Active Flutter Suppression Control Law Definition Via Least Square Synthesis," AIAA-80-0765, May 1980.

4. Hwang, C. and Pi, W.S., "Application of Optimal Control Techniques to Aircraft Flutter Suppression and Load Alleviation," AIAA-82-0724.

5. Ramaswami, B. and Ramar, K., "Transformation to the Phase-Variable Canonical Form," IEEE Transactions on Automatic Control, Volume AC-13, No. 6, December 1968.

6. Franklin, G.F. and Powell, D.J., "Digital Control of Dynamic Systems," Addison-Wesley Publishing Company, June 1981.

7. Johnson, E.H., Hwang, C., Joshi, D.S., Kesler, D.F., and Harvey, C.A., "Test Demonstrations of Digital Control of Wing/Store Flutter," AIAA 82-0645, AIAA/ASME/ASCE/AHS 23rd Structures, Structural Dynamics and Materials Conference, New Orleans, LA, May 1982.

ACKNOWLEGEMENTS

The analytical results in this paper were part of a Northrop Independent Research and Development study. The wind tunnel test were conducted by Northrop under U.S. Air Force Contract No. F33615-80-R-3217. Lt. Chris Worsowicz of AFFDL provided data for some of the Tustin mechanizations.

NASA/RAE COLLABORATION ON NONLINEAR CONTROL USING THE F-8C DIGITAL FLY-BY-WIRE AIRCRAFT*

G. F. Butler, M. J. Corbin, and S. Mepham
Flight Systems Department, Royal Aircraft Establishment
Farnsborough, Hampshire, U.K.

and

J. F. Stewart and R. R. Larson
Dryden Flight Research Facility, NASA Ames Research Center
P.O. Box 273, Edwards, California 93523, U.S.A.

SUMMARY

A cooperative advanced digital research experiment (CADRE) was established by the National Aeronautics and Space Administration (NASA) and the Royal Aircraft Establishment (RAE), in which nonlinear control algorithms developed by the RAE were tested on the F-8C digital fly-by-wire (DFBW) aircraft based at the Dryden Flight Research Facility. In the initial phase of the collaboration, some variable-gain algorithms, referred to collectively as variable integral control to optimize response (VICTOR) algorithms, were flight tested. With VICTOR, various measures available within the control system are used to vary gains and time-constants within the closed loop and thereby enhance the control capability of the system, while reducing the adverse effects of sensor noise on the control surfaces. A review of design procedures for VICTOR and results of preliminary flight tests are presented. The F-8C aircraft is operated in the remotely augmented vehicle (RAV) mode, with the control laws implemented as FORTRAN programs on a ground-based computer. Pilot commands and sensor information are telemetered to the ground, where the data are processed to form surface commands which are then telemetered back to the aircraft. The RAV mode represents a single-string (simplex) system and is therefore vulnerable to a hardover since comparison monitoring is not possible. Hence, extensive error checking is conducted on both the ground and airborne computers to prevent the development of potentially hazardous situations. Experience with the RAV monitoring and validation procedures is described.

SYMBOLS

DECL	on-board pitch command, deg
DEP	pitch stick command, deg
DERAV	pitch downlink elevator command, deg
DEUP	pitch uplink elevator command, deg
DRATE	maximum floating limit draft rate, 2.5 deg/sec
DYNP	dynamic pressure, lb/ft^2
G_a	closed-loop gain
G_q	baseline proportional gain
G_{qv}	proportional gain
G_θ	baseline integral gain
$G_{\theta v}$	integral gain
K_a	feed-forward gain
M_q	normalized pitching moment derivative due to pitch rate
M_α	normalized pitching moment derivative due to angle of attack
M_η	normalized pitching moment derivative due to elevator deflection
Q,q	pitch rate, deg/sec
q_D	pilot pitch-rate demand, deg/sec
$\dot{q}$	pitch acceleration, deg/sec^2
s	complex frequency variable
T	time delay
V_q	VICTOR pitch-rate gain

*Crown copyright subsists in Sec. 2 of this paper.

AD-A125 687 ADVANCES IN GUIDANCE AND CONTROL SYSTEMS(U) ADVISORY GROUP FOR AEROSPACE RESEARCH AND DEVELOPMENT NEUILLY-SUR-SEINE (FRANCE) JAN 83 AGARD-CP-321

3/3

UNCLASSIFIED F/G 17/7 NL

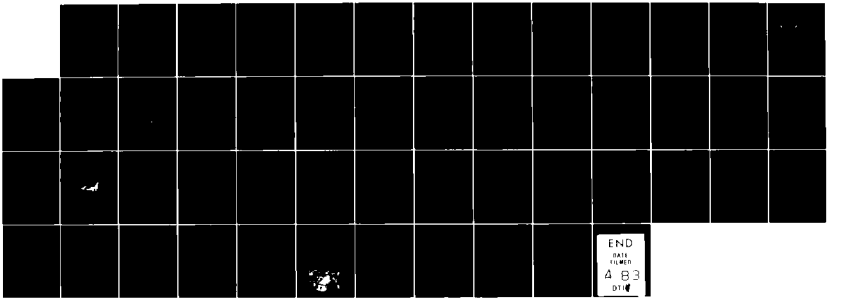

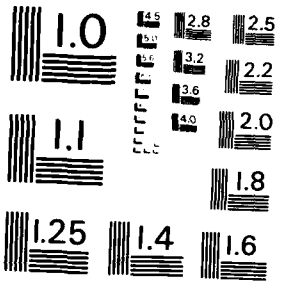

MICROCOPY RESOLUTION TEST CHART
NATIONAL BUREAU OF STANDARDS - 1963 - A

V_θ VICTOR integral pitch-rate gain

Z_α negative of lift force due to angle of attack

Z_η negative of lift force due to elevator deflection

α angle of attack, deg

$\dot{\alpha}$ angle-of-attack rate, deg/sec

δ VICTOR error threshold level

δ_1 second VICTOR error threshold

ε error

ε_V error between pitch-rate response and pilot demand

η elevator deflection from trim position

η_D CADRE elevator command, deg

τ_a lead-time constant for phase advance

τ_N time-constant of noise filter and phase advance

τ_{Nv} time-constant of noise filter

τ_z time-constant of pilot's filter

τ_{1_ε} VICTOR error lead-time constant

τ_{2_ε} VICTOR error lag-time constant

1. INTRODUCTION

Following discussions in 1979 between RAE and NASA on collaboration in the fields of active control technology and handling qualities, a joint program of nonlinear control was established. In this program, known as the cooperative advanced digital research experiment (CADRE), nonlinear flight-control techniques developed by RAE have been implemented and tested on the F-8C digital fly-by-wire (DFBW) research aircraft based at Ames Research Center's Dryden Flight Research Facility.

The F-8C DFBW aircraft is operated in the remotely augmented vehicle (RAV) mode (Ref. 1), in which control laws are implemented as FORTRAN programs on a ground-based computer; the control loop from the pilot and aircraft sensors to the actuators is completed by two-way telemetry. Since this represents a simplex system, extensive error checking is performed to prevent the development of potentially hazardous situations. Experience gained with the RAV monitoring and validation procedures is described in this paper.

The control concept was initially developed by RAE. F. R. Gill, the principal RAE advocate of nonlinear control concepts, has proposed several novel control concepts offering potential benefits in both control performance and handling qualities (Refs. 2-5). One of these concepts, the variable control to optimize response (VICTOR), has formed the basis of the initial stage of the collaboration.

Although the F-8C DFBW aircraft used for the flight testing is fitted with triplex on-board computers, the RAV mode is used for CADRE. Control laws are implemented in a high-level language (FORTRAN) on a ground-based computer, with the control loop from pilot inputs and aircraft sensors through the computer to the control actuators being completed by two-way telemetry (Fig. 1). The RAV mode is a simplex system and is therefore vulnerable to a hardover, since command voting or comparison is not possible. Hence, extensive error checking is carried out in both the ground and airborne computers and, if an error is detected, control is restored to the on-board system. Further details of the F-8C RAV flight-test technique, including modifications introduced for the CADRE flights, are given in Sec. 3.

With VICTOR, measures available within the control system are used to vary the gains within the closed loop and, hence, to enhance the control capability of the system while reducing the adverse effects of sensor noise on the control actuators. The operation of VICTOR is illustrated in Fig. 2. Normally, as the closed-loop gains increase, the control improves and the noise effects become greater. On the other hand, as the gains decrease, the noise effects decrease, but the control also becomes less effective. The VICTOR method overcomes this conflict by allowing the gain to vary as a function of error signals within the system, so that the gains increase when control is required as a result of pilot input or external disturbance, but are allowed to reduce to a much lower level once the control requirement has been satisfied. The design and operation of a variable-gain algorithm, known as VICTOR-E, implemented for a pitch-rate-to-elevator controller as part of CADRE, is described in Sec. 2.

Initial flight tests of the variable-gain control laws commenced early in 1982; they are described in Sec. 4. The principal aim of the flight tests was to establish whether a variable-gain controller could offer improved control performance over a linear baseline system, and whether any adverse handling problems were introduced by the rapidly varying gain. The task chosen for this assessment was an air-to-air tracking task, with the F-8C aircraft required to track an accompanying chase aircraft through a pushover/pull-up maneuver. These tests have demonstrated that a variable-gain controller can be designed to give improved control performance while maintaining acceptable handling qualities. In addition, the flight tests have shown that modifications introduced into the RAV system software for the CADRE tests have been successful

in allowing the assessment of the nonlinear control laws without undue restriction on the maneuver envelope of the aircraft. Finally, enhancements to the VICTOR control law and the introduction of other nonlinear control techniques into the CADRE program are discussed in the light of experience with the initial flights.

2. DESIGN OF THE VARIABLE-GAIN CONTROLLER[1]

The general structure of the CADRE nonlinear pitch-rate controller is shown in Fig. 3. The controller consists of two parallel loops: a baseline loop with fixed gains to provide a datum; and a higher-bandwidth VICTOR loop, the contribution from which is governed by the variable-gain algorithm. This parallel structure of the VICTOR and baseline loops embodies part of the concept of class A/B control architecture (Refs. 6, 7). The class A system is that needed to keep the aircraft flying, and the class B system combines with A to provide high performance. In this case, when the system errors are small, the class B (VICTOR) gains are reduced to zero; but once a significant error caused by pilot demand or external disturbance is detected, the gains in the class B system are allowed to increase rapidly to drive the error toward zero.

The CADRE control laws were developed in two stages: the initial design of the baseline and nonlinear control laws by RAE (Refs. 8, 9), using a simplified model of the F-8C short-period dynamics; and the simulation and assessment of the control laws at Dryden using a full six-degree-of-freedom model of the aircraft, together with the introduction of modifications to the RAV system software needed to ensure flight safety (see Sec. 3).

The first stage of the design was performed at RAE, using the computer-based control systems design package, TSIM (Refs. 10, 11). The major part of the design exercise was carried out using a continuous representation of the system, but a discrete implementation was also simulated and the characteristics checked as the design progressed. In addition, real-time engineer-in-the-loop simulations were used to check the system performance for a simple tracking task. Finally, the CADRE control laws were converted to difference-equation form and specified as a set of FORTRAN subroutines for the RAV ground computer. The CADRE control-law subroutines were then evaluated by NASA, and some modifications were introduced, as specified in Ref. 12.

This paper includes a summary of the principal design criteria and constraints, including the aircraft and actuator dynamics (Sec. 2.1), time delay (Sec. 2.2), and command prefilter (Sec. 2.3). The baseline system parameters are defined in Sec. 2.4, and the design of the VICTOR-E algorithm is discussed in Secs. 2.5 and 2.6. The final CADRE software includes eight combinations of parameters defining a range of control-law options; these are summarized in Sec. 2.7. The implementation of the control laws as FORTRAN subroutines is described in Sec. 2.8.

2.1 Aircraft Model

The pitch-rate controllers were designed for a fixed flight condition with a Mach number of 0.67 and an altitude of 6100 m. The short-period dynamics of the F-8C were modeled by linearized second-order equations of the form

$$\begin{bmatrix} \dot{q} \\ \dot{\alpha} \end{bmatrix} = \begin{bmatrix} M_q & M_\alpha \\ 1 & Z_\alpha \end{bmatrix} \begin{bmatrix} q \\ \alpha \end{bmatrix} + \begin{bmatrix} M_\eta \\ Z_\eta \end{bmatrix} \eta$$

where q is pitch rate, α is angle of attack, and η is elevator deflection from trim position.

The values of the normalized derivatives (such as M_q and M_α) were taken from the linearized six-degree-of-freedom data given in Ref. 13.

The primary and secondary actuators were represented by the first- and second-order transfer functions, $1/(1 + 0.08s)$ and $3969/(s^2 + 88s + 3969)$, respectively.

As noted previously, an important effect of the F-8C RAV facility is the time delay introduced by the telemetry link hardware and the ground computer. In the early design stages the delay was represented by the continuous second-order approximation

$$e^{-Ts} \cong \frac{12 - 6Ts + T^2s^2}{12 + 6Ts + T^2s^2}$$

where T is the delay time.

A total delay of 50 msec was assumed for the system design, but the initial flight tests indicate that the total delay in the RAV mode is about 100 msec, which leads to some reduction in the damping of the systems (see Sec. 4).

2.2 Command Prefilter and Feed-Forward

The initial design goal for the system response to a pilot demand was that the pitch-rate response to a step input on the stick should be rapid and exhibit as small an overshoot as possible. Normally, if no prefilter is included, the aircraft zero causes a large overshoot in pitch-rate response to a step input. To alleviate this effect, a command prefilter of the form $(1 + \tau_a s)/(1 + \tau_z s)$ is introduced. For a second-order model, the aircraft zero time-constant τ_z is given, in terms of normalized derivatives, by

---

[1]Crown copyright subsists in Sec. 2 of this paper.

$$\tau_z = \frac{M_\eta}{M_\alpha Z_\eta - M_\eta Z_\alpha}$$

For the design flight condition, $\tau_z = 1.02$.

The value of the lead-time constant, τ_a, allows some control over the size of the pitch-rate overshoot. For $\tau_a = 0$, simulations showed that the response was too slow for accurate tracking. On the other hand, as τ_a approaches τ_z, the lag is effectively canceled, which leads to an increasing tendency to overshoot. Air-to-air tracking at long distance (≥300 m) requires accurate control of pitch attitude through dead-beat pitch-rate response, whereas when the target is close, height errors play a more important part in the task, and hence there is an increasing emphasis on faster normal acceleration response. Therefore, the original dead-beat rate-response goal was changed for close tracking. Because of the inherent lag between pitch rate and normal acceleration response to an elevator input, more rapid normal acceleration requires an increased pitch-rate overshoot, with a consequent increase in the lead-time constant, τ_a. Two values of τ_a were included as options in the final software specification (Ref. 12) (also see Sec. 2.7):

$\tau_a = 0.2$ for distant tracking (>150 m)

$\tau_a = 0.6$ for close tracking (<150 m)

If no integral term is included in the control system, Gill (Ref. 4) shows that a feed-forward of the pilot demand with gain K_a will lead to a steady-state error of zero. For a second-order aircraft model, the feed-forward gain K_a, of Fig. 4, can be expressed in terms of normalized derivatives as

$$K_a = \frac{Z_\alpha M_q - M_\alpha}{Z_\alpha M_\eta - M_\alpha Z_\eta} = 0.62$$

for the design flight condition. Although the baseline controller includes an integral term, which will itself act to reduce the steady-state error to zero, the integral acts relatively slowly, and it has been found advantageous to retain the feed-forward element.

2.3 Baseline Loop Parameters

The selection of the gain values, G_q and G_θ, and the time-constant, τ_N, is considered in detail in Ref. 8. It should be noted that for convenience, the proportional and integral gains are scaled by a factor related to the elevator effectiveness, $G_a = 1/M_\eta$ (which is equal to 0.087 at the design flight condition), so that the total gains for the proportional and integral loops are given by $G_a G_q$ and $G_a G_\theta$, respectively (Fig. 4). The primary design criterion was to maintain a damping level of about 0.5 on the short-period mode, while making the response speed as rapid as possible and keeping noise effects on the elevator at a reasonable level. The values selected were as follows:

Time-constant: $\tau_N = 0.033$ sec

Proportional gain: $G_q = 3.6$

Integral gain: $G_\theta = 4.15$

2.4 Design of VICTOR-E Algorithm

Design guidelines for the structure and implementation of variable-gain control laws are currently under investigation at RAE. In particular, Gill has evolved several strategies for gain variation, which are described in detail in Refs. 4 and 5. One feature that stands out from this work is that in order to derive the full benefit of a high-gain system, the variable gain must be increased rapidly once the decision has been made that control is required. Hence, for the variable-gain algorithm described here (VICTOR-E), the starting point for gain variation in the VICTOR control loop is a straightforward on/off switch controlled by an error threshold. In other words, given an error ε and a threshold level δ, the system is switched to a higher gain when $\varepsilon \geq \delta$ and is switched back to a lower gain when $\varepsilon < \delta$. Some modifications have been introduced to this criterion to reduce the effects of switching transients, but VICTOR-E remains intrinsically a switching algorithm.

To retain reasonable levels of damping, the higher gain of the VICTOR system must be associated with a greater bandwidth. In the single-loop VICTOR systems described by Gill (Refs. 4, 5), the noise filter time-constants (and hence the bandwidth of the system) are slaved to the gain variation. As noted earlier, however, an important feature of the VICTOR-E implementation is the parallel structure (Fig. 3), in which the variable-gain elements are confined to a separate loop. One advantage of this parallel architecture is that the wider bandwidth of the VICTOR loop can remain fixed, with the contribution of this loop being controlled by the gain term alone, and, hence, the need for filter time-constant variation is removed.

The structure of the VICTOR control-loop includes variable proportional and "leaky" integral control in addition to fixed-phase advance and noise filter elements. The overall gains are varied by means of VICTOR gearings V_q and V_θ, which are in the range of 0 to 1 (for VICTOR-E, V_q is set equal to V_θ), and the maximum gains of the VICTOR loop are set by parameters G_{qv} and $G_{\theta v}$. For the design case, the integral gain $G_{\theta v}$ is set to zero, and the proportional gain G_{qv} is set to 3.6 (equal to the value of G_q in the baseline loop). The time-constant of the noise filter and phase elements in the VICTOR loop advance, τ_{Nv}, is set to 0.0125. Other values of these parameters are, however, included in the eight systems selected for flight (see Sec. 2.7).

2.5 Operation of VICTOR-E

The VICTOR-E algorithm operates by means of an error signal ε_V, which controls the V_q gearing ($0 \leq V_q \leq 1$). To ensure that V_q responds quickly to the pilot's stick movements, ε_V is based on the difference between the pitch-rate response q and the pilot demand q_D. The error is then filtered and washed out to eliminate noise and steady-state components, finally yielding the VICTOR error ε_V, defined by

$$\varepsilon_V = \left| (q - q_D) \left(\frac{\tau_{1_\varepsilon} s}{1 + \tau_{1_\varepsilon} s} \right) \left(\frac{1}{1 + \tau_{2_\varepsilon} s} \right) \right|$$

Time-constant values of $\tau_{1_\varepsilon} = 10$ and $\tau_{2_\varepsilon} = 0.05$ have produced satisfactory control behavior. Initially, the VICTOR gearing was increased by switching V_q from 0 to 1 when the error threshold δ was exceeded. To smooth out differences in control behavior experienced when pilot demand is close to the threshold, however, a second threshold, δ_1, was introduced so that when ε_V is increasing and $\delta \leq \varepsilon_V \leq \delta_1$, then $V_q = (\varepsilon_V - \delta)/(\delta_1 - \delta)$.

When the control demand has been satisfied and the error is reduced to a low level, the VICTOR algorithm must take account of this and reduce V_q toward zero. Gill (Refs. 4, 5) finds that the response is sensitive to the rate of reduction of the gain, and that it is important to ensure that the gain is not reduced too rapidly. Hence, if ε_V is decreasing, the maximum value of V_q is held until $\varepsilon_V < \delta$, after which V_q is reduced to zero linearly with time. A ramp decay time of 2 sec has proved to be suitable.

The operation of the VICTOR-E algorithm is illustrated in Fig. 5, using the results from simulation studies for a 0.1-sec lagged-step pilot input of 1 deg/sec. It should be noted that in the example shown, ε_V does not reach a high enough level to force V_q to its limiting value of unity.

2.6 Parameter Combinations for Flight Tests

Following simulation of the CADRE control laws at RAE and NASA, eight combinations of parameters were identified as possible candidates for flight testing. These eight functions can be commanded from a mode-panel on the ground; they allow the control law on the RAV system to be changed without leaving real time (see Sec. 3). The eight combinations comprise four basic systems, with two values of the lead-time constant on the pilot's prefilter, $\tau_a = 0.2$ or 0.6, specified for each (see Sec. 2.3). The basic systems are as follows.

1. Baseline: Here the proportional and integral gains in the VICTOR loop G_{qv}, $G_{\theta v}$ are set to zero, leaving only the baseline loop in operation. Even though the VICTOR loop is ineffective, the gearing V_q continues to vary and can be used as an indication of system performance (see Sec. 4). The baseline systems are numbered 5 and 6 with $\tau_a = 0.2$ and 0.6, respectively.

2. VICTOR (design gain): For this case, the VICTOR proportional gain G_{qv} is set at 3.6, with the integral gain $G_{\theta v}$ again set at zero. This corresponds to the design case described in Ref. 9 and is intended to give an enhanced control performance over that of the baseline system. These systems are denoted by 1 and 2, corresponding to $\tau_a = 0.2$ and 0.6, respectively.

3. VICTOR (half design gain): Here, G_{qv} is set at 1.8, which represents half the design value of 3.6. This case was included to allow G_{qv} to be increased progressively from zero to the design value. Systems 3 and 4 refer to this controller with $\tau_a = 0.2$ and 0.6, respectively.

4. VICTOR (emulation of baseline): For this case, the baseline system is degraded by halving the gains G_q and G_θ and allowing the VICTOR gains G_{qv} and $G_{\theta v}$ to make up the deficit. The VICTOR noise filter time-constant τ_{NV} is reset to the baseline value τ_v. Systems 7 and 8 correspond to $\tau_a = 0.2$ and 0.6, respectively.

2.7 Implementation of Control Laws in FORTRAN

The control laws described previously in this section have been converted to difference-equation form and specified as a set of subroutines written in standard FORTRAN IV. One of the principal aims of the software design was to produce well-commented, easy-to-follow coding, to ensure that the programs comprised an exact definition of the computing task to be performed. The development of the difference equations used in the software is described in more detail in Refs. 14 and 15. The structure of the software is shown in Fig. 6. Different versions of the coding are given in Refs. 8, 9, and 12, but each version is referred to by a unique one- or two-letter identifier xx. With reference to Fig. 6, each version contains three subroutines:

1. The initialization routine, QINIxx, is called once before engagement to set up the system parameters (gains and filter coefficients, etc.) and to initialize the filters.

2. The control program, QCONxx, takes in pitch rate and longitudinal stick position and generates an elevator demand signal. To minimize computing time delays from input to output, this routine performs only as much of each filter calculation as is needed to produce the output.

3. The filter completion routine, QFILxx, completes the filter calculations ready for the next input sample.

3. RAV SYSTEM OVERVIEW

The F-8C DFBW aircraft contains a triply redundant, full-authority, digital fly-by-wire flight-control system with provisions for accepting single-string (simplex) control-surface commands from a ground-based computer while in a special remotely augmented vehicle (RAV) mode. This mode allows advanced control concepts, such as the CADRE control laws, to be programmed into the ground-based computer. The necessary data are transmitted to the ground and the computer commands are transmitted back to the aircraft, as shown earlier in Fig. 1. The RAV mode is selectable by the pilot. It is a single-string (simplex) system; therefore, if there is any failure, the system automatically switches or can be manually switched back to the on-board digital SAS mode. The CADRE RAV mode allows implementation and changes to the CADRE control laws, which are written in FORTRAN, without disrupting the integrity of the on-board flight system.

In addition to programming the control laws in the ground-based computer, the development and flight qualification of the CADRE system involved an effort in system development. Significant changes and improvements were required for the existing ground and airborne software, Ref. 1, for the CADRE program. Additional failure-detection and identification methods were required for maneuvering flight. An effort was made from the start to develop a failure management strategy that would allow full elevator authority during maneuvering while allowing no failure in the F-8C RAV system to compromise either the fail-operational integrity of the triplex on-board systems, or the flight safety of the aircraft.

Monitoring command software was used for both the simulator testing and during flight. This allowed significant time saving during evaluation, verification, validation, and during flight testing.

Although the rigorous flight qualification standards developed in previous RAV experiments were used, modifications were made in the testing techniques and the procedures to meet the unique requirements of the CADRE system.

3.1 CADRE RAV System

The CADRE RAV system involved mechanization and implementation of various ground and airborne hardware, as well as software interfaces. The primary elements of the hardware used in the F-8C RAV facility are shown in Fig. 7; they are divided between ground systems and airborne systems.

The process starts with parameters being downlinked, including aircraft sensor signals and pilot commands. These signals are received at the telemetry-receiving station and are passed to a downlink telemetry computer which performs the required subframe decommutation and discrete processing of the downlink data. It also formats a data buffer for access by the control-law computer. The downlink data are then interfaced to the CADRE computational algorithms in the control-law computer. An additional computer interface, shown in Fig. 7, is to an external mode-control box. This provides a flexible change to the CADRE control laws between the eight different control algorithms.

The function of the CADRE control-law computer is first to compute the CADRE control algorithms. Secondary functions are real-time input/output computation, fault detection, and ground preflight testing. The program structure has two primary segments. One is a real-time segment which is synchronized to the uplink encoder and operates at an 18.75-msec frame rate. It contains all elements for the eight CADRE control-law configurations, logic for switching between control laws, and the set of failure detection and isolation algorithms that is discussed in Sec. 2. In addition, it contains the input and output routines required for the reformatting of the downlink and uplink parameters and the discrete interface to the mode-control box. The other segment of the program structure is the non-real-time or background segment. All initialization functions and several display routines are processed in this segment. The display routines, which are formatted for a CRT terminal, were designed for ground checkout and testing. In addition, the CRT terminal interface allows selected control system parameters, for example, G_{QV}, to be changed during flight, if desired. The display routines permit the easy monitoring of many of the hardware-to-software interface parameters, internal control variables and states, and failure detection functions. The ground computer software also contains a preflight module that is divided into static checks and a maximum/minimum dynamic check. The CADRE preflight is a monitor-only program; therefore, it can be used during flight if desired. Hard copies may be obtained of not only the preflight tests but of any of the CRT displays.

The CADRE control-law uplink commands are formatted as four 16-bit words of command information and operate on an 18.75-msec frame rate. Each command word contains 10 bits of proportional information; the remaining six bits are used for discrete uplink signals which provide for ground-commanded RAV disengagement. Although the RAV program uplinks the four words *pitch command*, *roll command*, *yaw command*, and *flap command*, the CADRE system only uses the pitch command. The uplink decoder outputs the four digital uplink words, which are then interfaced to the on-board flight-control system. The RAV commands are also sent to the on-board instrumentation system and transmitted via the downlink telemetry for monitoring in ground-based facilities during flight. The CADRE RAV system interface to the on-board flight system was designed to be an independent, pilot-selectable mode. Special care was taken to ensure that the operation of the CADRE RAV mode did not compromise the overall redundancy management and failure strategies of the DFBW flight systems. Therefore, the RAV on-board computer software mechanization included a series of logic statements specifying the conditions for the engagement and disengagement of the CADRE RAV mode; these are discussed in detail in Sec. 3.2.

In addition to pilot selection of the CADRE control modes, all of the engagement conditions had to be satisfied before the CADRE RAV mode became suitable for flight testing. The CADRE system was automatically disengaged, and control was transferred to the on-board SAS, if any of the disengage conditions appeared. In addition, the RAV on-board software contained functions that provided transient-free mode engagement, and command-rate reasonability checks. The on-board computer software was also modified to include command authority floating limits and ultimate g limits. This allows full elevator authority for maneuvering flight, which was needed for CADRE flight-test evaluation, while providing additional on-board protection.

The authority limits and rate-check thresholds were all chosen to ensure that aircraft transients were acceptable in the event of a worse-case hardover failure.

3.2 *Failure Detection and Identification*

The CADRE experiment was designed using a single-string (simplex) RAV system; therefore, redundancy management algorithms commonly used for multiple systems were impossible. Although a previous RAV system had successfully been developed (Ref. 1), it was not a full-authority system and did not require some of the additional concepts developed for this program. The primary features of the CADRE RAV mode-failure-detection system are (1) continuous rate-check testing of the uplink and downlink signals every minor cycle by both the flight and ground computers; (2) inhibition of RAV engagement until certain criteria are satisfied for both computer systems; (3) a wrap test that compares the RAV uplink command with itself sent back on a downlink word; (4) use of a floating window command limiter in the flight computer; and (5) imposition of a g envelope boundary for RAV operation. If a hard failure is declared by either computer system, a RAV downmode automatically occurs whereby the RAV command is faded to the on-board command in 2 sec. The particular cause of the RAV downmode is immediately identified and displayed in real time for downmodes originating from the ground computer. Piloted action is required to activate the RAV failure display code for RAV disconnects originating in the flight computer, and that information is then relayed to the flight controller. The failure detection tests and RAV limiting restrictions will now be discussed.

Ground computer— There are 11 tests for failure monitoring:

1. RAV engagement bias
2. DEUP rate check
3. Stick/trim opposition
4. Wrap test
5. DEP downlink rate check
6. Q downlink rate check
7. DECL downlink rate check
8. DFRAV downlink rate check
9. DYNP downlink rate check
10. Downlink telemetry computer fail
11. CADRE control-law computer fail

Failure identification is displayed in real time both on a strip chart and on a light display on the mode-control panel. Since the RAV mode is susceptible to data spikes caused by temporary loss of the telemetry signal, a hard failure is not declared unless a threshold has been exceeded for n or more consecutive iterations. Once a RAV downmode is commanded, the error must be reset before another RAV attempt is made. Each test will now be described.

Before RAV engagement, the CADRE command is compared with the current SAS command. The difference between the two must be 5° or less, otherwise an engagement bias error is declared that inhibits the RAV mode from engagement. Any command difference less than 5° is added to the CADRE command which then forms the RAV uplink command (DEUP). This bias then becomes fixed upon a successful RAV engagement.

Rate-check testing is performed on the CADRE RAV uplink signals. If the command rate exceeds the rate-check limit, the current command is replaced with the previous one and a counter starts incrementing. As long as this condition exists the RAV command remains frozen until the counter limit is reached and a RAV downmode is declared. If the RAV command becomes less than the rate-check value before the counter limit is reached, the RAV command is allowed to update to the new value, and the counter is reset to zero.

A test is performed that determines whether the trim command is in the same direction as the stick displacement. If the stick deflection exceeds the threshold, and a trim command is in opposition, a counter starts incrementing. When the counter limit is reached, a RAV downmode is declared.

A wrap test performs a closed-loop check of the RAV uplink command with itself which is sent back on a downlink channel. If the difference between these signals exceeds a given tolerance, a counter starts incrementing. When the counter limit is reached, a RAV downmode is commanded.

The proportional downlink words are rate-checked in their raw PCM format form before they are converted to engineering units. If the rate of change exceeds the tolerance level, the previously passed signal replaces the current one and a counter starts incrementing. As long as this condition exists, the passed signal remains frozen until the counter reaches a limit, at which time a RAV downmode is commanded. If the input signal becomes less than the tolerance before the counter limit has been reached, the new signal will be passed through, and the counter will be reset to zero.

The discrete downlink word is tested in a different way. For any discrete change to be recognized it must exist for at least three consecutive iterations; if not, the change is ignored, although no RAV downmode will result. This logic produces a two-sample delay for all discrete changes.

The downlink telemetry computer that first receives the downlink signals is tested in the following way. The computer expects to receive fresh downlink data at a rate of 200 sps, and when it does, a counter is incremented. If the counter fails to advance for five consecutive iterations, a RAV downmode is commanded.

The control-law computer is tested for failures by use of an external hardware watchdog timer. Each time the real-time loop begins execution, a pulse is sent to a timer. Failure to receive another pulse within about 20 msec causes a time out and a RAV downmode will be commanded through hardware.

Flight computer— There are 15 conditions that must be satisfied by the flight computer in order to engage the RAV mode and to stay in that mode. These conditions are as follows:

Not in SAS mode	Not SAS, surface and flap-rate check
Surface rate check	Autopilot engaged
Not SAS and surface rate check	Autopilot disconnect
Engage tolerance failed	Sensor failed
Flap-engage tolerance failed	Uplink failed
Flap rate check	Low-g limit exceeded
Not SAS and flap-rate check	High-g limit exceeded
Surface and flap-rate check	

The display codes are accessible to the pilot upon his request to execute the RAV failure display code program. The major failure testing will now be discussed.

A RAV engage tolerance test is first performed. It looks at the current RAV uplink command and compares it with the present on-board command. They must be within 1° for this test to pass, otherwise a RAV inhibit error will be set to prevent an engagement.

Once the RAV mode has been engaged, the command is rate checked. This test is similar to that of the RAV rate-check test which is done in the ground computer. If the rate of change of the RAV command exceeds 50°/sec, the current RAV command is replaced with the previous one until the counter reaches the limit of 3. When this situation occurs, a RAV downmode is declared from the airborne computer.

A floating window command limiter was added to the airborne software for the CADRE RAV program as a final test to prevent an undetected hardover just below the rate check from coming through to the surface directly. This limiter is illustrated in Fig. 8. Initially, the window is centered at ±3° about the current RAV command. Command rates up to 50°/sec are allowed within the 6° window. The window continuously tries to stay centered on the RAV command, but is only allowed to drift at a maximum rate of 2.5°/sec. Eventually, the RAV command will be rate-limited to the drift rate value until the command rate is decreased or reversed and the window is allowed to recenter as shown in the figure. A rate-limit signal is telemetered to the control room during the flight test whenever the RAV command is rate-limited.

The floating limiter, in combination with the rate-check testing that is resident in the triply redundant on-board systems, provides protection for a full-authority, single-string (simplex), ground-based control system. However, because of other safety considerations, RAV operation at the outer airplane g limits was deemed undesirable. Therefore, a g envelope limit for RAV operation was also added to the airborne system. These limits were set at +5 and -2 g's. If these limits are exceeded, an automatic RAV downmode will result.

3.3 RAV Software Development

Simulation– The CADRE control laws were developed by RAE and supplied to NASA DFRF. The simulation developments at NASA DFRF were performed in two principal stages. The first stage involved development of a real-time, all-digital simulation of the CADRE system – a duplication of the system developed by RAE. Data supplied by RAE were used to validate the simulation. This allowed for consistency checking between results and provided a timely method for evaluating modifications to individual control system filters or combinations of filters for selected inputs.

The second stage was the major simulation effort; it consisted of a CADRE simulation using the F-8C DFBW iron-bird simulation facility (Fig. 9). The iron-bird simulation consists of a decommissioned F-8C aircraft with the following equipment: triplex primary digital system; triplex analog computer bypass; a full set of flight actuators; triplex electrical buses with batteries; triplex hydraulic system; operable auxiliary aircraft systems; and operable cockpit instruments.

The iron bird interfaces with a nonlinear simulation of the F-8C aerodynamics which uses actual surface positions as inputs. The RAV ground computers were used as elements of the total CADRE simulation. The uplink and downlink hardware interfaces were simulated in the simulation computer, and the control laws were implemented on the same type of ground computer that was used during flight.

The iron-bird facility was the key element in the system verification, validation, and flight qualification.

CADRE software verification– The CADRE software verification tests were designed to insure compliance with the software specification. The verification process, which included element-by-element verification, required written procedural descriptions and produced hard-copy test results. All dynamic elements, such as filters, were exercised in a dynamic environment, and responses were compared with independent computer responses based on the desired characteristics. All path combinations of the CADRE control laws were executed. Each test was accompanied by a written verification test report that is under software control management. These reports contain descriptions of test, objective, setup, results, and conclusions.

A comprehensive software configuration control policy was developed based on the previous RAV experience (Ref. 1). Procedures were implemented to govern the verification test requirements, software changes, discrepancy reporting and reconciliation, software manufacture and loading, and documentation requirements.

Not only were written verification tests and results required, as discussed above, but all program changes also required the same documentation. Before the implementation of any program change, approval had to be given by a software control board.

CADRE configuration validation– The overall CADRE system configuration testing was designed to qualify the CADRE ground and vehicle systems and to insure proper system operation. The analysis and validation of the basic system design and mechanization initially used the iron-bird simulation. This facility was used to verify the proper control-law implementation through static and dynamic response tests and through extensive piloted evaluation. The RAV ground computer was used as elements of the total simulation, and the uplink and downlink hardware interfaces were simulated. The RAV simulation ground and on-board

software interfaces were identical to those of the actual aircraft and ground facilities, and the software developed and validated in the CADRE system simulation was used during the CADRE flight operation.

Qualification testing— A series of failure-mode demonstration tests was conducted to insure proper system response to any critical fault. These tests were first conducted on the F-8 iron-bird simulator, then a subset of these tests was repeated during aircraft/ground facility systems tests. In addition, an integrated closed-loop preflight of the total CADRE system was accomplished in which all CADRE input and output parameters were checked both statically and dynamically. As a final step in the flight qualification process, the RAV system operational parameters were monitored during a sequence of flight tests in which the CADRE control laws were operating open-loop. These open-loop monitoring flight tests verified RAV uplink and downlink communication links, telemetry signal strength, and the ground and aircraft synchronization strategies.

4. FLIGHT TESTS

Flight tests of the VICTOR variable-gain control laws commenced in February 1982. The main objective of the tests was to establish whether the variable-gain controller could offer improved control performance over that of a fixed-gain baseline system and whether any adverse handling problems were introduced by the rapidly varying gains. In addition, a comparison has also been made between the baseline controller and a variable-gain system, designed to reproduce, rather than improve, the performance of the baseline. The task used for this assessment has been an air-to-air tracking task, in which the F-8C pilot is required to track an accompanying chase aircraft through a pushover/pull-up maneuver. Details of the maneuver and other test procedures are given in Sec. 4.1. No direct measurement of the accuracy of tracking is available, but indirect indications are obtained from recordings of the system activity and from pilot ratings of the different controllers. These results are presented in Sec. 4.2.

The initial flight tests have highlighted the need for some enhancements of the current variable-gain control laws. Improvements planned include the provision of gain scheduling with dynamic pressure to widen the flight envelope, and the introduction of a rate-limiting term in the variable-gain logic to alleviate the effects of transient, rapid increases in gain, which can lead to the RAV rate limit being exceeded and to a consequent RAV downmode. Following this, it is proposed that three further concepts that have been studied at RAE be introduced into the CADRE control laws. These are (1) overshoot control (Ref. 5), in which the damping properties of the control loop are adjusted during the response to prevent undesirable overshoots; (2) a nonlinear command prefilter (Ref. 16), which is designed to give good response for both target acquisition and tracking; and (3) the self-adaptive technique, INFAIR (Ref. 17), in which the parameters of the command prefilter are adjusted to maintain invariant control response across the flight envelope. Some of these developments are discussed in Sec. 4.3.

4.1 Test Procedure

During the CADRE flight-test program, the F-8C takes off and climbs to the design conditions, normally Mach 0.6 and an altitude of 6100 m, with the on-board stability augmentation system (SAS) engaged in pitch, roll, and yaw. After trimming the aircraft, the pilot engages the RAV pitch mode, thus allowing the longitudinal control to be provided by the experimental CADRE control laws on the RAV ground computer.

The initial tests included testing of the eight CADRE control modes and the longitudinal SAS mode under the following conditions:

1. Nose-up and nose-down pitch pulses input by the pilot
2. Steps input by ground control
3. Rapid climb and descent between 5500 and 6700 m
4. 3-g windup turn

These tasks were used primarily to allow both the pilot and flight-test personnel to evaluate the control-law performance from a stability standpoint before the pilot rated its ability to perform the required task.

The major part of the flight test has been devoted to an evaluation of the CADRE controller for an air-to-air tracking task in which the F-8C pilot attempts to track the accompanying chase aircraft through a maneuver. In this maneuver, the pilot of a target aircraft rolls into a stabilized 3-g turn while endeavoring to keep the designed altitude and speed condition, but allowing altitude loss, if necessary. After turning 180°, the target pilot unloads the aircraft, reverses the direction of roll and pulls a stabilized 3 g's in the opposite direction, again through 180°. A tracking distance of about 300 m has been used to allow assessment of low overshoot CADRE controllers 1, 3, 5, and 7.

For this tracking task, the F-8C pilot was asked to assign a Cooper-Harper pilot rating (Ref. 18); this rating, as well as any other pilot comments on the system, was recorded. In general, the pilot was not told which CADRE controller was in operation. On the flight instruction card, the different controllers were simply referred to as modes A, B, C, etc., with the relationship to the CADRE controllers (1 to 8) known only to the flight-test engineers. This enabled the inclusion of repeat points to establish whether the pilot rating changed during the course of a flight.

Although more complex tracking tasks have been attempted, they have usually led to a RAV downmode because of the elevator rate of g-limit checks. It is possible that the inclusion of a rate-limit controller and gain scheduling (Sec. 4.4) within the CADRE control laws will allow the more complex tracking tasks to be achieved.

4.2 Flight Results

The initial flight tests concentrated on the tracking tasks described in Sec. 4.1, with the target aircraft at a range of about 300 m. The control laws that are designed for the task are modes 1, 3, 5, and 7. For these modes the lead-time constant on the pilot's prefilter is set at 0.2, giving a relatively low overshoot (Sec. 2.3). The controller, with $\tau_a = 0.6$ (cases 2, 4, 6, and 8), giving an overshoot in pitch rate have also been flown for this task, but have usually been given lower ratings. A summary of the ratings of two pilots (pilots A and B) for the eight CADRE controllers defined in Sec. 2.7, together with the on-board SAS system, is given in Table 1. The ratings in the table are for two particular flights but they are representative of ratings assigned after all five flights to date. The SAS mode uses washed out pitch-rate feedback to improve the short-period damping; since it is implemented on the on-board system, no additional RAV time delay is involved.

From Table 1, it can be seen that the pilots have consistently rated the mid-gain VICTOR system (mode 3) higher than the other CADRE controllers. Some basis for this rating can be found in Fig. 10 where flight records for the tracking maneuver for case 5 (baseline) and case 3 are compared. First, from the pilot input traces of Fig. 10a, it can be seen that the pilots were able to reproduce the maneuver very accurately, in that the variation of pitch-rate demand with time is virtually identical for the two modes. The low-amplitude, high-frequency bursts on the elevator demand signal for mode 3 of Fig. 10b show the influence of the VICTOR loop in widening the bandwidth of the controller. That the extra bandwidth is significant can be judged from the pilot ratings and a comparison of the VICTOR gearing (VQ) time histories of Fig. 10c. The activity of the VICTOR gearing is a convenient measure of how well the control demand is being satisfied, since the gearing increases toward unity when the difference between demand and response exceeds a prescribed threshold. In the traces of Fig. 10c, the VICTOR gearing is below one for a considerably greater part of the maneuver in case 3 than in case 5, indicating the greater degree of control afforded by the VICTOR controller.

Further observations of the different controllers in the tracking task and pilot comments about them are summarized below.

1. Baseline system (case 5): Generally, the baseline pitch-rate controller was rated slightly better than the on-board SAS controller. Control was precise and stable, but the initial response to a stick input was thought to be rather slow. The pilot rating was 4 to 5.

2. High-gain VICTOR system (case 1): There were stability problems with the design case (case 1) of VICTOR. In particular, the short-period mode was poorly damped and any attempt to use this controller for tracking led to a rate limit and a RAV downmode. The inadequate damping for this case was due to the time delay in flight, which has been estimated at about 100 msec. This was greater than the 50-msec delay used in the original design. It is anticipated that the performance of this controller will be improved by the introduction of rate limit and overshoot control elements. These are discussed in Sec. 4.3. No pilot ratings were given because of the stability problems.

3. Mid-gain VICTOR system (case 3): In general, this controller was preferred for the tracking task, giving precise control with at most one overshoot. A consistent pilot rating of 3 was obtained and flight traces indicate that the error between demand and response was usually smaller than with the other systems, with the result that the VICTOR loop was active for less time (see Fig. 10). One test has been performed with gain between the mid- and high-gain system, cases 3 and 1. Indications are that there is an improvement in pilot rating from 3 to 2 for small increments in maximum variable gain ($G_{qv} = 2.2$). This may imply that an optimal value of G_{qv} may be determined, given the present system.

4. VICTOR emulation of baseline (case 7): The pilot rating for this case was similar to that for the baseline (case 5). Nevertheless, the pilots could detect a difference between the two controllers, in that case 7 was thought to give less precise control, with slightly lower damping than the baseline. (In fact, the damping levels for cases 7 and 5 are the same; therefore, the perception of lower damping levels may be the start of a PIO as the pilot reacts to the controller breaking out from the low-gain condition.) Flights are planned with different values of the threshold, which will give further information on this effect.

5. System with pitch-rate overshoot (cases 2, 4, 6, and 8): These systems were designed for tracking at a range of under 150 m, but have been assessed in the 300-m tracking task. It can be seen from Table 1 that the pilot ratings are less consistent and more adverse for their controllers than the low overshoot modes. Pilot comments would seem to show some influence of the time delay in that the systems appeared to give very little reaction initially followed by a sudden rapid response which did not find favor with the pilots. For close-range tracking, this effect may not be so pronounced, since the task is governed by height changes which tend to lag the pitch-attitude changes. These will be evaluated in future flight tests, using a simulated refueling task.

5. FURTHER DEVELOPMENTS

Enhancements to the CADRE controller to be introduced in the near future are described below. These are concerned with gain scheduling, rate-limit control, and the reduction of overshoots.

5.1 Gain Scheduling

The CADRE controllers were designed for a fixed flight condition (Mach 0.67 at 6100 m). During the pushover/pull-up tracking maneuver, the pilots experienced some difficulty in maintaining the design conditions, with the result that as Mach number increased or altitude decreased, some loss of stability was experienced. To overcome this problem, the closed-loop gains are to be scheduled with the reciprocal of the measured dynamic pressure q, so that as altitude decreases or Mach number increases, the gains will reduce and stability will be restored. A scheduling relationship for the closed-loop gain G_a and for the feed-forward gain K_a (Fig. 4), has been selected and is being incorporated in the CADRE software.

5.2 Rate-Limit Control

One of the safety checks incorporated in the RAV system ensures that control reverts to the on-board system should the demand to the elevator exceed a certain rate (Sec. 3). This has proved a limiting factor in testing some of the CADRE controllers, particularly the high-gain VICTOR systems (1 and 2). Further design studies have shown that the high rate of change within the VICTOR loop is due mainly to the rapid increase in the gearing V_q associated with an increase in control demand. In fact, the successful operation of the variable-gain controller is not significantly affected by these high rates and hence a form of rate-limit control can be introduced with little or no performance penalty. In Ref. 19, several alternative rate-limiting strategies are compared for both fixed- and variable-gain controllers. The schemes proposed are based on continuous representations of the control system and require an estimation of the extent to which the rate-limit is exceeded, so that the effective gain can be reduced by using an appropriate feedback whenever rate limiting is imminent. However, for an implementation such as that used in CADRE, a relationship between the variable gearing V_q and the demanded control rate exists, so that the rate of control can be limited by adjusting V_q directly.

5.3 Overshoot Reduction

A nonlinear technique for reducing the magnitude of response overshoots has been proposed recently (Ref. 5). It is based on the argument that when the control is reducing, the magnitude and rate of change of this error can be used to predict a possible overshoot. In such a case, an additional control term can be introduced to increase the effective damping. The dramatic effect of such a term is shown in Fig. 11, where the technique is applied to the high-gain VICTOR system (case 1) with a time delay of 100 msec. It can be seen that the undesirable oscillatory response is much reduced, without a significant effect on the initial rate of response when the overshoot control term is introduced. It is expected that the influence of the time delay will be crucial in this application, with an effect not only on the damping of the system but also on the timing of the overshoot control term. Figure 11 also illustrates the effect of rate-limit control, with the onset of the overshoot control switch held back to ensure that the elevator demand rate does not exceed 50°/sec.

5.4 F-8C RAV Facility

One current constraint associated with the RAV facility is the time delay introduced by the telemetry communication with the ground-based computer. The RAV system mechanization for future programs will have significantly less delay. Improvements in the uplink hardware systems provide at least a tenfold increase in system bandwidth, as well as an uplink and downlink synchronization capability. These features will allow the RAV time delay to be reduced to a minimum.

6. CONCLUDING REMARKS

A major benefit of the NASA Dryden F-8C remotely augmented vehicle (RAV) facility is a reduction in the resources required to implement experimental control laws in the flight-test program, since the safeguards built into the facility obviate the need to produce flight-critical, high-integrity software. Furthermore, the control-law software is written in a high-level language (FORTRAN) and the structure and logic are, therefore, readily understood by the engineers and scientists working on the program. Additional safeguards introduced to the RAV facility for the NASA/RAE CADRE program have proved very successful in widening the maneuver envelope of the aircraft, while maintaining a low level of uncommanded reversions to the on-board system.

The additional time delay associated with the current RAV facility did influence both the stability and handling assessment of the experimental control laws. Nevertheless, meaningful results can be obtained by comparing the behavior of different control laws when the time delay is present.

The initial stage of the CADRE program has successfully illustrated the potential of variable-gain control laws, which allow the closed-loop gains to rise transiently to levels that would not be desirable for continuous operation owing to excessive noise-induced actuator activity. As a result of experience gained during the first stage of flight experiments, the introduction of improvements to the variable-gain control laws and the inclusion of further nonlinear techniques developed by RAE are planned in the near future.

REFERENCES

1. Petersen, K. L.: Flight Experience with a Remotely Augmented Vehicle Test Technique. AIAA/SETP/SAE Flight Testing Conference, Las Vegas, Nevada, Nov. 11-13, 1981.

2. Gill, F. R.: Ideas for Future Efficient Flight Control Systems. RAE Tech. Memo FS 256, 1979.

3. Gill, F. R.: Design Considerations for Optimal Flight Control Systems. AGARDograph 251, Theory and Applications of Optimal Control in Aerospace Systems, 1979.

4. Gill, F. R.: Nonlinear Pitch Rate to Elevator Control Laws for a Combat Aircraft. RAE Tech. Report 79075, 1979.

5. Gill, F. R.: Design Study of Nonlinear Control Laws for Automatic Approach and Landing: Part 1, Airspeed Hold. RAE Tech. Report 80096, 1980.

6. Gill, F. R.: Engineering of Control Systems and Implication on Control Law Design. AGARD Lecture Series 89, 1977.

7. Jones, J. G.: Design of Control Laws to Implement ACT Benefits. Aeronaut. J., vol. 84, 1980, pp. 13-21.

8. Butler, G. F.; Mepham, S.; and Corbin, M. J.: The Design and Software Specification of a Variable Gain Pitch Rate Control Algorithm, VICTOR-E, for the NASA F-8C Digital Fly-by-Wire Aircraft. RAE Tech. Memo FS 415, 1981.

9. Corbin, M. J.; and Winter, J. S.: TSIM — A Combined Analysis Package for the Design of Flight Control Systems. RAE Tech. Memo FS 185, 1978.

10. Corbin, M. J.: A Computer Package for the Analysis of Discrete-Time Flight Control Systems. RAE Tech. Report 80106, 1980.

11. Butler, G. F.; Mepham, S.; and Corbin, M. J.: Nonlinear Control Laws for the NASA F-8C Digital Fly-by-Wire Aircraft: Final Software Specification for VICTOR-E. RAE Tech. Memo FS 416, 1981.

12. Hartmann, G. L.; Hauge, J. A.; and Hendrick, R. C.: F-8C Digital CCV Control Laws. NASA CR-2629, 1976.

13. Corbin, M. J.: The Design of Digital Filters for Time-Varying Flight Control. RAE Tech. Report 80149, 1980.

14. Corbin, M. J.: A Nonlinear Prefilter for Digital FBW Control Systems. RAE Tech. Memo F[illegible]50, 1982.

15. Winter, J. S.: A Nonlinear Control Law for FBW Aircraft and Its Use in Target Acquisit[illegible]and Tracking. RAE Tech. Memo FS 177, 1978.

16. Gill, F. R.; and McLean, D.: A New Model-Reference Adaptive Scheme for Aircraft Flight [illegible]rol Systems. Trans. Inst. Measure. Control, vol. 1, no. 1, Jan. 1979.

17. Cooper, G. E.; and Harper, R. P.: The Use of Pilot Rating in the Evaluation of Aircraf[illegible]g Qualities. NASA TN D-5153, 1969.

18. Murphy, L. M.: A Comparison of Aircraft Flight Control Laws Designed to Reduce the Effects of Actuator Rate Limiting. RAE Tech. Report TR 82005, 1982.

TABLE 1. SUMMARY OF PILOT RATINGS FOR AIR-TO-AIR TRACKING TASK

System	Description	Rating	
		Pilot A	Pilot B
On board			
SAS	Stability augmentation system; no time delay	5-6	5
Low overshoot controllers			
Baseline	CADRE baseline controller	4	5
VICTOR	High-gain variable-gain controller	--	--
VICTOR	Mid-gain variable-gain controller	3	3
VICTOR	Variable-gain simulation of baseline	4	5
Higher overshoot controllers			
Baseline	CADRE baseline controller	4	7
VICTOR	High-gain variable-gain controller	--	--
VICTOR	Mid-gain variable-gain controller	4	5
VICTOR	Variable-gain simulation of baseline	4-5	10

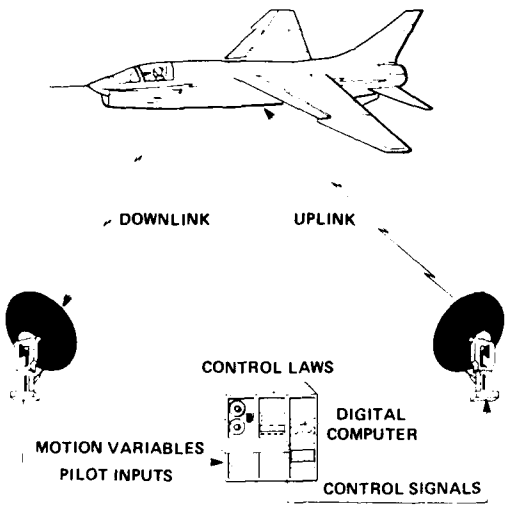

Fig. 1. F-8C DFBW RAV flight test technique.

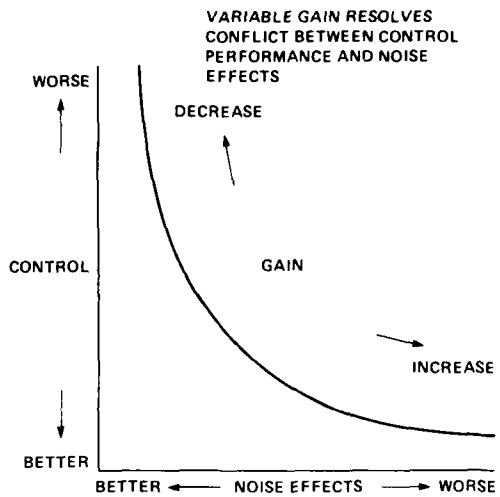

Fig. 2. VICTOR nonlinear control policy.

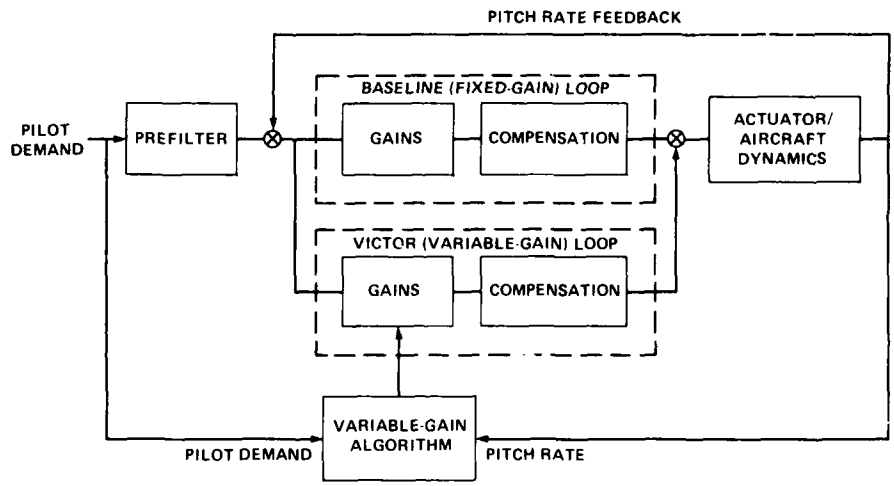

Fig. 3. General structure of RAE nonlinear pitch-rate controller.

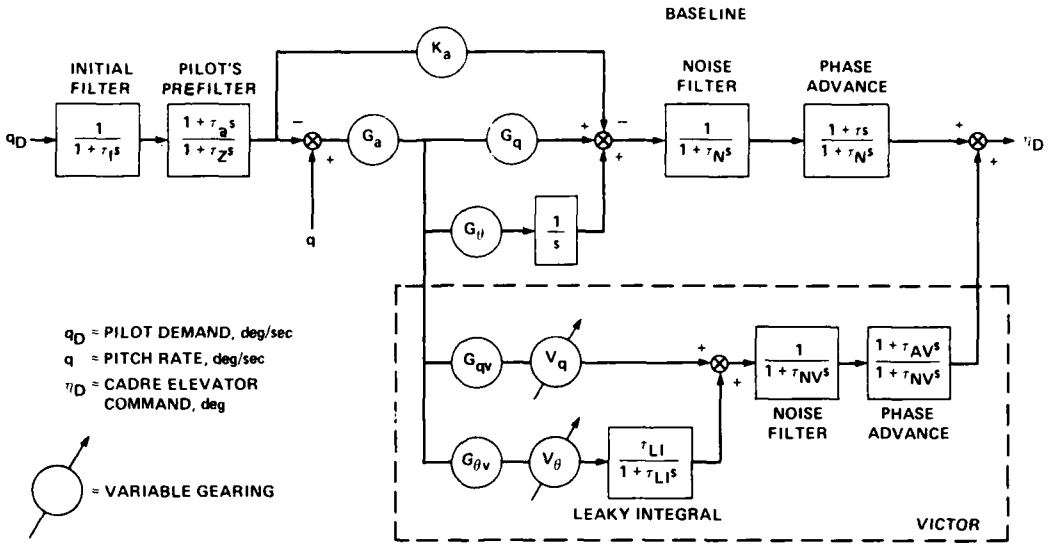

Fig. 4. Baseline plus VICTOR-E pitch-rate controller.

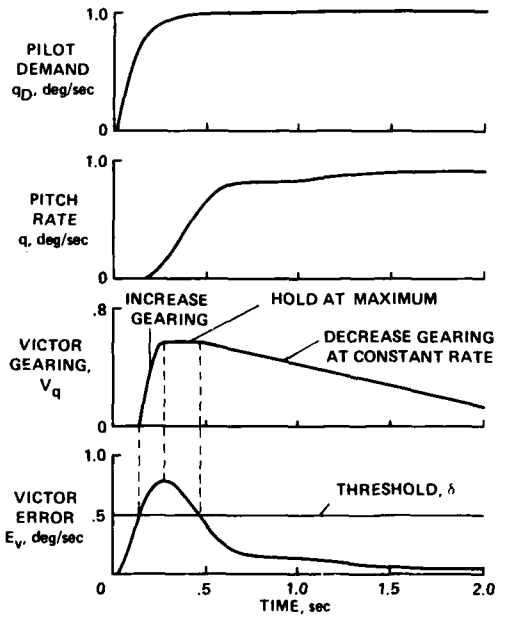

Fig. 5. Operation of VICTOR-E algorithm.

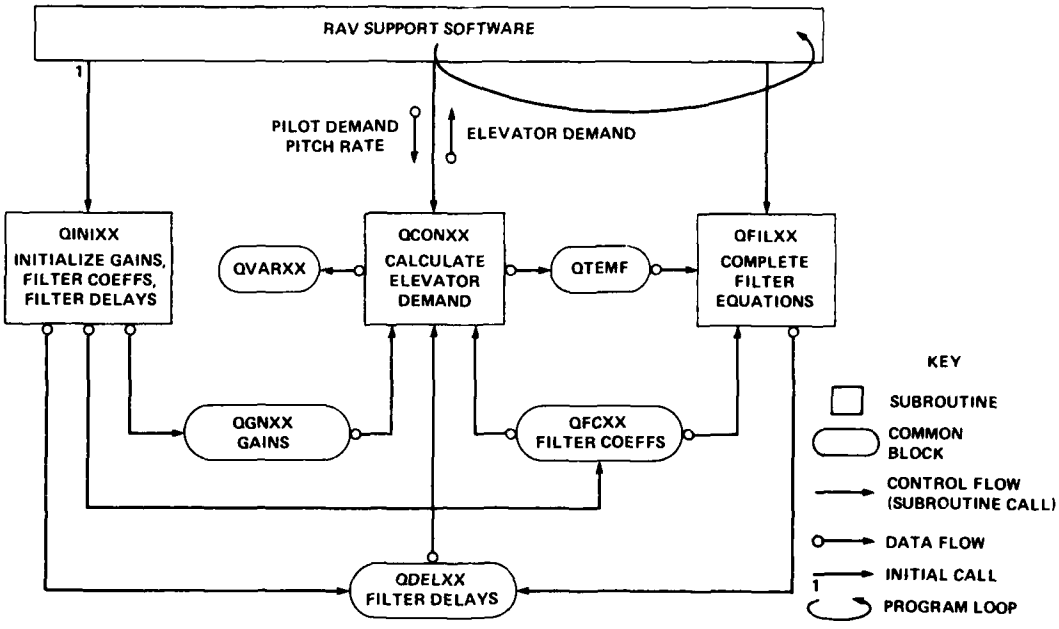

Fig. 6. Software structure for CADRE control laws.

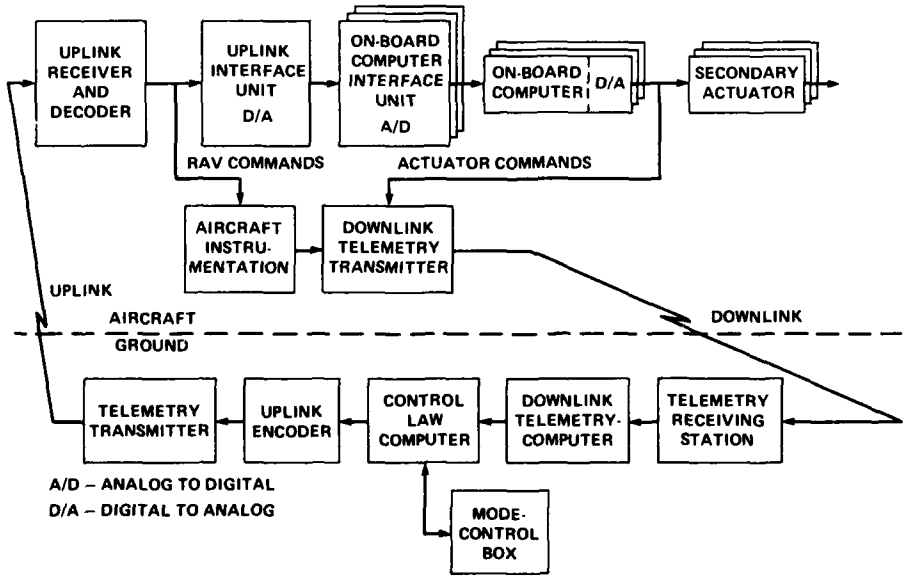

Fig. 7. Primary hardware elements of RAV system.

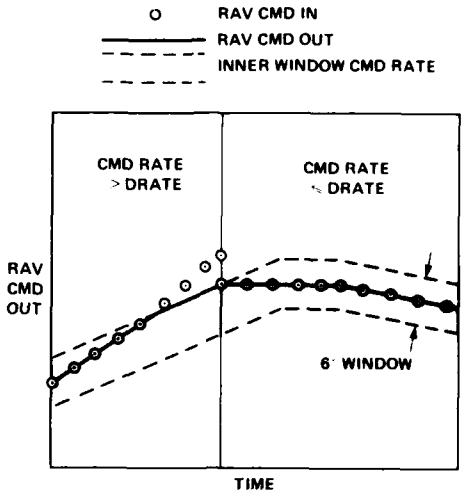

Fig. 8. F-8C DFBW floating RAV limiter.

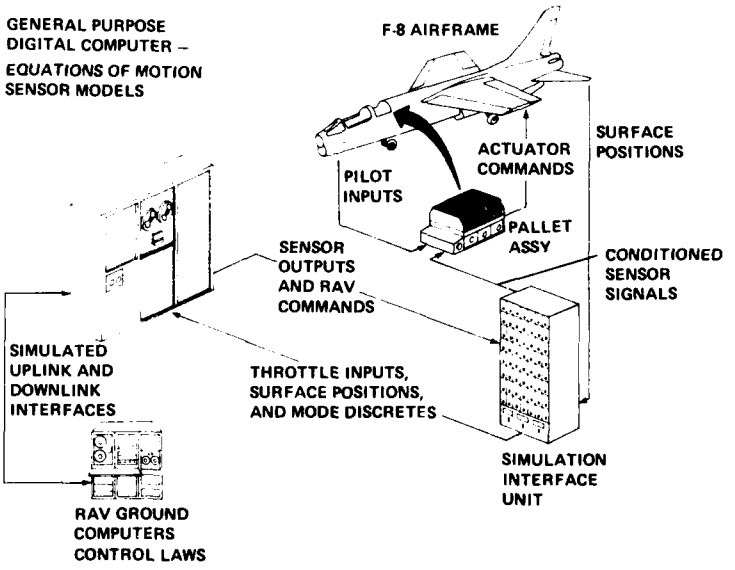

Fig. 9. F-8C DFBW iron-bird simulation facility configured for RAV system testing.

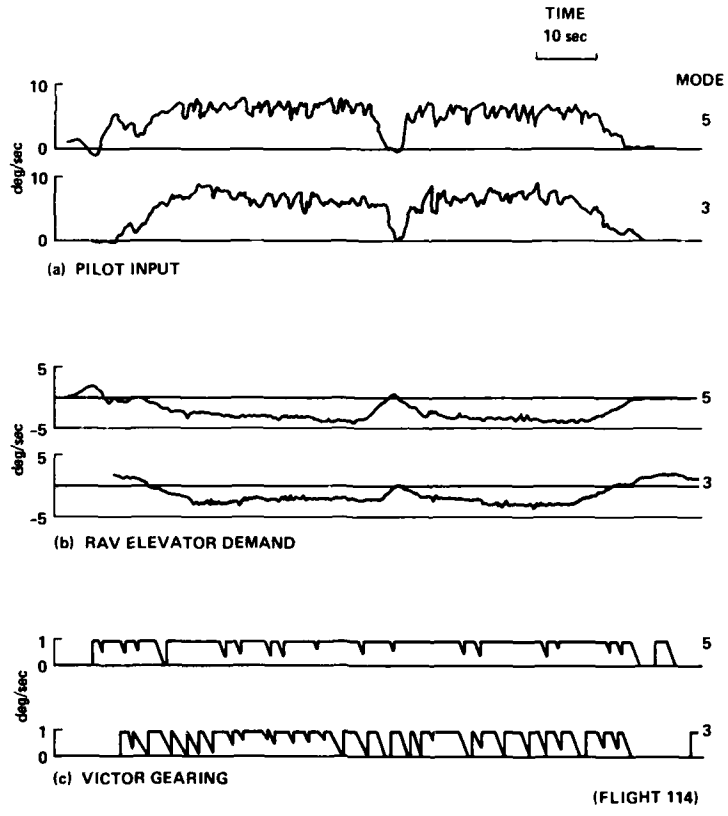

CONTROL MODE: BASELINE, PILOT RATING (4)
CONTROL MODE: MID-GAIN VICTOR, PILOT RATING (3)

Fig. 10. Flight traces for baseline and mid-gain VICTOR systems.

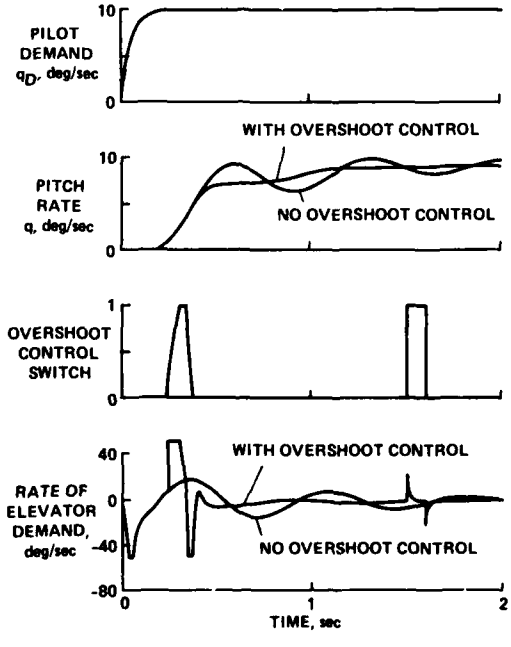

Fig. 11. Effect of overshoot control.

FLIGHT TEST EXPERIENCE WITH A DIGITAL INTEGRATED GUIDANCE AND CONTROL SYSTEM IN A CCV FIGHTER AIRCRAFT

by
U. Korte
MESSERSCHMITT-BÖLKOW-BLOHM GMBH
Aircraft Division
8000 München, Postfach 801160
FRG

SUMMARY

A quad redundant digital FBW Control System for a highly unstable fighter aircraft has been developed and flight tested by MBB in a single seater F-104 G which had been modified as a CCV demonstrator. The CCV program was funded by the German MOD.

From Dec. 1977 to Nov. 1981 a total of 118 flights has been conducted. During these flights the quadruplex system was successfully tested for five different configurations starting with the highly stable basic aircraft and ending up with the highly unstable canard configuration with a static instability up to 22% mean aerodynamic chord (MAC).

Some of the results obtained regarding control system design, handling evaluation and redundancy management with the digital system will be presented.

1. INTRODUCTION

The objectives of the German CCV-Demonstrator Program were to develop and flight test a quadruredundant digital fly-by-wire control system and to investigate the stability and control characteristics of a supersonic aircraft throughout the flight envelope with up to 20% negative static margin. (Optimum performance improvement of future aircraft resulting from relaxed static stability will be reached at an degree of instability of 10 ~ 20% MAC.)

First a brief description of the system and control concept will be given. Thereafter some problems and results of the flight tests will be discussed.

2. PROGRAM DESCRIPTION

2.1 Destabilisation and Flight Test Sequence

The desired degree of instability of the demonstrator aircraft was obtained by mounting a canard surface above the forward fuselage and adding 660 kg aft ballast (Fig. 1).

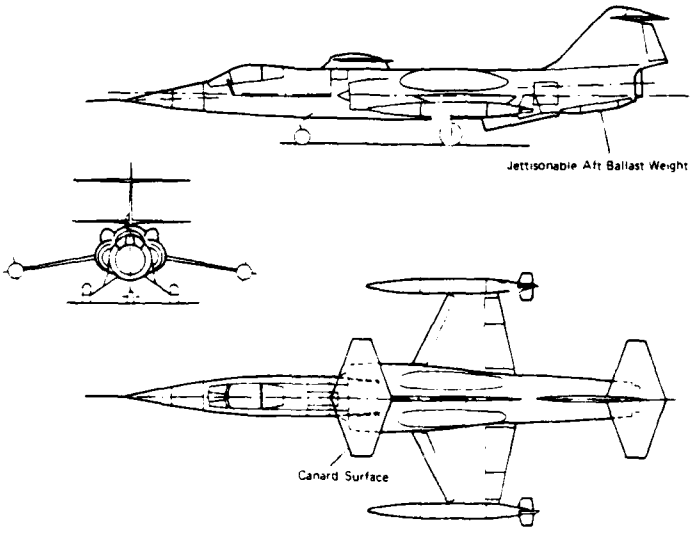

Fig. 1 DESTABILISATION CONCEPT

By the fixed canard the aerodynamic center is moved forward by approximately 35% whereas by the tail ballast the center of gravity (c.g.) is moved to the tip-up aft limit.

Destabilization of the CCV aircraft was done in several steps. This is shown in Fig. 2.

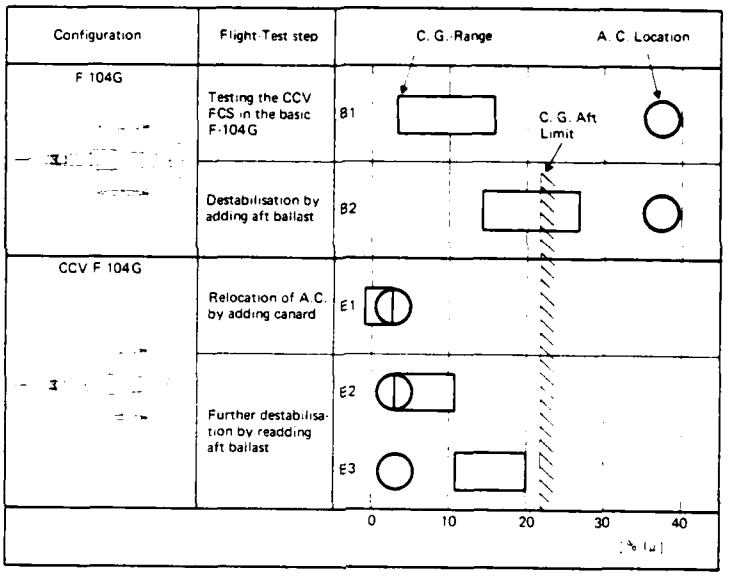

Fig. 2 FLIGHT TEST SEQUENCE

The B 1 configuration is the basic F-104 G configuration which was used for a thorough flight testing of the newly developed digital FBW system. In B 2 600 kg aft ballast were added thus reducing static stability to approximately 10% MAC. In E 1 the canard was mounted. As forward tank fuel is not used here and 212 kg front ballast are added this configuration is still stable and can still be flown manually if necessary. It was therefore the back up configuration for the unstable E 2 and E 3 configuration. In E 2 the canard configuration is destabilized by 400 kg aft ballast. In E 3 further destabilization is reached by increasing the aft ballast to 660 kg and by reversing the sequence of fuel usage. Now forward tank fuel and then main tank fuel is used before tip tank fuel.

2.2 Safety system

Due to limited funding no iron-bird ground test rig could be built. Therefore the original FCS of the F-104 G was maintained as a mechanical back up.

By pulling the stick trigger the pilot can always switch from the FBW-System to the mechanical system.

2.3 Restabilization

In an emergency situation the unstable demonstrator aircraft can be restabilized by dropping the aft ballast (E 2 configuration). In the E 3 configuration fuel transfer from the tips to the forward tank is additionally required. Thereafter the aircraft can be flown with the mechanical back up. In E 2 and E 3 switch over to MEC is coupled with the tail ballast dropping mechanism.

Ballast jettisoning was successfully demonstrated in FBW Mode in the B 2 configuration (400 kg lead shot).

3. THE CCV FLIGHT CONTROL SYSTEM

3.1 Main features

The newly developed CCV-FCS has already been described in detail in Ref. 1. Therefore only the main features of the system are repeated here:

- Double fail-operational redundancy
- Digital data processing and system monitoring
- Application of multivariable control theory
- Integration of ADC, CSAS, Autopilot, Navigation and BITE functions in each computer
- Central inertial sensors with strap down capability
- Skewed flow direction sensors (α, β)
- Modular, selfmonitoring secondary actuators

The double fail-operational redundancy is provided by a four channel system (quadruplex) with parallel signal processing where failures are detected, localized and isolated by majority vote. A system overview is given in Fig. 3.

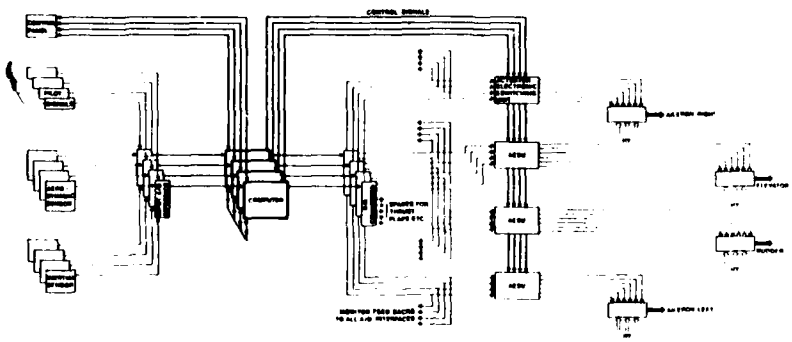

Fig. 3 SYSTEM OVERVIEW

The four identical computers are 16 bit computers with 16 K memory. They run identical software and communicate with each other via fast data lines (direct memory access). Each computer performs the following functions:

- Stabilization and Control
- Autopilot
- Air Data Computation
- Inertial Navigation (Strap down)
- Preflight Check out
- Redundancy Management

The necessary signals for the guidance and control system are supplied by a number of sensors which can be seen in the more detailed picture of Fig. 4.

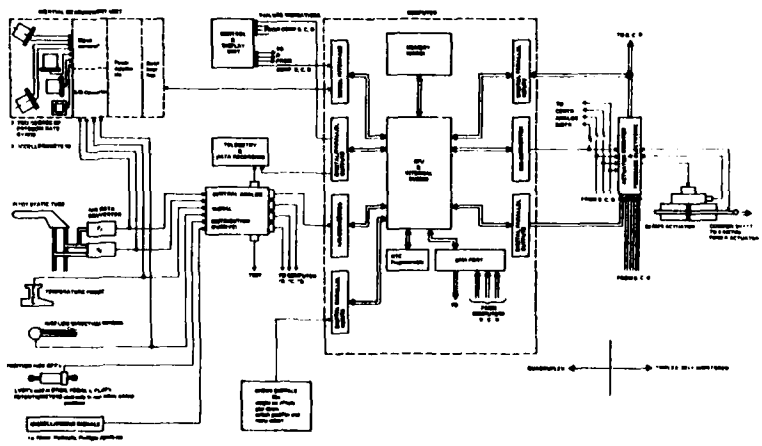

Fig. 4 CCV-F-104 G
GUIDANCE & CONTROL SYSTEM
(One Channel)

A list of the measured variables is given in Fig. 5.

α	– angle of attack	$\dot{h}$	– vertical velocity
β	– angle of sideslip	V_{GSP}	– ground speed
p	– roll rate } body fixed	χ	– ground track angle
q	– pitch rate } body fixed	γ	– flight path angle
r	– yaw rate } body fixed	Δy	– cross track error
Φ	– roll angle	Φ^*	– geographic latitude
Θ	– pitch angle	λ	– geographic longitude
Ψ	– heading	P_s	– static pressure
V	– total velocity	q_c	– dynamic pressure
h	– altitude	T_t	– total temperature

Fig. 5 MEASURED VARIABLES

3.2 Control System Design

The FCS of the CCV aircraft is a digital FBW-System with 100% authority. In this system the pilot no longer commands control surface deflections but desired values of normal acceleration, roll rate (around the velocity vector) and sideslip respectively. With the pedals untouched, automatic turn coordination is provided. Fig. 6 shows a 360°-roll for the unstable E 3 configuration.

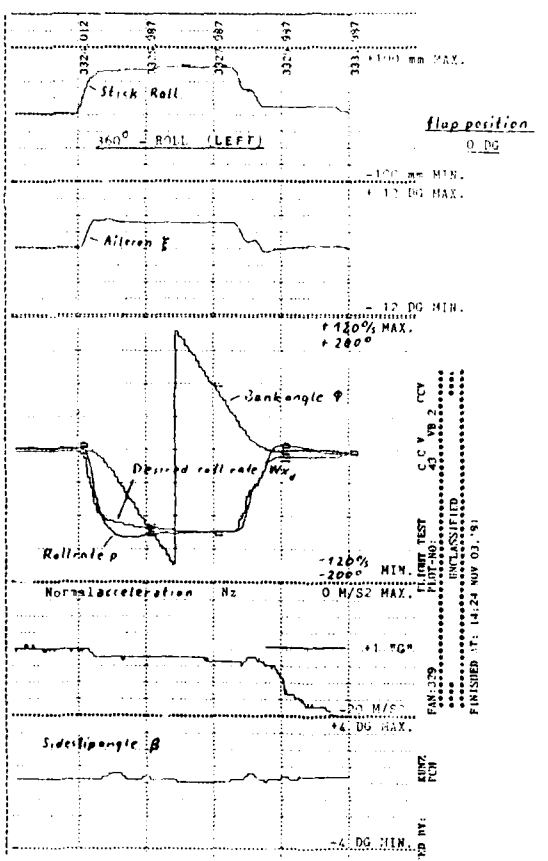

Fig. 6 360° - ROLL (LEFT)

It can be seen that there is no variation of load factor and sideslip with bank angle. Sideslip at the beginning and the end of the manoeuvre is less than 0,5 degrees.

One of the unusual features of the control system is attitude feedback in the manual control mode (switched off in ground operation). This leads to a reduction of pilot workload by making the aircraft more 'stable' and was commented favourably by the pilots who judged this feature as an excellent means for general aircraft handling although there was some criticism regarding the aircraft flare behavior. This is discussed in section 4.

Fig. 7 shows the basic structure of the control system which was remained for all five different configurations.

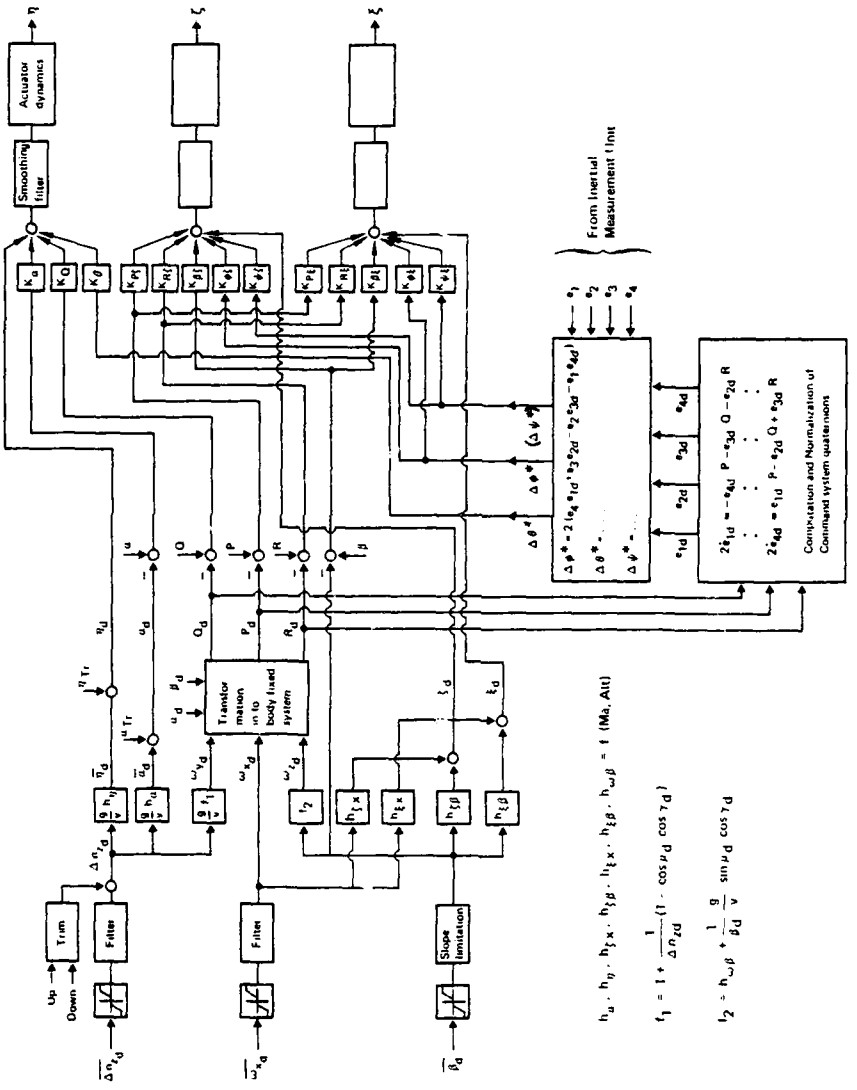

Fig. 7 CCV-GUIDANCE AND CONTROL SYSTEM (SCHEMATIC)

Linear controllers with proportional output vector feedback are used for the longitudinal and lateral motion. Feedback signals are angle of attack α, sideslip β, rates p, q, r and pitch and roll attitude Θ, ϕ.

Compensation of coupling effects is done via the nonlinear command system which interconnects all three axes of the aircraft (Ref. 2).

Design of the control laws was based on linear control theory for multivariable systems using computer aided design methods. It was done in the discrete time domain.

Therefore no compensation for the effects of sampling was required which otherwise would have been necessary due to the low sampling rate of 16 2/3 Hz.

The feedforward and feedback coefficients were evaluated for each configuration for a number of reference points in a Mach, altitude grid. They are stored in the computer memory. Between the reference points the coefficients are linearly interpolated. The maximum allowed desired values Δn_{zd}, w_{xd} and β_d are also functions of Mach and altitude.

Structural coupling ground tests with the closed loop system showed the necessity for filtering of pitch and roll rate. (The rate gyros of the IMU-System are mounted in the nose cone.) Therefore structural filters had to be introduced.

For the yaw axis ground test had shown sufficient structural damping but during the first closed loop flights a yaw oscillation of 6,8 Hz occurred and lead to the aposteriory installation of a yaw rate notch filter. Due to the flexibility of the digital system this was no problem at all and could be done within a few days. All filtering was done digitally, with a sampling rate of 50 Hz for the structural filters.

4. FLIGHT TEST EXPERIENCE

4.1 Testing of the Different Configurations

Before the first closed loop flight with the new control system, direct link flights (1:1) in FBW were conducted with 50 Hz sampling first and then with 16 2/3 Hz to see whether the low sampling rate would degrade aircraft handling. This was not the case.

For the B 1 and B 2 configuration the MIL-Spec requirements for frequency and damping of the short period and dutch roll mode were fulfilled from the beginning. Therefore, no change of the theoretical feedback coefficients was required. However, some modifications became necessary for pitch and roll control during landing. In roll pilots complained about the late roll onset and to high a minimum achievable roll rate. The problem could be solved by the following measures:

- Change of the roll stick shaping filter from second order to first order.
- Minimisation of the dead zone (software) around the roll sticks neutral position. These measures reduced the phase lag.
- Reduction of maximum desired roll rate w_{xd} below Ma = 0,4 (fading between Ma = 0,4 and Ma = 0,3).
- Adaptation of the direct link gain (aileron angle due to commanded roll rate)

In a second step the time constant of the stick shaping filter was reduced to 50%. Thereafter pilot ratings were good for all weather conditions.

In pitch an overcontrol tendency was observed during the landing flare phase which was unpredicted by PIO-evaluations. It was not considered safety critical but pilots wanted improvement. After removing the stick command pitch filter pilot ratings (Cooper-Harper) of 3-4 were given.

In some flights (B 2 and E 1 configuration) the attitude feedback was switched off by the pilot before landing. Here Cooper-Harper ratings of 2 were given. This indicates that not any phase lag in the low sampled digital system was responsible for the deficiencies, but the different control strategy during round out in attitude 'on' mode. In the attitude feedback system definite forward stick pushing is required if the pilot wants to lower the nose of the aircraft whereas with attitude 'off' he just has to release the stick. This is the conventional procedure he is used to.

The first flight in the canard configuration E 1 (practically a new aircraft) was without any problems. Handling characteristics were very favourably commented on by the pilot.

The whole first flight was made in FBW-Mode because simulator studies had shown better handling in FBW than in the mechanical back up mode. Especially take off in MEC might have been critical due to a strong pitch up tendency.

In later flights bad damping at high Mach numbers was observed. This was due to an incorrect description of the aerodynamics of the canard aircraft at higher Mach numbers. Parameter identification and subsequent modification of the controller coefficients solved the problem.

When enough experience had been gathered with the stable canard aircraft E 1 flight testing of the unstable canard configurations E 2 and E 3 was taken up. After the prior thorough flight testing these tests could be completed rather fast. From July to November 1981, 22 flights were conducted, 14 flights in the moderately unstable E 2- and 8 in the highly unstable E 3 configuration. The highest instability reached in normal flight was up to 22% MAC at about 11° α.

The aircraft was always easily controllable with the CCV-FCS even when during landing - not quite planned - an instability of 16% was reached due to an malfunctioning of tip fuel feeding.

Fig. 8 shows a wind up turn in the unstable E 3 configuration. With increasing angle of attack the instability becomes obvious by the stabilizer moving in a positive direction (contrary to the stick). For comparison in Fig. 9 the same manoeuvre is shown for the stable E 1 configuration. Here stick and stabilizer move in the same direction. The pilot reported good control and very nice constant stick force gradients.

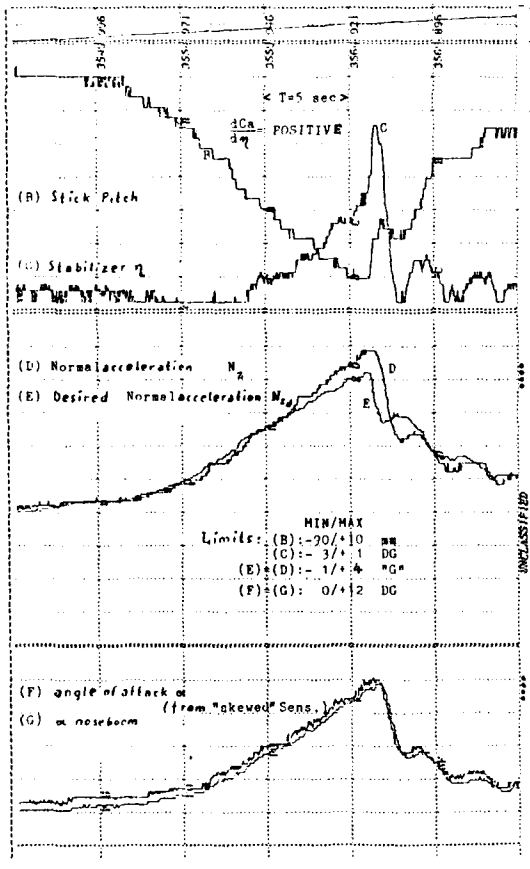

Fig 8 WUT: UNSTABLE E 3 CONFIGURATION

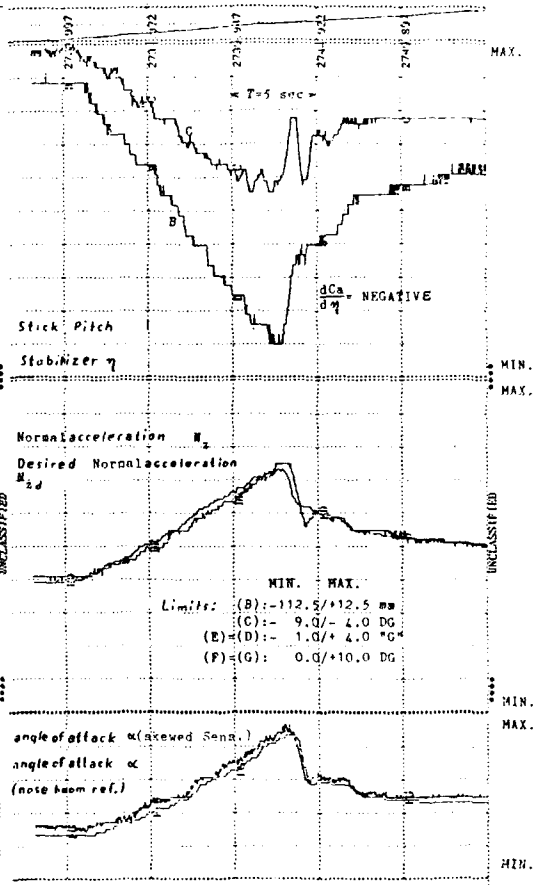

Fig. 9 WUT: STABLE E 1 CONFIGURATION

4.2 The 'Backswing' Problem

One problem which was mainly observed in the canard configuration was a two-step-rate response with 'backswing' after a pitch stick command (Fig. 10). Although for manoeuvering, limited tracking and wind up turn, aircraft control seemed very good, this control behaviour caused problems for small attitude changes, speed changes and precise small pitch corrections.

By introducing stick shaping filters aircraft behaviour could be significantly improved. In Fig. 11 pitch step response after introduction of the filter is shown (same flight condition, same configuration).

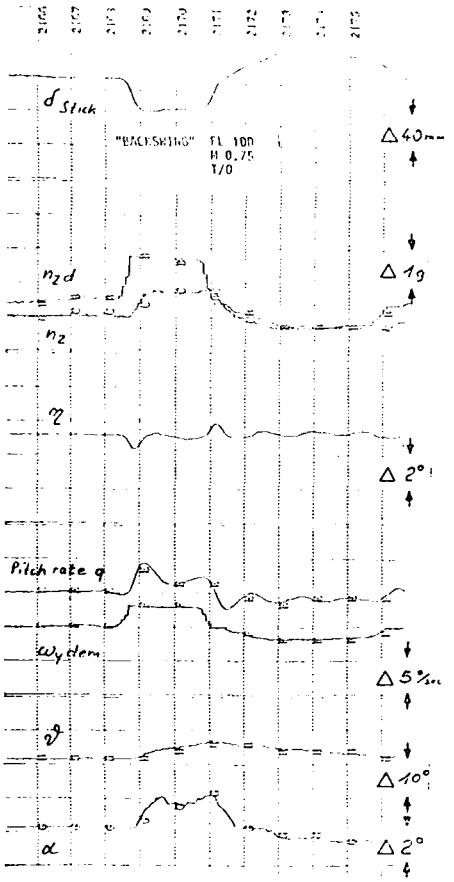

Fig. 10 BACKSWING

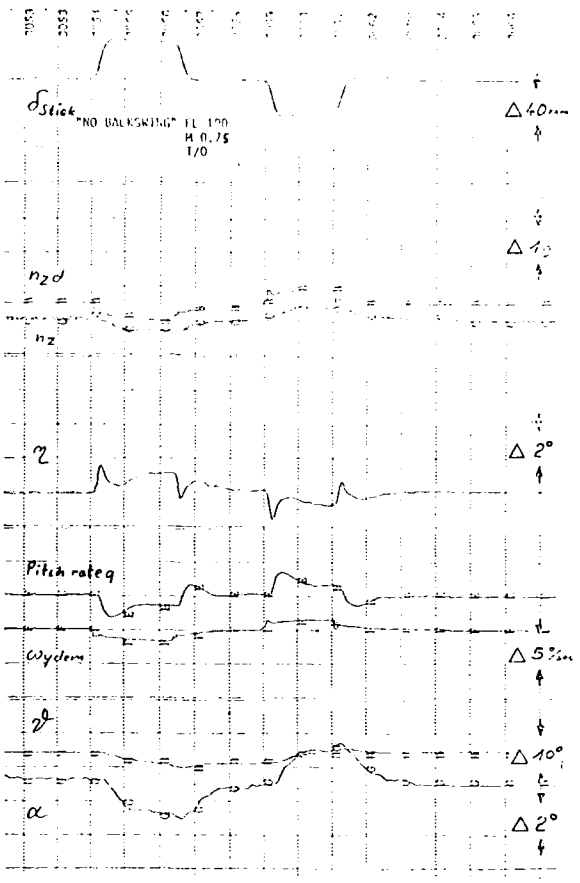

Fig. 11 NO BACKSWING

After termination of the unstable aircraft testing some additional flights in the E 1 configuration were made in 1982 where the coefficients of the shaping filters were changed depending on Mach numbers and altitude thus further optimising pitch response - as the pilot wrote in his flight report 'to an almost excellent level exceeding aircraft handling in stable configurations with mechanical control systems'.

Such sophisticated mechanizations are no problem in digital systems. The required program change (assembler) and testing was done within less than a fortnight.

In the shaping filters a direct throughput was maintained to avoid increased time delay.

4.3 Trimming in Pitch and Roll

One last problem which shall be addressed is pitch and roll trim.

When the FCS was first designed it was thought unnecessary to have a special trim possibility because in a rate command system the stick is in the neutral position for steady flight. But after the first simulations pilots insisted on the introduction of a trim possibility - first in pitch, than in roll too -.

In the FBW mode no trim motor is used because it would be counteracted by the controller (unlimited authority). Trim inputs are given via the non-linear command system, that is, they are identical to small stick inputs.

In roll a fixed value $w_{xd\ TR}$ is commanded by the trim button. It becomes zero again when the button is released.
Small precise roll angle corrections can be made with this system.

Different to roll in the first mechanization the pitch trim button commanded an increasing Δn_{zdTR} which was held constant at release. This was for enabling trimmed turns (for 60° bank a Δn_{zd} of 1 is required equivalent to a load factor of 2). However, with this system it was very hard to find the trim neutral point and quick stabilization was not possible. The problem was pronounced by the 'backswing' behaviour.

Therefore, now a mechanization similar to that in roll has been installed with the trim signal filtered.

5. THE SAFETY PROBLEM

As already mentioned the CCV-FCS is a quadruplex system with fail-op, fail-op capability. The decision to go quadruplex proved right because during all 118 (125) flights no critical failure of the FCS occurred - in spite of a lot of computer hardware trouble (bad multilayer connections - design problem - and ray clad solder sleeve failures) and - at the beginning - actuator trouble.

Without a reliable system flight testing of the unstable configurations would have been impossible because malfunctioning might have been catastrophic.

The main work with regard to the redundancy management had already been done during the development phase before flight test. But some modification and optimization had to be done during the flight phase - this was partly due to the lack of an iron bird ground test rig.

5.1 Signalconsolidation

To avoid drift of the computer outputs in the different lanes and therefore failures, the input signals had to be consolidated. This is done in the following way:

Each computer sends one set of signals it has received from its A/D-inferface to the three other computers. So each computer has four sets of data available in its memory. Each computer now generates the average of the different signals.

In order not to spoil the average value only those signals are taken which have been found error free. That means that prior to consolidation the input signals have to pass a failure detection procedure.

As not only the signals can fail but the data transmission between the computers as well, transmission failures are detected via check sum generation and comparison.

Where possible the same software routines have been used for failure detection and signal consolidation to keep the program small. Because during tests some failures occurred which were due to the fact that the computers in spite of their internal clock were slowly drifting apart, exact synchronization became necessary. This was reached by hardware interconnect which forced all computer clocks to the same frequency.

5.2 Failure Display

In the failure routine each computer compares its own input signals with those of the other three channels. As there are always small discrepancies between the signals due to sensor- and interface tolerances failure limits had to be defined. Each trespassing of the limits leads to the immediate exclusion of the failed signal in the averaging process but not to immediate failure display. Only if the limits are exceeded for more than a prescribed period of time (number of cycles) a failure indication on the Control and Display Unit (CDU) is given (Fig. 12). Thus unnecessary irritation of the pilot in case of short trespassings is avoided. Final definition of the failure limits and counter cycles was a development process during flight testing. The number of cycles (and of course the limits) are different for different signals.

The computer output signals for example which go to the actuators must exceed the limits for at least 4 cycles (cycle time is 60 ms) before a failure is indicated.

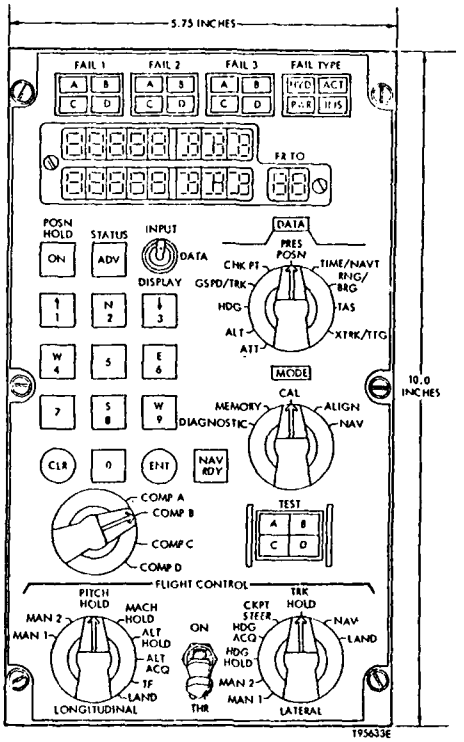

Fig. 12 CCV-CONTROL AND DISPLAY UNIT

5.3 Software Validation

In a digital system there always arises the problem of generic software errors which cannot be overcome by redundancy because each channel contains the same error. Therefore, effective software test methods are of great importance. In case of the CCV-FCS software testing is done in several steps.

Each program for the flight computers was written in assembler using a cross assembler that has been specially developed for a PDP 11/70. The program has a block structure. For each block a check sum is evaluated. If there is any program change the dedicated check sums are changed too. Thus it is easy to find on a compare list which parts have to be tested after program changes.

Each new program is loaded into a flight computer via punched paper tape and then checked in the laboratory with different input signals. Output of internal values is on the Control and Display Unit (digitally) or via the flight computer telemetry program on a plotter - a telemetry set is available in the lab.

Thereafter closed loop simulations follow with the flight computer in the loop where pilots 'fly' the digitally simulated aircraft from a cockpit.

For test purposes a second non-linear simulation program has been written on a VAX 11/780. There is no interface for analog inputs or outputs.

This program (aircrafts equation of motion and controller) is written in Fortran whereas in first simulation SL1 is used for the aircraft and assembler for the controller (flight computer program). As both simulations are based on the same set of aerodynamic data simulation results can be compared to check for programming errors.

Redundancy procedures, safety routines and limitations can only be checked with all four systems in the aircraft. Therefore after each change in the flight computer program a special ground test was conducted with the aircraft.

Additionally, before each flight the pre-flight test program was run.

During flight tests some software problems were detected which had not been found in ground tests. Most of them were due to 'wrong thinking' that is to introducing logic functions, software limitations or quick program changes which had not been considered in all consequences.

In this context the otherwise so valuable flexibility of the digital system was kind of dangerous because changes from one flight to the next - just to try something new - could be made so easily.

One failure which might be of interest here was due to a scaling error (in the quaternion program part) which was very difficult to detect. We might have flown with it for years if not by chance the pilot would have flown exactly 180° heading with exactly zero bank and zero pitch attitude. Only when these conditions were fulfilled overflow occurred. This overflow led to a moderate step input in roll.

6. CONCLUSIONS

A newly developed quadruredundant digital flight control system has been installed in a CCV demonstrator aircraft and flight tested up to 22% negative static margin.

The aircraft was always easily controllable even in the highly unstable configuration. All three pilots who have flown the system confirmed generally good handling qualities. Areas of criticism and improvements have been discussed.

The flights have demonstrated that the redundancy management problems have been successfully solved and that an unstable aircraft can be flown safely.

They have also demonstrated that digital systems are superior to analog systems as they allow the installation of complex systems with subsequent changes and optimization by pure software change in very short time.

The CCV program will be continued. Future work amongst other will be on simple back up software, which can be easily checked for programming errors (first flights in September this year) and on dissimilar software.

7. REFERENCES

[1] Kubbat, W. — A Quadruredundant Digital Flight Control System for CCV Application, AGARD-Symposium Flight Mechanics Panel and Guidance and Control Panel, 16.10.1974, Paris (MBB-UFE report 1116 (Ö))

[2] Beh, H.; Korte, U.; Löbert, G. — Stability and Control Aspects of the CCV-F 104 G, AGARD Flight Mechanics Panel Meeting on Stability and Control, 25.-28.9.1978, Ottawa (MBB-UFE report 1447 (Ö))

GROUND AND FLIGHT TESTING ON THE FLY-BY-WIRE JAGUAR EQUIPPED WITH A FULL TIME QUADRUPLEX DIGITAL INTEGRATED FLIGHT CONTROL SYSTEM

BY

T. D. SMITH

C. J. YEO

British Aerospace P.L.C.
Aircraft Group, Warton Division
Warton Aerodrome, Preston
Lancashire PR4 1AX

R. E. W. MARSHALL

Marconi Avionics Ltd.
Combat Aircraft Controls Division
Airport Works, Rochester
Kent ME1 2XX

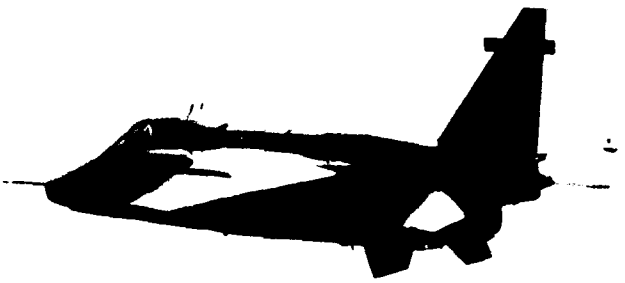

SUMMARY

A national (U.K.) research programme has been undertaken with the aim of the design, development and demonstration of a safe, practical full time fly-by-wire flight control system for a combat aircraft. Throughout the programme, the flight control system was to be treated in all airworthiness aspects as though it were intended for production. The flight trials were to include flight assessment of an integral spin prevention system and aircraft configurations which are unstable in pitch. The first major objective of the programme has been achieved, namely the generation of confidence in the airworthiness of such a system, by the successful completion of the design, development, ground testing and initial flight test assessment of a fully representative system.

1.0 INTRODUCTION

The first flight of the British Aerospace Fly-By-Wire Jaguar in October 1981 represented the culmination of a national (U.K.) research programme. The FBW demonstrator programme formally began in 1977 with the award of a contract to British Aerospace by the Ministry of Defence. Prior to 1977, British Aerospace (then the British Aircraft Corporation) had begun studies into Active Control Technology (ACT) with a view to utilising the benefits of such technology in future combat aircraft. Also in the early 70's Marconi Avionics were continuing the development of digital processors in a number of aircraft applications including the Tornado and the YC14; and Dowty Boulton Paul were developing a novel actuator design based on the principle of failure absorption. When the research contract was awarded to British Aerospace, Marconi Avionics were selected to supply the Flight Control System which was to comprise a quadruplex digital system and Dowty Boulton Paul were selected to supply the powered flying controls which would comprise a duo-triplex actuation system. The technical sponsors of the research programme were to be the Flight Systems Division of the Royal Aircraft Establishment (RAE) at Farnborough.

The aim of the research programme was defined as the design, development and demonstration of a safe, practical, full time, fly-by-wire flight control system for a combat aircraft. Throughout the programme, the flight control system was to be treated in all airworthiness aspects as though it were intended for production. Although it was not intended to demonstrate the aerodynamic benefits of ACT, the programme included flight demonstration of the aircraft in an unstable configuration in pitch and of a Stall Departure Spin Prevention System. Since the integrity standard of the flight control system was designed to be comparable with existing mechanical systems, and in addition, the aircraft was to be flown in an unstable configuration, it was decided early in the definition phase to remove all the mechanical control rods. Thus the FBW Jaguar quadruplex digital flight control system has no emergency back up flight control system of any kind.

This paper describes the extensive rig and ground testing performed which resulted in the first major objective being achieved, a clearance for the first flight of the aircraft. It then describes the first phases of the flight test assessment which were completed ahead of schedule and a series of simulated whole aircraft lightning tests which were carried out prior to the next phase of the flight assessment.

2.0 AIRCRAFT AND SYSTEMS DESCRIPTION

2.1 Aircraft

The FBW Jaguar demonstrator aircraft is a modified single seat Sepecat Jaguar. The aircraft started life as the sixty-second production Jaguar and it served with the Royal Air Force for several years before being returned to Warton to be extensively modified to become the FBW demonstrator aircraft. In general, only minor changes to the structure have been made to accommodate the new equipment. Some internal equipment, principally the guns and ammunition trays were removed to make way for the flight control system computers and the very extensive instrumentation system fitted to the aircraft. All the mechanical control rods, the autostabiliser equipment and the original powered flight control units were also removed. Thus the external appearance of the aircraft is little changed. However, for the high incidence trials, an anti-spin parachute will be fitted in place of the standard brake parachute; and later in the flight trials programme, leading edge strakes will be fitted along the air intake boxes.

The aircraft has provision for a large block of fixed internal ballast to be carried in the rear fuselage. This ballast and some alterations to the fuel management procedures will enable the centre of gravity to be moved aft to give a manoeuvre point of -3%$\bar{c}$ to -5%$\bar{c}$.

The addition of the leading edge strakes will move the centre of pressure forward to give a manoeuvre point of -10%$\bar{c}$.

2.2 Flight Control System

The flight control system (FCS) is basically a quadruplex digital system with no manual reversion. All mechanical control rods downstream of the trim and feel units have been removed. Quadruplex position sensors (QPS) are used to sense pilot control demands in terms of stick, pedal and trim inputs and quadruplex rate gyros sense aircraft pitch, roll and yaw rates. Four identical digital flight control computers (FCC) are used to process these signals together with a variety of other sensors. The resulting command signals are used to control the two taileron, two spoiler and one rudder actuators. In order to convert the quadruplex signals from the FCCs into the sextuplex signals required by the duo-triplex actuators, the four FCCs are supplemented by two actuator drive and monitor computers (ADMC). This system layout was a result of the following considerations.

- Overall system loss probability (including first stage actuation) shall be no greater than 10^{-7} per hour.
- Any two electrical failures in the system shall be able to be survived.
- The electrohydraulic first stage actuation would have only two independent hydraulic supplies with no interconnection between them.
- The system shall be able to survive a hydraulic system failure followed by an electrical system failure or an electrical followed by a hydraulic failure.
- The system shall rely on majority voting of the redundant elements for failure survival rather than self-monitoring within each redundant element.
- Similar redundant digital implementation shall be adopted without any reliance on any back up flight controls (eg: mechanical or simple analogue links).

The Jaguar FBW system configuration is illustrated in Figure 1 which presents a simplified schematic of the primary control path. In addition to the quadruplex primary input sensors, sensors of lower redundancy are used for those functions which may be necessary for optimum handling qualities but which are not necessary for safe flight. These are dynamic pressure, static pressure, incidence and sideslip which are all triplex secondary sensors; and lateral acceleration, flap position and airbrake position which are duplex sensors. Triplex dynamic and static pressures are provided by three pitot static probes (the standard nose boom and two side mounted probes). Triplex incidence and sideslip

signals are provided by four airstream direction detector probes (ADD) mounted around the nose of the aircraft.

The FCS also uses a number of quadruplex and duplex discrete inputs for switching functions. A simplified overall system configuration is illustrated in Figure 2. A more detailed description of the system architecture and the system LRUs can be found in reference 1.

Powered Flying Control Units

The taileron, rudder and spoiler PFCUs each consist of a duo-triplex first stage actuator block and a duplex tandem jack. All five are similar in design, differences between them being limited to valve port sizes, jack strokes and diameters, connector handing etc.

The PFCUs contain six flapper nozzle servo valves which convert electrical inputs from the FCCs and ADMCs into hydraulic signals which are then used to drive a pair of first stage spool/control valves. Each servo valve is connected to two pairs of opposing pistons inside one of these first stage actuators. The pistons act on flanges mounted on the actuator spools, two pairs being used to prevent asymmetric loading. Both flanges are therefore driven by six pairs of opposing pistons, two pairs from each of three servo valves. A mechanical link between the two actuators ensures that the spools and thus the flanges move in unison, so that all six servo valve outputs are effectively summed together. In this way failures in at least two lanes can be absorbed within the actuators, the four good lanes overriding the failed lanes. Movement of the first stage actuators results in hydraulic fluid being supplied to the control surface jack. The jacks are conventional tandem units. Hydraulic supplies from the two aircraft systems are routed through the first stage actuators, each system also supplying the actuator's associated trio of servo valves. Failure of one of these hydraulic supplies can be tolerated by the PFCUs in addition to at least one electrical failure in the lanes supplying the unaffected side of the actuator.

2.3 General Aircraft Systems

Electrical Power Supplies

DC electrical power is normally supplied by two engine driven alternators via two transformer rectifier units (TRUs). A third TRU, not present on standard Jaguar, was added to cover the additional loading of the fly-by-wire system and ancillaries. To meet the power supply integrity requirements of the FCS (including supply following double engine flameout) revised power distribution and emergency systems were introduced.

The three TRUs supply three busbars, the two normal busbars and a dedicated FC busbar. The flight control system is then supplied from the three busbars. For emergency operation, each of the normal busbars supplying the FCS is battery backed. Each is supplied by a 40 amp-hour battery, and provides power for the two electrohydraulic pumps in addition to the FCS. The dedicated FC busbar is supplied by a 23 amp-hour battery.

Hydraulic Power Supplies

Engine driven pumps are the primary source of power in the Jaguar's two independent hydraulic systems. They are supplemented by a power transfer unit (PTU) which allows the transfer of power but not fluid between systems, and an emergency electrohydraulic pump (EHP) on the number two system. Higher power and integrity requirements of the fly-by-wire aircraft have necessitated replacement of the engine driven pumps and the electrohydraulic pump by units with greater capacity, and the provision of a new, second EHP. This new EHP provides pressure to the number one system in an emergency. Both EHPs provide power primarily to the flying control actuators, services being supplied via a priority valve (which maintains pressure to the controls) and an isolation valve (which is closed by a low level signal to protect against hydraulic leaks in the services). At present, it has not been found necessary to fit the priority valves but they are available if future testing indicates a requirement.

Air Conditioning

The normal Jaguar air conditioning system was retained but with additional ducts and ground fans to allow cooling air to be supplied to the FCS computers.

Flight Test Instrumentation

An extensive on board data acquisition system was fitted to the aircraft during the conversion phase.

This comprises pulse code modulation (PCM) and analogue systems which record data on an on-board 14 track tape recorder and a limited telemetry system (described in more detail in Section 8) which includes a 'hot mike' facility. In addition, flutter mode excitation equipment in the form of groups of lateral thrust units (LTU) or 'bonker packs' were fitted to the fin and tailplane together with a pilot operated LTU fire control panel. Also fitted to the aircraft are special cockpit displays for high incidence test flying and these include wide range incidence and sideslip indicators and visual and audio warnings for low altitude and high levels of longitudinal acceleration. The instrumentation system only interfaces with FCC4 for integrity reasons but a considerable

amount of FCS data is recorded. The inter FCC serial digital link has an instrumentation 'window' which is programmable and allows access to any data in the FCC store.

2.4 FCS Control Laws

The design aim of the control laws is to give the FBW Jaguar handling qualities at least as good as the standard Jaguar over the full flight envelope and in a wide variety of configurations. The FCS also has to provide an integral stall departure and spin prevention system (SDSP) as well as to respect those load limits which are not restricted by flight limitations - for example fin loads.

Two sets of control laws are used; one for the stable and one for the unstable pitch configurations. Both sets of laws can be stored in the FCC, but for safety reasons are loaded separately into the computers. Provision for a further two modes has been made which may be selected using the gain change switch on the pilots control panel. It is planned to use this option during the highly unstable flying to enable assessment of development modes of the unstable control laws.

Longitudinal Laws

The longitudinal control laws are based on a pitch rate plus incidence demand system. The pilot's control input is converted to a pitch rate demand and the incidence into equivalent pitch rate before being compared with pitch rate feedback. The pitch rate error signal is converted to a tailplane demand signal via a proportional, integral and differential (PID) controller. This type of controller minimises the spread in stick force per g variation with aircraft configuration and manoeuvre margin and ensures good handling qualities. Pitch axis gains are scheduled with airspeed, altitude, incidence and undercarriage position. A non-linear "manoeuvre boost" path is also included as an additional forward path in the pitch loop. This gives a marked improvement in shortterm response to stick inputs by combining good tracking ability with rapid response in large perturbation manoeuvres. The incidence limiting function of the SDSP is an integral part of the longitudinal control laws.

Lateral Laws

The lateral control loop is a roll rate command system wherein roll rate demand from the lateral stick is compared with actual roll rate to produce a roll rate error signal which commands spoiler and differential tailplane deflection. A feed forward path provides a good roll acceleration and the control demand necessary to maintain the desired roll rate in a steady roll. At low incidence roll control is basically provided by the spoilers. Differential tailplane is used to augment the spoilers as a function of airspeed and incidence and rudder is used as a function of incidence. These interconnects provide good co-ordination and roll performance and the SDSP functions are inherent in the control law scheduling.

Directional Laws

The directional control laws consist of a wind axis yaw damper with sideslip feedback to augment directional stiffness. The wind axis yaw rate is synthesised from body axis yaw and roll rates. Turn entry and exit at low speed is improved using a synthesised bank angle term from a further roll rate to rudder crossfeed.

Sideslip feedback is used to augment directional stability at high incidence although it is also available for augmentation at low incidence for low directional stability store configurations.

As in the roll axis, the SDSP function is inherent in the gain scheduling, for example rudder pedal authority with undercarriage up is progressively reduced as incidence is increased in order to prevent pilot induced departures.

Fixed Gains and Train Mode

In the event of a double failure in the triplex secondary sensors (ie: incidence, sideslip, airspeed or altitude) the control laws are switched to a fixed gain mode. In this condition all scheduling functions are set to fixed values and undercarriage position is used to select the appropriate gains. In order to allow pilot assessment of this condition, a Training mode is provided in the control laws which is equivalent to the fixed gains mode and the pilot can select and deselect this mode via a cockpit switch.

Spin Recovery Mode

The spin recovery mode is only intended for recovery from developed spins where the rate feedback terms in the normal control modes would apply adverse control inputs and hinder recovery. The spin recovery mode provides a direct position control of mean and differential tailplane, rudder and spoilers with no other motion feedback. The mode is really only a test facility for emergency use when proving the SDSP system and strictly is not therefore an integral part of the control laws.

3.0 FCS BUILT IN TEST FACILITIES

The Built-In-Test (BIT) requirement and facilities were broadly defined by BAe in their Jaguar FBW Integrated Flight Control System (IFCS) base specification. This may be summarised by noting that the BIT features were to provide an accurate decisive and repeatable method of measuring equipment functional characteristics using built-in-test facilities.

In particular, the BIT was to be used to clear the flight control system in the aircraft prior to each flight and thus its integrity and ability to detect faults was to be comparable with the overall integrity aims of the FCS. A very useful fall out of such a system is that it can be used for FCS commissioning on the aircraft and reclearance of the FCS following LRU changes.

Built in Test Functions Available

The facilities provided by the BIT equipment can be grouped into three main categories of test class.

1. Those tests and checks performed prior to take-off which give the pilot confidence that the Flight Control System (FCS) is functioning correctly. This comprises the Pre-Flight Check (PFC) series of tests. The PFC series of tests fall into two groups, those tests which are conducted automatically and those tests which require pilot participation for their completion.

2. Those tests and checks which can be initiated by the pilot and need not be performed compulsorily prior to flight. They enable the pilot to test other ancillary functions on the aircraft that, in their execution, require the co-operation of the ground crew. These tests are called First Line Checks (FLC). Tests in this class include checks on incidence and sideslip probes.

3. Those tests and checks which are conducted automatically in a background mode whilst the FCCs are executing the In-Flight software of the FRS. These tests are referred to as In-Flight Monitoring (IFM) and perform continual checks on the processor and system operation during flight. There are also signal consolidation voter/monitor algorithms which are used to select the control input information from the multiple redundant transducer and sensor sources.

The conduct and the results of the BIT are displayed to the pilot via the Central Warning Panel (CWP) and the Pilots Control and Switch Panel (PCSP). The PCSP uses coloured annunciators to inform the pilot of test failures in PFC, or FLC or in the case of IFM, a first or second failure of a primary or secondary sensor or processing. The ground crew can receive information via a Diagnostic Display Unit (DDU) which is located in the port undercarriage bay. It is used to inform the ground crew of software identity status, PFC test sequence number, and the identity of test failures. The FCCs have a capacity to store 100 failure codes for each lane which uniquely identify those tests which have failed and permit identification of the failing lane and the function within that lane that has caused the failure.

3.1 Design and Development of BIT System

The tests required to check out the installed IFCS were evolved using both a top down and bottom up approach to test philosophy. From this assessment a basic systems orientated test strategy was produced which identified the required system test functional areas and those module areas where test interfaces would have to be supported. The tests would be controlled through software and appropriate interfaces were accordingly developed.

The test objectives need to be simple with clearly defined outcomes in order that the assessment of the result may be easily and unambiguously made. A complex test can have responses the assessment of which can be demanding due to the number and complexity of interrelated and interactive parameters which need to be correlated in order to define a good or bad outcome. Software can be written which will effectively perform such a service but its commissioning and any subsequent modification can be a difficult and time consuming task. In a research programme one must expect changes as flight trials and development proceeds. It is important therefore to design the flight control system to accommodate such changes efficiently and to minimise penalties both in terms of time and cost.

The practical outcome of this strategy was the requirement that tests should be simple and understandable in structure and generally capable of modification by changes to the data constants leaving the coding structure unaltered. Checks requiring more sophisticated testing methods should make use of parametric changes or combinations of simple tests.

The basic reasoning behind the development of each of the tests followed a similar pattern where test methods were assessed against the test objectives. In some instances what might be considered the normal methods of checking were found to have shortcomings in that the probability objectives could not be met. This led to the introduction of more sophisticated methods to achieve the test objective. An example of this is reflected in the use of a sum check sequence to check the test patterns in both the program and constant stores. A straightforward analysis of the probability of bit

corruption in a 16K 16 bit PROM store showed that there was a probability greater than 1: 10^{-7} of a successful sum check with 2 or more bits being corrupted. This led to the introduction of cyclic redundancy check methods. This enabled comparisons to be made with a probability error of less than 2.3×10^{-10} (ref. 2 and 3).

A further type of problem that had to be solved is exemplified by the requirement to checkout the failure absorbing duo triplex actuators. These units are capable of providing normal performance in the presence of two electronic or an electronic and a hydraulic failure. The use of tests which fail multiples of input commands to the units could not be used as the response of the actuators was indeterminate in certain open loop or null command states. Using such a method it would not be possible therefore to obtain definitive results to assess performance. The solution ultimately conceived was simple in concept, it involved a series of dynamic tests in which pairs of commands were set to servo saturation at opposite extreme limits. The remaining pair of command lanes were then used to stimulate the system with an impulse function. With this configuration and test condition the actuator system had a predictable dynamic response. This simple test was then applied sequentially to combinations of saturated and stimulated command lanes to check the complete actuation system.

3.2 Entry and Performance of Pre-Flight Check

Entry to Pre-Flight Test

Precautions are taken to prevent the inadvertent entry into the Pre-Flight Check sequence whilst the aircraft is in flight by a series of interlock actions.

For entry to occur, the aircraft must have "weight on wheels" the BITE press button cover must be raised and the BITE press button operated. On entry the automatic tests are performed, these take approximately 60 seconds to complete. Errors are automatically loaded into the Failure Identification Table (FIT).

Automatic Test Sequence

The computer functions check is a sequence of instructions which are more complex and not used in the initial running of the Flight Resident Software (FRS). The program/constant store check operates as previously described using cyclic redundancy check techniques. Additionally on completion of the check in each FCC the result is transmitted between lanes and subject to further correlation to confirm identical store bit patterns in each FCC. Errors may be identified by display on the DDU to a specific store. Lane coding and stability setting checks follow. The stability setting defines whether FRS for stable or unstable control laws is required, it is predetermined by wire links in the aircraft wiring. The scratchpad checks test that all locations are capable of storing ones and zeros. Those locations in the Autonomous Data Transfer (ADT) area, where autonomous updating can take place, have the opportunity of a second check should the first fail due to an ADT updat operation. Checks on the serial data transmission system are conducted intra lane by looping the data transmitter output to the data receivers. Dedicated bits in an output logic word are used to control a series of checks which test both rate and failure states for correct operation of the failure response. The discrete outputs are checked by loading the scratchpad with special binary patterns which are re-read into the scratchpad after processing by the discrete output logic. The check is completed by comparison via software. Analogue to digital and digital to analogue conversion is checked by looping back analogue output signals to the analogue inputs. The loop is formed by operating analogue BITE switches incorporated into the analogue input signal conditioning. Checks are conducted at both positive and negative levels as well as the zero state. The analogue output voltage and the corresponding input voltages are assembled in the scratchpad and compared using software. An important feature of the FCC is its treatment of overflow conditions in the processor. The processor is designed to behave in a similar way to an analogue computer in that exceeding the maximum positive or negative magnitudes will not result in a sign inversion. Use is made of the property in the control law processing so to maximise the resolution performance. It is thus an important function and is checked continually during flight as well as in pre-flight test. All combinations of instruction that would lead to overflow are exercised and the result checked for correct response. A feature of the processor operational checks is a check-word monitor. This is a piece of hardware which checks both a bit pattern and its output rate from the processor. A persistent error in either of these causes the data from that lane to be inhibited, the other FCCs are informed of this action by a default error code from the serial data transmitter. Both the rate gyros and the accelerometers are provisioned with inputs which enable them to be stimulated. Signals of defined levels are used to torque the units, the responses are input to the scratchpad where they are checked. The operation of the auto-trim motors is checked by confirming the rate and direction of movement resulting from forcing functions output from the FCC.

After the completion of the automatic tests the opportunity is available to interrogate the FIT through the use of the DDU. At this stage it is also possible to display the software issue number. This is unique to each issue of FRS and has to correlate between lanes before it is possible for the In-Flight Software to be entered. Any error is identified to a specific lane.

Crew Participation Checks

The second phase of the PFC requires the participation of the crew to complete them. This can entail an observation or an action to complete each section. The ADMC's have BIT which operates autonomously on receipt of the correct commands from the FCC's. Once initiated they run to completion and in the first part require the pilot to observe and note the operation of failure warning annunciators. The completion of sections of the test are signalled to the PFC by the pilot operating the BITE press button on the pilot's control and switch panel. During this series of tests the consolidation of the dual power supplies at each FCC and ADMC are checked by the pilot manually interrupting each supply at the control panel. This is followed by pilot checks on the operation and input range of the column, rudder pedal and trim inputs together with some discrete inputs (push buttons and switches). The actuator checks described in Section 3.1 are conducted in this section of testing despite the fact that the test is entirely automatic. This was done to enable as many tests as possible to be executed prior to the need to power the hydraulic systems via the aircraft's engines.

First Line Checks

These tests are optional and may be omitted prior to flight if so desired. The pilot can select to continue testing at the conclusion of the pilot participation tests. The first line checks require the co-operation of the ground crew for their completion. They cover the operation of the DDU, the pilot's control panel and the air data triplex transducers. A full list of the pre-flight and first line checks is given in Annex 2.

3.3 In-Flight Monitoring

The In-Flight Monitoring (IFM) software operates contemporaneously with the flight control software. It serves two main functions:-

- to monitor the flight control sensor inputs
- the continual check of certain hardware functions.

Flight Control Sensor Input Monitoring

Flight control sensor information is provided with redundancy levels ranging from quadruplex for primary data to triplex and duplex for secondary information. The selection of flight control data for presentation to the voters is achieved by associated monitors which continually check complementary inputs across lanes. Monitors are provided for both analogue and discrete digital input signals.

The checks performed compare each lane's data against the others. When a lane is identified as being out of tolerance, an error count is commenced. A pre-determined count has to be reached before a voter has an input disconnected. This is to limit or prevent the occurrence of nuisance disconnects that could otherwise occur. Recovery from a potential disconnect situation is achieved when the out-of-tolerance signal returns to tolerance within the error count maximum. This causes the error count to be decremented at half the incrementation rate. This procedure ensures that cyclic errors can be detected. When a predetermined count has been reached, the lane sensor data in error is inhibited from its associated voter and the voting algorithm is rescheduled to reflect the new number of valid inputs. The detection of an error is indicated to the pilot by the CWP where, according to whether the failure is a first or second similar failure, an Amber or Red warning is displayed. With the Amber warning the pilot can attempt re-engagement of the system by depressing the status button on the pilot's control panel.

Voter/monitors are provided for all the sensor inputs each operating against a given threshold and error count figure. Any detected error causes an entry to be made in the FIT. This can then be read, after landing, via DDU to ascertain the cause of any warning indications given to the pilot.

In-Flight Hardware Checks

Checks conducted on the hardware primarily relate to the operation of the processor, storage and conversion sub-systems. The instruction function and overflow checks ensure that data is correctly manipulated by the processor and that sign inversions do not occur with instructions that could normally cause overflow. The analogue to digital converter module has scratchpad locations linked to a dedicated A-D loop. This loop is continually exercised during flight to check the performance of the module. Any error causes an entry to be made into the FIT.

The operation of the FCC is monitored by a hardware rate and bit pattern detection module. This is the On-Line Monitor which accepts predetermined bit patterns at the frame running rate and checks that both bit pattern and the rate at which it is being received are correct. If erroneous data or excessive rates are detected, the remaining FCC lanes are informed via the serial digital data link by the transmission of an error signal. This is used in the receiving lanes to reject data from the faulty lane and to adjust the voter algorithms accordingly.

A series of continual tests are conducted on the scratchpad, program and constant stores. The scratchpad checks confirm operation of each location (1 bit and 16 bit) of the scratchpad with true and inverse checkerboard patterns. The program and constant stores are subject to cross lane checks which compare the entire contents of each of the stores with one another cross lane. The entire comparison process is completed approximately every 2.5 minutes. Any failures in the cross lane communications system result in a receiver status being set. This causes the receiving lane to ignore the data from that receiver.

The sequential operation of the software is checked through the use of the frame execution monitor. This is a piece of software which operates in each processing frame to confirm that:

- it is the correct frame of processing (i.e. the preceding frame number is one less than the current frame)
- that processing was completed in the preceding frame
- that lanes are in frame synchronism.

If a lane is detected as being out of frame synchronism (i.e. master resets occur at the right time but frame numbers are different), action is taken to correct the frame count and to note the failure by an entry to the FIT. The synchronisation maintenance algorithm utilises an assessment table to determine the action to be taken (i.e. shorten or lengthen frame by 20 microseconds) in order to keep that lane in synchronism. If the adjustment period falls outside that achievable by the sync. maintenance algorithm, an error is flagged up, and the Amber warning is signalled to the pilot. He can attempt a re-sync. by operating the status press button.

The quadruplex voter/monitors associated with the rate gyros incorporate inputs derived from gyro fail discretes. These inputs when associated with out of tolerance input signals cause the failure counts to be at an accelerated rate thus leading to a faster disconnect. The fail discretes by themselves can also cause deselection of a gyro input by incrementation of the error count. A list of the checks performed by IFM are given in Annex 2.

3.4 Failure Display Selection

Pre-Flight Check

At the conclusion of each phase of PFC there is the opportunity to interrogate the FIT and also to read the software issue status. This information is available from the DDU which also monitors test progress by display of test numbers. The DDU display holds the current test number for 5 seconds and then reverts to the display of software identity. This is recognised by having the numeral 6 displayed in the hundreds position, the ten and units displaying the software issue state number. When failure identify information is required, the DDU read button is pressed for each output of failure information. When the FIT has been read completely, the DDU displays 8888. Further operation of the read button causes a repeat of the previously displayed failure information.

In-Flight Check

As already indicated, failures detected by the In Flight Monitoring are stored in the FIT and in the majority of cases a warning is given to the pilot via the central warning system. However, there are some hardware checks which only give an entry into the FIT. This is because their immediate impact on the system integrity is not considered significant enough to warn the pilot but their occurrence indicates possible incipient failure conditions. In order to tell the ground crew that the FIT contains failure information, and so initiate maintenance procedures, the DDU contains a caption which is illuminated whenever entries are made into the FIT. Thus part of the after-landing check to be performed by the groundcrew is a check of the DDU.

4.0 GROUND TEST FACILITIES

Early in the programme definition phase, it was decided that a representative ground test rig should be built rather than use the aircraft for system qualification tests. The comprehensive rig facility illustrated in Figure 3 comprises the following:

- flight control computer system test bench
- powered controls actuator test bench including representative actuator mounting structure and simulated aerodynamic loading facilities
- representative cockpit including actual pilot's flying controls, flight instruments with head up display and computer generated outside world display
- a three axis rate table
- a sensor bench for secondary sensor testing

- a flight simulation computer capable of closing the aerodynamic loop as well as simulating the control laws and driving the 'outside world' and cockpit displays.
- a power bench to provide hydraulic and electrical power supplies for the FCS
- simulation benches for primary sensors and actuators
- a comprehensive data acquisition system.

The facility can be run in a number of configurations enabling simultaneous testing to be performed on different benches or in a fully closed loop mode whereby a complete set of FCS hardware can be 'flown' by the pilot. For example, loaded actuator performance can be measured on the power controls bench while control law development can be carried out using the cockpit and simulation computer. The outside world display is confined to a runway, a blue sky and a random scattering of coloured squares on a green background together with a number of cloud layers. Although very simple, this display together with the HUD was adequate for pilot assessment of visual flying tasks.

For aircraft test work, automatic test equipment (ATE) was provided on a purpose-built trolley. This powerful tool enabled direct access to the FCC serial digital data streams and could be set up for a number of automated monitoring tasks as well as enabling detailed diagnostic testing to be performed.

The ground rig is used for four primary and two secondary tasks. The primary tasks are:

1. To verify the control laws by pilot assessment before encoding into the computers.
2. To integrate the hardware, the software and the instrumentation.
3. To validate the final software before flight.
4. To gain confidence in the overall system.

The secondary tasks are:

1. Each flight test schedule is flown on the ground rig immediately prior to the actual flight.
2. The rig provides an excellent pilot training aid. Experienced pilots can practise the failures peculiar to the FBW aircraft. New pilots can gain first-hand experience of the control systems and control laws, as well as experiencing all the possible failures. As with more conventional simulators familiar to military pilots, the FBW engineers have become adept at thinking up the most convoluted and esoteric emergencies.

The final task of the ground rig prior to commencement of the flight test programme proper was 50 one-hour periods of closed loop testing using the full flight cleared hard and software.

5.0 SIMULATOR TESTING

Before the full system rig, which is described in the next section, became available, the initial investigation and development of the flight control laws was carried out on one of the Warton Division's general research simulators. By this method much of the early development of the control laws was completed far earlier than would otherwise have been the case.

5.1 Simulator System Description

Cockpit - Unlike the Rig Cockpit the simulator cockpit was not modelled on the Jaguar, or for that matter any other particular aircraft, but had a general HDD instrument display and an early version of the Jaguar HUD.

Outside World Display - The simulator used a simple Tector electronically generated outside world display. The display was basically a sky/ground presentation with fields, clouds and visibility effects. Runways and targets could be simulated so that take off and landings and air to ground tracking could be explored. The simulator outside world display was very similar to that used in the full system Rig.

Flight Conditions - Turbulence, crosswinds and gusts were required for handling evaluation during take off and approach and flight at low level and to examine the increase in control system activity. Discrete gusts of larger than typical levels could be injected vertically and laterally at random from the computer console. Crosswinds with magnitudes up to and in excess of the standard Jaguar crosswind limit were frequently used. These facilities were considered to be essential to a thorough handling evaluation and are also used on the full system Rig.

Take Off and Landing Simulation - The landing and take-off simulation on both the research simulator and the Rig contained only a simple model of the aircraft's undercarriage dynamics and ground effects were limited to a series of ground restraints upon the aircraft model which came into effect below a pre-defined minimum height. During flight trials it has been found that the stick forces to rotate during take-off are consistently lighter than those suggested by the basic simulation.

Aircraft Model Validation - Before any research work concerning the FBW control laws could be undertaken, the basic aircraft model had to be validated. To accomplish this validation a comparison of a series of step inputs at several flight conditions was made using an IBM computer which contained the 'Jaguar Master Data File'. The inputs were made for models of the FBW Jaguar, Autostabilised Jaguar and Basic Jaguar. These inputs were repeated on the simulator and the frequency, dampings and response of the two computer data sets compared. Once a good match was achieved, experienced Jaguar pilots were asked to evaluate the simulator model for fidelity with the real aircraft.

5.2 Results of Simulation Testing

Phase 1

Phase 1 represented a very early exposure of the proposed control laws to pilot comment. Four configurations were examined; a and b were for a longitudinally stable aircraft, c and d were for a longitudinally unstable aircraft.

a. Clean aircraft

b. Centreline fuel tank, 4 x 1,000 lb bombs inboard, 2 x 1,000 lb bombs outboard

c. 2 x fuel tanks inboard plus leading edge strakes

d. Clean aircraft plus leading edge strakes.

Even at this very early stage of development, the pilots found much that they liked about the aircraft. The following features were highlighted for further development:

High Stick Forces - The stick force per g and the stick force to rotate was found to be high in the mid Mach number range from 0.5 to 0.8 and during rotation on take-off. In most cases this criticism was accompanied by comments concerning the incidence limiting system. It was concluded that the incidence scheduling was restricting pitch control at incidences lower than desirable. Further development of the incidence scheduling resulted in satisfactory stick force per g. The high stick force during rotation was a simulator characteristic produced by the simple model of ground effects; the actual aircraft can be rotated to the take-off attitude with a light stick force.

Trim Change with Flap Extension - The pitch trim change when both mid and full flap was extended was excessive with flap travelling in either direction. The direction of the trim change was in the unsafe sense, i.e. a pitch down on flap retracting, leading to poor overshoot handling. A modification to the flap compensation control law reduced the trim change with flap movement to almost negligible proportions.

Poor Pitch Response - Pitch response was criticised in the clean aircraft configurations during take off and landing and at 400 KIAS at low altitude. Further control law development overcame this problem and the aircraft now has a snappy, quick pitch response at all flight conditions.

Low Roll Rate - The target roll rate of 150°/second was not achieved. However, variation in rate with normal acceleration was almost eliminated. For example, at 5,000 ft, 0.9 IMN full stick rolls produced 130 to 140°/second at -1g and at 5g as well as at 1g. Further refinement of the control laws has achieved the target roll rate.

Departure Prevention - It was possible to induce departure by using rudder at high incidence with a centreline tank and six bombs. However, at this early stage of development, rudder scheduling with incidence had not been introduced. Once this was incorporated the problem no longer existed.

Light Stick Forces in the Unstable Configurations - The unstable configurations, particularly with inboard fuel tanks, were found to have lighter than desirable stick forces and poor pitch stability. This criticism applied throughout the flight envelope, including take off and landing. Further control law development eliminated this problem and current studies on the Rig show the aircraft to have pleasant handling characteristics in the unstable configurations throughout the flight envelope.

Phase 2

Phase 2 of the simulator studies of the FBW control laws examined the changes made to develop and improve the laws, and also looked for the first time at some of the reversionary control laws following sensor failures. As has already been noted, all the problems were successfully overcome prior to flight and good handling qualities were obtained throughout. The Phase 2 simulator study identified the following characteristics:

Pitch Transient with Undercarriage Selection - An increase in incidence occurred when the undercarriage was selected 'up' in all stable configurations and failure states. This was due to the change in control law gains effected by the undercarriage selector lever. The transient was substantially reduced for the full system modes although it can still be detected in the failure states. Thus even in the failure states, it is no more than a minor nuisance.

Departure Prevention - Only one case was found, in the heavy stores configuration, where it was possible to induce departure. If the stick was moved forward during a rapid roll and then moved rapidly aft, the aircraft would depart. Further control law development eliminated such problems from the practical flight envelope. Later Rig testing has confirmed that departure is prevented throughout the cleared flight envelope. It can only be provoked if the aircraft's negative 'g' limit is exceeded and rolling continued through more than 720^{o}, which is also beyond the clearance envelope.

Stable/Unstable Boundary Assessment - In configurations with near neutral stability, fuel transfer problems can cause the centre of gravity to move from the stable to the unstable region and vice versa. This situation was investigated by flying the simulator in the "wrong" control law mode for the actual centre of gravity. An assessment was made across the flight envelope from low speed to 550 KIAS, and during landing. No problems specific to the case were encountered within the extremes of centre of gravity movement, indeed the pilots were pleasantly surprised by the way in which the good handling qualities were retained in this failure case.

After the completion of Phase 2 of the simulator studies, the control law testing was moved to the dedicated FBW Rig which is described in the next section of this paper.

6.0 RIG TESTING

The Rig facility was used extensively during the initial development phase and throughout the validation and flight clearance phases. The particular aspects of Rig testing included here are the validation of the FCS software prior to flight and the confirmation testing for the failure mode and effect analysis (FMEA) of the hydraulic and electrical systems.

The validation of the FCS software on the Rig prior to flight is only one part of the overall clearance to flight procedure as described in Reference 4. The actual Rig testing performed can be broken down as follows:

1. Initial testing on the Rig to confirm that all previous system queries have been cleared.

2. Initial closed loop evaluation where the Rig was operated closed loop using FCS computer hardware. The project pilot flew a series of flight profiles to assess aircraft handling and system behaviour over a wide range of flight conditions to identify any deficiencies and to give early warning of any software errors. This test technique proved particularly effective in identifying potential errors in the software and a number of iterations were necessary before the software was judged to be satisfactory. Having established confidence in the system, more detailed testing was then commenced as follows:

3. Full evaluation of preflight check and first line BIT functions.

4. Open loop static and dynamic testing.

5. Open loop transient testing.

6. Synchronisation testing. These tests were performed to assess the ability of the system to obtain synchronisation on start up and to re-establish synchronisation after interruption. In addition, system performance checks, including a closed loop pilot assessment, were carried out with the system deliberately forced into asynchronous operation. The synchronisation algorithm proved to be very effective in obtaining and maintaining synchronisation, and even with the FCCs deliberately driven out of synchronisation, pilot control and system performance in terms of handling qualities was completely unaffected.

7. Open loop failure testing. Failures were induced in each set of sensors to demonstrate correct operation of all aspects of failure detection and identification.

8. Closed loop dynamic testing. Closed loop dynamic and end to end transient tests were conducted initially using an analogue aircraft model for frequencies up to 50 Hz, then later with the digital simulation computer.

9. Closed loop failure testing. With the Rig in the closed loop configuration, the project pilots were given a comprehensive selection of single and multiple failures to assess. These included 'ramp' and oscillatory failures at various flight conditions over the whole flight envelope.

10. Pilot in the loop evaluation. A series of comprehensive schedules were 'flown' by the project pilots to thoroughly identify the aircraft handling throughout the flight envelope. This was done in all system modes and included such unlikely failure cases as approach and landings in spin recovery mode and undercarriage up control laws.

11. Confidence testing. The final confidence testing of the system comprised 50 representative 1 hour sorties flown with the Rig in a flight representative state including flight standard FCS equipment. These were 'flown' closed loop by pilots and engineers and each sortie included power up, pre-flight checks, take off, full handling flight schedule, as well as arbitrary general handling, landing and power down.

The Rig testing carried out to verify the FMEA of the hydraulic and electrical systems included endurance testing in terms of battery supplies and EHP capacity as well as comprehensive short circuit tests to demonstrate the integrity of each independent electrical power supply. These results were used in the compilation of comprehensive failure drills designed to cope with all conceivable systems failures. These drills were then practised by the project pilot and the project engineers under realistic conditions by using the cockpit and simulator and introducing 'failures' via the cockpit central warning system while the pilot 'flew' a typical flight profile.

7.0 AIRCRAFT GROUND TESTING

The task of verifying the performance and behaviour of the flight control system was primarily a task for the ground test rig. However, a considerable amount of testing could only be accomplished in the actual aircraft environment and this can be conveniently divided into four categories; flight control system testing, electromagnetic compatibility testing, aircraft systems testing and simulated lightning testing.

7.1 Flight Control System Testing

This represented the build of the FCS into the aircraft and each sensor LRU had to be checked out. With a full equipment fit, the integral BIT facility was used extensively to check correct function of each sensor and proved extremely useful in identifying such items as a broken wire in the extensive cable runs or a faulty LRU. This facility together with the A.T.E. enables a very comprehensive system check out to be performed rapidly as well as providing a powerful diagnostic tool.

The other major item of FCS testing was structural coupling testing. With the introduction of a high gain control system, interaction between the FCS and aircraft structural modes is potentially catastrophic in that any instabilities can result in the fatigue life of the airframe being consumed in a very short period of time. To protect the aircraft, gyros and other sensors are positioned to give minimal structural feedback and notch filters are used to attenuate structural modes. The first series of aircraft tests defined the actuator/airframe characteristics and the level of structural mode pick up for each sensor. This was done using external test equipment to drive the actuators. The Jaguar represented a unique problem in this respect as the rear fuselage structure is such that there is a strong interaction between the tailplane actuator and the various aircraft structural modes. This first series of tests emphasised the value of early on-aircraft testing in that it identified below specification phase characteristics in the failure absorbing actuator under certain double electrical failure conditions and the actuator was modified to overcome this. These tests also indicated that only the rate gyros were sensitive to structural pick up to the extent that notch filters were required.

The next series of tests identified the notch filter requirements to cover all possible aircraft configurations including variations in fuel state, external stores etc. Prior to first flight, a final series of tests were carried out with the flight standard actuators to confirm satisfactory margins. It is of interest to note that between these tests and the previous tests, the pitch feel system had been modified to optimise the stick force per g characteristics. This was shown to have had a significant effect on the structural mode pick up at the pitch stick sensor to the extent that a filter change was necessary to maintain adequate stability margins.

7.2 Electromagnetic Compatibility and Transient Testing

Electromagnetic interference (EMI) represents a serious problem in that it provides a potential common mode failure in a multi-redundant flight control system. In the light of this, a considerable amount of electromagnetic compatibility (EMC) testing was performed on the FBW Jaguar prior to first flight. The automatic test equipment was used extensively during this testing to monitor a large number of signals within the FCS via a fibre optic link. The parameters to be monitored, warning thresholds and signal alarms were programmed-in prior to each test. During each test continuous monitoring was available and if the preset thresholds were exceeded, an immediate alarm was available as well as a replay of the appropriate signal.

The aim of the EMC testing was to give a general flight clearance with no limitations so that the aircraft could be cleared to fly in areas of intentional and unintentional sources of radio frequencies (r.f.).

To determine the safety margins of the installed system against the test levels of r.f., it was necessary to establish the operating characteristics of the equipment in isolation from the aircraft. The tests to determine these characteristics were conducted by Marconi during the qualification test phase of the flight control system. With the equipment installed in the aircraft, interaction tests with other on-board equipment were carried out to ensure that the flight control system was not degraded. Further flight control system functioning tests were conducted to ensure no degradation or uncommanded responses were observed in the presence of internally and externally generated r.f. fields. During these latter tests the induced interference currents were measured for analysis and comparison against equipment immunity levels. It was considered that the induced interference currents should be less than 25% of the equipment immunity levels. The flight computer internal data buses were monitored for extraneous effects during aircraft ground tests.

The on-aircraft tests covered the interaction of other on-board systems with the Flight Control System and also the behaviour of the FCS during transmission of the on-board transmitters, the local airfield transmitters and other aircraft transmitters including radars. During the tests the aircraft was in a 'flight ready' state so that monitoring of the other critical aircraft systems for malfunction during the test transmissions was possible. The aircraft transmission levels were enhanced either by injecting higher power into the on-board antennae (antenna re-injection) or by opening equipment bay doors - the power levels being enhanced by at least a factor of 4, again with the aim of demonstrating a safety margin.

The bench measurements of the flight control computer susceptibility were compared with the aircraft bulk current measurements and satisfactory margins of safe operation (i.e. the on-aircraft induced currents were less than 25% of the computer susceptibility thresholds) were demonstrated for the VHF and UHF bands. A comparison was not possible for on-board transmitters above UHF (Telemetry, Radar Altimeter, IFF and Tacan) due to bulk current measuring limitations, however, no EMI effects were noted with all relevant access panels removed and this was considered an adequate safety margin. Again it was not possible to make a comparison at frequencies of 26 to 100 MHz as no on-board transmitters existed. At HF frequencies an acceptable safety margin could not be demonstrated as comparison of aircraft and bench measurements did not satisfy the 4/1 criterion and also since uncommanded movements were noted on the control surfaces when the on-board transmitter was operated on particular frequencies. The aircraft was thus prohibited from airborne HF on-board transmissions.

Using the results obtained on the susceptibility of the flight control system, a national survey of known transmitters was carried out in conjunction with MOD, and aircraft operating limits with respect to the transmitters defined. These limits do not cause any major difficulties in the operation of the FBW Jaguar.

Transient Testing

The flight control system is normally supplied from separate power supplies but under certain failure conditions it is possible that single source transients can affect all busbars. The electrical generation system had been studied and the equipment specified to cope with the worst cases found in the failure analysis. During the equipment qualification tests and the flight clearance tests on the ground rig, the equipment was exposed to transients and in all cases was satisfactory. The interaction between the flight control system and the other aircraft systems cannot be adequately checked on the ground test rig, and specific interaction tests were conducted on the aircraft in collaboration with a specialised MOD team from A&AEE, Boscombe Down. The latter tests were carried out with engines running and also in the hangar, and consisted of observing the effects of conducted and radiated transients during the operation of all aircraft equipments singly and in normal combinations. The major transient, not unexpectedly, came from the electrohydraulic pumps, both on switch-on and switch-off. The resultant transients were within the capability of the flight control computers both with and without the busbar support batteries connected.

7.3 Aircraft Systems Testing

As already described in Section 6, the FMEA of aircraft systems identified all the safety critical failure cases which were then tested on the rig. However, a number of these cases were aircraft configuration dependent and so some repeat testing was performed on the aircraft. This testing included hydraulic system behaviour in terms of primary flight control actuator performance under specific failure conditions such as:

- engine failure on take-off
- loss of a single hydraulic system with the EHP taking the load
- loss of both engine driven pumps as a result of a double engine flame out in a spin and the two EHPs taking the load.

The testing also assessed the electrical generation system behaviour with particular emphasis on system loading and battery endurances under a variety of failure conditions. This testing demonstrated a good margin above the theoretical endurances and also revealed that the priority valves were unnecessary for the initial flying programme.

7.4 Simulated Lightning Testing

During the design and build of the FCS into the Jaguar demonstrator aircraft, extensive lightning protection measures were built into the FCS and its aircraft interfaces. However, it is well known that the effects of a lightning strike on an aircraft are unpredictable, particularly on an aircraft such as the FBW Jaguar due to the highly complex interactive effects of the aircraft structure, equipment layout and cable runs. Thus for the initial flight trials, the aircraft was prohibited from flying in areas where lightning activity was likely. On completion of the first stage of the flight assessment, a series of simulated whole aircraft lightning tests were carried out. The objective of these tests was twofold:

- to evaluate the overall effectiveness of the design features incorporated into the aircraft and the FCS in order to protect the FCS from large electromagnetic pulses

- to obtain a relaxation of the flight limitations.

The testing was carried out at B.Ae Warton in conjunction with the Lightning Studies Unit from Culham Laboratories (UKAEA) and RAE Farnborough. The aircraft was configured into an effectively 'flight ready' condition with certain exceptions commensurate with the considerable safety precautions necessary to protect both the aircraft and personnel involved in the tests. The aircraft test configuration is illustrated in Figure 4 where it can be seen that the aircraft was placed on a test frame of 'return conductors' which provide a return path for the high current pulse and create the correct electric field around the airframe. The simulated lightning pulses were produced by discharging a high voltage and high di/dt generator into the aircraft at the base of the pitot probe with the return conductors attached to the required part of the aircraft structure, e.g. tail-cone or fin tip. Very extensive monitoring equipment was used with the aircraft measurements being transmitted via fibre optic data links to a screened room where the recording equipment was positioned.

A progressive sequence of tests was performed beginning with low level pulses (20 KV) working up to high level pulses 80 KV and 100 KA. These high level pulses were discharged into the aircraft in a fully powered (electrically and hydraulically) condition with FCS engaged, and there was no corruption or interference on the FCS. This was a highly satisfactory result as the high level pulses are equivalent to moderate to severe lightning strikes. Some extrapolation of results is necessary to cover the full lightning threat, and the extrapolated results will be used to assess the behaviour of the FCS as a basis for a final clearance. This work is still in progress but it is hoped that the present limitations which prohibit the aircraft from flying in and around predicted areas of lightning activity will be rescinded in the near future. Obviously considerable confidence has been generated in the design technique used in providing lightning protection for the FCS on the FBW Jaguar.

8.0 FLIGHT TESTING

One of the design aims of the FBW Jaguar programme was that the control laws implemented in the FCS should provide handling qualities as good if not better than the standard Jaguar. The standard Jaguar has a mechanical control system with a simplex three axis autostabiliser system. Thus the objective of the flight assessment was not only to demonstrate the basic performance and integrity of the FCS but to carry out an assessment of the aircraft handling qualities. In this respect, the flight trials of the FBW Jaguar aircraft can be compared with those for a new aircraft and the overall flight programme reflects this.

The current overall flight trials programme can be divided into five test phases; Phase 1 comprised a general aircraft and systems shakedown together with an initial aircraft handling assessment. This led straight into Phase 2 of the trials which comprised a detailed flight envelope expansion programme. The whole of these two phases was carried out with "Issue 1" of the FCS software which provided the fixed gains mode of the control laws. In this condition, the quadruplex primary sensors are fully operational whereas the secondary sensors (airspeed, altitude, incidence and sideslip) although operational, are set to fixed values which are dependent upon undercarriage position (see section 2.2).

Phase 3 comprises a detailed assessment of the Issue 2 fully scheduled control laws in a number of aircraft store configurations. This will include a high incidence handling investigation of the SDSP function and an assessment of the stable control laws at progressively smaller manoeuvre margins. Phase 4 comprises a detailed assessment of the unstable control laws at stability levels down to -4%$\bar{c}$ manoeuvre margin. Phase 5 comprises an assessment of the straked aircraft over the stability range of +3 to -10%$\bar{c}$ manoeuvre margin. At the time of writing, the third test phase is about to begin and so results are given for the first two test phases only.

8.1 Telemetry

From the start of the FBW Jaguar Project it was planned to use real time telemetry between the aircraft and a ground station at Warton. Fortuitously a Jaguar telemetry cabin, which was last used during the initial development of the aircraft, was still available. Modifications were carried out to suit the existing facility to its new role and it has been used throughout every flight trial to date and it will be used for the foreseeable future. The aircraft parameters which were transmitted to the ground station during the first phases of the flight assessment are shown at Annex 1. These were chosen so that the project engineers could monitor the FBW system response and aircraft reaction during all the test manoeuvres.

Useful though the transmission of data has been in its own right, both the project engineers and the pilots have found the continuous voice ("hot mike") communication channel of the greatest benefit. The engineers are able to follow the aircraft through the test schedule and discuss unusual or unexpected results with the pilot and then take immediate decisions on the future course of the flight. In addition, test points which take the aircraft near to corners of the envelope can be carefully monitored.

For the pilot, the telemetry has several benefits, not least being that of a willing scribe to record his comments about every facet of the aircraft's handling at the conclusion of each test point. In addition, the project engineers are able to give immediate advice based upon their detailed knowledge of the aircraft's instrumentation and FBW systems. To date no serious malfunction of the aircraft systems has occurred during the flight trials, but in anticipation of such an event the telemetry engineers and the pilots routinely practice their handling of aircraft emergencies together on the FBW system rig. All the foreseen possible failures and the corrective drills are contained in the aircraft's flight reference cards (FRC) and are, of course, practiced many times so that the pilots can correctly handle any of them without telemetry assistance; however, engineering advice could be critical in the unlikely event of an unexpected and perhaps esoteric fault. Finally, B.Ae makes it a rule that all high incidence trials are conducted with telemetry and a ground safety pilot.

8.2 Flight Test Results

Phase 1 of the flight trials commenced with a high speed taxi during which basic aircraft systems were checked out as well as giving the pilot confidence in the abili'y of the FCS to rotate the aircraft into a flying attitude.

The first flight took place on 20th October 1981 and a total of 5 flights were carried out in 4 weeks. This completed the aircraft and systems shakedown together with the initial handling assessment one flight ahead of schedule. The flight trials proceeded immediately into the second phase, the envelope expansion programme. The new taileron and rudder actuators represented a new standard in terms of flutter modes and so flutter testing was necessary to expand the flight envelope beyond the initial flutter clearance. The next 8 flights were completed in 10 weeks despite the loss of $4\frac{1}{2}$ weeks due tc various external factors including a period of severe winter weather. An indication of the reliability of the aircraft and its systems including the FCS is given by the fact that the programmed successful flying rate was exceeded and the test phase was completed in 13 flights compared with the programmed 14 to 22 flights. This is illustrated in Figure 5. In fact the flying rate of the aircraft was not limited during this period by any problems with the FCS but by the large amounts of data for analysis produced after each flight.

The aircraft proved to be very easy and straightforward to fly with excellent FCS reliability. The control laws implemented provided handling qualities which were in general as good as if not better than the standard Jaguar despite having fixed gains. The detailed results of the flight trials can be divided into two areas of interest; FCS behaviour and aircraft handling qualities provided by the FCS control laws.

Flight Control System Behaviour

During the whole of the first two flight trials phases only one in-flight FCS failure warning was encountered and only one FCS LRU had to be changed because of a defect. The LRU change was a flight control computer (FCC) which was rejected during routine servicing when the BIT revealed a digital cross lane transmission malfunction. No computing malfunctions occurred in flight throughout the flight trials. The in-flight FCS failure warning which occurred just prior to landing on Flight 13 was caused by a delay in the quadruplex switch on the undercarriage selector. This particular switch is a standard Jaguar item and its design is such that it is possible for there to be a delay in operation between two pairs of switches. The FCS detected this delay on a slow undercarriage selection and gave the pilot a RED FCS warning. However, the design of the logic was such that it successfully dealt with this two versus two situation and provided the correct signal to the control laws. After this particular flight, the in-flight check function of the BIT was interrogated via the DDU and immediately identified the cause of the RED FCS warning. To prevent a recurrence of what was effectively a "nuisance warning" the software algorithm which monitors the quadruplex undercarriage selector has been modified to allow these delays between switches. Thus, in overall terms, the flight control system reliability and performance was excellent, generating a very high level of confidence in the system. Pilot confidence in the serviceability of the system prior to each flight was enhanced by the thoroughness of the BIT function which is a prerequisite for system engagement. Obviously in such a demonstrator aircraft, the BIT contained a good deal of pilot interaction which could be automated to a large extent in a production aircraft environment. However, even this BIT could be completed in about three minutes after a few practices.

Aircraft Handling Qualities

The aircraft handling qualities were assessed by a combination of qualitative and quantitative assessments. A large number of classical handling tests were performed, including stick jerks, rudder doublets, slowdowns, wind-up turns, inversions, partial rolls and rapid rolls. In addition, specific tests were undertaken including ground attack dive manoeuvres and formation flying as well as aerobatics. The flight envelope explored is illustrated in Figure 6 where it can be seen that a maximum speed of 550 kts, 1.26 Mach was achieved.

From the first flight the handling of the aircraft proved to be excellent, instilling a high level of pilot confidence in the flight control system. Over much of the envelope the aircraft combined pleasantly light control forces with good response. It was not over sensitive to handle and there were no PIO tendencies in any phase of flight examined. It was particularly easy to fly near the ground and to land accurately and gently. The ground

attack manoeuvres revealed good tracking performance and formation flying was very straightforward.

The wind-up turns demonstrated good manoeuvring characteristics over the whole of the flight envelope assessed which included subsonic turns up to 7.5g and supersonic turns up to 5g. Target 'g's' could be achieved smoothly and accurately and could be held with ease even through the transition from supersonic to subsonic flight.

The rapid rolling assessment included 360° rolls from 1g entry conditions over a range of speed and altitude and 180° in accelerated flight with entry conditions of up to 4g. The rolling performance was very good with a smooth and rapid roll acceleration together with a high sustained rate. Figure 7 illustrates how the peak roll rate was maintained both at low speed and at high levels of normal acceleration. The aircraft response to stick jerks was typically deadbeat and the dutch roll response to rudder doublets always moderately to heavily damped. The accuracy of the predictions is clearly illustrated in Figure 8 where the flight measured dutch roll characteristics virtually overlay the predicted behaviour.

As the flight trials were carried out during the autumn and winter months, considerable experience was obtained of flying in turbulent weather conditions. In clear air turbulence at altitude the aircraft held its flight path well and at low level during ground attack manoeuvres in moderate to heavy turbulence the aircraft would drive its way through in an impressive fashion. Take-off and landings were performed in gusty conditions with crosswind components in excess of 15 kts. The aircraft was always easy to fly in these conditions and there was never any suggestion of over-controlling or PIO in any axis.

The aerobatic manoeuvres performed included loops, barrel rolls and slow rolls. From a pilot's point of view the slow roll is a very good test of a flight control system as it requires a well co-ordinated control system in order to achieve a smooth, steady roll rate about a level axis. The rolls proved to be very smooth and straightforward to fly and clearly demonstrated the effectiveness of the FBW Jaguar FCS.

A characteristic of the fixed gains control laws was that with undercarriage up control laws the aircraft was neutrally stable in pitch due to the presence of the integrator with a fixed value of incidence. Above 240 kts this gave the aircraft a very pleasant characteristic described by one pilot as if "the aircraft was flying along rails" which was very beneficial, particularly in ground attack manoeuvres. Below 240 kts the lack of static stability became more apparent and it was necessary to monitor incidence carefully in order to prevent inadvertent speed loss. However, practice approaches to low overshoots (200 ft) were flown in order to demonstrate that it was entirely practical to land the aircraft in the very unlikely event that such a failure to undercarriage up control laws should occur.

The accuracy of the simulation carried out prior to flight proved to be of a very high order and a frequent pilot comment was "just like the simulator". Only in its lack of motion cues did the fixed base simulation fall short of accurate flight predictions. This accounted for the interesting phenomenon encountered during partial rolls at high subsonic speeds described by the pilots as "roll hunting". If a rapid and abrupt partial roll stick input was made at these conditions, the initial roll acceleration was rapid enough to move the pilot's torso and hand away from the direction of the roll. Under certain conditions, this could reduce the roll stick demand which in turn reduced the roll acceleration and hence resulted in an oscillatory roll acceleration and sustained roll rate which gently damped out. Initially only one pilot encountered this behaviour but the second pilot was subsequently able to find it by modifying his grasp of the stick and elevating his arm.

This 'hunting' phenomenon was shown to be caused by a combination of low roll stick control circuit damping and good roll acceleration from sharp roll stick inputs which coupled through the bob weight effect of the pilot's arm and torso to give a closed loop coupled motion. The natural frequency and damping of the mechanical control circuit between the stick and the position sensor on the FBW Jaguar is significantly different from the standard Jaguar because of the absence of control rods linked to a main valve on a hydraulic jack. In fact the damping on the FBW Jaguar roll stick circuit was of the order of 0.06f_n. Theoretical modelling which included the bob weight effect of the pilot's arm confirmed the coupling phenomenon and indicated that an increase in stick damping together with a slight reduction in roll loop gain would provide a satisfactory solution. A viscous damper has been introduced in the roll circuit and the Issue 2 control laws contain the slight reduction in roll gain. This it is expected that the partial roll response will now be satisfactory throughout the flight envelope. This experience demonstrated the difficulties involved in designing a single set of control laws to cover all aircraft configurations from clean aircraft to heavy wing stores as well as modifying an existing mechanical control circuit. The roll gain was defined by the high roll inertia, heavy wing store configuration and was thus overgeared for the clean aircraft. However, it is still expected that the single set of control laws will produce satisfactory roll handling over a variety of store configurations. The FBW team believe that the aim of a single set of control laws is a highly desirable one if it can be achieved without a significant loss of performance.

The overall results of the flight trials completed to date have been highly satisfactory. The project pilots have consistently praised the aircraft handling qualities and as a production standard flight control system, the FCS reliability and performance has been very good.

A high degree of confidence has been generated in the aircraft and its systems for the continuing flight trials programme.

In conclusion, the authors would like to acknowledge the special team effort that such a programme involves. Its success depends upon the efforts of British Aerospace, Marconi Avionics and Dowty Boulton-Paul. In particular, the programme could not have gone ahead in the first place, nor have been sustained through several years of financial stringency, were it not for the enthusiastic support from the British Ministry of Defence and RAE Farnborough.

.....

REFERENCES

1. R. E. W. Marshall, K. S. Snelling, J. M. Corney. "The Jaguar Fly-by-Wire Demonstrator Integrated Flight Control System". 1981 Proceedings of Advanced Flight Controls Symposium. USAF Academy.

2. W. W. Peterson, E. J. Welden. "Error Correcting Codes". Pub. M.I.T. Press Appendix C.

3. I. N. Steward. "Galois Theory". Pub. Chapman and Hall. Chapter 4

4. E. Daley, R. B. Smith. "Flight Clearance of the Jaguar Fly By Wire Aircraft". 1982 Proceedings of the Royal Aeronautical Society Avionics Systems Group Symposium "Certification of Avionic Systems".

.....

ANNEX 1

FBW JAGUAR TEMELETRY PARAMETERS FOR GENERAL FLYING

1. Indicated Airspeed
2. Altitude
3. Central Warning Panel Events (6)
4. Longitudinal Stick Position
5. Lateral Stick Position
6. Incidence
7. Sideslip
8. Yaw Rate
9. Roll Rate
10. Rudder Ram Position
11. Starboard Tailplane Ram Position
12. Port Tailplane Ram Position
13. Pilot Continuous Speech

Note: Alternative signals are available for Specific Flight Trials - for example, high incidence flying

ANNEX 2

BUILT-IN TEST FUNCTION

1. PRE-FLIGHT CHECK

Automatic Tests

- Computer Functions
- Program/Constant Store Check
- Lane Coding/Stability Selection
- ADT Scratchpad Checks
- 16 Bit Scratchpad Checks
- 1 Bit Scratchpad Checks
- Intralane Outputs
- Discrete Outputs
- Discrete Inputs
- Weight On Wheels Undercarriage Select
- Analogue/Digital - Digital/Analogue Check
- Analogue Loop Check
- Overflow Operation
- Checkword Monitor Operation
- Sensor Torqueing
- Autotrim Operation
- Quadruplex Tracking
- Failure Display Selection

Crew Participation Tests

- ADMC Checks (Part 1)
- Power Supplies
- Column, Rudder Pedal and Trim Inputs
- Spin Recovery/Training Mode Selection
- Actuators Check
- Failure Display Selection

Pilot's decision on whether to carry out FLC or enter FRS

First Line Checks

- Diagnostic Display Unit Operation
- Pilot's Control Panel
- Triplex Transducers
- Failure Display Selection

2. IN-FLIGHT MONITORING

- Functions Check
- Overflow Check
- Analogue Loop Check
- On-Line Monitor
- Scratchpad Operation
- Program Store Comparison
- Constant Store Comparison
- Interchannel Communication Valid
- Frame Execution Monitor
- Synchronisation Operation Monitor
- Voter/Monitor Data Selection (Quadruplex to Duplex)
- Rate Gyros Valids

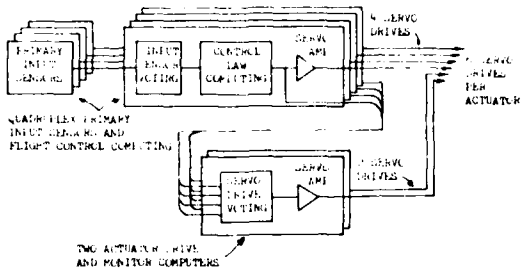

FIGURE 1. SIMPLIFIED SCHEMATIC OF PRIMARY CONTROL PATH

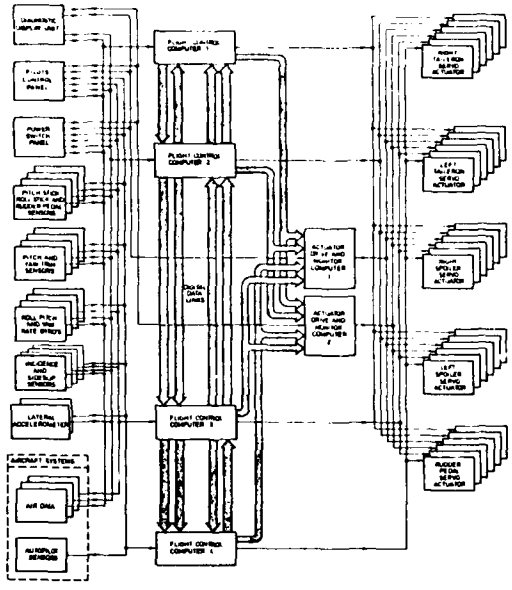

FIGURE 2. FBW JAGUAR IFCS CONFIGURATION

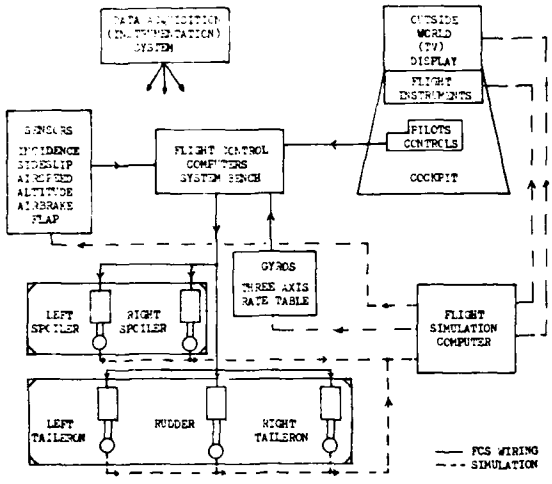

POWER CONTROLS MOUNTED IN REPRESENTATIVE STRUCTURE

FIGURE 3. GROUND TEST RIG FACILITIES

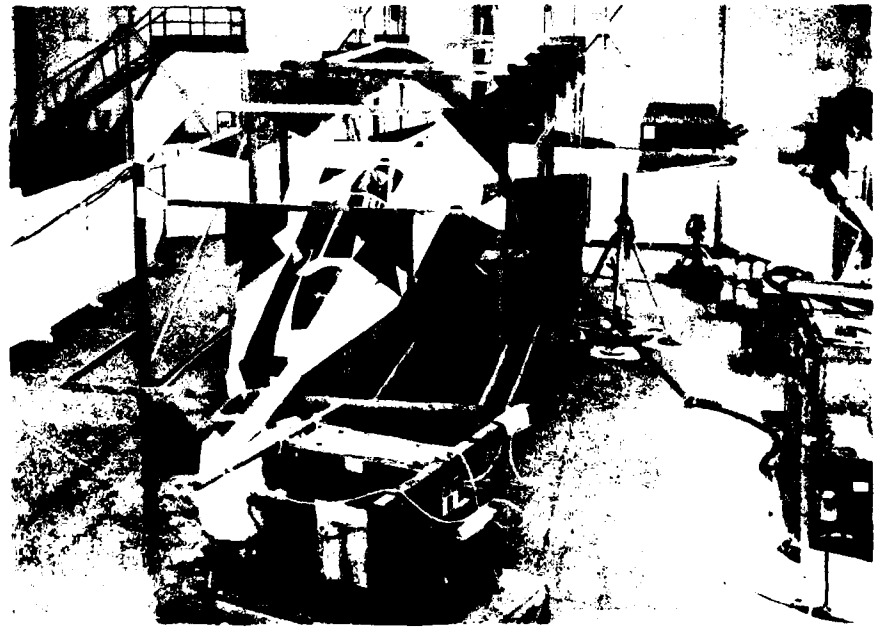

FIGURE 4 FBW JAGUAR IN SIMULATED LIGHTNING TEST RIG

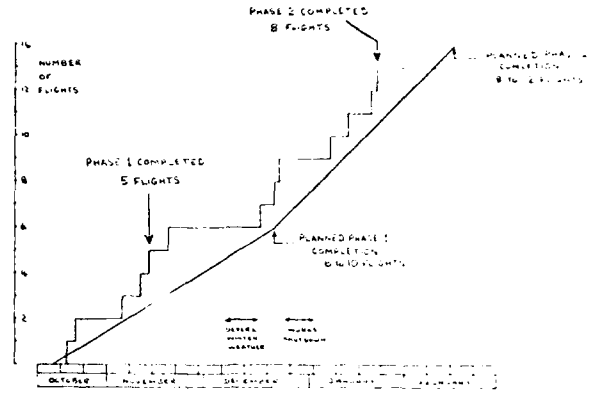

FIGURE 5 FBW JAGUAR FLYING HRS ACHIEVED

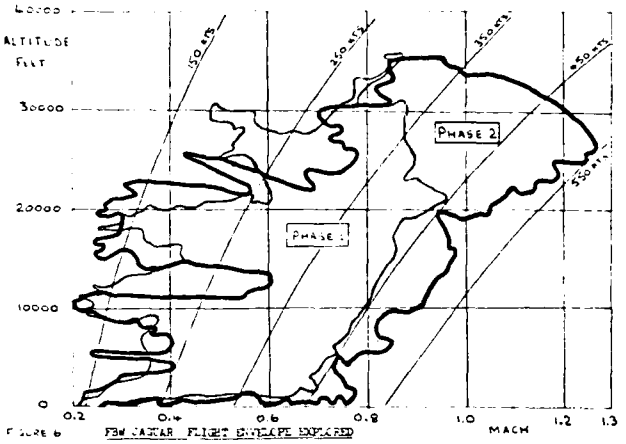

FIGURE 6 FBW JAGUAR FLIGHT ENVELOPE EXPLORED

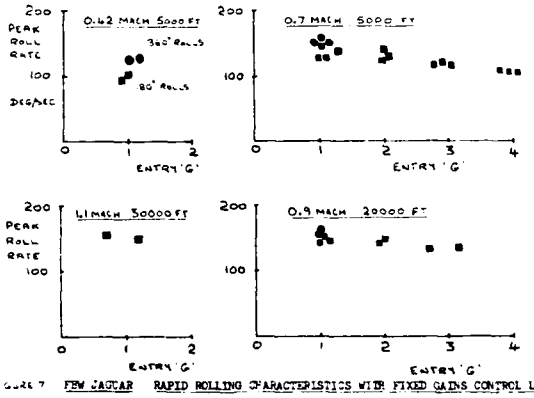

FIGURE 7 FBW JAGUAR RAPID ROLLING CHARACTERISTICS WITH FIXED GAINS CONTROL LAWS

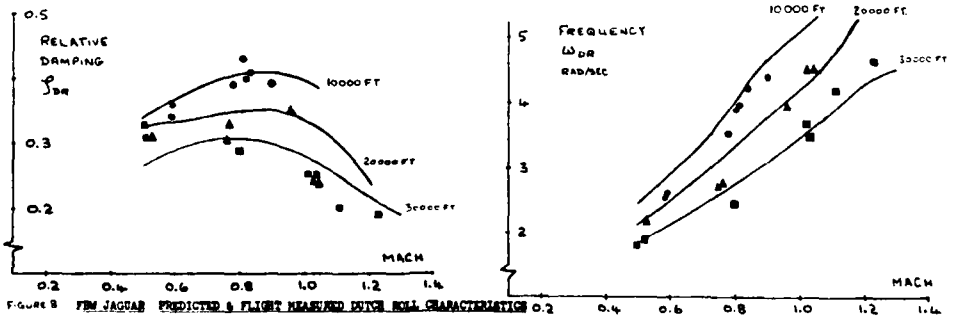

FIGURE 8 FBW JAGUAR PREDICTED & FLIGHT MEASURED DUTCH ROLL CHARACTERISTICS FIXED GAINS CONTROL LAWS

REPORT DOCUMENTATION PAGE

1. Recipient's Reference	2. Originator's Reference	3. Further Reference	4. Security Classification of Document
	AGARD-CP-321	ISBN 92-835-0324-4	UNCLASSIFIED

5. Originator Advisory Group for Aerospace Research and Development
North Atlantic Treaty Organization
7 rue Ancelle, 92200 Neuilly sur Seine, France

6. Title

ADVANCES IN GUIDANCE AND CONTROL SYSTEMS

7. Presented at

the Guidance and Control Panel 35th Symposium held in Lisbon, Portugal, 12–14 October 1982

8. Author(s)/Editor(s)	9. Date
Various	January 1983
10. Author's/Editor's Address	**11. Pages**
Various	252

12. Distribution Statement This document is distributed in accordance with AGARD policies and regulations, which are outlined on the Outside Back Covers of all AGARD publications.

13. Keywords/Descriptors

Control theory	Design
Control equipment	Guidance
Systems engineering	

14. Abstract

This publication contains part of the papers presented at the Guidance and Control Panel 35th Symposium on Advances in Guidance and Control Systems.

1 Keynote Address and 23 papers were presented, 19 of the papers appear in this book – the balance of 5 papers appear in CP-321(S) – a classified publication.

The topics covered are as follows:–

- Advances in control (Keynote)
- Applications of control theory
- Advanced design concepts
- Advanced system design
- Systems synthesis – simulation and validation
- Recent systems experience

AGARD Conference Proceedings No.321 Advisory Group for Aerospace Research and Development, NATO ADVANCES IN GUIDANCE AND CONTROL SYSTEMS Published January 1983 252 pages This publication contains part of the papers presented at the Guidance and Control Panel 35th Symposium on Advances in Guidance and Control Systems. 1 Keynote Address and 23 papers were presented, 19 of the papers appear in this book the balance of 5 papers appear in CP-321(S) a classified publication. P.T.O.	AGARD-CP-321 Control theory Control equipment Systems engineering Design Guidance	AGARD Conference Proceedings No.321 Advisory Group for Aerospace Research and Development, NATO ADVANCES IN GUIDANCE AND CONTROL SYSTEMS Published January 1983 252 pages This publication contains part of the papers presented at the Guidance and Control Panel 35th Symposium on Advances in Guidance and Control Systems. 1 Keynote Address and 23 papers were presented, 19 of the papers appear in this book the balance of 5 papers appear in CP-321(S) a classified publication. P.T.O.	AGARD-CP-321 Control theory Control equipment Systems engineering Design Guidance
AGARD Conference Proceedings No.321 Advisory Group for Aerospace Research and Development, NATO ADVANCES IN GUIDANCE AND CONTROL SYSTEMS Published January 1983 252 pages This publication contains part of the papers presented at the Guidance and Control Panel 35th Symposium on Advances in Guidance and Control Systems. 1 Keynote Address and 23 papers were presented, 19 of the papers appear in this book the balance of 5 papers appear in CP-321(S) a classified publication. P.T.O.	AGARD-CP-321 Control theory Control equipment Systems engineering Design Guidance	AGARD Conference Proceedings No.321 Advisory Group for Aerospace Research and Development, NATO ADVANCES IN GUIDANCE AND CONTROL SYSTEMS Published January 1983 252 pages This publication contains part of the papers presented at the Guidance and Control Panel 35th Symposium on Advances in Guidance and Control Systems. 1 Keynote Address and 23 papers were presented, 19 of the papers appear in this book the balance of 5 papers appear in CP-321(S) a classified publication. P.T.O.	AGARD-CP-321 Control theory Control equipment Systems engineering Design Guidance

The topics covered are as follows:

- Advances in control (Keynote)
- Applications of control theory
- Advanced design concepts
- Advanced system design
- Systems synthesis – simulation and validation
- Recent systems experience

Papers presented at the Guidance and Control Panel 35th Symposium held in Lisbon, Portugal, 12–14 October 1982.

ISBN 92-835-0324-4

The topics covered are as follows:

- Advances in control (Keynote)
- Applications of control theory
- Advanced design concepts
- Advanced system design
- Systems synthesis – simulation and validation
- Recent systems experience

Papers presented at the Guidance and Control Panel 35th Symposium held in Lisbon, Portugal, 12–14 October 1982.

ISBN 92-835-0324-4

The topics covered are as follows:

- Advances in control (Keynote)
- Applications of control theory
- Advanced design concepts
- Advanced system design
- Systems synthesis – simulation and validation
- Recent systems experience

Papers presented at the Guidance and Control Panel 35th Symposium held in Lisbon, Portugal, 12–14 October 1982.

ISBN 92-835-0324-4

The topics covered are as follows:

- Advances in control (Keynote)
- Applications of control theory
- Advanced design concepts
- Advanced system design
- Systems synthesis – simulation and validation
- Recent systems experience

Papers presented at the Guidance and Control Panel 35th Symposium held in Lisbon, Portugal, 12–14 October 1982.

ISBN 92-835-0324-4

END

DATE
FILMED

4-83

DTIC